DISTINCT SURVIVAL STRATEGIES OF PDAC CELLS UNDER STRESS: ECM-DEPENDENT ADAPTATION TO NUTRIENT DEPRIVATION AND QUIESCENCE UPON KRAS INHIBITION

IFEOLUWA OYELADE

A THESIS SUBMITTED IN PARTIAL FULFILMENT OF THE REQUIREMENT FOR THE DEGREE OF DOCTOR OF PHILOSOPHY

THE UNIVERSITY OF SHEFFIELD

FACULTY OF SCIENCE

SCHOOL OF BIOSCIENCES

NOVEMBER 2025

Abstract

Pancreatic cancer remains one of the most lethal forms of cancer, due in part to its ability to adapt to stressful conditions such as a nutrient-deprived microenvironment or chemotherapy. Here, we investigated the role of the extracellular matrix (ECM) in supporting the growth of PDAC cells in nutrient-deprived conditions. We found that the ECM supported PDAC cell proliferation under nutrient deprivation. Our metabolomics analysis revealed that PDAC cells upregulated the Arginine and proline metabolic pathway in the presence of Matrigel, coupled with a Matrigel-dependent increase in ASS1 expression, the rate-limiting enzyme in the de novo synthesis of Arginine. Furthermore, Matrigel-dependent mTORC1 activation was required for Matrigel-dependent proliferation of glucose-deprived PDAC cells. In contrast, Matrigel internalisation mediated Matrigel-dependent proliferation of glutamine-deprived PDAC cells. We also investigated the effects of MRTX1133, a KRAS G12D inhibitor, on PDAC cells and showed that MRTX1133 caused a significant reduction in cell number and EdU incorporation in PDAC cells with the KRAS G12D mutation, with no corresponding increase in cell death. Flow cytometry analysis confirmed that MRTX1133-treated cells were in the quiescent G0 phase of the cell cycle, and dye retention assay revealed that MRTX1133-treated cells retained the dye compared to cells treated with the vehicle control, where proliferation resulted in dye dilution. This suggests that MRTX1133-treated cells are not dividing or are dividing at a significantly slower rate than vehicle control. Importantly, upon MRTX1133 removal, cells resumed proliferation, indicating that quiescence induced by MRTX1133 was reversible. Finally, metabolomics analysis showed that β-oxidation of fatty acid-related metabolites were upregulated in MRTX1133-treated cells, suggesting their reliance on β-oxidation of fatty acid for survival. Overall, our study established that the ECM remodels PDAC cell metabolism to support their growth under nutrient-limiting conditions, while KRAS inhibition induces a quiescent state in PDAC, potentially resulting in treatment resistance and survival of PDAC cells.

Acknowledgement

This PhD would not have been possible without the divine leading, teachings, inspiration, and support of the Holy Spirit.

I am deeply grateful to my parents and siblings. Their unwavering support and belief in my dreams have brought me to this point, and I do not take it for granted.

A heartfelt thank you to my supervisor, Dr Elena, who has been nothing short of exceptional. I truly appreciate her guidance, patient and gentle teaching approach, and, most importantly, her openness to my ideas. She has given me the space to take full ownership of my project while providing invaluable support and direction. Thank you for making my PhD journey both enjoyable and as stress-free as a PhD can be.

This PhD would not have been completed without the support of Prof. Liz Smythe and Prof. Carl Smythe. Beyond Prof. Liz Smythe's guidance as my Scientific Advisor, I will always be grateful for their unwavering support, especially during the moments when I almost had to walk away from my PhD.

A huge thank you to Dr Heather Walker for running my metabolomics experiments and for always being gracious and available to answer my questions, and to Dr Helen Matthews for her helpful suggestions during lab meetings and for providing the antibodies, PDAC cell lines, and kits for my experiments.

Finally, to my incredible lab members—Mona, Bella, Bian, Vic, Zhe, Rachele, Eric, Rachel, and Fatmagul—thank you for your support and for being the absolute best team to work with. A special shout-out to Mona for always being available to answer my questions with such grace and clarity and for allowing me to bounce ideas off her; she made my PhD so much easier.

Declaration Page

I declare that this thesis is the result of my work. I confirm that this thesis has not been previously submitted to the University of Sheffield or any other institution. I confirm that the source is cited where I have quoted the work of others.

Ifeoluwa Oyelade

10/11/2025

Table Of Contents

List Of Figures

CHAPTER 1

CHAPTER 2

CHAPTER 3

CHAPTER 4

CHAPTER 5

CHAPTER 6

CHAPTER 7

List Of Tables

CHAPTER 1

CHAPTER 2

CHAPTER 5

CHAPTER 7

Abbreviations

AA - Amino acid

ADAMTS - A disintegrin and metalloproteinase with thrombospondin motifs

ADM - Acinar-to-ductal metaplasia

AMPK - AMP-activated protein kinase

ATG - Autophagy Related Gene

ASS1 - Arginine succinate synthetase 1

BAD - Bcl-2–associated death promoter

BM - basement membrane

BSA - Bovine serum albumin

CAF - cancer-associated fibroblasts

CPT1 - Carnitine palmitoyl transferase 1

CRC - Colorectal cancer

DDRs - discoidin-domain receptors

DF1 - DharmaFect-1

dFBS - Dialysed FBS

DMEM - Dulbecco's Modified Eagle's Medium

DMSO - Dimethyl sulfoxide

ECM - extracellular matrix

EdU - 5-ethynyl-2´-deoxyuridine

EGF - Epidermal growth factor

EGFR - Epidermal growth factor receptor

EMT - epithelial-to-mesenchymal transition

ERK1/2 - Extracellular signal-regulated kinase-1/2

ER - Estrogen receptor

FAO - Fatty acid oxidation

FBS - Fetal bovine serum

FGF - Fibroblast growth factor

FN - Fibronectin

GA - Glutaraldehyde

GAPs - GTPase-activating proteins

GAPDH - Glyceraldehyde 3-phosphate dehydrogenase

GDH - Glutamate dehydrogenase

GEFs - Guanine nucleotide exchange factors

GFs - Growth factors

GLU - Glucose

GLS - Glutaminase

GLN - Glutamine

GOT1 - Glutamic-Oxaloacetic Transaminase 1

GOT2 - Glutamic-Oxaloacetic Transaminase 2

GS - Glutamine synthetase

HCC - Hepatocellular carcinoma

HK - Hexokinase

HNCSS - Head and neck squamous cell carcinoma

IF - Interstitial fluid

IM - Interstitial matrix

KD - Knockdown

KRAS - Kirsten rat sarcoma viral oncogene homolog

LDHA - Lactate Dehydrogenase A

MAPK - Mitogen-activated protein kinase

MEF - Mouse embryonic fibroblasts

MMP - Matrix metalloproteinase

MS - Mass spectrometry

mTOR - Mammalian target of rapamycin

mTORC1 - Mammalian target of rapamycin complex 1

mTORC2 - Mammalian target of rapamycin complex 2

NADH - Nicotinamide adenine dinucleotide

NADPH - Nicotinamide adenine dinucleotide phosphate

NHE1 - Na^+/H^+ exchanger 1

NSCLC - Non-small cell lung carcinoma

Nt - Non-targeted

PAICS - Phosphoribosylaminoimidazole succinocarboxamide synthetase

Pb - Palbociclib

PDAC - Pancreatic ductal adenocarcinoma

PDGF - Platelet-derived growth factors

PFA - Paraformaldehyde

PI3K - Phosphoinositide 3-kinases

PIP_3 - Phosphatidylinositol (3,4,5)-trisphosphate

PK - Pyruvate kinase

PPP - Pentose phosphate pathway

PSCs - Pancreatic stellate cells

RAPTOR - Regulatory-associated protein of mTOR

ROS - Reactive Oxygen Species

RT - Room temperature

S6 - Ribosomal subunit S6

S6K - Ribosomal S6 kinase

SLC2A1 - Solute Carrier Family 2 Member 1

SMPDB - Small Molecule Pathway Database

TCA - Tricarboxylic acid

TGF-β - transforming growth factor beta

TIFM - Tumour Interstitial Fluid Media

TME - Tumour microenvironment

ULK1 - Unc-51 Like Autophagy Activating Kinase 1

UPLC-MS - Ultra-Performance Liquid Chromatography - Mass spectroscopy

5′ terminal oligopyrimidine tracts mRNAs - 5′ TOP mRNAs

1 Introduction

1.1 Overview of Pancreatic Cancer

The pancreas is a vital organ located behind the stomach, close to the duodenum, spleen and hepatic hilum (Valente et al., 2024). It is made up of two major components, the endocrine and exocrine pancreas, both of which play distinct roles in the body. The endocrine pancreas consists of the islets of Langerhans and regulates blood glucose homeostasis through the secretion of hormones, including insulin, glucagon and somatostatin (Hu et al., 2025). On the other hand, the exocrine pancreas facilitates digestion by secreting digestive enzymes such as amylase, lipase, and proteases, which break down carbohydrates, lipids, and proteins (Hu et al., 2025). The exocrine pancreas is composed of acinar and ductal cells. The acinar cells are the predominant cells in the endocrine pancreas and are responsible for the synthesis and secretion of digestive enzymes (Valente et al., 2024; Hu et al., 2025). In contrast, the ductal cells transport these enzymes to the duodenum and secrete them to neutralise gastric acid and maintain an optimal pH for enzymatic digestion (Hu et al., 2025).

The abnormal growth of endocrine cells leads to Pancreatic Neuroendocrine Tumour (PNET). In contrast, malignant transformation of exocrine cells results in either acinar cell carcinoma or Pancreatic Ductal Adenocarcinoma (PDAC) (Lanfredini et al., 2019). According to the American Cancer Society, PDAC accounts for approximately 90% of pancreatic cancer cases and has a poorer prognosis than PNET and acinar cell carcinoma. Most PDAC cases originate in the head of the pancreas, with the liver being the most common site of metastasis, followed by the lungs and spleen in some cases (Hezel et al., 2006). Some common risk factors for pancreatic cancer include age, smoking, type 2 diabetes, family history, obesity, excessive alcohol consumption, and genetic mutations (Hidalgo, 2010).

The latest statistics on pancreatic cancer **(Table 1.1)** from Cancer Research UK and the American Cancer Society show that pancreatic cancer is fast becoming one of the leading causes of cancer death in the UK and the USA. Unlike breast and prostate cancers, which have well-known and reliable biomarkers for early detection, there is a lack of dependable biomarkers for identifying pancreatic cancer early.

Table 1.1- Latest statistics of pancreatic cancer
The table shows some of the latest statistics in pancreatic cancer Worldwide, the UK and the USA.
Data from World Cancer Research Fund International (2025), Cancer Research UK (2025) and the SEER Program, National Cancer Institute (2025). The table was generated using draw.io

	INCIDENCE	MORTALITY	5-YEAR SURVIVAL RATE	PROJECTIONS
Worldwide	12th most common cancer	7th cause of cancer death	NA	NA
United Kingdom	10th most common cancer	5th cause of cancer death	8.3%	Incidence rate projected to rise by about 5% between 2023 and 2025 and 2038-2040
United States of America	10th most common cancer	3rd cause of cancer death	13.3%	Expected to become the 2nd leading cause of cancer death by 2030

Common biomarkers such as CA19.19, CEA, and CA125 are available; however, their lack of specificity to pancreatic cancer and undetectable levels in some patients make them unreliable (Hidalgo, 2010; Yu et al., 2025). Consequently, most patients are diagnosed at an advanced metastatic stage, with very low chances of survival. Supporting this, the 2024 report by the National Pancreatic Cancer Audit states that most individuals diagnosed with pancreatic cancer in England and Wales between 2020 and 2021 already had metastatic disease, with only about 10% surviving for one year after diagnosis. Furthermore, according to the American Cancer Society, standard treatment methods such as surgery, chemotherapy, and radiotherapy are largely ineffective for disease-free survival, highlighting the severity of the disease (Cancer facts & figures 2025).

1.1.1 Common mutations in PDAC

Pancreatic acinar cells show a marked degree of plasticity that allow them to undergo acinar-to-ductal metaplasia (ADM) in response to inflammation or injury (Marstrand-Daucé et al., 2023). ADM is a cellular reprogramming process in which pancreatic acinar cells lose their differentiated state and adopt ductal-like characteristics. Under non-oncogenic conditions, ADM is a reversible process that enables regeneration of pancreatic acinar tissue following injury. However, upon persistent inflammation and sustained oncogenic KRAS activation, ADM becomes irreversible and drives the formation of pancreatic intraepithelial neoplasia (PanIN) followed by progression to PDAC (**Figure 1.1)** (Marstrand-Daucé et al., 2023; Aliar et al., 2026).

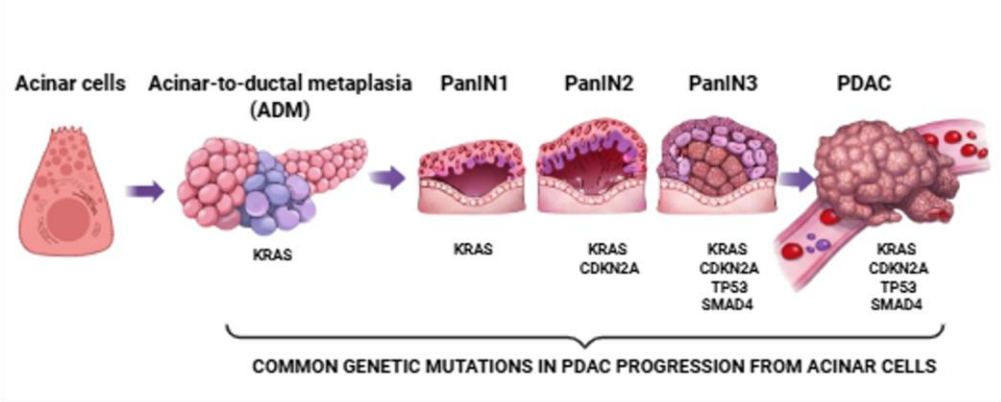

Figure 1.1 - Genetic alterations driving the progression of pancreatic ductal adenocarcinoma (PDAC).
Under inflammatory conditions such as pancreatitis, acinar cells can undergo acinar-to-ductal metaplasia (ADM), a reversible process in which acinar cells adopt a duct-like phenotype. However, in the presence of oncogenic KRAS activation, ADM becomes stabilised and promotes the formation of precursor lesions of pancreatic intraepithelial neoplasia (PanIN). Progressive accumulation of genetic alterations, including loss of CDKN2A, TP53, and SMAD4, drives the transition from low-grade PanIN lesions (PanIN1) to high-grade lesions (PanIN2 and PanIN3) and ultimately to invasive PDAC. This model highlights the role of KRAS signalling in locking ADM into a neoplastic state and illustrates the stepwise genetic evolution of PDAC from normal pancreatic cells. The figure was generated using Biorender.com.

Activation of the KRAS oncogene, found in more than 90% of all PDAC cases, is a key driver mutation in PDAC and is also necessary to maintain the progression of the disease (Halbrook et al., 2023; Wei et al., 2024). Among the KRAS mutations in PDAC **(Figure 1.2)**, the KRAS G12D mutation accounts for about 42%, followed by G12V (32%), G12R (16%) and the less common G12C (2%) (Wei et al., 2024). In addition to the KRAS mutation, inactivation of the tumour suppressor genes TP53, CDKNA and SMAD4 is also seen in most PDAC cases (Hidalgo, 2010; Halbrook et al., 2023). Some less common mutations are in DNA repair proteins, BRCA2, MSH2 and MLH1 (Hingorani et al., 2005).

RAS is a small GTPase that switches between an inactive GDP-bound and an active GTP-bound form via guanosine exchange factors (GEFs) and GTPase-activating proteins (GAPs). GAPs promote RAS GTPase activity, resulting in GTP hydrolysis, to switch RAS into an inactive GDP-bound state, while GEFs displace GDP from RAS to allow binding of GTP (Pantsar, 2020) **(Figure 1.3).**

In its active GTP-bound state, RAS activates downstream signalling pathways such as the Mitogen Activated Protein Kinase/ Extracellular Signal-Regulated Kinase (MAPK/ERK) pathway, the Phosphoinositide 3-kinase/Protein Kinase B/Mammalian Target of Rapamycin (PI3K/AKT/mTOR) pathway and the Ral Guanine nucleotide Dissociation Stimulator (RalGDS)/Ral pathway. There are 3 RAS proteins: Kirsten rat sarcoma (KRAS), Harvey-RAS (HRAS) and Neuroblastoma-RAS (NRAS), all of which can be mutated in cancers, with KRAS being the most commonly mutated RAS in all cancers, including pancreatic cancer (Shi et al., 2025). The common KRAS mutations in PDAC are caused by a point mutation on codon 12, which replaces the amino acid glycine with aspartate (G12D), arginine

(G12R), valine (G12V) or cysteine (G12C). These mutations affect GTP hydrolysis, allowing a sustained activation of RAS's downstream signalling proteins (Hezel et al., 2006).

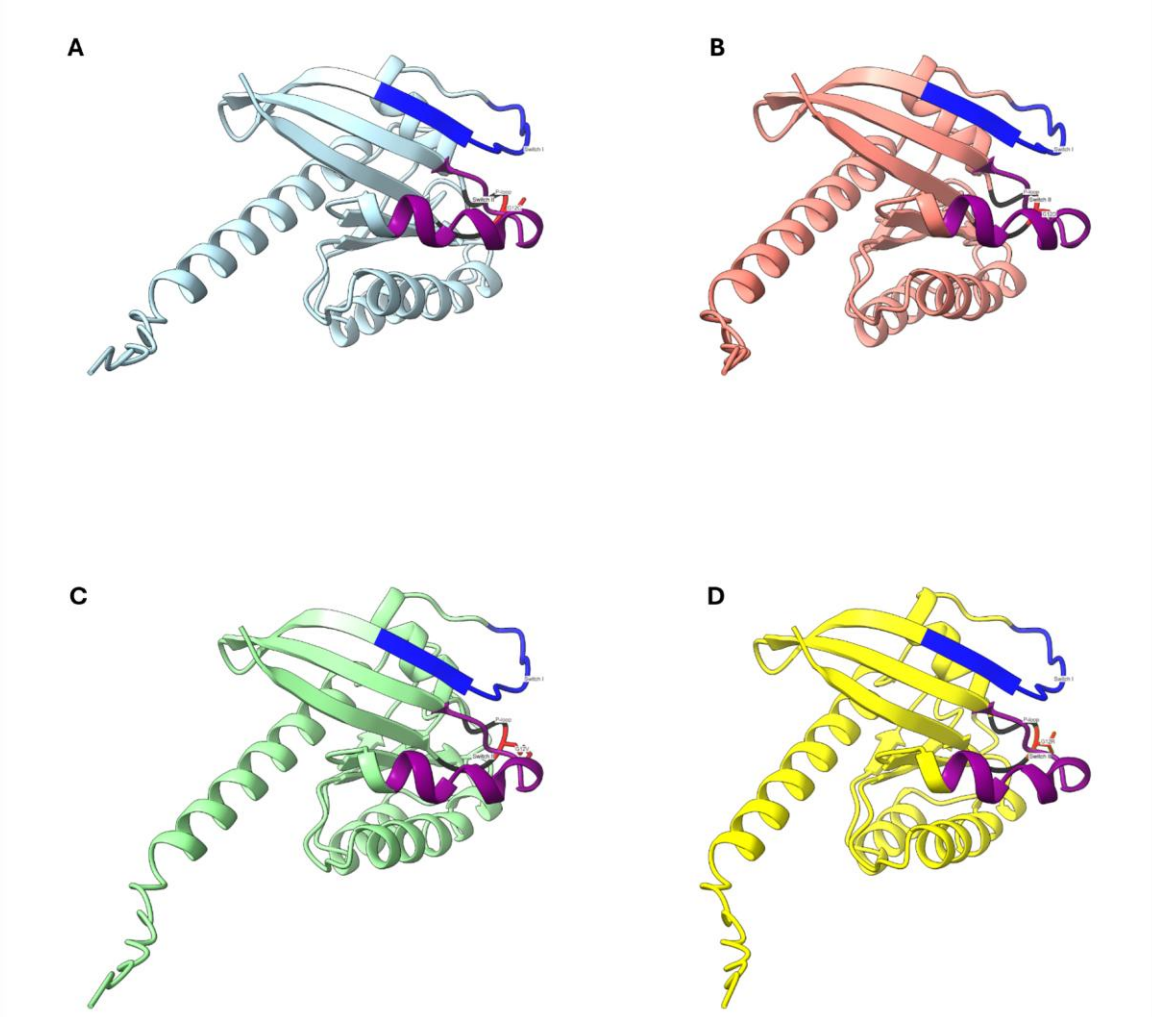

Figure 1.2 - Structural visualisation of KRAS G12 mutation hotspots.
Ribbon diagram of human KRAS protein generated from the AlphaFold Protein Structure Database (UniProt P01116) and visualised in UCSF ChimeraX. Functionally critical regions are highlighted: P-loop (residues 10–17, black) coordinates GDP/GTP phosphates, Switch I (residues 30–40, blue), and Switch II (residues 58–72, purple) undergo conformational changes upon GTP binding and mediate interactions with downstream effector proteins. The G12 mutation site (red) is the most frequently mutated position in KRAS-driven pancreatic cancer. (A) G12C mutation (cysteine, ~1–2% of PDAC cases). (B) G12D mutation (aspartate, ~40–45% of PDAC cases). (C) G12V mutation (valine, ~30–35% of PDAC cases). (D) G12R mutation (arginine, ~15–20% of PDAC cases). Functional residue domain adapted from Pantsar, 2020.

Given the vital role of KRAS in PDAC and other cancers like lung and colon cancers, several studies have focused on effectively inhibiting KRAS, resulting in the recent development of MRTX849, a KRAS G12C inhibitor. But, given the rarity of the KRAS G12C mutation in PDAC, a more impactful discovery came with the development of MRTX1133, a non-covalent, small-molecule KRAS G12D inhibitor. MRTX1133 has been reported to produce promising results in both PDAC in vivo and in vitro studies (Wei et al., 2024). Following this is an even more recent development of pan-RAS inhibitors, such as

RMC-7977 and RMC-6236, that inhibit the different isoforms of RAS as well as both the wild-type and mutant forms of RAS (Cregg et al., 2025).

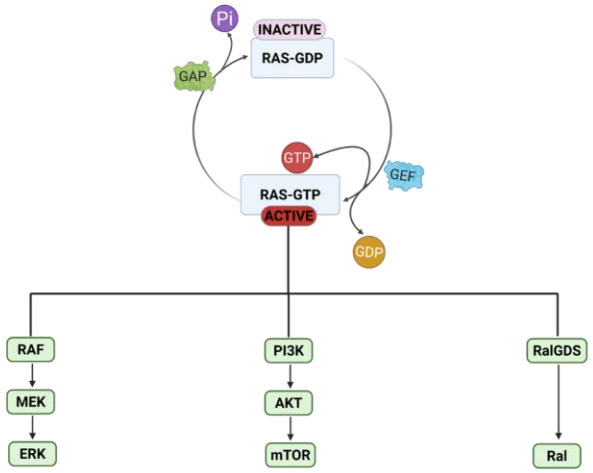

Figure 1.3 - Activation and Inactivation of RAS
RAS is bound to GDP in its inactive form and GTP in its active form. GTPase-activating protein (GAP) promotes RAS's intrinsic GTPase activity to hydrolyse GTP, allowing RAS to bind to GDP and making it inactive. Guanosine exchange factor (GEF) displaces GDP from RAS and allows the binding of GTP to RAS, making it active. This activates its main downstream effector pathways – the RAF/MEK/ERK pathway, PI3K/AKTmTOR pathway and the RalGDS pathway, all implicated in cell differentiation, proliferation, migration and survival. The figure was generated using Biorender.com, adapted from Hezel et al., 2006.

Furthermore, as a driver of progression of PDAC, mutated KRAS have also been found to play a role in metabolic remodelling of PDAC cells, allowing them to upregulate different metabolic pathways, nutrient transporters and nutrient scavenging mechanisms like macropinocytosis to provide the required nutrients needed to sustain their aberrant growth facilitated by KRAS (Yun et al., 2009; Ying et al., 2012; Jeong et al., 2018). Additionally, in PDAC, mutated KRAS has been shown to play a role in remodelling the tumour microenvironment (TME) by driving changes that result in activation of fibroblasts, immune cells recruitment and the expression of matrix-remodelling enzymes such as MMP7, all of which contribute to the dense fibrotic TME of PDAC (Collins et al., 2012).

Interestingly, studies have found that the effects of different KRAS mutations on downstream signalling and metabolic pathways, disease severity and patient prognosis vary (Hobbs et al., 2020; Ardalan et al., 2025). For example, using different PDAC cell lines, Hobbs and colleagues reported that while cell lines with both G12D and G12V mutations efficiently interact with PI3Kα (p110α) to activate the PI3K-AKT signalling pathway and drive macropinocytosis in a MYC-dependent manner, G12R-mutant cell lines are impaired in their ability to interact with PI3Kα due to structural perturbations in the switch II domain, resulting in reduced PI3K-AKT pathway activation. Despite this, G12R-mutant PDAC cells maintain macropinocytosis through upregulation of KRAS-independent PI3Kγ activity,

representing a compensatory alternative mechanism. Consistently, siRNA knockdown of KRAS reduced macropinocytosis in G12D and G12V-mutant PDAC cell lines but not in G12R-mutant lines, confirming that macropinocytosis in G12R-mutant PDAC operates independently of KRAS (Hobbs et al., 2020).

Furthermore, Ardalan et al, analysed the molecular distinctions between patients with G12D-mutated tumours and those with G12R-mutated tumours and reported that patients with G12R mutations had significantly better overall survival than those with G12D mutations. They found that patients with G12D-mutated tumours displayed higher expression of genes involved in glucose metabolism, including Solute Carrier Family 2 Member 1 (SLC2A1), Lactate Dehydrogenase A (LDHA) and glutamine metabolism including Glutamic-Oxaloacetic Transaminase 1 and 2 (GOT1 and GOT2) compared to G12R-mutated tumours. Their gene set enrichment analysis further indicated a trending enrichment of PI3K/AKT/mTOR pathway gene expression in G12D compared to G12R tumours, collectively suggesting greater metabolic activity in G12D-mutated PDAC (Ardalan et al., 2025). Altogether, these findings demonstrate that KRAS variants are not functionally interchangeable and highlight the importance of KRAS mutation-specific stratification when considering therapeutic vulnerabilities and clinical management in PDAC.

1.2 The Tumour Microenvironment of PDAC

The TME is the natural environment of the tumour. It comprises cellular components such as immune cells, blood vessels, fibroblasts, and an acellular component, the extracellular matrix (ECM). The PDAC TME is characterised by altered and excessive ECM deposition, resulting in a dense fibrotic stroma, also called desmoplasia, which creates an environment conducive to cancer cell sustained proliferation and survival (Mahadevan and Von Hoff, 2007; Papalazarou et al., 2020). Hence, it is vital to understand the roles of the PDAC ECM and its contribution to pancreatic cancer severity.

1.2.1 Role of the ECM in PDAC

The PDAC TME is characterised by the accumulation of ECM components such as collagen-I, collagen-III, collagen-IV, laminin and fibronectin (**Table 1.2)**, with collagens being the most abundant ECM in PDAC. The ECM comes in two forms - the interstitial matrix (mainly composed of collagens I, III, V and fibronectin), which provides structural support to tissues and organs and supports cell differentiation and migration (Winkler et al., 2020), and the basement membrane (BM), mainly consisting of collagen-IV, laminins, nidogen and perlecan, that separates epithelial organs from the interstitial matrix and aid in cell differentiation and tissue repair (Zhou et al., 2022). Among the BM components, laminins have been linked to early embryonic development and formation of BMs, collagen-IV is responsible for

maintaining the structural integrity of the BM and acts as a scaffold to aid the binding of other BM proteins, perlecan aids in the formation of muscular tissue, while nidogen aids in the stabilisation of the BM (Zhou et al., 2022).

ECM proteins bind to the cell surface receptors, including integrins, discoidin domain receptors (DDRs) and CD44, mediating cellular processes such as cell proliferation, migration and apoptosis (Winkler et al., 2020; Huang et al., 2021). Different ECM receptors have been implicated in various cancers (Sipos et al., 2004; Huang et al., 2021). For example, αvβ6, which binds to fibronectin and tenascin-C, is overexpressed in pancreatic cancer, and it was found to promote both cell proliferation and metastasis and could represent a bad prognostic indicator in PDAC (Sipos et al., 2004; Li et al., 2016). Similarly, high expression of Discoidin-domain receptor 1 (DDR1), a collagen-binding receptor tyrosine kinase that mediates cell–extracellular matrix signalling to regulate processes such as cell adhesion, migration, proliferation, differentiation and survival (Huo et al., 2015; Chen et al., 2021), has been implicated in pancreatic cancer (Huo et al., 2015). A 2015 study by Huo and colleagues on the roles of DDRs in PDAC revealed that expression of DDR1 at both the mRNA and protein levels was significantly higher in the tissue specimens of pancreatic cancer patients compared to non-tumour tissues. They also highlighted its role as a poor prognostic indicator in pancreatic cancer; however, the molecular mechanism behind its role in pancreatic cancer was not described in this study (Huo et al., 2015).

Table 1.2 - ECM proteins and their roles in Cancer
The table shows some ECM proteins that have been implicated in pancreatic cancer. The table was generated using draw.io

ECM PROTEINS	ROLE IN CANCER	CANCER REPORTED	REFERENCES
Collagen-I	Promotes Tumorigenesis Promotes Metastasis Promotes cancer drug resistance Reactivation of dormant breast cancer cells	Breast cancer Pancreatic cancer Prostate cancer Lung cancer	Barkan et al., 2010 Miyamoto et al., 2004
Collagen-IV	Promotes cancer drug resistance Promotes cell proliferation and metastasis Promotes liver metastases in different tumours	Breast Cancer Pancreatic Cancer	Miyamoto et al., 2004
Fibronectin	Reactivation of dormant breast cancer cells Promotes cancer drug resistance Survival and migration of tumour cells Maintain cells in a state of dormancy	Breast Cancer Pancreatic Cancer	Barkan et al., 2010 Miyamoto et al., 2004
Laminin-332	Promotes cell proliferation, migration and invasion	Pancreatic cancer	Huang and Cheng, 2021
Hyaluronic acid	Promotes chemotherapy resistance and metastatic relapse	Pancreatic cancer	Provenzano et al., 2012

Additionally, a study by Miyamoto and colleagues found a positive correlation between expression of ECM proteins such as collagen-I, collagen-IV and fibronectin, increased cell proliferation and resistance to anti-cancer agents in human PDAC cell lines (Miyamoto et al., 2004). Also, ECM proteins have been proposed to be a marker of relapse and poor survival in pancreatic cancer (Ohlund et al., 2009). In this study, Ohlund and colleagues first investigated whether type IV collagen in pancreatic tumours originates only from stromal cells or cancer cells themselves. Using two pancreatic cancer cell lines, HPAC and CFPAC-1, their Western blotting analysis of both cell lysate and conditioned media revealed that collagen-IV subunits (α1 and α2) were strongly expressed in both the media and cell lysates, suggesting that the cells express and secrete collagen-IV. Subsequently, they measured the levels of circulating collagen-IV in pancreatic cancer patients and healthy controls via ELISA. Before surgery, they saw a significantly higher concentration of collagen-IV in pancreatic cancer patients compared to controls, which they hypothesised to be a result of the production and secretion of collagen-IV by pancreatic cancer cells. Next, they found a consistently high level of collagen-IV in some pancreatic cancer patients after surgery. They saw that higher levels of collagen-IV post-surgery are directly proportional to a higher chance of relapse and low survival (Ohlund et al., 2009). Their study further highlights the contribution of ECM proteins to the severity of PDAC, making it a viable target for effective treatment.

1.2.2 ECM Remodelling in PDAC

A hallmark of PDAC is its highly desmoplastic TME, which is characterised by a complex network of Cancer Associated Fibroblasts (CAFs), immune cells, and ECM components that collectively promote tumour progression and therapeutic resistance (Halbrook et al., 2023). In PDAC, the ECM is constantly remodelled by cancer cells, CAFs, and immune cells to drive sustained cell proliferation and survival (Prakash and Shaked, 2024). ECM remodelling is a process characterised by a change in the composition, abundance, structure and organisation of the ECM, all of which alter cell behaviour (Winkler et al., 2020). Two of the most characterised mechanisms of ECM remodelling are ECM deposition and ECM degradation (Winkler et al., 2020)

1.2.2.1 ECM Deposition

Excessive ECM deposition alters the abundance and composition of the ECM and contributes to its dense fibrotic stroma. The dense stroma is enriched with collagens (I, III and IV), laminins, hyaluronic acid and fibronectin (Ferrara et al., 2021). In PDAC, both cancer-associated fibroblasts (CAFs) and pancreatic stellate cells (PSCs) play a vital role in ECM deposition (Perez et al., 2021; Yang et al., 2023a).

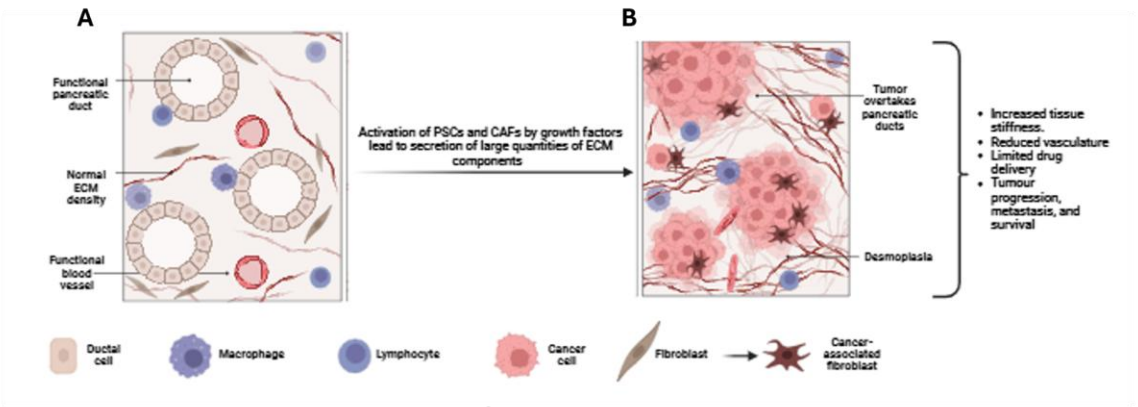

Figure 1.4 – ECM remodelling during progression from healthy pancreas to PDAC
In the healthy pancreas (A), the extracellular matrix (ECM) is maintained at low density, supporting normal tissue architecture and function. During PDAC development (B), growth factors including TGF-β and PDGF drive the activation of quiescent PSCs into CAFs, which subsequently secrete abundant ECM components. This subsequently results in the formation of a dense desmoplastic stroma characterized by abundant ECM deposition, creating a tumour microenvironment that promotes disease progression and limits therapeutic access. The figure was generated using BioRender.com.

PSCs and CAFs are activated by growth factors such as platelet-derived growth factors (PDGFs), fibroblast growth factors (FGFs) and transforming growth factor beta (TGFβ1). Upon activation, CAFs and PSCs secrete large quantities of ECM components (Hidalgo, 2010), driving the desmoplastic reaction that remodels the TME of PDAC. This excessive ECM accumulation increases tissue stiffness, reduces vasculature, impedes drug delivery (Mahadevan and Von Hoff, 2007), and enhances tumour progression, metastasis, and survival (Papalazarou et al., 2020) **(Figure 1.4)**.

1.2.2.2 ECM Degradation

ECM degradation is the process of breaking down ECM components. The two main mechanisms of ECM degradation identified are extracellular degradation by proteases and intracellular lysosomal degradation following ECM internalisation (Rainero, 2016).

For extracellular degradation, the ECM is broken down by specific proteases such as Matrix metalloproteinases (MMPs), A disintegrin and metalloproteinase with thrombospondin motifs (ADAMTS), as well as serine and cysteine proteases (Winkler et al., 2020). MMPs, one of the most studied ECM degradation enzymes, are a family of zinc and calcium-dependent proteolytic enzymes responsible for the breakdown of ECM proteins. They are classified into collagenases, gelatinases, stromelysins, matrilysins, membrane-bound MMPs and others based on their enzymatic function **(Table 1.3)** (Murphy and Nagase, 2008). Studies have found that MMPs and MMP-degraded ECM proteins are differentially expressed in pancreatic cancer patients and healthy patients. For example, Willumsen et al reported a 2-fold increase in the levels of MMP-degraded collagens I, III and IV in the serum of pancreatic cancer patients compared to the healthy control group (Willumsen et al., 2013).

Table 1.3 - MMPs and their roles in ECM degradation
Adapted from Murphy and Nagase, 2008 and Alipour et al., 2016. The table was generated using draw.io

MMPs	TYPES	SUBSTRATES
Collagenases	MMP-1, MMP-8, MMP-13, MMP-18	Collagens I, II, III, IV, VIII, X, fibronectin, osteonectin
Gelatinases	MMP-2, MMP-9	Collagens IV, V, XI, fibronectin, osteonectin, elastin, laminin
Stromelysins	MMP-3, MMP-10, MMP-11, MMP-17	Collagens III, IV, V, IX, osteonectin
Matrilysins	MMP-7, MMP-26	Collagens IV, X, laminin, fibronectin, proteoglycans
Membrane-bound MMPs	MMP-14, MMP-15, MMP-16, MMP-17, MMP-24, MMP-25	Collagens I, II, III, fibronectin, laminin, proteoglycan, vitronectin

Furthermore, various studies have highlighted the tumour-promoting roles of different MMPs in PDAC. An early work on the roles of MMPs in pancreatic cancer by Ellenrieder and colleagues revealed that MMP-2 was highly expressed in pancreatic cancer tissues compared to the normal pancreas. Furthermore, they found that MMP-2 was highly expressed in PDAC cell lines, PANC-1 and IMIM-PC1, and these cell lines had higher invasive ability than PDAC cell lines that have low or minimal MMP-2 activity, highlighting the correlation between MMPs and invasion in PDAC (Ellenrieder et al., 2000).

1.2.3 ECM Internalisation and Lysosomal Degradation

ECM internalisation and lysosomal degradation is a process whereby cells take up ECM components via phagocytosis or different endocytic processes (Rainero, 2016), such as macropinocytosis, clathrin-mediated endocytosis or caveolae-mediated endocytosis **(Figure 1.5)**, followed by delivery into the lysosome for lysosomal degradation. In the lysosome, intra- and extracellular components such as the internalised ECM proteins are broken down and recycled to yield metabolites for use in cellular metabolism to fuel the tricarboxylic acid (TCA) cycle, biosynthesis of other lipids, nucleotides and proteins, as well as activation of mTORC1 (Lawrence and Zoncu, 2019; Miao et al., 2020).

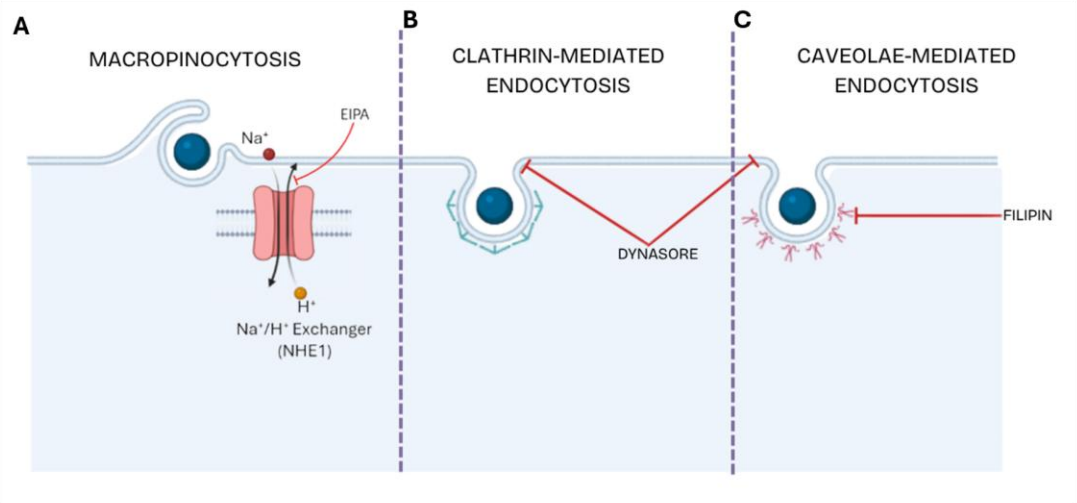

Figure 1.5 – Overview of Endocytic pathways associated with ECM internalisation and their pharmacological inhibitors

(A) Macropinocytosis, an actin-mediated endocytic process, is inhibited by EIPA. (B, C) Both clathrin- and caveolae-mediated endocytosis require the small GTPase dynamin, which is inhibited by dynasor. Filipin inhibits lipid-raft mediated endocytosis, including but not limited to caveolae-dependent. Created with Canva and Biorender.com

The first step in ECM internalisation is the recognition and attachment of cells to ECM components through ECM receptors such as integrins and Discoidin Domain Receptors (DDRs), followed by internalisation via endocytic processes (Sprangers and Everts, 2019). Indeed, ECM receptors such as α2β1 integrin, Endocytic receptor 180 (Endo180), and β1 integrin mediate collagen phagocytosis, clathrin-dependent collagen internalisation, and caveolae-dependent fibronectin internalisation (Rainero, 2016). Furthermore, a recent study in our lab reported that α2β1 integrin is required for ECM internalisation, facilitating invasion and migration of breast and pancreatic cancer cells (Martinez et al., 2024). Mechanistically, they found that in MDA-MB-231 cells, disruption of β1 integrin via siRNA knockdown reduced Matrigel internalisation, and disruption of α2 integrin (by siRNA or pharmacological inhibitor) reduced collagen-I and Cell-derived matrices (CDM) internalisation. Similarly, they found that inhibition of α2 integrin by BTT-3033 reduced migration of pancreatic cancer cells, confirming the requirement of α2β1 integrin–mediated ECM internalisation for cancer cell invasion (Martinez et al., 2024). Moreover, ECM internalisation is reported to be upregulated and facilitates the survival of PDAC, colorectal cancer, lung cancer and breast cancer cells, especially in nutrient-limited conditions (Olivares et al., 2017; Hsu et al., 2022; Nazemi et al., 2024; Martinez et al., 2024).

Additionally, lysosomal degradation enzymes are upregulated in cancer. Quintanilla-Dieck and colleagues reported that Cathepsin K (CatK), a lysosomal cysteine protease that degrades collagens in the lysosomes, is upregulated in melanoma cells to support collagen degradation following internalisation, thereby enhancing invasion and metastasis (Quintanilla-Dieck et al., 2008). Western blot analysis revealed that melanoma cell lines (MM-AN, LIBR, and MeWo) strongly expressed the

active form of CatK, whereas primary melanocytes did not. Furthermore, using Oregon Green–labelled collagen-IV, the authors found that melanoma cell lines (MM-AN and MeWo) internalised collagen-IV, which subsequently colocalised with LAMP1 (lysosome-associated membrane protein 1), indicating lysosomal localisation. Also, inhibition of CatK led to a twofold increase in the number of cells containing detectable internalised collagen-IV, indicating that inhibition of CatK blocked collagen degradation and increased its detectability (Quintanilla-Dieck et al., 2008).

1.3 Nutrient Deprivation

All cells (normal and cancerous) require an optimal amount of nutrients such as glucose and essential amino acids to maintain their growth and ensure their survival. Indeed, most cells are committed to progress through the cell cycle only with available nutrients and growth factors. Moreover, cancer cells are more susceptible to nutrient deprivation due to their uncontrollable growth and largely hypovascular microenvironment that limits the transport of oxygen and nutrients (especially in solid tumours). As a result, most cancer cells do not survive in a nutrient-starved state and succumb to apoptosis, while some have been found to survive in a quiescent state (Terzi et al., 2016). Unfortunately, some cancer cells have found ways to retain their ability to thrive and continue cell proliferation under nutrient-limiting conditions **(Figure 1.6)**. As a result, recent work in cancer metabolism has focused on understanding how these cells survive in nutrient-deprived conditions, intending to target their various survival pathways.

1.3.1 Tumour cell Quiescence

Tumour dormancy is a clinically observed stage in cancer progression in which residual disease persists but remains asymptomatic, with cancer patients capable of developing recurrent metastatic disease following latency periods ranging from years to decades (Aguirre-Ghiso, 2007). Studies have shown that ERK(MAPK) activity is a determinant of tumour growth and dormancy and that the balance between ERK and p38 MAPK signalling determines whether cancer cells proliferate or enter dormancy (Aguirre-Ghiso et al., 2003). Using breast, prostate, melanoma, and fibrosarcoma cell lines, the authors demonstrated that the ERK/p38 activity ratio predicted in vivo behaviour in approximately 90% of cell lines tested, with a high ERK/p38 ratio favouring tumour growth and proliferation and a high p38/ERK ratio inducing tumour growth arrest and dormancy in vivo (Aguirre-Ghiso et al., 2003). Importantly, the authors show that modulating the ERK/p38 ratio can switch tumour cells between proliferative and dormant states, suggesting that this signalling balance is a key determinant of metastatic behaviour and a potential therapeutic target.

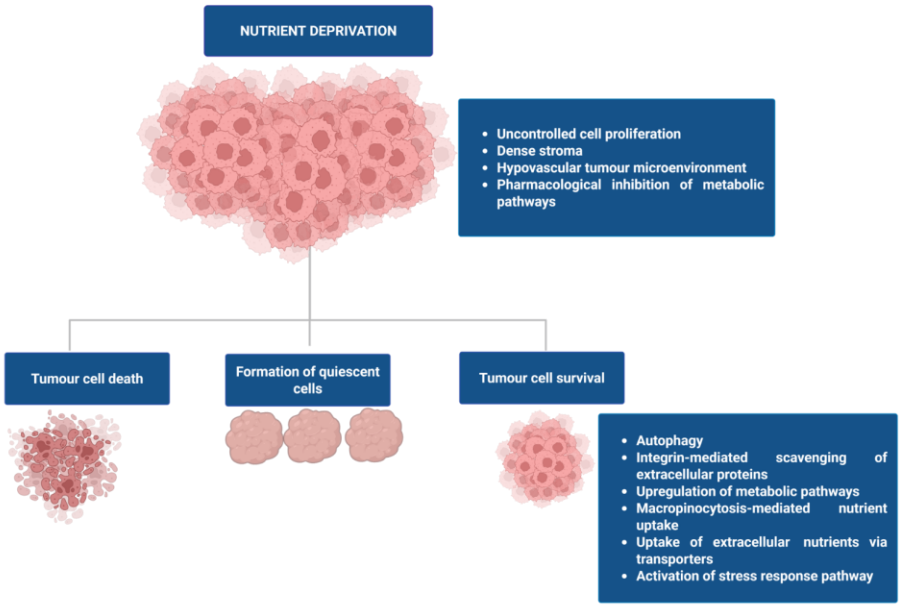

Figure 1.6 - PDAC cell fate under nutrient deprivation.
Nutrient deprivation in PDAC arises due to uncontrolled cell proliferation, a dense desmoplastic stroma, a hypovascular tumour microenvironment, and pharmacological inhibition of metabolic pathways. In response to nutrient deprivation, PDAC cells can undergo one of three fates: cell death, quiescence, or survival. Cells that survive nutrient deprivation do so by employing adaptive strategies, including autophagy, macropinocytosis, integrin-mediated extracellular protein scavenging, upregulation of metabolic pathways, and activation of stress response pathways. The figure was generated using Biorender.com.

Tumour dormancy can arise through at least three distinct mechanisms. The first and most important to this thesis is cell dormancy/quiescence, which describes a state in which individual cells enter G0 arrest or a quiescent state. Next is angiogenic dormancy, wherein micrometastatic lesions fail to expand due to insufficient vascularisation, and immune-mediated dormancy, a state in which anti-tumour immune surveillance constrains tumour outgrowth (Aguirre-Ghiso, 2007).

Cells have been found to enter a reversible quiescent state as an adaptive response to unfavourable microenvironmental conditions, including nutrient deprivation, growth factor withdrawal, and oxidative stress imposed by chemotherapeutic agents (Nik Nabil et al., 2021). These quiescent cells are not responsive to chemotherapeutic agents as they are non-proliferative, and most cytotoxic therapies preferentially target actively dividing cells. However, they retain their cancer-specific mutations and can re-enter the cell cycle upon exposure to appropriate reactivation signals and cause cancer relapse **(Figure 1.7)**. Some common markers of quiescent cells are upregulation of cyclin-dependent kinase inhibitors, such as p21 and $p27^{KIP1}$, lack of Ki-67 (a marker of cell proliferation found in all phases of the cell cycle except G0), inactivation of mTORC1 and activation of autophagy (Li et al., 2019).

Furthermore, nutrient deprivation has been widely implicated as a driver of tumour cell quiescence. To study the contributions of nutrient deprivation to the formation of quiescent tumour cells, White et al found that upon serum deprivation, prostate cancer cell lines were insensitive to H_2O_2-induced oxidative stress compared to their serum-replete counterparts. In addition, they observed a proliferation arrest, cell cycle arrest, lack of apoptotic phenotype, rounder and flatter phenotype, a lack of pRB and accumulation of $p27^{KIP1}$ in the nucleus, all indicators of a quiescent state (White et al., 2020).

Furthermore, Ortmayr and Zampieri found that exposing ovarian, lung or colon cancer cells to glutamine-free conditions resulted in a population of cells where at least 40% of the cells were in the G0 phase of the cell cycle, suggesting that nutrient scarcity may actively drive cancer cells into a quiescent state (Ortmayr and Zampieri, 2022). Another study by Li and colleagues demostrated that serum-starved nucleus pulposus stem cells (NPSCs) adopted a quiescent phenotype marked by reduced Ki-67, accumulation of $p27^{KIP1}$, as well as flow cytometry-based confirmation of a G0 phase. Additionally, they found that upon supplementation with serum, the cells became reactivated and could differentiate, indicating that the quiescent state was reversible (Li et al., 2019). This reversibility is of relevance as it suggests that nutrient-deprived cancer cells may similarly enter a protective quiescent state that allows long-term survival, with the potential to reactivate upon restoration of a nutrient-replete microenvironment, contributing to disease recurrence.

In addition to nutrient deprivation, downregulation of the KRAS oncogene in KRAS-driven cells has been found to result in the formation of cells with quiescent features such as lack of proliferation, lack of apoptosis and ability to resume proliferation upon re-expression of KRAS (Viale et al., 2014; Rajbhandari et al., 2017). Also, some ECM proteins are associated with the formation and reactivation of quiescent tumour cells (Barkan et al., 2010; Di Martino et al., 2022). Using both in vivo and in vitro models of human head and neck squamous cell carcinoma (HNSCC), Di Martino and colleagues found that collagen-III induced the formation of quiescent tumour cells, and it was required for the cells to maintain their quiescent properties (Di Martino et al., 2022).

Conclusively, understanding the changes in cancer cells that enable them to go from a proliferative to a quiescent state and become reactivated to return to a proliferative state is crucial, since this could be the key to preventing cancer relapse and metastasis.

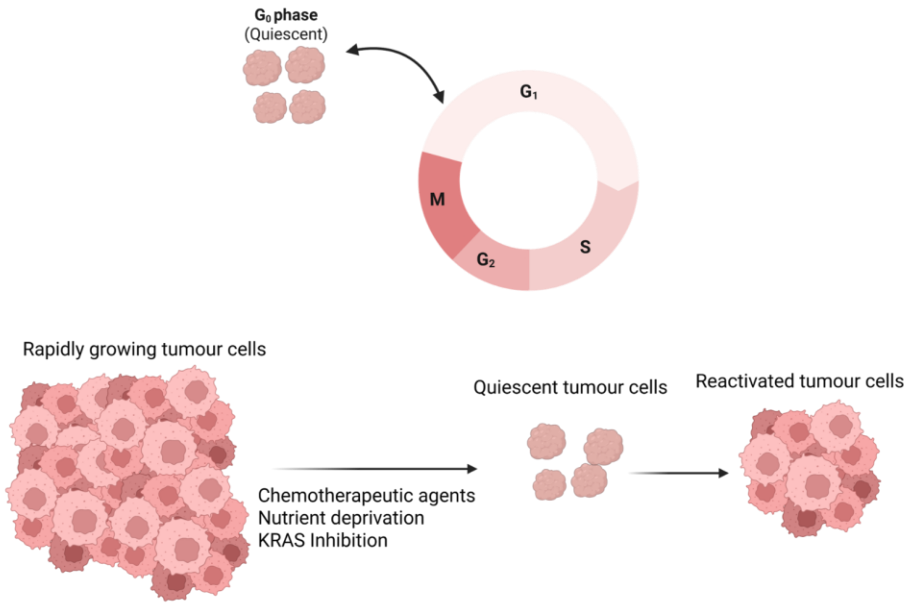

Figure 1.7 - Tumour quiescence
Quiescent tumour cells can temporarily exit the cell cycle because of stressful conditions or assault from chemotherapeutic agents. They can re-enter the cell cycle in the presence of appropriate triggers to become reactivated to rapidly proliferating cells. The figure was generated using Biorender.com

1.3.1.1 Targeting quiescent tumour cells

The latest advances in targeting quiescent tumour cells have focused on three main approaches: quiescent cell reactivation, maintenance of the quiescent state, and targeting quiescent cells.

The goal of stimulating quiescent tumour cells with proliferative signals is to reactivate them into rapidly proliferating cells, making them sensitive to chemotherapeutic agents. However, one drawback of this approach is that the cells might have acquired some adaptive features while in their quiescent state that would make them less sensitive to chemotherapeutic agents, even in their proliferative states. This would result in uncontrollable and non-targetable tumours that could progress faster into overt metastasis.

The second approach focuses on maintaining tumour cells in a quiescent state and preventing their reactivation ability to become rapidly proliferative. This approach was demonstrated in a study by Di Martino and colleagues. Using both in vivo and in vitro models of head and neck squamous cell carcinoma (HNSCC), they found that not only does collagen-III induce a quiescent phenotype in these cells, but tumour-derived collagen-III is also required to maintain the cells in a quiescent state via its interaction with DDR1, a collagen receptor. Importantly, they observed that a disruption of the interaction between collagen-III and its receptor, DDR1, resulted in the reactivation of the cells, leading to renewed proliferation (Di Martino et al., 2022). These findings highlight the therapeutic potential of collagen-III in maintaining cells in a dormant state to prevent reactivation and cancer

relapse. Again, in theory, this could be a viable option; however, due to the evolutionary nature of cancer and the fact that the cells in a quiescent state still have the genetic properties of cancer, keeping the cells in a quiescent state may not be the best option, as there will always be the possibility of reactivation.

The last and arguably the most viable option is to target and kill quiescent cells in their quiescent state. This approach eliminates the possibility of reactivating cell proliferation and eventual relapse arising from the other two methods. Indeed, researchers have amplified efforts into this approach. A work led by Ortmayr and Zampieri identified the roles of fatty acid β-oxidation in the survival of quiescent lung and breast cancer tumour cells, and they found that disrupting this metabolic pathway sensitised quiescent cells to apoptosis (Ortmayr and Zampieri, 2022).

Also, a recent study led by Dwyer demonstrated that inhibiting autophagy resulted in dormant mammary tumour cell death in vivo (Dwyer et al., 2024). Using a known doxycycline-inducible HER2-driven mouse model that recapitulates minimal residual disease, dormancy and recurrence as seen in human breast cancer, they showed that withdrawal of doxycycline (and thus HER2 downregulation) produced a quiescent population of residual tumour cells. Their microscopy data revealed an increased expression of GFP-tagged Light Chain 3 (LC3) in the quiescent models compared to the actively growing models, indicating increased autophagy upon quiescence. Interestingly, treatment with chloroquine (an autophagy inhibitor), 3 weeks after HER2 downregulation (to ensure the formation of a quiescent population), resulted in a 38% reduction in quiescent cells compared to the vehicle control. Their findings indicate that autophagy is required for the survival of the quiescent population (Dwyer et al., 2024). This highlights the potential benefits of combining autophagy inhibitors with standard breast cancer therapies to reduce the burden of quiescent tumour cells and the chances of tumour relapse.

In conclusion, understanding the mechanism of action behind the formation and reactivation of quiescent tumour cells to either prevent their formation or target and kill these cells would be a breakthrough in cancer therapy. Furthermore, identifying their metabolic requirements, nutrient sources, and survival mechanisms while in the quiescent state and targeting these means of survival would be an effective approach to kill these cells before they become reactivated.

1.3.2 How do PDAC cells survive in a nutrient-deprived microenvironment?

PDAC tumours are poorly vascularised, resulting in insufficient availability of nutrients and oxygen required for survival. They are known to survive and thrive in an environment deprived of nutrients

that should ideally be unfavourable for their survival (Izuishi et al., 2000). In their study, Izuishi and colleagues reported that normal human fibroblasts died after 24 hours of culture in serum-free media, glucose-free media or amino acid-free media. In contrast, they demonstrated that upon exposing human PDAC cell lines (PANC-1, AsPC-1, BxPC-3 and KP-3) to similar nutrient-deprived conditions, more than half of the cell population survived 48 hours post-starvation (Izuishi et al., 2000), highlighting the ability of PDAC cells to withstand stressful nutrient-starved conditions.

Understanding the molecular mechanisms behind nutrient starvation adaptation will be vital to improving the treatment of pancreatic cancer. Indeed, one of the hallmarks of KRAS-driven tumours like PDAC is their ability to scavenge the extracellular molecules to match their rapid proliferation needs in nutrient-deprived environments (Kamphorst et al., 2013). Several studies have highlighted macropinocytosis-dependent uptake of extracellular proteins, autophagy, metabolic plasticity, increased expression of nutrient transporters and integrin-mediated scavenging of ECM proteins as the main ways through which PDAC cells acquire nutrients to support their continuous cell proliferation and survival **(Figure 1.6)** (Yun et al., 2009; Guo et al., 2011; Jeong et al., 2018; Finicle et al., 2018).

1.3.2.1 Macropinocytosis

Macropinocytosis **(Figure 1.8)** is an endocytic process involving the uptake of large extracellular proteins/fluids through vesicles called macropinosomes. This is followed by macropinosome fusion with lysosomes and lysosomal enzymes' degradation of the proteins, before the final release of amino acids and sugars into the cytosol (Finicle et al., 2018). Various studies have reported that PDAC cells take up extracellular proteins via macropinocytosis (Commisso et al., 2013; Kamphorst et al., 2015). Kamphorst and colleagues assessed the internalisation of tetramethylrhodamine-conjugated dextran (TMR-dextran, a known marker of macropinocytosis) by human PDAC cells. Using fluorescent microscopy, they found significantly higher TMR-dextran-positive macropinosomes in human PDAC tissues incubated with TMR-dextran than in normal tissues. Further in the study, using KPC cells harvested from KRAS G12D-mutated mouse model, they found that PDAC cells deprived of leucine did not survive past day 3, however, when the cells were supplemented with Bovine Serum Albumin (BSA), even without leucine, the cells continued to proliferate rapidly, demonstrating that the cells sustained proliferation by scavenging extracellular proteins (Kamphorst et al., 2015).

Furthermore, mutant KRAS has been reported to upregulate macropinocytosis, especially in nutrient-starved conditions (Jeong et al., 2018). To confirm the roles of activated KRAS in macropinocytosis, the Commisso lab assessed the ability of human PDAC cell lines, MIA PaCa-2, harbouring a KRAS G12C

mutation, and wild-type KRAS BxPC-3, to internalise TMR-dextran. They found that MIA PaCa-2 cells showed a significantly higher uptake of TMR-dextran than BxPC-3 cells. To further confirm the role of macropinocytosis in this uptake, upon addition of 5-(N-ethyl-N-isopropyl)amiloride (EIPA), a known macropinocytosis inhibitor, there was a dose-dependent reduction in the uptake of TMR-dextran (Commisso et al., 2013). Additionally, using a similar technique, Jeong et al found that both pancreatic and lung cancer cell lines expressing mutant KRAS upregulate macropinocytosis as evidenced by a higher uptake of TMR-dextran compared to their corresponding wild-type cell lines (Jeong et al., 2018).

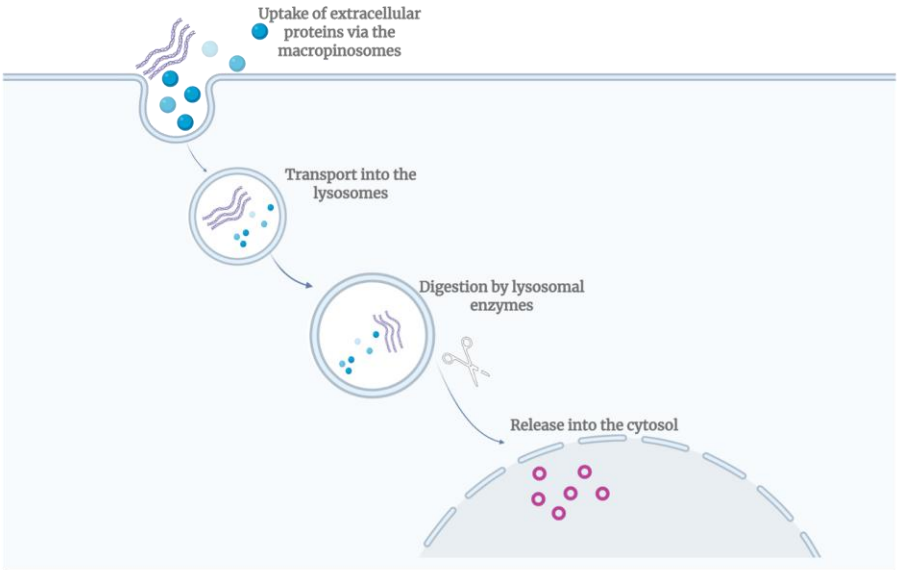

Figure 1.8 - Macropinocytosis
In macropinocytosis, extracellular proteins are internalised into the macropinosomes. Upon fusion with lysosomes, the internalised proteins are digested by lysosomal enzymes, releasing amino acids and sugar into the cytosol. The figure was generated using Biorender.com

Finally, to demonstrate the roles of macropinocytosis in nutrient uptake and breakdown in nutrient-starved PDAC cells, Olivares et al studied the roles of macropinocytosis in the uptake and breakdown of collagen-I and IV in glucose and glutamine-deprived PDAC cells. Using DQ-fluorescein collagen-I and IV (which shows fluorescence following protein breakdown), they found that inhibiting macropinocytosis resulted in reduced uptake and breakdown of collagens I and IV in glucose-deprived PDAC cells, suggesting that macropinocytosis plays a role in the uptake and breakdown of collagens I and IV in a glucose-deprived environment. However, they did not see similar effects under glutamine starvation, suggesting that other pathways might be involved in matrix uptake in this condition (Olivares et al., 2017).

The highlighted studies suggest that understanding the molecular mechanisms behind the macropinocytic uptake of nutrients is vital to developing novel anti-cancer treatments, especially in the context of KRAS-dependent and nutrient-deprived PDAC cells.

1.3.2.2 Autophagy

Autophagy is another nutrient-scavenging mechanism cancer cells employ to meet their energy demands. It is a process where cells break down their cellular components, especially in nutrient-limiting conditions or hypoxia, to obtain nutrients to maintain their metabolic needs (Levine and Kroemer, 2008).

Autophagy is initiated when the cell senses nutrient deprivation or hypoxia. This initial stage of this process is regulated by the Mammalian target of rapamycin complex 1 (mTORC1), AMP-activated protein kinase (AMPK) and the Unc-51-like kinase (ULK) family (ULK1, ULK2, Autophagy related gene 13 (ATG13) and ATG101). Upon mTORC1 activation, ULK1 is phosphorylated, which inactivates its kinase activity, preventing autophagy initiation. On the other hand, AMPK is activated during low-energy or low-glucose conditions and activates the kinase activity of ULK1, initiating autophagy. Upon activation of the ULK family, autophagosome formation is triggered to allow the engulfment of macromolecules or damaged cellular organelles from the cytosol in a process regulated mainly by the Light Chain 3 (LC3) protein. This is followed by fusion of the autophagosome with the lysosome, called an autolysosome, and degradation of the engulfed substances into amino acids by lysosomal enzymes (Parzych and Klionsky, 2013; Sneeggen et al., 2020).

While autophagy is primarily believed to be activated under nutrient starvation, PDAC cells have been shown to have a high basal level of autophagy in nutrient-replete conditions compared to normal pancreatic cells (Yang et al., 2011). In their study, Yang et al assessed the degree of autophagy activation in breast cancer cell lines (MCF7), lung cancer cell lines (H460), normal pancreatic cells and PDAC cells based on the recruitment of GFP-tagged LC3 (GFP-LC3) into the autophagosomes. Interestingly, their data revealed that although the cells were cultured in nutrient-replete conditions, all the PDAC cell lines tested had a higher recruitment of GFP-LC3 than the normal pancreatic cells or breast and lung cancer cells, indicating the importance of autophagy in PDAC. Additionally, they saw that upon chloroquine treatment (which inhibits autophagy by blocking lysosomal degradation of the autophagosome), there was a reduction in PDAC cell growth. At the same time, there was little or no reduction in the proliferation of MCF7 and H460, both of which had a low level of autophagy (Yang et al., 2011). This led them to conclude that autophagy was required for PDAC cell proliferation even in nutrient-replete conditions.

Furthermore, autophagy has been shown to support the maintenance of quiescent cells (Valcourt et al., 2012). In a study examining the effects of serum starvation on nucleus pulposus stem cells (NPSCs), Li et al found that induction of quiescence was associated with increased expression of the autophagy marker LC3II/I, as detected by Western blot. Inhibition of autophagy using chloroquine caused serum-starved cells to revert to a proliferative phenotype, characterised by decreased $p27^{KIP1}$ and increased Ki-67 expression (Li et al., 2019). These findings suggest that autophagy is also important for maintaining the quiescent state, rather than being strictly required for cell survival.

1.3.3 Mammalian Target of Rapamycin Complex 1 (mTORC1)

Mammalian target of rapamycin (mTOR) is a serine/threonine protein kinase that is divided into two complexes - Mammalian target of rapamycin complex 1 (mTORC1) and Mammalian target of rapamycin complex 2 (mTORC2). The main difference between mTORC1 and mTORC2 is their sensors. mTORC1 senses stress, nutrients (amino acids such as arginine and lysine, and glucose), oxygen availability and growth factors, while mTORC2 is found to be nutrient-insensitive (Guertin and Sabatini, 2007). Hence, mTORC1 has been the focus of nutrient-deprivation studies.

Mechanistically, in the presence of amino acids and growth factors, mTORC1 **(Figure 1.9)** is translocated from the cytoplasm to the lysosome, where it is activated by GTP-bound Rheb (Ras homolog enriched in the brain). This is followed by the recruitment of S6 kinase 1 (S6K1) and 4E-BP1 by a regulatory protein associated with mTOR (RAPTOR). Once activated, mTORC1 phosphorylates S6K1, which in turn phosphorylates the ribosomal protein S6. This prompts the synthesis of ribosomal proteins by enhancing the translation of 5' terminal oligopyrimidine tracts mRNA (5' TOP mRNAs) to promote protein synthesis (Ben-Sahra and Manning, 2017; Mehta et al., 2024).

Concurrently, upon activation, mTORC1 phosphorylates 4E-BP1. 4E-BP1 is a member of the e1F4E-binding protein family with both tumour-supporting and tumour-inhibiting roles. To inhibit cell proliferation, 4E-BP1 binds to e1F4E to prevent the formation of the e1F4F complex (e1F4G, e1F4E and e1F4A), thereby blocking cap-dependent mRNA translation and negatively regulating cell proliferation. Upon its phosphorylation by mTORC1, it dissociates from e1F4E and allows e1F4E to bind with other members of the e1F4F complexes to initiate cap-dependent translation that promotes protein synthesis and cell proliferation (Musa et al., 2016; Shin et al., 2022)

Several studies have highlighted the inactivation of mTORC1 under nutrient-deprived conditions (Palm et al., 2015; Lowman et al., 2019). Using Western blot to assess the phosphorylation of S6 as a marker for mTORC1 activity in mouse embryonic fibroblasts (MEFs), Lowman et al found that under glutamine

and arginine deprivation, mTORC1 was inactive (Lowman et al., 2019). Additionally, mTORC1 signalling has been linked to tumour quiescence. Khalil et al reported that upon activation of tumour quiescence in an in vivo model of HNSCC, in addition to the commonly known quiescent markers (high p21 and $p27^{KIP1}$ and low Ki-67), there was a reduction in mTORC1 activation, shown as a reduction in the phosphorylation of S6 in the quiescent-induced cells (Khalil et al., 2021).

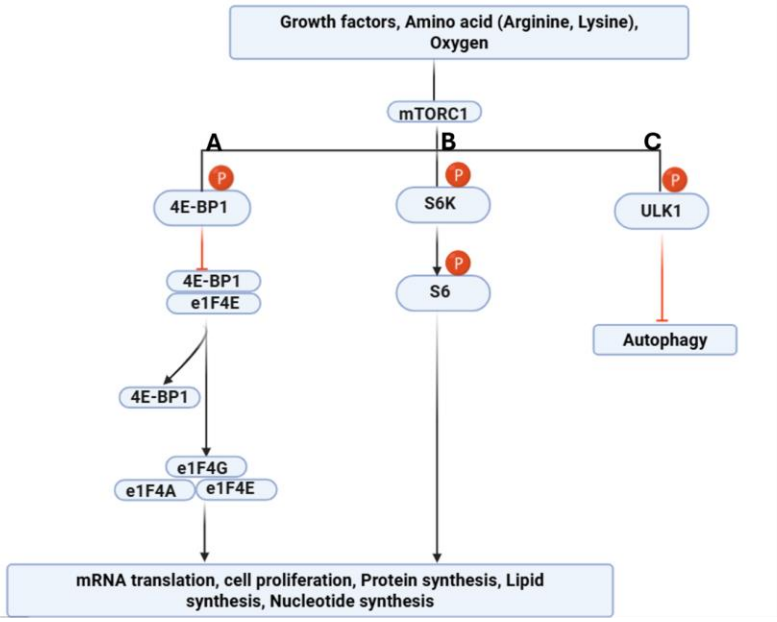

Figure 1.9 - mTORC1 activation results in protein, lipid and nucleotide synthesis
In the presence of growth factors, oxygen, and amino acids such as arginine and lysine, (A) mTORC1 phosphorylates 4E-BP1, resulting in the dissociation of 4E-BP1 from e1F4E. This dissociation allows the formation of the e1F4F complex (e1F4E, e1F4A and e1F4G), allowing cap-dependent mRNA translation. (B) mTORC1 phosphorylates S6K, which in turn results in the phosphorylation of S6 to activate cellular processes such as protein synthesis and nucleotide synthesis. (C) mTORC1 is a negative regulator of autophagy. When mTORC1 is activated, it phosphorylates ULK1. ULK1 is required for the initiation of autophagy; upon phosphorylation, it becomes deactivated, thereby suppressing autophagy. The figure was generated using Biorender.com

1.4 Metabolic remodelling in PDAC

Advances in cancer research have improved our understanding of cancer cells and our knowledge of their specific features that could improve our approach to cancer therapy. One of the main advances is our understanding of the hallmarks of cancer. In 2000, Hanahan and Weinberg identified six main features of cancer, which they described as hallmarks of cancer (Hanahan and Weinberg, 2000). In 2011, an updated version of the hallmarks was published, and they included avoiding immune destruction and altered cellular metabolism as part of the hallmarks of cancer **(Figure 1.10)** (Hanahan and Weinberg, 2011). The latest update was released in a review by Hanahan in 2022, and it has some emerging hallmarks such as senescent cells and non-mutational epigenetic reprogramming (Hanahan, 2022).

In normal and cancer cells, metabolic processes ensure adequate nutrient and energy availability to support growth and survival (Vander Heiden et al., 2009). However, tumour cells often exist in nutrient-deprived environments and must adopt alternative survival strategies. These include nutrient scavenging and metabolic reprogramming to meet their elevated energy and biosynthetic demands under resource-limited conditions (Olivares et al., 2017; Wu et al., 2024).

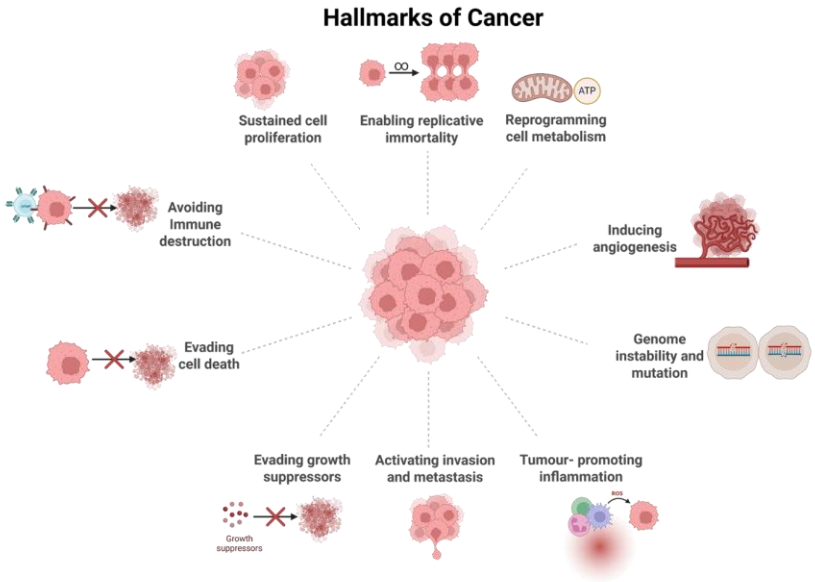

Figure 1.10 - Hallmarks of Cancer
The 6 initial hallmarks of cancer, as reported by Hanahan and Weinberg in 2000, have continued to evolve as our understanding of cancer has evolved. This has resulted in the addition of 4 new characteristics necessary for cancer growth and survival. They are reprogramming cell metabolism, avoiding immune destruction, tumour-promoting inflammation, and inducing angiogenesis. The figure was adapted from Hanahan 2022 and generated using Biorender.com.

For example, using metabolomics and proteomics techniques, Biancur et al found that although CB-839, a potent glutaminase inhibitor, resulted in reduced proliferation of PDAC cells in vitro, it did not affect tumour growth in an autochthonous mouse model of PDAC (LSL-KRAS G12D; p53L/+; Pdx1-Cre). This led them to hypothesise that PDAC cells in vivo may have adaptive properties that allow them to survive the disruption in the glutamine metabolic pathway. Furthermore, they chronically exposed mPDAC cells (derived from primary tumours of an LSL-KRAS G12D; p53L/+, Pdx1-Cre mouse model of PDAC) to CB-839. Metabolomics analysis revealed an upregulation of glycine, serine and threonine metabolism, arginine and proline metabolism, ammonia recycling, urea cycle and β-oxidation of branched-chain fatty acid in PDAC cells with acquired resistance to CB-838, demonstrating the adaptive metabolic plasticity of PDAC in response to glutaminase inhibition (Biancur et al., 2017).

Hence, it is important to understand the metabolic dependencies of PDAC cells and highlight the key metabolic enzymes that are upregulated in PDAC, which could be a targetable option to improve the treatment of pancreatic cancer.

1.4.1 Metabolic Dependencies of PDAC

Anabolic metabolism is a hallmark of most proliferating cells, supporting their growing energy demands (Shi et al, 2025). Hence, cancer cells have a unique requirement for nutrients that can be used for further anabolic processes such as the synthesis of amino acids, lipids and nucleotides, all of which are required for the survival of cancer cells. Glucose, glutamine, arginine, and fatty acids play a role in this anabolic process **(Figure 1.11)** and the overall survival of PDAC cells. PDAC cells remodel their metabolic pathways to increase the availability of these nutrients to aid their survival in their nutrient-deprived state.

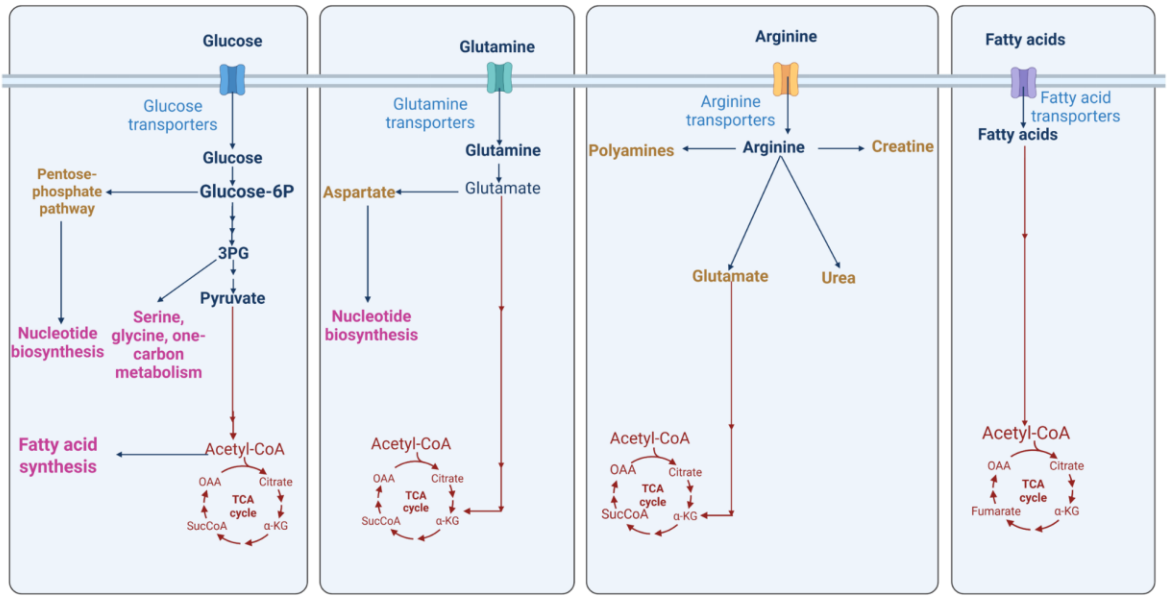

Figure 1.11 - Anabolic roles of Glucose, Glutamine, Arginine and Fatty acids
Glycolysis, the breakdown of glucose, produces intermediates for nucleotide synthesis, fatty acid synthesis and synthesis of other amino acids. Glucose is transported into the cell via glucose transporters, and it is broken down in a series of reactions to produce pyruvate and acetyl-CoA. Acetyl CoA aids in the synthesis of fatty acids and also feeds into the TCA cycle. On the other hand, glucose, via the pentose phosphate pathway, produces intermediates for nucleotide synthesis and, via 3-phosphoglutarate, aids in the synthesis of serine and glycine. Upon transport into the cell via glutamine transporters, glutamine feeds into the TCA cycle via Ɑ-ketoglutarate and synthesises nucleotides via aspartic acid. Arginine is broken down to produce polyamines, creatine, glutamate and urea. It feeds into the TCA cycle via glutamate that's converted to Ɑ-ketoglutarate. Beta oxidation of fatty acids generates acetyl-CoA, which feeds into the TCA cycle. The figure was generated using Biorender.com

Unlike rapidly proliferating cancer cells, quiescent cancer cells have a minimal requirement for anabolic metabolism due to their lack of proliferation; hence, their metabolic requirements are expected to differ. Indeed, they have been found to favour metabolic pathways that generate the

needed energy to maintain their state and generate the least amount of reactive oxygen species (ROS) to reduce their exposure to oxidative stress, such as mitochondrial fatty acid oxidation and oxidative phosphorylation (Du et al., 2023; Wang et al., 2025b).

1.4.1.1 Glucose

Glucose is one of the primary nutrients required for the survival of cells in culture. Glycolysis, the breakdown of glucose to pyruvate and acetyl-CoA, not only provide cells with ATP to support excessive cell proliferation but also provides the intermediates required for lipid, amino acid and nucleotide biosynthesis, all needed for adequate cell growth and survival (DeBerardinis et al., 2008). In addition to glycolysis, other glucose-dependent metabolic pathways are the pentose phosphate pathway (PPP), which yields NADPH and pentose phosphates, the hexosamine pathway, gluconeogenesis and the serine biosynthesis pathway (Hay, 2016). Glucose deprivation reduces the level of NADPH produced in the cells, accumulates reactive oxygen species and leads to oxidative stress-induced cell death (Hay, 2016).

Several studies have highlighted the ability of cancer cells to alter glucose metabolism to meet their energy demands (Yun et al., 2009; Ying et al., 2012; Yan et al., 2019). Mutant KRAS supports glucose metabolism by increasing the expression of the glucose transporter GLUT1, to promote glucose uptake (Yun et al., 2009). In their study, Yun and colleagues found that under low glucose conditions (0.5mM), KRAS and BRAF-mutated colorectal cancer cells survived better than wild-type KRAS and BRAF cells. Their transcriptomics data revealed that KRAS and BRAF-mutated cells upregulate the GLUT1 gene compared to the wild-type cells. Upregulation of GLUT1 was associated with enhanced glucose uptake from the extracellular space and the subsequent survival of these cells (Yun et al., 2009). Additionally, using an in vivo model of KRAS G12D-mutated pancreatic cancer, Ying and colleagues found that doxycycline-induced withdrawal of the KRAS oncogene resulted in a reduction in the by-products of glycolysis (glucose 6-phosphate and fructose 6-phosphate) as well as a reduction in both glucose uptake and lactate production (Ying et al., 2012).

1.4.1.2 Glutamine

Apart from glucose, glutamine, a non-essential/semi-essential amino acid, is another main requirement for cell growth and survival. Glutamine is especially vital to cancer cells as it is the primary nitrogen source for amino acid and nucleotide biosynthesis and is a carbon source for the TCA cycle. Moreover, glutamine also plays a role in de novo synthesis of some amino acids, such as proline,

aspartic acid and alanine (Garcia-Bermudez et al., 2020) as well as in the synthesis of fatty acids via the TCA cycle (Altman et al., 2016).

To break down glutamine for further metabolic processes, glutamine is converted to glutamate by glutaminase enzymes, glutaminase 1 (GLS1) in the kidney and glutaminase 2 (GLS2) in the liver. Given the role of glutamine in proliferating cells as highlighted above, it is unsurprising that GLS enzymes play a role in various cancers. GLS1 has been reported to be upregulated in multiple cancers, including PDAC, breast cancer, non-small cell lung carcinoma (NSCLC) and colorectal cancer (Yu et al., 2021), and it has been a target for cancer therapy (Shi et al., 2025). However, while GLS1 is upregulated in various cancers, expression of GLS2 is suppressed in most cancers (López de la Oliva et al., 2020).

Furthermore, due to its essential role in anabolic metabolism, cancer cells have an increased demand for glutamine, leading them to scavenge the extracellular environment for more sources of glutamine outside of the de novo synthesis. For example, in glutamine-deprived conditions, glutamine can be transported to the cells by amino acid transporters like SLC1A5, SLC38A1, SLC38A2, and SLC6A14, which, unsurprisingly, have been reported to be upregulated in various cancers (Altman et al., 2016; Jin et al., 2023). In addition to transporters, cancer cells can obtain glutamine via uptake and breakdown of extracellular proteins in the lysosome (Li et al., 2024).

1.4.1.3 Arginine

Arginine is another semi-essential amino acid that is vital to tumour cell survival. Arginine plays a crucial role in the de novo synthesis of polyamines, creatine, and feeds in the urea and TCA cycles (Garcia-Bermudez et al., 2020). As a non-essential amino acid, arginine is synthesised from aspartate and citrulline, catalysed by arginosuccinate synthetase (ASS1) and arginosuccinate lyase (ASL), with ASS1 being the rate-limiting enzyme in the de novo synthesis of arginine. Interestingly, various cancers like PDAC, prostate and ovarian cancer have been found to either completely lack or have a low ASS1 expression (Garcia-Bermudez et al., 2020), making these cells dependent on the transport of extracellular arginine into the cell. This suggests that arginine deprivation might represent a viable therapeutic strategy for these cancers. On the other hand, some cells have been seen to upregulate ASS1 protein, allowing de novo arginine synthesis under arginine-deprived conditions. Melanoma cancer cell lines, as reported by Tsai and colleagues, upregulate the expression of ASS1 upon treatment with arginine-deaminase-based chemotherapeutic agent, ADI-PEG20, that depletes arginine from the cells (Tsai et al., 2009) to facilitate their survival.

In addition, Apiz Saab et al found that PDAC cells upregulate ASS1 to survive under nutrient-limited conditions (Apiz Saab et al., 2023). Building on an earlier study that characterised the nutrient

composition of the interstitial fluid (IF) of a mouse model of PDAC (mPDAC) (Sullivan et al., 2019), the authors formulated a medium, Tissue Interstitial Fluid Media (TIFM), to mimic the physiological nutrient environment of PDAC. Metabolomics analysis revealed that arginine was the most depleted amino acid in TIFM, but mPDAC cells cultured in TIFM maintained cell proliferation by upregulating ASS1 expression, allowing them to produce the required arginine for sustained cell proliferation. Functional analysis of the role of ASS1 revealed that genetic knockout of ASS1 impaired proliferation of mPDAC cells in TIFM (Apiz Saab et al., 2023), further solidifying the role of arginine biosynthesis in the survival of PDAC cells.

Furthermore, arginine is transported from the extracellular space via arginine transporters such as SLC7A1, which is upregulated in breast, colorectal, and hepatocellular carcinoma (HCC) (Mossmann et al., 2018). Using miR122, a negative regulator of SLC7A1, Kishikawa et al. found that silencing miR122 in HCC cells upregulated SLC7A1, resulting in significantly higher levels of arginine compared to the control (Kishikawa et al., 2015).

In addition to its role in metabolic pathways, arginine is one of the main amino acids that activate mTORC1 to promote protein translation, cell proliferation and cell survival. To highlight the importance of arginine in mTORC1 activation, Lowman et al demonstrated that mouse embryonic fibroblasts (MEFs) deprived of both arginine and glutamine showed inactivation of mTORC1, as indicated by reduced phosphorylation of S6 compared to control cells. Interestingly, when arginine was reintroduced to glutamine-deprived cells, mTORC1 activity was restored. In contrast, adding glutamine to arginine-deprived cells failed to reactivate mTORC1. These findings emphasise the critical role of arginine in mTORC1 activation (Lowman et al., 2019)

1.4.1.4 Fatty acids

Fatty acid metabolism involves both fatty acid synthesis and fatty acid β-oxidation (fatty acid breakdown), and these two processes have been seen to be altered in cancer. Fatty acid β-oxidation (FAO) involves the breakdown of acetyl-CoA to generate ATP to maintain energy balance. FAO is especially vital for energy production in glucose-starved conditions, where most tissues rely on FAO as an energy source (Houten and Wanders, 2010). Also, FAO has been considered to be a more efficient way to generate ATP than glycolysis, suggesting its importance in meeting the high energy demands of cancer cells (Chen and Huang, 2019). Carnitine palmitoyl transferase 1 (CPT1) is the rate-limiting enzyme in FAO that catalyses the transport of acetyl-CoA from the cytosol into the mitochondria, where β-oxidation occurs. This makes it a viable target to block β-oxidation of fatty acids. Indeed, a CPT1 inhibitor, ST1326, was found to inhibit cell proliferation and induce apoptosis in

leukaemia cell lines (Ricciardi et al., 2015), suggesting the metabolic dependence of these cells on the β-oxidation pathway.

Similarly, Schlaepfer et al demonstrated that targeting lipid catabolism represents a potential therapeutic strategy for prostate cancer (Schlaepfer et al., 2014). In their study, human prostate cancer cell lines (VCaP, LNCaP, and PC3), normal prostate epithelial cells (BPH-1), and patient-derived prostate cancer and benign epithelial cells were treated with etomoxir, a CPT1 inhibitor, either alone or in combination with orlistat, an inhibitor of fatty acid synthesis. Both prostate cancer cell lines and patient-derived cancer cells exhibited greater sensitivity to these treatments compared to non-malignant counterparts, as shown by decreased cell viability and proliferation. Mechanistically, Western blot analysis revealed that etomoxir treatment suppressed mTORC1 signalling, evidenced by reduced phosphorylation of S6K and 4E-BP1. In addition, etomoxir decreased phosphorylation of the Bcl-2–associated death promoter (BAD) protein, a pro-apoptotic member of the Bcl-2 family that induces apoptosis via mitochondrial outer membrane permeabilisation (Howells et al., 2011), further indicating activation of the apoptotic pathway (Schlaepfer et al., 2014). Collectively, these findings highlight lipid catabolism as a critical metabolic vulnerability in prostate cancer cells and support the potential of CPT1 inhibition as a therapeutic approach.

Furthermore, FAO plays a role in the survival of quiescent tumour cells (Hampsch et al., 2020; Ortmayr and Zampieri, 2022; Wang et al., 2025b). Using an estrogen receptor-positive (ER+) breast cancer model of quiescence, Hampsch and collaborators used transcriptome-wide RNA sequencing to reveal that the quiescent cells upregulated FAO and were sensitive to etomoxir-induced inhibition of FAO (Hampsch et al., 2020). Collectively, these findings highlight the therapeutic potential of targeting FAO in cancers.

1.4.2 Latest advances in targeting metabolic dependencies of PDAC

PDAC cells and other KRAS-mutant tumours overcome nutrient limitations by reprogramming their metabolism to exploit alternative nutrient sources, particularly glucose, glutamine, arginine and fatty acids, which fuel their proliferation and survival (Shi et al., 2025). This makes these cancer cells reliant on specific metabolic pathways, creating a window of opportunity for targeted therapy. Targeting these pathways could be selectively toxic to cancer cells. Indeed, researchers are starting to explore ways to inhibit these metabolic pathways, resulting in several small-molecule inhibitors against different metabolic pathways that favour cell growth and survival.

For example, PDAC cells with KRAS mutation depend on glutamine metabolism for sustained cell proliferation, making this a targetable option in cancer therapy (Son et al., 2013). Before its failure in clinical trials due to its excessive toxicity, 6-Diazo-5-oxo-L-norleucine (DON), a glutamine analogue that blocks the conversion of glutamine to glutamate by glutaminase (GLS), among other pathways that utilise glutamine, has been suggested as a small molecule inhibitor of glutamine metabolism (Encarnación-Rosado et al., 2024). Fortunately, DRP-104 and CB-839, other glutaminase inhibitors, are currently in clinical trials (Shi et al., 2025). L-asparaginase (an enzyme that depletes serum of the non-essential amino acid asparagine) is also used as a chemotherapeutic agent for acute lymphoblastic leukaemia (Garcia-Bermudez et al., 2020).

In 2009, Yun et al reported that KRAS mutant cells upregulate GLUT1, a glucose transporter (Yun et al., 2009). Their follow-up study in 2015 revealed that exposure to high levels of vitamin C was selectively toxic to human colorectal cancer cells with the KRAS G12D mutation. They found that upregulation of GLUT1 increased the uptake of dehydroascorbate, an oxidised form of vitamin C, resulting in a ripple of effects that involves accumulation of reactive oxygen species (ROS), depletion of glutathione, oxidative stress and depletion of the glycolytic enzyme glyceraldehyde 3-phosphate dehydrogenase (GAPDH), resulting in the death of glycolysis-dependent KRAS-mutated cells (Yun et al., 2015). An important discovery from their study is that the toxicity of high doses of vitamin C is not seen in cells with wild-type KRAS, highlighting the selectivity of the treatment.

Furthermore, some targets of fatty acid metabolism have shown promising results in clinical trials. For example, acetyl-CoA carboxylase (ACC) inhibitors that catalyse the conversion of acetyl-CoA to malonyl-CoA in fatty acid synthesis have shown promising results in hepatocellular carcinoma. Inhibitors of fatty acid synthase (FASN), which catalyse the synthesis of palmitate in fatty acid synthesis, are also in clinical trials for patients with advanced solid tumours (Shi et al., 2025)

All the studies highlighted above have shown that targeting nutrient dependency in cancer cells shows promising therapeutic benefits in cancer treatment. It should, however, be noted that, as much as targeting metabolic pathways could be a promising way to target cancer cells, these cells may switch to other pathways, resulting in cancer relapse (Shi et al., 2025). Hence, apart from understanding the specific mechanisms involved in the adaptability and survival of cancer cells in a nutrient-deprived environment, a more promising therapeutic procedure would be to focus on combinations of targets of different metabolic pathways or different nutrient scavenging pathways with chemotherapeutic agents to prevent metabolic adaptability and improve treatment efficacy.

1.5 Aim of the Thesis

1.5.1 Scope

Previous studies have shown that PDAC cells are hypovascular, making them more susceptible to nutrient deprivation. Furthermore, PDAC cells are notorious for relapse after initial treatment, which significantly contributes to its bad prognosis and high mortality rate. We hypothesise that this is because:

- PDAC cells can obtain nutrients by scavenging ECM proteins to survive in a nutrient-deprived state.
- PDAC cells have been shown to enter a reversible quiescent state, whereby upon reactivation, they can resume proliferation and disseminate to distant organs, driving the development of metastatic disease characterised by secondary tumour formation, and poorer patient outcomes

1.5.2 Aim

- To investigate the roles of ECM components in supporting the growth of nutrient-deprived PDAC cells.
- To investigate the molecular mechanisms behind the ECM-dependent proliferation of PDAC cells in a nutrient-deprived microenvironment.
- To investigate the conditions that result in the formation of quiescent PDAC cells.
- To investigate the molecular mechanisms behind the formation, reactivation and survival of quiescent PDAC cells.

2 Materials and Methods

2.1 MATERIALS

2.1.1 Cell culture media

Table 2.1 Cell culture media

MEDIA	SUPPLIER
Dulbecco's Modified Eagle Medium (DMEM), high glucose, pyruvate	Gibco
RPMI-1640, L-Glutamine	Gibco
DMEM, no glutamine	Gibco
DMEM, no glucose	Gibco
11130 - MEM Amino Acid Solution 50X	Gibco
RPMI, no glutamine	Gibco
RPMI, no glucose	Gibco
TIFM	A gift from the Muir Lab

2.1.2 Reagents and Suppliers

Table 2.2 Reagents and Suppliers

REAGENT	SUPPLIER
Foetal bovine serum (FBS)	Gibco Gilson
Dialysed Foetal bovine serum (dFBS)	Gibco
Trypsin EDTA solution 1x	Sigma
Propidium Iodide	Invitrogen

Pyronin Y	Sigma-Aldrich
VECTASHIELD Antifade Mounting Medium with DAPI	VECTOR laboratories
Paraformaldehyde	Fluka Chemika
Hoechst33342, trihydrochloride trihydrate	Invitrogen
Cell tracker™ Red CMTPX	Invitrogen
DRAQ5™	Rocher
pH Rodo™Red, succinimidyl ester	Invitrogen
5x siRNA buffer	Horizon Discovery by Perkin Elmer
DharmaFect 1 (DF1) Reagent	Dharmacone
Ambion™ Nuclease-free water	Life Technologies Corp.
High-Capacity cDNA Reverse Transcription Kit	Appliedbiosystems
Microplate PCR 384 well	Alphalaboratories
qPCRBIO SyGreen Blue Mix Lo-ROX	PCRBIOSYSTEMS
RNeasy Mini Kit (50)	QIAGEN
Click-iT™ EdU Alexa Flour™ 555 Imaging Kit	Invitrogen
EdU Cell Proliferation Image Kit (Orange Fluorescence)	Antibodies.com
Collagen type I (Rat tail high concentration)	Ibidi/ Corning
Matrigel	Corning
Laminin/entactin complex	Corning
Senescence β-Galactosidase cell staining kit	Cell signalling
Dimethyl sulfoxide (DMSO)	Fisher Scientific
Glutaraldehyde solution	Sigma Aldrich
Glycine	Sigma
Tris(hydroxymethyl)aminomethane (Tris)	Sigma-Aldrich
Triton X-100	Sigma

Trypan Blue stain 0.4%	Gibco by Life Technologies
Tween-20	Sigma
PVDF membrane	IMMOBILON-FL
QiaShredder	QIAGEN
Bovine Serum Albumin	Sigma Aldrich
Skim milk powder	Sigma Aldrich
Protein ladder	Colour protein standard broad range. Bio-Labs

2.1.3 Solutions

Table 2.3 Solutions and Recipes

SOLUTION	**RECIPE**
PBS (10x)	For 1L - 80g NaCl, 2g KCl, 14.4g Na_2HPO_4 , 2.4g KH_2PO_4, 800ml dH_2O (pH 7.4)
TBS	10mM Tris-HCl pH7.4, 150mM NaCl
TBS-T	TBS, 0.1% Tween-20 (v/v)
Towbin buffer (10x)	1.92M Glycine, 0.25M Tris
Transfer buffer	10% 10x Towbin buffer, 20% methanol
SDS Lysis buffer	1% SDS (v/v), 50mM Tris-HCl pH7.0
Metabolite extraction buffer	5 MeOH: 3 AcN: 2 dH_2O
Running buffer	25mM Tris, 192mM Glycine and 1% SDS in dH_2O
TIFM	For 500ml - 1.560g of TIFM all pools, 3.22g of pool 3, 1g sodium bicarbonate, 450mL of dH_2O, 50mL of dFBS

2.1.4 siRNAs used in the study

Table 2.4 siRNAs used in the study

siRNA	TARGET	SUPPLIER	CATALOG NUMBER
Non-targeting (NT)	ON TARGET plus non-targeting siRNAsiRNA SMART Pool	Dharmacon	D-001810-04
ASS1	siGENOME Human ASS1 (445) siRNA - SMART pool	Dharmacon	M-010257-03-0005
NHE1	ON TARGET plus human NHE1 (3242) siRNA SMART Pool	Dharmacon	L-005277-01-0005

2.1.5 Primary Antibodies used in the study

Table 2.5 Primary Antibodies used in the study

ANTIBODY	HOST	DILUTION	SUPPLIER/CATALOG NUMBER
Phospho-S6 Ribosomal Protein (ser235/236)	Rabbit	Western blot (1:1000)	Cell signalling/2211L
GAPDH	Mouse	Western blot (1:1000)	Santa Cruz Biotechnology/ (SC-47724)
p44/42 MAPK (ERK1/2)	Rabbit	Western blot (1:1000)	Cell signalling/9102S
P-p44/42 MAPK (pERK)	Rabbit	Western blot (1:1000)	Cell signalling/9101S
p4E-BP1	Rabbit	Western blot (1:1000)	Cell signalling/9459S

NHE-1	Mouse	Western blot (1:1000)	Santa Cruz Biotechnology/ (SC-136239)

2.1.6 Secondary Antibodies used in the study

Table 2.6 Secondary Antibodies used in the study

ANTIBODY	HOST	DILUTION	SUPPLIER
IRDye® 800CW Anti-Mouse IgG	Goat	Western blot (1:30K)	LI-COR
IRDye® 680CW Anti-Rabbit IgG	Donkey	Western blot (1:20K)	LI-COR

2.1.7 Primers used in the study

Table 2.7 Primers used in the study

PRIMER	ASSAY NAME	STOCK CONCENTRATION
ASS1	Hs_ASS1_1_SG	10X
GAPDH	Hs_GAPDH_1_HS	10X

2.2 METHODS

2.2.1 Cell culture

Human PDAC cell lines SW-1990, PANC-1, MIA PaCa-2 and BxPC-3 cells were used for this study (**Table 2.8**). SW-1990, PANC-1 and MIA PaCa-2 cells were cultured in high-glucose Dulbecco's Modified Eagle's Medium (DMEM) while BxPC-3 cells were cultured in RPMI media. All culture media were supplemented with 10%(v/v) Foetal Bovine Serum (FBS). Cell lines were maintained at 37°C, 5% CO_2 and passaged every 3-4 days. All cell lines used were routinely tested for mycoplasma. To split the

cells, the media was removed, and the cells were washed twice with PBS. 0.25% (w/v) trypsin-EDTA was added to the cells and incubated at 37°C and 5% CO_2 for approximately 5 minutes to detach the cells from the surface completely. The cells were resuspended in the appropriate media and transferred into a new 10cm dish.

Table 2.8 Pancreatic ductal adenocarcinoma (PDAC) cell lines used in this study, including tissue of origin and KRAS mutation status.

CELL LINES	ORIGIN	KRAS MUTATION
SW-1990	Spleen metastasis	G12D
PANC-1	Primary tumour	G12D
MIA PaCa-2	Primary tumour	G12C
BxPC-3	Primary tumour	Wild type

To preserve the cells for long-term use, they were frozen and placed in liquid nitrogen to cryo-preserve them. To do this, cells in a 10cm dish at about 85-90% confluency were washed, trypsinised, and resuspended in the required media. After resuspension, the cells were centrifuged at 1000rpm for 3 minutes. The freezing solution was prepared as follows:

Solution A - 50% FBS and 50% media

Solution B - 80% FBS and 20% DMSO

After 3 minutes, the supernatant was removed and 500µL of solution A was added to the pellet and placed in a cryovial, followed by a drop-wise addition of 500µL of solution B. The vial was placed in a Biocision™ CoolCell™ LX freezing container, stored at -80°C for a few days before transferring to liquid nitrogen for long-term storage.

2.2.2 ECM Preparation

96-well plates - Collagen-I, Laminin/Enactin and Matrigel were diluted to a final concentration of 2mg/ml, 3.5mg/ml and 3mg/ml, respectively, in ice-cold PBS. The plates were coated with 15µl of the ECM solution and incubated at 37°C for at least 3 hours to polymerise.

35mm dishes - Matrigel was diluted to a final concentration of 1mg/ml in ice-cold PBS. The dishes were coated with 100µl of the Matrigel solution and incubated at 37°C for at least 1 hour to polymerise.

6-well plates - Matrigel was diluted to a final concentration of 3mg/ml in ice-cold PBS. The dishes were coated with 300µl of the Matrigel solution and incubated at 37°C for at least 3 hours to polymerise.

2.2.3 ECM Internalisation Assay

Matrigel-coated 35mm dishes were labelled with 20µg/ml pHrodo diluted in PBS and 0.1M sodium bicarbonate and placed on the rocker for 1 hour. The labelled dishes were washed with PBS and incubated at 37°C and 5% CO_2 overnight. Following this, $5x10^5$ cells/well were seeded and placed in the incubator overnight.

- For ECM internalisation in the presence of pharmacological inhibitors, the required concentration of the inhibitors **(Table 2.9)** and vehicle control were added to the cells before placing them in the incubator overnight.

Table 2.9 Inhibitors used in the study

INHIBITORS	**CONCENTRATION**	**SUPPLIER**	**CATALOGUE NUMBER**
CB-839	200nM and 500nM	MedChemExpress	HY-12248
EIPA	25µM	Sigma	A3085-25MG
Filipin	5µg/ml	Sigma	480-49-9
Dynasore	40µM	Sigma	1202867-00-2
TORIN-1	15nM	APExBIO	A8312
MRTX1133	200nM	MedChemExpress	HY-134813
MRTX849	100nM	MedChemExpress	HY-130149
PALBOCICLIB	1µM	MedChemExpress	HY-50767

- For ECM internalisation under nutrient deprivation, the cells were seeded in full media and placed in the incubator for 3 hours for the cells to attach to the surface. Afterwards, the media was changed to the required starvation media **(Table 2.1)** and incubated overnight.

Afterwards, the cells were stained with Hoechst33342 and imaged live using a NIKON A1 confocal microscope with a 60x oil immersion objective. ECM uptake was quantified using ImageJ software (https://imagej.net/ij/), as described in Nazemi et al., 2024 (**Figure 2.1**).

2.2.4 Cell Proliferation Assay

96-well plates were coated with collagen-I, Laminin/Enactin, or Matrigel as in **2.2.2.** 2000 cells/well were seeded in full media on the ECM-coated 96-well plates and placed in the incubator at 37°C and 5% CO_2 overnight. For nutrient deprivation studies, the media were changed to starvation media **(Table 2.1)** or full media, all supplemented with dFBS, in the presence of inhibitors **(Table 2.9)** or vehicle control, where indicated. The cells were left in the incubator at 37°C and 5% CO_2 for 7 days (PANC-1, SW-1990, BxPC-3 cells) or 6 days (MIA PaCa-2 cells). For quiescence studies, the media were changed to full media in the presence of inhibitors **(Table 2.9)** or vehicle control, where indicated. The cells were incubated at 37°C and 5% CO_2 for 4 days. The cells were washed twice with PBS and fixed with 4% PFA for 15 minutes.

Cells were stained and imaged using different approaches. (1) The nuclei were stained with 5µM DRAQ5 in PBS and incubated in the dark for 1 hour at RT. The cells were washed twice with PBS and incubated in PBS for another 30 minutes to remove background staining. The cells were imaged with a Licor Odyssey Sa system (offset 3mm, 169µm resolution, intensity 5, 700nm for DRAQ5), and the signal intensity was measured using Image Studio Lite software. (2) The nuclei were stained with 10µg/ml of Hoechst33342 for at least 15 minutes at RT. The cells were imaged with an InCell Analyzer 2200, 10x objective and the cell number was measured with Cell Profiler using a pipeline to detect the nuclei by covering the range of nuclei sizes **(Figure 2.2)**. (3) The cells were imaged with an ImageXpress microscope, 2x objective and DAPI filter. The cell number was measured using MetaXpress and the Costume Module Editor software (CME) using an algorithm that could detect the nuclei by covering the nuclei size and intensity range. Where indicated, the data were normalised by dividing the values at day 7 by the mean of the corresponding condition at day 2 on plastic. Values ≥1 indicate increased cell numbers compared to day 2, while values ≤1 indicate cell death.

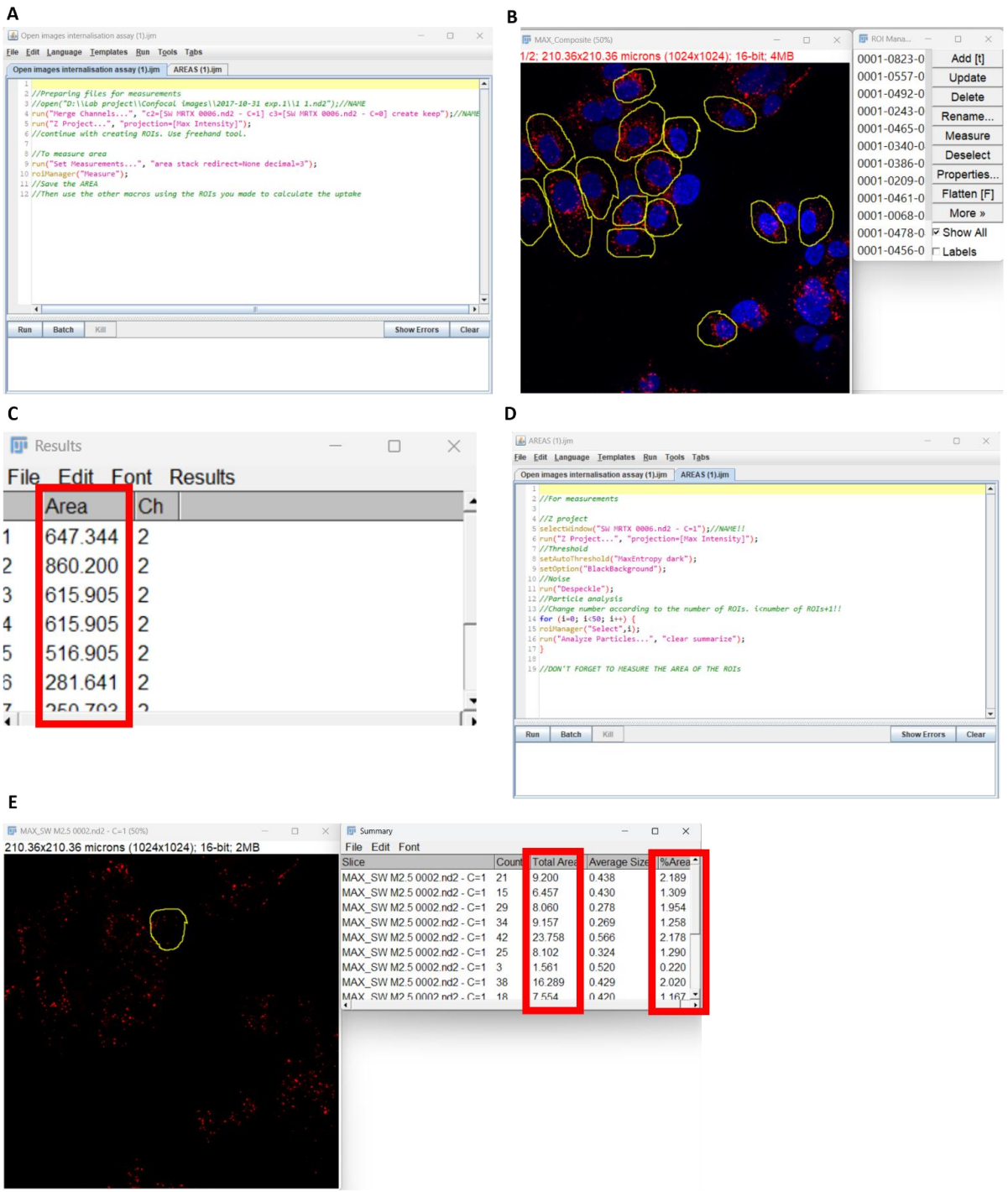

Figure 2.1. Quantification of ECM Internalisation using ImageJ

An ImageJ macro was used to quantify ECM internalisation. (A) The 'open images' macro is run to overlay the channels and create a max projection. (B, C) Individual cell areas were defined by manually outlining regions surrounding each nucleus, and the cell area was subsequently measured. (D, E) The 'area' macro is run to threshold the image, despeckle it and analyse the particles in each cell. ECM internalisation = Area/Total Area *100

2.2.4.1 Media composition for Cell Proliferation Studies

Table 2.10 Composition of different DMEM media used in the study

Components	DMEM, high glucose, pyruvate (mg/L)	DMEM, high glucose, no glutamine (mg/L)	DMEM, no glucose (mg/L)	DMEM, no amino acids
AMINO ACIDS				
Glycine	30	30	30	-
L-Arginine hydrochloride	84	84	84	-
L-Cystine 2HCl	63	63	63	-
L-Glutamine	580	-	580	-
L-Histidine hydrochloride-H_2O	42	42	42	-
L-Isoleucine	105	105	105	-
L-Leucine	105	105	105	-
L-Lysine hydrochloride	146	146	146	-
L-Methionine	30	30	30	-
L-Phenylalanine	66	66	66	-
L-Serine	42	42	42	-
L-Threonine	95	95	95	-
L-Tryptophan	16	16	16	-
L-Tyrosine	72	72	72	-
L-Valine	94	94	94	-
VITAMINS				
Choline chloride	4	4	4	4
D-Calcium pantothenate	4	4	4	4
Folic Acid	4	4	4	4
Niacinamide	4	4	4	4
Pyridoxine hydrochloride	4	4	4	4

Riboflavin	0.4	0.4	0.4	0.4
Thiamine hydrochloride	4	4	4	4
i-Inositol	7.2	7.2	7.2	7.2
INORGANIC SALTS				
Calcium Chloride ($CaCl_2 \cdot 2H_2O$)	264	200	200	265
Ferric Nitrate ($Fe(NO_3)_3 \cdot 9H_2O$)	0.1	0.1	0.1	0.1
Magnesium Sulfate ($MgSO_4 \cdot 7H_2O$)	200	97	97	97.67
Potassium Chloride (KCl)	400	400	400	400
Sodium Bicarbonate ($NaHCO_3$)	3700	3700	3700	-
Sodium Chloride (NaCl)	6400	6400	6400	6400
Sodium Phosphate monobasic ($NaH_2PO_4 \cdot 2H_2O$)	141	125	125	109
OTHER COMPONENTS				
D-Glucose (Dextrose)	4500	4500	-	1000
Phenol Red	15	15	15	15.9
Sodium Pyruvate	110	-	-	-

Table 2.11 Composition of different RPMI used in the study

Components	RPMI, high glutamine (mg/L)	RPMI, no glutamine (mg/L)	RPMI, no glucose (mg/L)
AMINO ACIDS			
Glycine	10.0	10.0	10.0
L-Arginine	200.0	200.0	200.0
L-Asparagine	50.0	50.0	50.0
L-Aspartic Acid	20.0	20.0	20.0
L-Cystine 2HCl	65.0	65.0	65.0
L-Glutamic Acid	20.0	20.0	20.0
L-Glutamine	300.0	-	300.0
L-Histidine	15.0	15.0	15.0
L-Hydroxyproline	20.0	20.0	20.0
L-Isoleucine	50.0	50.0	50.0
L-Leucine	50.0	50.0	50.0
L-Lysine hydrochloride	40.0	40.0	40.0
L-Methionine	15.0	15.0	15.0
L-Phenylalanine	15.0	15.0	15.0
L-Proline	20.0	20.0	20.0
L-Serine	30.0	30.0	30.0
L-Threonine	20.0	20.0	20.0
L-Tryptophan	5.0	5.0	5.0
L-Tyrosine disodium salt dihydrate	29.0	29.0	29.0
L-Valine	20.0	20.0	20.0
VITAMINS			
Biotin	0.2	0.2	0.2
Choline chloride	3.0	3.0	3.0
D-Calcium pantothenate	0.25	0.25	0.25
Folic Acid	1.0	1.0	1.0
i-Inositol	35.0	35.0	35.0
Niacinamide	1.0	1.0	1.0

Para-Aminobenzoic Acid	1.0	1.0	1.0
Pyridoxine hydrochloride	1.0	1.0	1.0
Riboflavin	0.2	0.2	0.2
Thiamine hydrochloride	1.0	1.0	1.0
Vitamin B12	0.005	0.005	0.005
INORGANIC SALTS			
Calcium Nitrate ($Ca(NO_3)_2 \cdot 4H_2O$)	100.0	100.0	100.0
Magnesium Sulfate ($MgSO_4$, anhydrous)	48.84	-	48.84
Magnesium Sulfate ($MgSO_4$-$7H_2O$)	-	100.0	-
Potassium Chloride (KCl)	400.0	400.0	400.0
Sodium Bicarbonate ($NaHCO_3$)	2000.0	2000.0	2000.0
Sodium Chloride (NaCl)	6000.0	6000.0	6000.0
Sodium Phosphate dibasic (Na_2HPO_4, anhydrous)	800.0	-	-
Sodium Phosphate dibasic (Na_2HPO_4-$7H_2O$)	-	1512.0	1512.0
OTHER COMPONENTS			
D-Glucose (Dextrose)	2000.0	2000.0	-
Glutathione (reduced)	1.0	1.0	1.0
Phenol Red	5.0	5.0	5.0

Table 2.12 Composition of Tumour Interstitial Fluid Media (TIFM) used in the study

Source: eLife Supplementary Table 1 (elife-81289)

Components	**mg/L**
Pool 1 — Vitamins	
Biotin	0.013694
(-)-Riboflavin	0.021334
Pyridoxine hydrochloride	0.029149
Choline chloride	28.466792
5-methyl-5,6,7,8-tetrahydrofolic acid calcium salt	1.129325
Myo-inositol	75.417643
Niacinamide	4.819355
4-Aminobenzoic acid	0.479973
D-Pantothenic acid hemicalcium	0.800786
Vitamin B-12	1.35537
Thiamine hydrochloride	2.691219
Pool 2 — Proteinogenic Amino Acids	
L-Phenylalanine	12.5519
L-Proline	13.069449
L-Histidine	13.859573
L-Isoleucine	16.389028
L-Valine	16.610359
L-Tryptophan	5.77736
L-Tyrosine	10.006224
L-Asparagine monohydrate	16.266199
L-Alanine	91.169368
L-Serine	20.068894
L-Lysine monohydrochloride	23.588827
L-Threonine	28.044572
L-Leucine	36.052678
Glycine	129.568647
L-Cystine	15.98052
L-Citrulline	11.727166

L-Ornithine monohydrochloride	49.678216
L-Methionine	10.443672
L-Aspartic acid	47.428445
L-Arginine monohydrochloride	0.478836
Pool 3 — Salts †	
Calcium nitrate tetrahydrate	0.1
Magnesium sulfate (anhydrous)	0.04884
Potassium chloride	0.4
Sodium chloride	5.12
Sodium phosphate dibasic (anhydrous)	0.8
Sodium bicarbonate	1000
Pool 4 — Glucose, Lactate, Pyruvate	
L(+)-Lactic acid	309.535171
D(+)-Glucose	702.097706
3-Hydroxybutyrate (R/D enantiomer acid)	7.637217
Pyruvic acid sodium	5.811062
Pool 5 — Glutamine, Glutamate	
L-Glutamine	109.240905
L-Glutamic acid	138.433466
Pool 6 — PCr, Cr, Taurine	
Creatine anhydrous	151.122869
Taurine	265.398027
Phosphocreatine disodium hydrate	90.619937
Pool 7 — TCA Cycle Intermediates	
α-Ketoglutaric acid	1.119033
cis-Aconitic acid	0.467212
Fumaric acid	0.257113
Succinic acid	11.257729
Di-sodium hydrogen citrate sesquihydrate	90.46767
L-(-)-Malic acid	18.551766
Pool 8 — Lowest Abundance	
5'-Deoxy-5'-methylthioadenosine	0.016239
N-Formyl-L-methionine	0.024216

2-Picolinic acid	0.02607
Cytidine 5'-triphosphate disodium salt	0.032253
Thymidine 5'-monophosphate disodium salt hydrate	0.036651
DL-Indole-3-lactic acid	0.080643
N6-Acetyl-L-lysine	0.107004
N-Acetyl-L-glutamine	0.110624
N-Acetyl-L-glycine	0.113834
Carbamoylaspartate	0.120107
Orotic acid potassium salt	0.139538
S-Adenosyl-L-homocysteine	0.141865
N-Acetyl-L-alanine	0.164712
Kynurenine	0.193968
Homocitrulline	0.199303
2'-Deoxycytidine	0.199829
Argininosuccinate	0.218973
D-Sorbitol	0.225158
N-Acetyl-L-glutamic acid	0.238413
Cytidine 5'-diphosphocholine sodium	0.251743
Sarcosine	0.281459
L-Carnosine	0.300924
2-Ketobutyric acid	0.359485
L-Methionine sulfoxide	0.498706
Thymidine	0.546108
Pipecolinic acid	0.673762
N-Acetyl-L-aspartic acid	0.674355
Pool 9 — Mid-Abundance	
Guanidinoacetate	0.704689
L-2-Aminobutyric acid	0.713881
D-Fructose-1,6-bisphosphate trisodium salt hydrate	0.747882
3-Methyl-2-oxopentanoic acid sodium salt	1.030957
β-Alanine	1.13845

D-Glyceric acid sodium salt	1.141444
Creatinine	1.296529
2-Hydroxybutyric acid sodium salt	1.360493
L-α-Hydroxyglutaric acid disodium salt	1.425524
Inosine 5'-monophosphate disodium salt hydrate	1.451272
Sodium 3-methyl-2-oxobutyrate	1.712561
Itaconic acid	2.0193
DL-3-Hydroxyisobutyric acid sodium salt	2.149278
L-2-Aminoadipic acid	2.208158
Cytidine	2.340854
Guanosine 5'-monophosphate disodium salt hydrate	2.582416
Cytidine 5'-monophosphate disodium salt	3.012786
Hypotaurine	3.352282
Xanthine	3.380965
Phospho(enol)pyruvic acid monopotassium salt	3.415537
UDP-Glucose	4.654322
O-Acetyl-L-carnitine hydrochloride	5.535477
Pool 10 — Highest Abundance	
D-(-)-3-Phosphoglyceric acid disodium salt	6.04034
L-Carnitine hydrochloride	7.062211
Inosine	8.907947
Uracil	9.146651
Uridine 5'-monophosphate disodium salt	10.35388
Adenosine 5'-monophosphate disodium salt	10.615894
Uridine	13.50733
Hypoxanthine	13.766215
Betaine hydrochloride	13.935533
L-Glutathione oxidized disodium salt	15.851827
Uridine 5'-diphospho-N-acetylglucosamine sodium salt	16.06222
Allantoin	16.834751

α-D-Glucose 1-phosphate disodium salt	23.757527
D-Glucose-6-phosphate sodium salt	26.77607
D-Ribose 5-phosphate disodium salt	29.688318
L-α-Glycerophosphorylcholine	33.117285
O-Phosphoethanolamine	66.263168
Phosphocholine chloride calcium salt tetrahydrate	66.8885
L-Glutathione reduced	90.122616

2.2.5 ECM Crosslinking

2.2.5.1 ECM crosslinking for ECM Uptake analysis

35mm dishes were coated with 1mg/ml Matrigel as in **2.2.2.** Matrigel was crosslinked with 1% or 2.5% sterile glutaraldehyde in PBS for 30 minutes at RT and washed twice with PBS. The crosslinking agent was quenched with 1M sterile glycine in water for 20 minutes at RT and washed with PBS until all the quenching agent was washed off. Afterwards, Matrigel was labelled with 20µg/ml pHrodo diluted in PBS and 0.1M sodium bicarbonate and placed on the rocker for 1 hour. The labelled dishes were washed with PBS and incubated at 37°C and 5% CO_2 overnight. Then, $5x10^5$ cells/dish were seeded, incubated and imaged as in 2.2.3.

2.2.5.2 ECM crosslinking for Cell proliferation studies

96-well plates were coated with 3mg/ml Matrigel as in **2.2.2.** Matrigel was crosslinked with 2.5% sterile glutaraldehyde in PBS for 30 minutes at RT and washed twice with PBS. The crosslinking agent was quenched with 1M sterile glycine in water for 20 minutes at RT and washed with PBS until all the quenching agent was washed off. PBS was added to the crosslinked Matrigel and placed in the incubator at 37 °C and 5% CO_2 overnight. 2000 cells/well were seeded in full media and placed in the incubator at 37°C and 5% CO_2 overnight. The media was changed to starvation media **(Table 2.1)** or full media, all supplemented with dFBS. The cells were incubated at 37 °C and 5% CO_2 for 7 days. The cells were washed twice with PBS and fixed with 4% PFA for 15 minutes at RT. The nuclei were stained with10µg/ml of Hoechst33342 for at least 15 minutes at RT. The cells were imaged with an InCell Analyzer 2200, 10x objective. The cell number was measured with Cell Profiler using an algorithm that detects the nuclei, covering the range of nuclei size and intensity **(Figure 2.2)**.

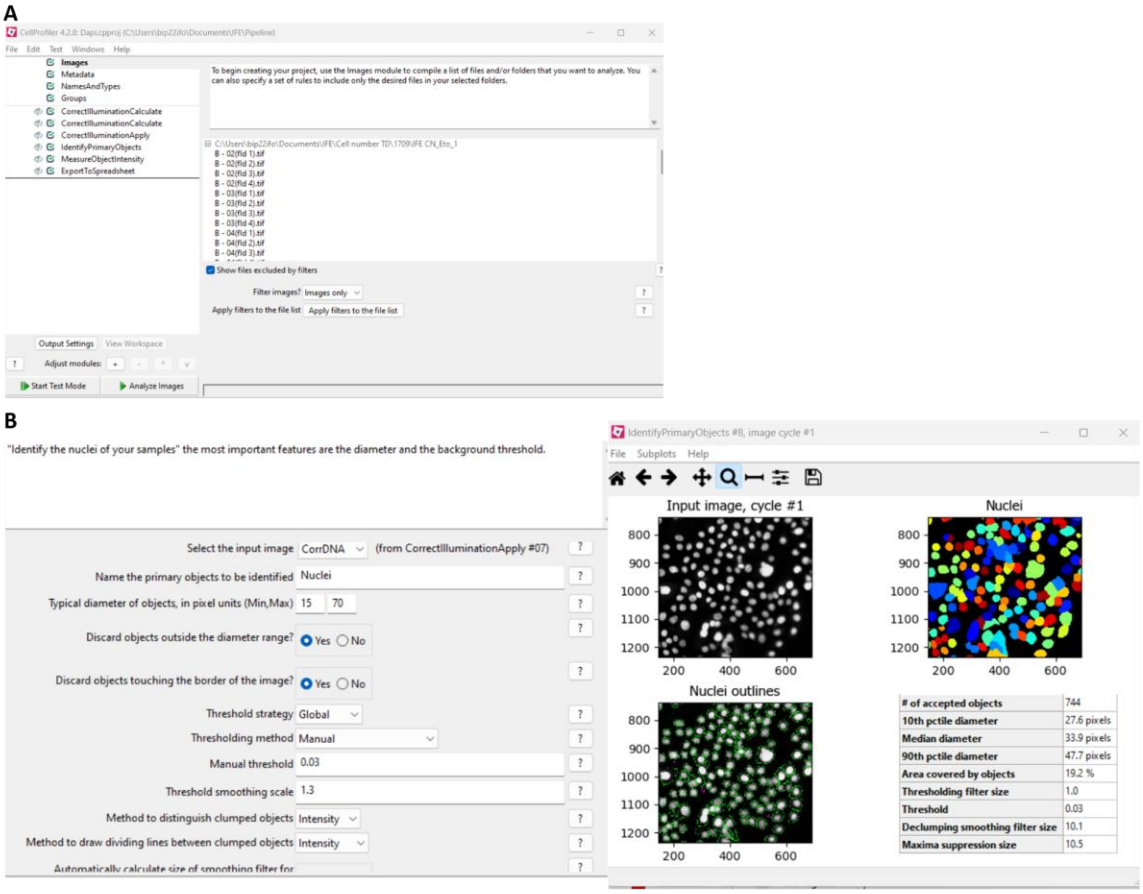

Figure 2.2. Quantification of cell number using CellProfiler.
(A) Images from each condition were analysed in CellProfiler using a custom pipeline that quantifies cell number based on the DAPI channel. (B) The 'Identify Primary Object module' was used to detect individual nuclei. The 'typical diameter of object' parameter was optimised to define nuclear size based on the nuclei sizes of the image (objects outside of the range are discarded), and the Global manual threshold was applied to enable accurate nuclei segmentation. The cell count was automatically quantified from each image and exported for statistical analysis.

2.2.6 EdU Incorporation Assay

96-well plates were coated with 3mg/ml Matrigel as in **2.2.2.** 2000 cells/well were seeded in full media on the ECM-coated 96-well plates and placed in the incubator at 37°C and 5% CO_2 overnight. For nutrient deprivation studies, the media were changed to starvation media **(Table 2.1)** or full media, all supplemented with dFBS. The cells were incubated at 37°C and 5% CO_2 for 7 days. For quiescence studies, the media were changed to full media containing DMSO and the indicated inhibitors **(Table 2.9)**. The cells were incubated at 37°C and 5% CO_2 for 4 days. The cells were incubated with 10µM EdU for 24 hours. Next, the cells were fixed with 4% PFA for 15 minutes at RT, and the nuclei were stained with 10µg/ml of Hoechst33342 for at least 15 minutes at RT. Afterwards, the cells were permeabilised with 0.25% Triton X for 20 minutes and stained with Antibodies EdU mix (10x reaction buffer, $CuSO_4$, Alexa Fluor 555 azide, 10x reducing agent) for 30 minutes in the dark at RT with gentle rocking. The cells were imaged with an InCell Analyzer 2200, 10x objective, using DAPI wavelength for nuclei and

Cy3 wavelength for EdU. The %of EdU-positive cells were measured with Cell Profiler using an algorithm to detect the total number of nuclei and nuclei positive for EdU **(Figure 2.3)**.

2.2.7 Propidium Iodide Incorporation Assay

96-well plates were coated with collagen-I or Matrigel as in **2.2.2.** 2000 cells/well were seeded in full media on the ECM-coated 96-well plates and placed in the incubator at 37°C and 5% CO_2 overnight. For nutrient deprivation studies, the media were changed to starvation media **(Table 2.1)** or full media, all supplemented with dFBS. The cells were left in the incubator at 37°C and 5% CO_2 for 7 days (SW-1990 cells) and 6 days (MIA PaCa-2 cells). For quiescence studies, the media were changed to full media containing DMSO or the indicated inhibitors (**Table 2.9)**. The cells were incubated at 37°C and 5% CO_2 for 4 days. The cells were co-stained with 5µg/ml Hoechst33342 and 1µg/ml PI (diluted in PBS) and incubated at 37°C and 5% CO_2 for 30 minutes. Afterwards, the cells were washed with PBS, and media without phenol red was added. The cells were imaged live with an ImageXpress microscope, 10x objective, using DAPI wavelength for nuclei and Cy3 wavelength for PI. The %PI was measured using MetaXpress and the Costume Module Editor software (CME) using an algorithm that could detect the total nuclei and nuclei positive for PI.

2.2.8 Tumour Quiescent Reactivation

2000 cells/well were seeded in full media in 96-well plates and placed in the incubator at 37°C and 5% CO_2 overnight. The media was changed to full media containing DMSO or 200nM MRTX1133. The cells were incubated at 37°C and 5% CO_2 for 4 days. Afterwards, the cells treated with MRTX1133 were washed, and the media were replaced with normal media and placed in the incubator at 37°C and 5% CO_2 for 8 days. The cells were washed twice with PBS and fixed with 4% PFA for 15 minutes at RT. The nuclei were stained with 10µg/ml Hoechst33342 for at least 15 minutes at RT. The cells were imaged with an InCell Analyzer 2200, 10x objective. The cell number was measured with Cell Profiler using an algorithm to detect the nuclei by covering the range of nuclei size and intensity **(Figure 2.1)**.

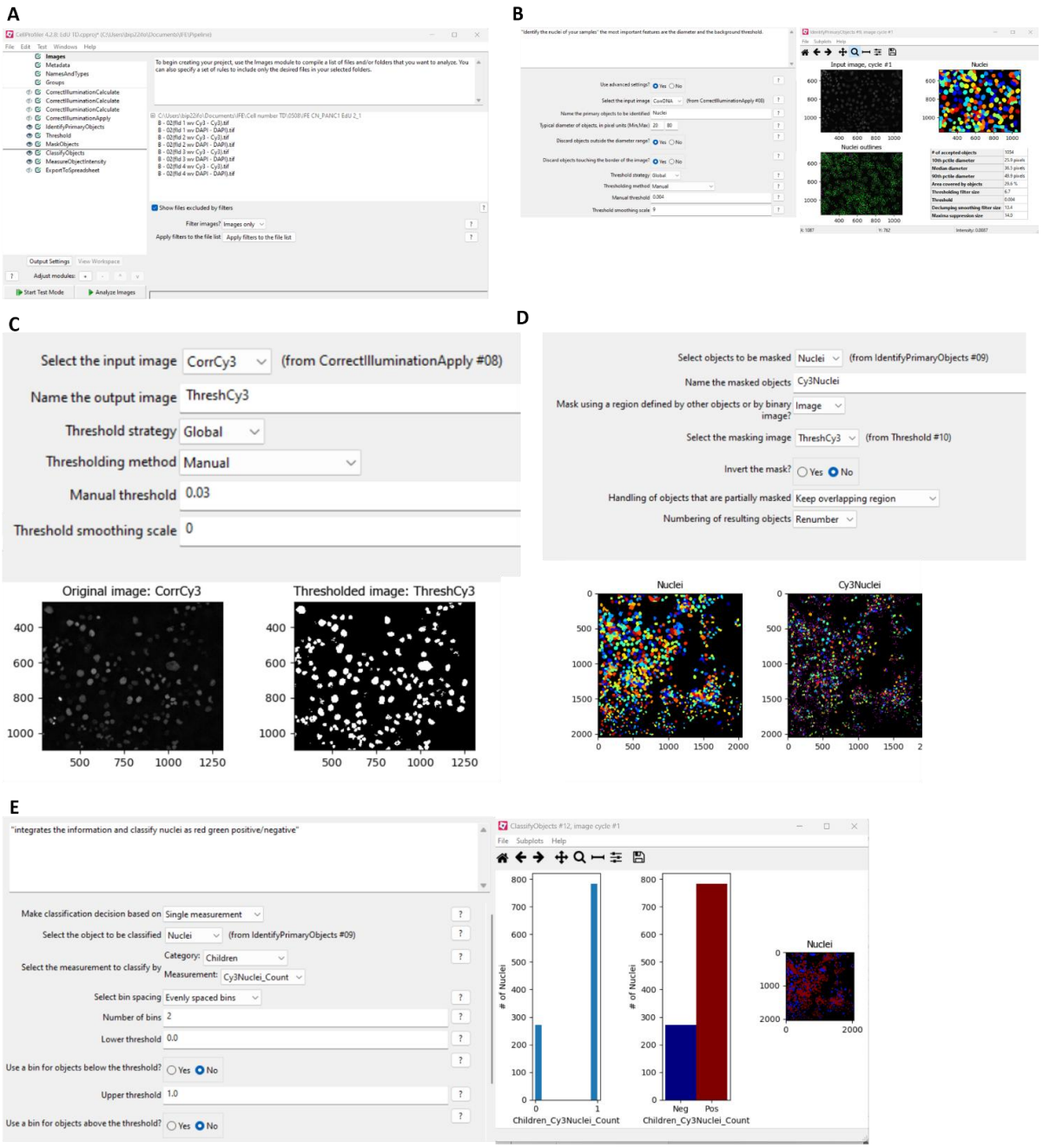

Figure 2.3. Quantification of EdU-positive cells using CellProfiler.
(A) Images from each condition were analysed in CellProfiler using a custom pipeline that quantifies cell number based on the DAPI (nuclei) and Cy3 (EdU) channels. (B) The 'Identify Primary Object module' was used to detect individual nuclei. The 'typical diameter of object' parameter was optimised to define nuclear size based on the nuclei sizes of the image (objects outside of the range are discarded), and the Global manual threshold was applied to enable accurate nuclei segmentation. (C) A Global manual threshold was applied in the Cy3 channel to identify EdU-positive cells. (D) The MaskObject module was used to mask the images by keeping only the overlapping region between DAPI-identified nuclei and Cy3 signal. (E) The ClassifyObjects module (based on single measurements) was used to assign each nucleus as either EdU-positive or EdU-negative. The percentage of EdU-positive cells was calculated as: %EdU-positive cells = Number of EdU+ cells/Total nuclei * 100

2.2.9 Western Blotting

2.2.9.1 Sample preparation

For nutrient deprivation studies, 6-well plates were coated with 3mg/ml of Matrigel as in 2.2.2. 10^5 cells/well were seeded on Matrigel-coated plates or on plastic and grown overnight at 37°C and 5% CO_2. Media were changed to starvation media and left in the incubator for 7 days. For the tumour quiescence studies, 10^5 cells/well were seeded in 6-well plates and incubated overnight at 37°C and 5% CO_2. 200nM MRTX1133 or DMSO were added to the media and left in the incubator for 4 days. The media was aspirated, and cells were washed twice with ice-cold PBS. Afterwards, cells were lysed with 100µl of lysis buffer **(Table 2.3)** and the lysates were transferred into QiaShredder columns and spun down at full speed for 5 minutes. The flow-through was transferred into a new Eppendorf tube, and the protein concentration was measured with a nanodrop. The samples were stored at -20°C.

2.2.9.2 Western Blotting

A loading buffer made up of 1mM DTT in NuPage buffer was prepared and added to the samples, and the samples were placed in a heating block at 70°C for 5 minutes. The required volume (based on the calculated protein concentration) of the samples and 1µL of molecular weight ladder (BioLabs) were loaded on 4-15% Mini-PROTEAN precast polyacrylamide 10-well or 12-well gels and allowed to run at 100V for ~2 hr 30 min in 1x running buffer. Afterwards, the gels were transferred onto FL-PVDF membranes at 100V for 80 minutes in the transfer buffer. Membranes were blocked in 5% (w/v) BSA or milk in TBS-T for 1 hour at RT, incubated with the protein of interest and GAPDH (housekeeping protein for normalisation) primary antibodies and placed in the cold room overnight. The primary antibodies were removed, and the membranes were washed 3 times in TBS-T for 10 min and placed on the rocker at RT during each wash. The required LICOR secondary antibodies were added and incubated for 1 hour at RT in the dark. Following this, the membrane was washed 3 times in TBS-T for 10 min, placed on the rocker at RT during each wash, and rinsed with water before imaging.

2.2.10 RT-qPCR

2.2.10.1 Sample preparation

6-well plates were coated with 3mg/ml of Matrigel as in **2.2.2**. 10^5 cells/well of SW-1990 cells were seeded on Matrigel-coated plates or on plastic and grown overnight at 37°C. The media were changed to the required starvation media and left in the incubator for 7 days.

2.2.10.2 mRNA Extraction

mRNA was extracted using the RNeasy® Mini kit (Qiagen) following the manufacturer's protocol. The media was removed and the cells were washed twice with ice-cold PDS. Afterwards, 350µl Buffer RLT was added directly to the wells, cells were scraped, the lysate was collected in a QIAshredder spin column placed in a 2ml collection tube and centrifuged for 2 min at full speed. 350µl of 70% ethanol in RNAse-free water was added to the flow-through, transferred into a RNeasy spin column, placed in a 2ml collection tube, and centrifuged for 30seconds at 10,000 rpm. The flow-through was discarded, and 700µl Buffer RW1 was added to the RNeasy spin column and centrifuged for 30seconds at 10,000 rpm. The flow-through was discarded, and 500µl Buffer RPE was added to the RNeasy spin column and centrifuged for 30seconds at 10,000 rpm. The flow-through was discarded again, and 500µl Buffer RPE was added to the RNeasy spin column and centrifuged for 2 minutes at 10,000 rpm to wash the spin column membrane. The RNeasy spin column was placed in a new 2ml collection tube and centrifuged at full speed for 1 minute to eliminate any possible carryover of Buffer RPE. Afterwards, the RNeasy spin column was placed in a new 1.5 ml collection tube and 30µl RNAse-free water was added directly to the spin column membrane and centrifuged for 1minute at 10,000rpm to elute the RNA. The mRNA concentration was measured with a nanodrop, and the samples were either stored at -80°C or used to synthesise the cDNA immediately.

2.2.10.3 cDNA Synthesis

1000ng of mRNA per sample was used to synthesise cDNA, using High-Capacity cDNA Reverse Transcription Kit (Fisher). A 20µl reverse transcription reaction containing 5.8 µL of RNase-free RT mastermix, and RNase-free water to a final volume of 20 µL **(Table 2.10)**.

Table 2.13 RT Mastermix

Component	Volume (per sample)
10xRT buffer	2.0µL
25x dNTP Mix	0.8µL
10x RT Random Primers	2.0µL
MultiScribe™ Reverse Transcriptase	1.0µL

A negative control solution made up of mRNA and all other solutions in the master mix, except the reverse transcriptase, was also prepared. The 20µl solution was placed in a 0.2mL PCR tube. The samples were placed in a thermal cycler and run following the settings in **Table 2.11**. The synthesised cDNA was stored at -80°C

Table 2.14 Time and Temperature for cDNA Synthesis

	Step 1	Step 2	Step 3	Step 4
Temperature (°C)	25	37	85	4
Time	10 min	120 min	5 min	∞

2.2.10.4 qPCR

The cDNA was diluted in a 1:20 dilution using RNase-free water. The qPCR master mix was prepared as described in **Table 2.12.**

Table 2.15 qPCR Mastermix

	Volume/reaction (384-well)	Final concentration
2x QuantiFast SYBR Green PCR Master Mix	5µL	1x
10x QuantiTect Primer Assay	1µL	1x
Water	1µL	
Template cDNA (diluted)	3µL	≤100 ng/ reaction

10µl of the solution containing 3µl of cDNA solution and 7µl of the mastermix was loaded in a 384-well plate (3 technical repeats for each condition, including -RT control and blank water control). The plate was sealed and spun for a few seconds to mix the sample. The PCR reaction was set up as shown in **Table 2.13** and run for 40 cycles. The PCR was run and analysed using a QuantStudio 12K flex real-time PCR system. Expression levels of the target genes were calculated using the 2–ΔCt method (2-(ΔCt Target gene – ΔCt Housekeeping gene)) using GAPDH as the housekeeping gene. Three biological replicates were performed for each experiment, and the results were normalised to the mean of full media on plastic.

Table 2.16 Time and Temperature for qPCR

	Hold Stage	PCR Stage		Melt curve stage		
Temperature (°C)	95	95	60	95	60	95
Time (min: sec)	02:00	00:10	00:30	00:15	01:00	00:15

2.2.11 siRNA Knockdown

2.2.11.1 siRNA Knockdown in 6-well plates

190 µl of opti-MEM and 10µl of 5µM siRNA were added to a 6-well plate, and the plate was incubated for 5 minutes at RT. A mix of 4µl of Dharmafect 1 (DF1) and 196µl of opti-MEM was prepared and incubated for 5 minutes at RT. The DF1 mix was added to the 6-well plate. The plate was incubated for 20 minutes at RT on a gentle rocker. $3x10^5$ of SW-1990 cells in 1.6 ml of media were added to each well and placed in the incubator at 37°C and 5% CO_2 for 3 days.

2.2.11.2 siRNA Knockdown for Cell Proliferation Studies

96-well plates were coated with 3mg/ml Matrigel as in **2.2.2.** 3000 cells/well were seeded in full media on the ECM-coated 96-well plates and placed in the incubator at 37°C and 5% CO_2 for 3 hours. The media was removed, and a mix of 5 µl of opti-MEM and 5 µl of 500nM siRNA was added to each well, and the plate was incubated for 5 minutes at RT. A mix of 0.2µl of DF1 and 4.8 µl of opti-MEM was prepared and incubated for 5 minutes at RT. 10µl of the DF1 mix was added to each well of the 96-well plate (Final concentration of siRNA is 25nM). Afterwards, 80µl of full media was added and placed in the incubator at 37°C and 5% CO_2 overnight. The media was changed to the different starvation media **(Table 2.1)** or full media, all supplemented with dFBS and the cells were left in the incubator at 37°C and 5% CO_2 for 5 days. The cells were washed twice with PBS and fixed with 4% PFA for 15 minutes at RT. The nuclei were stained with 10µg/ml Hoechst33342 for at least 15 minutes at RT. The cells were imaged with an InCell Analyzer 2200, 10x objective. The cell number was measured with Cell Profiler using an algorithm to detect the nuclei by covering the range of nuclei sizes **(Figure 2.2)**.

2.2.12 Cell Cycle Analysis by Flow Cytometry

$15x10^4$ cells/well were seeded in a 6-well plate and incubated overnight at 37°C and 5% CO_2. 200nM MRTX1133 or DMSO were added to the media and left in the incubator for 4 days. The media was removed, and the cells were washed, trypsinised, centrifuged and placed in an Eppendorf tube. 10µg/ml of Hoechst33342 (dissolved in media) was added to the cells and placed in an incubator at 37°C and 5% CO_2 for 45 minutes. Afterwards, 5µg/ml of pyronin Y (dissolved in media) was added to the cell solution and incubated at 37°C and 5% CO_2 for 15 minutes. The cells were placed on ice, and the level of fluorescence emitted was measured and analysed by flow cytometry using FCS Express analyser. Hoechst33342 was detected at 450nm, while pyronin Y at 575 nm. The data were analysed using FCS Express software at the Flow Cytometry Core Facility, University of Sheffield, UK.

2.2.13 Dye retention assay

10^5 cells/well were seeded in a 6-well plate and incubated overnight at 37°C and 5% CO_2. 200nM MRTX1133 or DMSO were added to the media and left in the incubator for 4 days. 7.3µl of DMSO was added to the cell tracker mix. Afterwards, 1.5ml serum-free media was added to 0.5µl of cell tracker/DMSO mix (1:3000 dilution). The cells were washed, 1ml of the cell tracker mix was added, and the cells were placed in the incubator at 37°C and 5% CO^2 for 1 hour. Next, the cells were washed, trypsinised, counted and 2000 cells/well were seeded on a 96-well plate in full media with DMSO or MRTX1133 and placed in the incubator at 37°C and 5% CO_2 for 4 days. The cells were imaged live daily over 4 days with an InCell Analyzer 2200, 10x objective, using DAPI wavelength for nuclei and Cy3 wavelength for Cell Tracker Red. The % of Cell Tracker Red-positive cells were measured with Cell Profiler using an algorithm to detect the total number of nuclei and the number of nuclei positive for Cell Tracker Red **(Figure 2.3)**.

2.2.14 Mass Spectroscopy

2.2.14.1 Untargeted Mass Spectroscopy

Nutrient deprivation studies - 6-well plates were coated with 3mg/ml Matrigel as in **2.2.2.** 10^5 cells/well were seeded in full media on the ECM-coated 6-well plates and placed in the incubator at 37°C and 5% CO_2 overnight. The media was changed to starvation media **(Table 2.1)** or full media, all supplemented with dFBS. The cells were left in the incubator at 37°C and 5% CO_2 for 7 days (SW-1990 cells) and 6 days (MIA PaCa-2 cells).

Tumour quiescent studies - 10^5 cells/well were seeded in a 6-well plate and incubated overnight at 37°C and 5% CO_2. 200nM MRTX1133, 1µM palbociclib or DMSO were added to the media and left in the incubator for 4 days.

The cells were placed on ice, the media was removed, and the cells were washed with ice-cold PBS. Afterwards, 800µl of ice-cold metabolite extraction solution (5 MeOH: 3 ACN: 2 H_2O) was added for 5 minutes and transferred to an Eppendorf tube. The samples were centrifuged at 14,000 rpm at 4°C for 10 minutes, and the samples were preserved at -70°C. The samples were run at the Faculty of Science biOMICS Facility using the settings below:
Untargeted UPLC-MS **-** Samples were directly injected into the mass spectrometer Waters Synapt G2-Si using a Waters Acquity autosampler. Injection volume 10µl. Flow rate 0.05ml/min. Mobile phase A

= water + 0.1% formic acid, and mobile phase B = methanol + 0.1% formic acid. Isocratic flow 50:50 A: B.

Mass Spectrometry settings - Data were acquired in positive or negative mode with a 1 sec scan time over the mass range 50-800amu. Three replicates of each condition were combined and run at both positive and negative modes. Only the data from the positive node was used for subsequent analysis.

2.17 Tune Conditions for Positive and Negative Mode

Settings	Positive	Negative
Capillary (kV)	3	4.5
Sample Cone (V)	25	33
Source Offset (V)	75	48
Source Temp (°C)	100	100
Desolvation Temp (°C)	280	280
Desolvation gas Flow (L/h)	700	612

2.2.14.1.1 Untargeted Mass Spectroscopy Data Analysis

Untargeted metabolomics data were analysed using Perseus software (version 2.0.11.0). Log_2-transformed and normalised metabolite intensity values were subjected to two-sample t-test statistical analysis with parameters S_o = 0.1 and false discovery rate (FDR) = 0.05. To ensure robust statistical comparison, imputed values were replaced by NaN before testing. Metabolites with $p < 0.05$ were considered statistically significant, and the results were visualised using volcano plots. Metabolic pathway enrichment analysis of metabolites upregulated on Matrigel compared to plastic was performed using MetaboAnalyst 6.0 (https://dev.metaboanalyst.ca/), referencing the Homo sapiens Small Molecule Pathway Database (SMPDB) pathway library.

2.2.14.2 Targeted Mass Spectroscopy

The samples were prepared, and metabolites were extracted as in **2.2.14.1**. The samples were run at the Faculty of Science biOMICS Facility using the settings below:

Targeted UPLC-MS (Amino acids) - A Mass spectrometer Waters Synapt G2-Si coupled to Waters Acquity UPLC was used. Column Waters BEH C18 50x2.1mm. Injection volume 4µl. Flow rate 0.3ml/min. Mobile phase A = water + 0.1% formic acid and mobile phase B = acetonitrile + 0.1% formic acid.

2.18 Gradient table for UPLC (Targeted Amino acids)

Time (min)	% A	% B
0	99	1
3	35	65
6	1	99
6.9	99	1
7	99	1

Mass Spectrometry settings - Data were acquired in positive and negative modes with a 1 sec scan time over the mass range 50-300amu

2.19 Tune Conditions for positive and negative mode (Targeted Amino acids)

Settings	Positive	Negative
Capillary (kV)	3	4.5
Sample Cone (V)	25	33
Source Offset (V)	75	48
Source Temp (^{o}C)	100	100
Desolvation Temp (^{o}C)	280	280
Desolvation gas Flow (L/h)	700	612

The samples were run in both positive and negative modes. Only the data from the positive node was used for subsequent analysis.

Targeted UPLC-MS (Lipids) - A Bruker timsTOF fleX Mass spectrometer coupled to an Agilent 1290 Infinity II UPLC was used. Column Bruker Bio-AQ 100x2.1mm. Injection volume 4µl. Flow rate 0.3ml/min. Mobile phase A = water + 0.1% formic acid and mobile phase B = acetonitrile + 0.1% formic acid.

Table 2.20 Gradient table for UPLC (Targeted Lipids)

Time (min)	% A	% B
0	99	1
0.5	99	1
8	65	35
9	2	98
10	2	98
10.1	99	1
12	99	1

Mass Spectrometry settings - Data acquired in positive and negative modes with a 1-second scan time over the mass range 50-1300amu

2.21 Tune Conditions for positive and negative mode (Targeted Lipids)

Source type	VIP-HESI (Positive)	VIP-HESI (Negative)
Capillary (V)	3000	4500
Sample Cone (V)	25	33
Source Offset (V)	75	48
Source Temp (°C)	100	100
Desolvation Temp (°C)	280	280
Desolvation gas Flow (L/h)	700	612

Data Processing - Data was processed by Heather Walker at the biOMICS Mass Spectrometry Facility. A Bruker Metaboscape 2025 software with default settings for T-Rex 4D processing and ion deconvolution with a minimum 4D peak size of 85 points and an intensity threshold of 1000 counts, was used. Compounds were matched to a target list and lipid and spectral libraries, with tolerances and scores shown in the table below.

Table 2.22 Tolerance and scores for lipid data processing

Criteria	**Narrow Tolerance**	**Wide Tolerance**
m/z	2ppm	5ppm
Retention time	0.1min	0.5min
mSigma	20	100
MS/MS score	900	600
CCS	1%	3%

2.2.15 Statistical Analysis

All graphs were plotted using GraphPad Prism software. A Mann-Whitney U test was used to analyse experiments containing two groups. One-way ANOVA (Kruskal-Walli's test) was used to analyse experiments containing more than two groups, and Dunn's multiple comparison test was used to compare the different data sets. A two-way ANOVA was used to analyse experiments containing more than two groups with more than one variable, and Tukey's multiple comparisons test was used to compare the different groups. Superplots were generated as described by Lord and colleagues (Lord et al., 2020). Data points from the same experiments were presented in similar colour, and the mean

value of each biological replicate was presented in the colour of each experiment, but in larger symbol sizes. Statistical analysis for non-targeted metabolic profiling was performed by Perseus software (described in section 2.2.14.1.1).

3 The ECM supports the proliferation of PDAC cells in nutrient-deprived conditions

3.1 Introduction

PDAC cells exist in a nutrient-deprived microenvironment in vivo (Kamphorst et al., 2015). In addition to the increased need for nutrients to support rapidly proliferating cells in all cancers, some studies have attributed PDAC's nutrient-deprived state to its dense stroma that results in collapsed blood vessels and low vasculature, negatively impacting the transport of nutrients to the cells (Ren et al., 2023). Indeed, while analysing the metabolic profile of human PDAC tissues, Kamphorst et al reported that PDAC tumours are low in glucose, glutamine and serine (Kamphorst et al., 2015). In addition, Sullivan and colleagues analysed the interstitial fluid of murine PDAC models and found that the tumours are low in glucose, lactate, arginine, tryptophan and cysteine (Sullivan et al., 2019). Despite this, PDAC cells have been found to survive in this nutrient-deprived environment (Kamphorst et al., 2015).

The TME comprises cellular components like fibroblasts, CAFs and immune cells, and the largest and acellular component, the ECM (Kamphorst et al., 2015). More specifically, the PDAC TME is dense and highly fibrotic (Liot et al., 2021), due to the excessive deposition of ECM from CAFs and PSCs. This desmoplastic reaction not only provides mechanical support (Weniger et al., 2018), but also negatively impacts drug delivery into the tumour (Ferrara et al., 2021) and serves as a source of nutrients (Olivares et al., 2017), all of which contribute to PDAC cell proliferation, migration, metastasis and survival. The typical ECM components found in PDAC are collagens, fibronectin, laminin and hyaluronan. In particular, collagens I, IV and laminins have been reported to be the most abundant ECM in PDAC (Ferrara et al., 2021; Perez et al., 2021), with a high serum concentration of collagen-IV being linked to the increased likelihood of relapse in pancreatic cancer patients (Ohlund et al., 2009).

Furthermore, in their study on the roles of collagen-I in pancreatic cancer, Ohlund and colleagues found that pancreatic cancer cells seeded on either collagen-I or IV showed increased cell proliferation and reduced apoptosis compared to pancreatic cancer cells seeded on a control matrix, BSA. Their wound healing assay also showed that pancreatic cancer cells grown on both collagen-I and IV matrices migrated faster than those grown on BSA, used as a control matrix (Ohlund et al., 2013). In addition, Olivares et al reported that nutrient-deprived PDAC cells internalised both collagens I and IV, and collagen-IV supported PDAC cell survival in glucose-starved conditions. Also, they found that PDAC cells supplemented with collagen-IV showed an increased phosphorylation of ERK, downstream of

KRAS, accounting for its role in promoting cell proliferation (Olivares et al., 2017). Besides, a recent study by Nazemi et al highlighted the role of collagen-I in breast cancer cells (also known to exist in an ECM-rich microenvironment). They found that collagen-I promoted the growth and survival of amino acid-deprived breast cancer cells. Using metabolomics, they discovered that under amino acid starvation, breast cancer cells seeded on a collagen-I-rich matrix have an increased level of tyrosine and phenylalanine, which they found was responsible for ECM-dependent growth of the cells in amino acid-deprived conditions (Nazemi et al., 2024).

The dense fibrotic stroma, characterised by an abundant accumulation of ECM that contributes to poor vasculature and a significantly reduced access to adequate nutrients, is a well-known feature of the PDAC TME (Mahadevan and Von Hoff, 2007). However, PDAC cells survive and continue to thrive in their nutrient-deprived environments (Kamphorst et al., 2015). Here, we wanted to assess the roles of the Matrigel and collagen-I in supporting PDAC cell growth in different nutrient-deprived conditions.

3.2 Results

3.2.1 Matrigel and collagen-I partially rescued the proliferation of PDAC cells under nutrient deprivation

Two ECM preparations, Matrigel and collagen-I, were used. Matrigel is extracted from Engelbreth-Holm-Swarm (EHS) mouse sarcoma, and it contains basement membrane components such as collagen-IV, different isoforms of laminin (with the most abundant being laminin 111) (Aisenbrey and Murphy, 2020), nidogen and perlecan. Additionally, Matrigel contains proteases and growth factors such as PDGF, EGF and FGF (Benton et al., 2011). Growth factor-reduced Matrigel was used in our study to mimic the basement membrane, while collagen-I was used to simulate the interstitial matrix.

To assess the roles of the ECM under nutrient deprivation, human PDAC cell lines with different KRAS mutations were used to assess the possible contributions of KRAS mutation to ECM-dependent support under nutrient deprivation. SW-1990 (G12D), PANC-1 (G12D), MIA PaCa-2 (G12C) and BxPC-3 (Wild-type KRAS) cells were seeded on plastic, Matrigel or collagen-I-coated plates and cultured in glucose-free, glutamine-free or amino acid-free media, supplemented with 10% dialysed FBS (dFBS). dFBS was used in our study because, unlike regular FBS, dFBS has been depleted of small molecules like amino acids, hormones, and other metabolites, thereby minimising the contribution of nutrients from other sources into our starvation conditions (Nazemi et al., 2024). The cells were fixed on days 2

and 6 for MIA PaCa-2 cells or days 2 and 7 for the remaining cell lines, stained with DRAQ5 and imaged using a LICOR Odyssey system.

In SW-1990 cells, in full media, there was a small but statistically significant increase in cell growth in the presence of both Matrigel and collagen-I compared to plastic **(Figure 3.1A)**. Furthermore, Matrigel rescued the growth of SW-1990 cells under glucose deprivation, with about an 8-fold increase in cell growth in the presence of Matrigel compared to plastic. While the cell growth on collagen-I was about 5 times more than on plastic, the increase did not reach statistical significance. **(Figure 3.1B).**

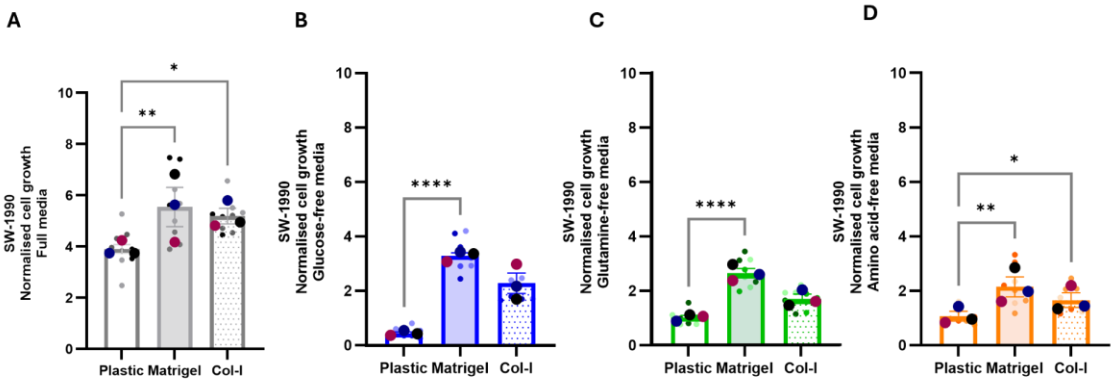

Figure 3.1 – Matrigel and Collagen-I partially rescued SW-1990 cell proliferation under nutrient deprivation
SW-1990 cells were seeded on plastic, 2mg/ml collagen-I (col-I) or 3mg/ml Matrigel-coated 96-well plates and incubated overnight. The media were changed to (A) full media, (B) glucose-free media, (C) glutamine-free media, (D) amino acid-free media, all supplemented with dFBS. The cells were fixed on day 2 or day 7, stained with DRAQ5 and imaged with a Licor Odyssey Sa system. The signal intensity was quantified using Image Studio Lite software. Data are presented as Mean ± SEM. The data was normalised to the mean of each condition on plastic on day 2. Significance was determined using Kruskal-Wallis and Dunn's multiple comparisons test. ****p<0.0001, **p<0.01 *p<0.05. N=3 independent experiments, and the bigger dots represent the mean of each experiment.

Similarly, in glutamine-deprived conditions, while there was a significant increase in cell growth in the presence of Matrigel compared to plastic (more than 2-fold), there was no significant difference in cell growth between collagen-I and plastic **(Figure 3.1C)**. Finally, unlike glucose and glutamine-free conditions, in amino acid-free conditions, Matrigel and collagen-I caused a significant ~ 2-fold increase in cell growth compared to plastic **(Figure 3.1D)**. Overall, that data suggests that Matrigel has a more significant effect on glucose and glutamine-deprived SW-1990 cells than collagen-I.

Next, in MIA PaCa-2 cells, the data showed that in full media, there was a significant increase in cell growth in the presence of Matrigel compared to both plastic and collagen-I (~2-fold). At the same time, there was no difference in the cell growth between the cells on plastic and the cells on collagen-I **(Figure 3.2A)**. Next, we saw that under glucose starvation, both Matrigel and collagen-I significantly increased cell growth compared to plastic, with a ~2-fold increase in the presence of either Matrigel or collagen-I compared to plastic **(Figure 3.2B)**. Similarly, both Matrigel and collagen-I partially rescued the growth of glutamine-deprived and amino acid-deprived MIA PaCa-2 cells (≥2 fold on both Matrigel

and collagen-I compared to plastic) **(Figure 3.2C, D)**. Together, these data indicate that both Matrigel and collagen-I partially rescued MIA PaCa-2 cell growth under starvation to similar extents.

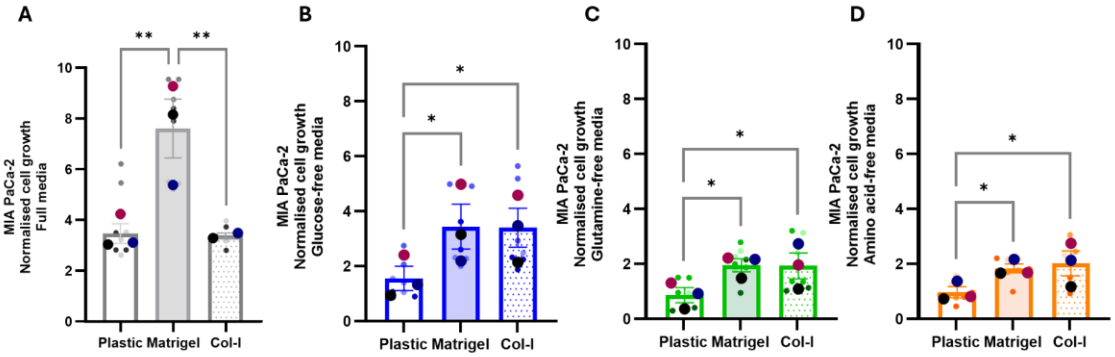

Figure 3.2 – Matrigel and Collagen-I partially rescued MIA PaCa-2 cell proliferation under nutrient deprivation
MIA PaCa-2 cells were seeded on plastic, 2mg/ml collagen-I (Col-I) or 3mg/ml Matrigel-coated 96-well plates and incubated overnight. The media was changed to (A) full media, (B) glucose-free media,(C) glutamine-free media, (D) amino acid-free media, all supplemented with dFBS and incubated. The cells were fixed on day 2 and day 6, stained with DRAQ5 and imaged with a Licor Odyssey Sa system. The signal intensity was quantified using Image Studio Lite software. Data are presented as Mean ± SEM. The data was normalised to the mean of each condition at day 2. Significance was determined using Kruskal-Wallis and Dunn's multiple comparisons test. **p<0.01 *p<0.05. N=3 independent experiments, and the bigger dots represent the mean of each experiment.

In BxPC-3 cells, there was no difference in cell growth in the presence of Matrigel or collagen-I compared to plastic in full media **(Figure 3.3A)**. In contrast, only Matrigel partially rescued cell growth of BxPC-3 cells under glucose deprivation, as there was a significant increase in cell growth in the presence of Matrigel compared to both plastic and collagen-I (more than a 2-fold increase), while there was no difference in cell growth between the cells on plastic and the cells on collagen-I **(Figure 3.3B)**. Similarly, under glutamine starvation, there was a Matrigel-dependent increase in cell growth (about 2 times more on Matrigel compared to plastic). At the same time, there was no significant increase in cell growth in the presence of collagen-I compared to plastic **(Figure 3.3C)**. Next, we saw that in amino acid-free conditions, Matrigel and collagen-I caused a small (≤ 2-fold), but statistically significant increase in cell growth compared to the cells on plastic **(Figure 3.3D)**. Overall, similar to SW-1990 cells, the data suggest that Matrigel has a more significant effect on glucose and glutamine-deprived SW-1990 cells than collagen-I.

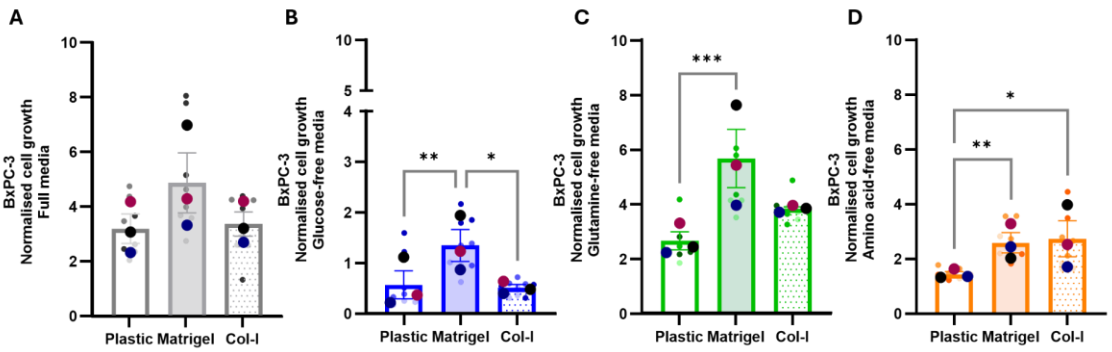

Figure 3.3 – Matrigel and Collagen-I partially rescued BxPC-3 cell proliferation under nutrient deprivation
BxPC-3 were seeded on plastic, 2mg/ml collagen-I (Col-I) or 3mg/ml Matrigel-coated 96-well plates and incubated overnight. The media was changed to (A) full media, (B) glucose-free media, (C) glutamine-free media, (D) amino acid-free media, all supplemented with dFBS and incubated. The cells were fixed on day 2 and day 7, stained with DRAQ5 and imaged with a Licor Odyssey Sa system. The signal intensity was quantified using Image Studio Lite software. Data are presented as Mean ± SEM. The data was normalised to the mean of each condition at day 2. Significance was determined using Kruskal-Wallis and Dunn's multiple comparisons test. ***p<0.001 **p<0.01 *p<0.05 N=3 independent experiments, and the bigger dots represent the mean of each experiment.

Finally, in PANC-1 cells, there was no difference in cell growth in the presence of Matrigel or collagen-I compared to plastic in full media **(Figure 3.4A)**. However, Matrigel and collagen-I caused a significant increase (~2-fold) in cell growth compared to the cells on plastic under glucose starvation **(Figure 3.4B**). In contrast to this, there was no increase in cell growth in the presence of Matrigel or collagen-I compared to plastic under glutamine-free conditions **(Figure 3.4C)**. Lastly, Matrigel and collagen-I significantly increased cell growth under amino acid deprivation. While the cell growth on collagen-I was about 3 times more than on plastic, the cell growth on Matrigel was about 5 times more than on plastic **(Figure 3.4D)**.

Overall, we saw that Matrigel had a more pronounced effect on rescuing the proliferation of glucose and glutamine-deprived SW-1990 and BxPC-3 cells than collagen-I. At the same time, there was no difference between Matrigel's and collagen-I's ability to support the growth of MIA PaCa-2 cells under nutrient deprivation. In PANC-1 cells, the data showed that Matrigel and collagen-I partially rescued cell growth under glucose and amino acid, but not glutamine starvation. Overall, Matrigel consistently promoted cell growth under nutrient deprivation in all the cell lines tested.

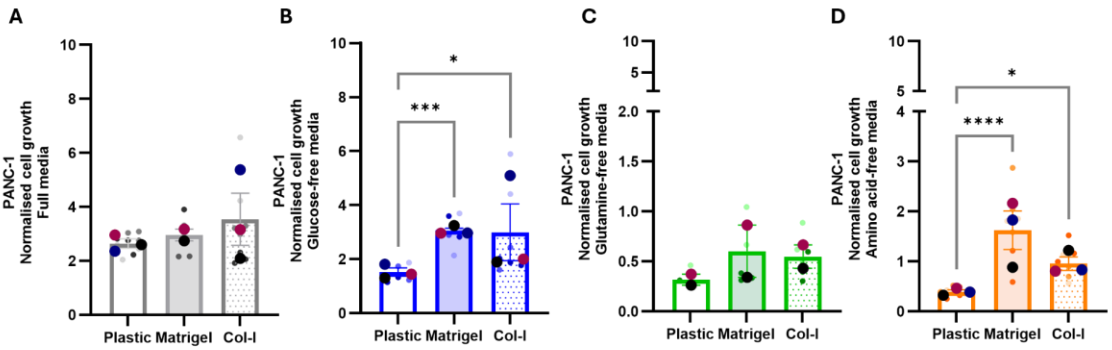

Figure 3.4 – Matrigel and Collagen-I partially rescued PANC-1 cell proliferation under glucose and amino acid deprivation

PANC-1 were seeded on plastic, 2mg/ml collagen-I (Col-I) or 3mg/ml Matrigel-coated 96-well plates and incubated overnight. The media was changed to (A) full media, (B) glucose-free media, (C) glutamine-free media, (D) amino acid-free media, all supplemented with dFBS and incubated. The cells were fixed on days 2 and 7, stained with DRAQ5, and imaged using a Licor Odyssey Sa system. The signal intensity was quantified using Image Studio Lite software. Data are presented as Mean ± SEM. The data was normalised to the mean of each condition at day 2. Significance was determined using Kruskal-Wallis and Dunn's multiple comparisons test. ****p<0.0001 ***p<0.001 **p<0.01 N ≥2 independent experiments, and the bigger dots represent the mean of each experiment.

3.2.2 Matrigel, but not collagen-I, partially rescued the proliferation of PDAC cells in Tumour Interstitial Fluid Media (TIFM)

The Interstitial fluid (IF) transports nutrients and waste between the cells and the bloodstream (Wagner and Wiig, 2015). In normal cells, the nutrient content in the IF is similar to the nutrient content in the blood; however, in tumours such as PDAC with poor vasculature, the nutrient content in the IF transported to the tumours is lower than the available nutrients in the bloodstream (Sullivan et al., 2019). This suggests that measuring the nutrient content of the IF is a better method of characterising the nutrient content of tumours.

To have a clearer picture of the nutrient content in PDAC, Sullivan et al used LC/MS-based quantitative metabolomics to measure the nutrient content in the IF of a murine model of PDAC and found that, in addition to glucose, cysteine, tryptophan and lactate, arginine was the most depleted nutrient in the IF of PDAC tumours (Sullivan et al., 2019). Using this data, they formulated Tumour Interstitial Fluid Media (TIFM), which they reported to better recapitulate the nutrient depleted and metabolically stressed state of PDAC in vivo. (Apiz Saab et al., 2023). Given the importance of physiological relevance in cancer modelling, TIFM was selected as the culture medium to more accurately recapitulate the nutrient microenvironment experienced by PDAC cells in vivo.

To assess the ability of Matrigel and collagen-I to support the proliferation of PDAC cell lines cultured in TIFM, SW-1990, PANC-1, MIA PaCa-2 and BxPC-3 cells were seeded on plastic, Matrigel or collagen-I-coated surfaces and cultured in TIFM supplemented with 10% dFBS. After 6 days (MIA PaCa-2 cells) and 7 days (remaining cell lines), the cells were fixed, stained with DRAQ5 and imaged using a LICOR Odyssey system. We saw that Matrigel, but not collagen-I, rescued SW-1990, MIA PaCa-2 and BxPC-3

cell growth **(Figure 3.5A, C, D)** while neither Matrigel nor collagen-I rescued PANC-1 cells cultured in TIFM **(Figure 3.5B)**. This further solidifies our initial observation that supplementing PDAC cells with Matrigel significantly affected nutrient-deprived PDAC cells more than collagen-I.

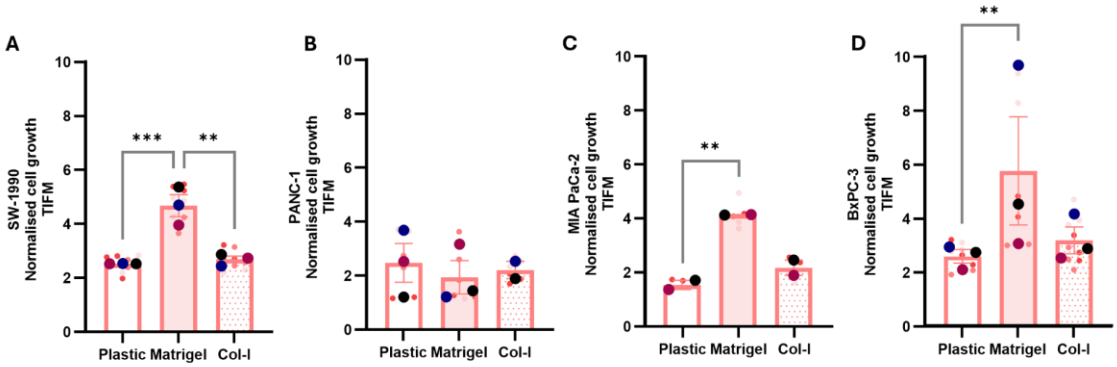

Figure 3.5 – Matrigel partially rescued PDAC cell proliferation in TIFM
(A) SW-1990 (B) PANC-1 (C) MIA PaCa-2 (D) BxPC-3 cells were seeded on plastic, 2mg/ml collagen-I (Col-I) or 3mg/ml Matrigel-coated 96-well plates and incubated overnight. The media was changed to TIFM supplemented with dFBS and incubated. The cells were fixed on days 2 and 6 for MIA PaCa-2 cells and days 2 and 7 for the remaining cell lines, stained with DRAQ5, and imaged using a Licor Odyssey Sa system. The signal intensity was quantified using Image Studio Lite software. Data are presented as Mean ± SEM. The data was normalised to the mean of each condition at day 2. Significance was determined using Kruskal-Wallis and Dunn's multiple comparisons test. ***p<0.001 **p<0.01 N ≥2 independent experiments, and the bigger dots represent the mean of each experiment.

3.2.3 Laminin/entactin partially rescued the proliferation of amino acid-deprived PDAC cells

To investigate the specific basement membrane component that could be responsible for the role of Matrigel and given that laminin is the most abundant basement membrane component in Matrigel (Kleinman and Martin, 2005), we measured the effects of laminin/entactin on nutrient-deprived PDAC cells. SW-1990 cells were seeded on plastic, Matrigel or laminin/entactin-coated plates and cultured in full, glucose-free, glutamine-free, amino acid-free media and TIFM supplemented with 10% dialysed FBS (dFBS). After 7 days, the cells were fixed, stained with DRAQ5 and imaged using a LICOR Odyssey system.

Culturing cells on Matrigel and laminin/entactin-coated surfaces significantly increased the proliferation of SW-1990 cells grown in full media **(Figure 3.6A)** and amino acid-free media **(Figure 3.6D)**. However, compared to Matrigel-coated surfaces, laminin/entactin did not rescue cell growth in glucose-free **(Figure 3.6B)**, glutamine-free **(Figure 3.6C)** media or TIFM **(Figure 3.6E)**. This suggests that laminin/entactin alone might not be responsible for Matrigel's ability to support PDAC cells in nutrient-starved conditions.

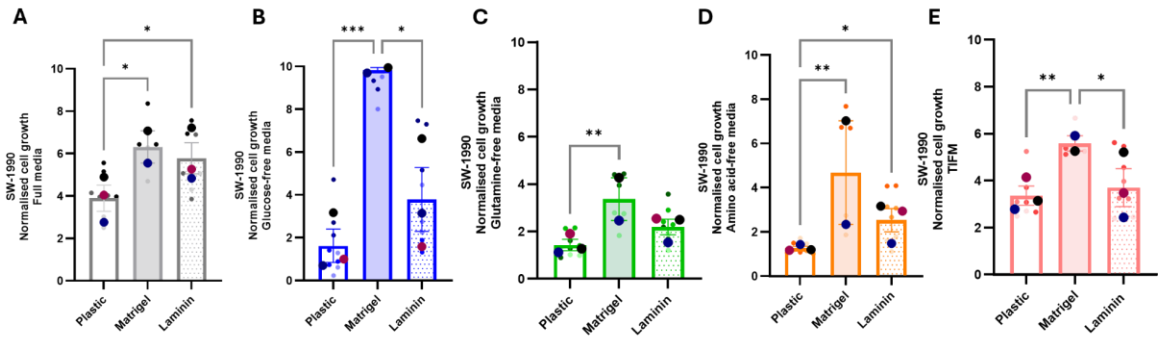

Figure 3.6 – Matrigel and Laminin partially rescued SW-1990 cell proliferation under nutrient deprivation
SW-1990 cells were seeded on plastic, 3.5mg/ml laminin or 3mg/ml Matrigel 96-well plates and incubated overnight. The media were changed to (A) full media, (B) glucose-free media, (C) glutamine-free media, (D) amino acid-free media, and (E) TIFM, all supplemented with dFBS and incubated. The cells were fixed on days 2 and 7, stained with DRAQ5, and imaged using a Licor Odyssey Sa system. The signal intensity was quantified using Image Studio Lite software. Data are presented as Mean ± SEM. The data were normalised to the mean of each condition at day 2. Significance was determined using Kruskal-Wallis and Dunn's multiple comparisons test. ***p<0.001, **p<0.01, *p<0.05, N ≥2 independent experiments, and the bigger dots represent the mean of each experiment.

3.2.4 Matrigel partially reversed the effects of the Glutaminase inhibitor, CB-839, in PDAC cells

Given the critical role of glutamine as a building block for other amino acids, nucleotides and fuelling the TCA cycle, it is no surprise that rapidly proliferating cells depend on glutamine as a metabolic fuel to support their proliferation (Son et al., 2013; Palm and Thompson, 2017). Consequently, targeting glutamine metabolism is a promising method of cancer therapy. The glutaminolysis process starts with converting glutamine to glutamate, catalysed by glutaminase (GLS). CB-839, a small-molecule inhibitor of GLS **(Figure 3.7A)**, showed anti-tumour effects in patients with solid tumours such as triple-negative breast cancer, renal cancer and non-small cell lung carcinoma in phase I/II clinical trials (Harding et al., 2021; Gouda et al., 2025). Given the ability of Matrigel to support the proliferation of PDAC cells cultured in glutamine-free media, we wanted to assess the effects of Matrigel upon pharmacological inhibition of glutamine metabolism.

Here, BxPC-3 cells were seeded on Matrigel-coated plates or on plastic, cultured in full media in the presence of different concentrations of CB-839 or glutamine-free media for 5 days. The cells were fixed and stained with Hoechst33342 and imaged using an InCell Analyzer. **Figure 3.7B** shows a concentration-dependent reduction in the cell number upon treatment with CB-839, similar to the decrease in cell number in glutamine-free media. Furthermore, Matrigel partially reversed the growth-inhibitory effect of CB-839, evidenced by the increase in the number of cells on Matrigel-coated plates compared to the cells on plastic.

This further solidifies the role of the ECM in supporting PDAC cell growth under nutrient deprivation and suggests that the abundant ECM in PDAC could contribute to resistance to therapeutic interventions that focus on disrupting glutamine metabolism of PDAC cells.

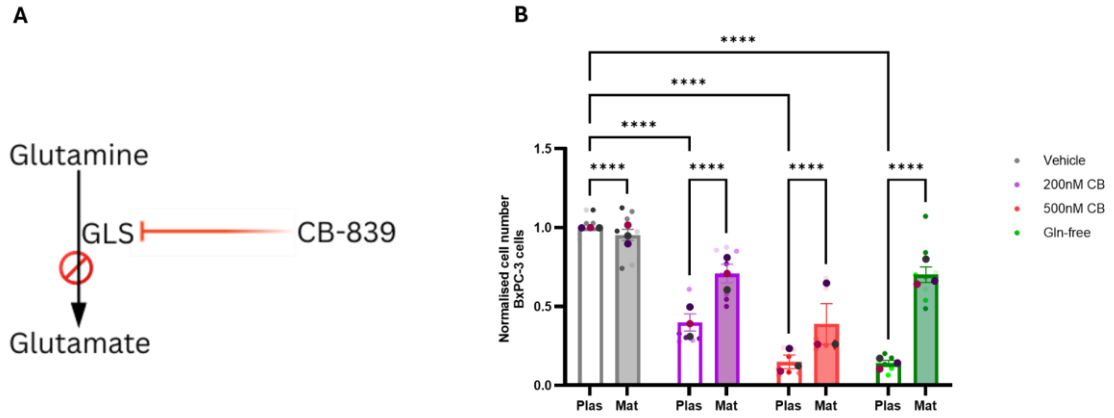

Figure 3.7 – Matrigel partially rescued PDAC cell growth under pharmacological inhibition of GLS1.
(A) Schematics of GLS inhibition by CB-839. (B) BxPC-3 cells were seeded on a plastic or 3mg/ml Matrigel-coated 96-well plate and incubated overnight. The media was changed to media containing DMSO (vehicle), 200nM CB-839, 500nM CB-839 or glutamine-free media supplemented with dFBS and incubated for 5 days. The cells were fixed and stained with Hoechst 33342, imaged using InCell Analyzer 2200 and analysed using Cell Profiler. Data are presented as Mean ± SEM. The data was normalised to the mean of the plastic vehicle control. Significance was determined by Two-Way Anova with Tukey's multiple comparisons test. ****p<0.0001. N=3 independent experiments, and the bigger dots represent the mean of each experiment

3.2.5 Matrigel and collagen-I did not reduce apoptosis in PDAC cells under nutrient deprivation conditions

It is known that nutrient starvation induces cell death in PDAC cells (Tsai et al., 2021). Here, we wanted to investigate the role of the ECM on the survival of nutrient-deprived PDAC cells. Propidium iodide (PI) staining was used as a cell death marker. PI is a membrane-impermeable nuclear stain that is not incorporated in live cells with an intact plasma membrane (Crowley et al., 2016), but it stains dying or dead cells in which the plasma membrane is damaged. Hoechst33342 is a membrane-permeable dye, making it appropriate to stain live cells. Co-staining the cells with both PI and Hoechst33342 allowed us to get a percentage of non-viable cells within our live cell solution.

SW-1990 and MIA PaCa-2 cells were seeded on plastic, Matrigel or collagen-I coated plates and cultured in full media, glucose-free media, glutamine-free media, amino acid-free media and TIFM, all supplemented with 10% dFBS. The cells were co-stained with PI and Hoechst33342 and imaged live 7- and 6-days post-treatment, respectively. In SW-1990 cells, there was a trend of an increase in the percentage of PI-positive cells across all the starvation conditions compared to full media, with the cells cultured in glucose-free media having the highest percentage of PI-positive cells (**Figure 3.8)**.

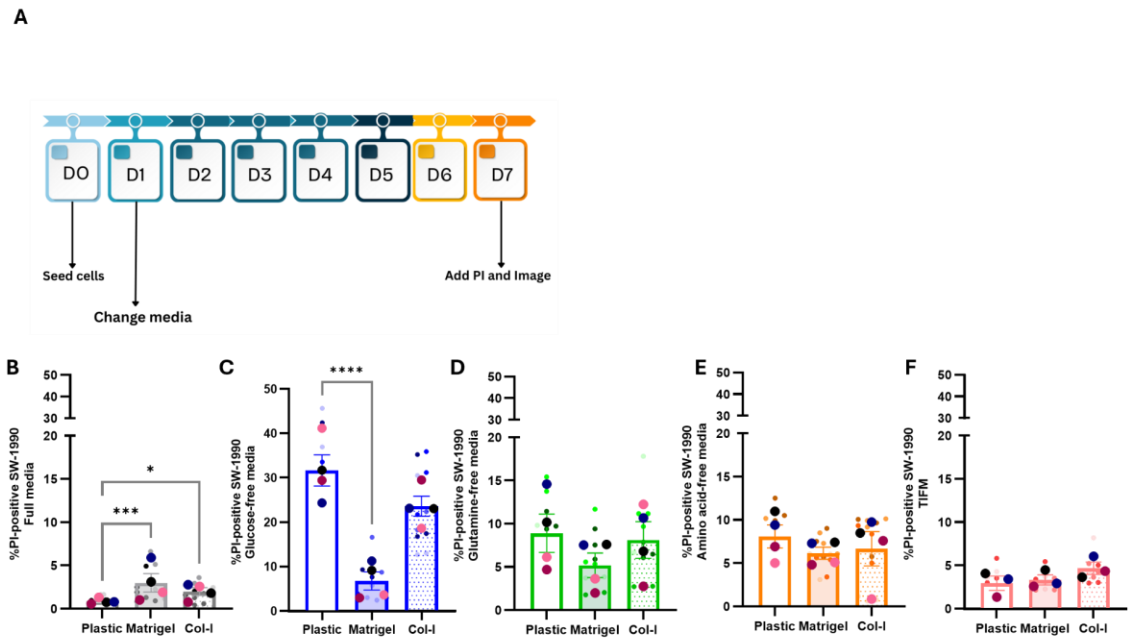

Figure 3.8 – The ECM did not reduce apoptosis in nutrient-deprived SW-1990 cells
(A) Timeline of PI incorporation experiment. SW-1990 cells were seeded on plastic, 2mg/ml collagen-I (Col-I) or a 3mg/ml Matrigel-coated 96-well plate and incubated overnight. The media were changed to (B) full media, (C) glucose-free media, (D) glutamine-free media, (E) amino acid-free media, and (F) TIFM, all supplemented with dFBS and incubated for 7 days. The cells were stained with both Hoechst 33342 and PI, imaged live with an Image Xpress microscope and analysed using the MetaXpress software. Data are presented as Mean ± SEM. Significance was determined using Kruskal-Wallis and Dunn's multiple comparisons test. ****p<0.0001,, ***p<0.001, *p<0.05. N ≥3 independent experiments, and the bigger dots represent the mean of each experiment.

Looking at the roles of ECM proteins, we saw that in full media, there was a small but statistically significant increase in the percentage of PI-positive cells in the presence of both Matrigel and collagen-I compared to plastic, suggesting that there was an increase in cell death in the presence of ECM proteins in full media **(Figure 3.8B)**. This could be attributed to the fact that the cells grew slightly faster in the presence of ECM and were too confluent. In contrast, there was a significant reduction in the percentage of PI-positive cells cultured in glucose-free media in the presence of Matrigel, and not collagen-I, compared to plastic **(Figure 3.8C)**. Finally, neither Matrigel nor collagen-I affected the percentage of PI-positive cells cultured in glutamine-free, amino acid-free media or TIFM **(Figure 3.8D, E, F).**

Similarly, in MIA PaCa-2 cells, there was a trend of an increase in the percentage of PI-positive cells across all the starvation conditions compared to full media **(Figure 3.9)**.

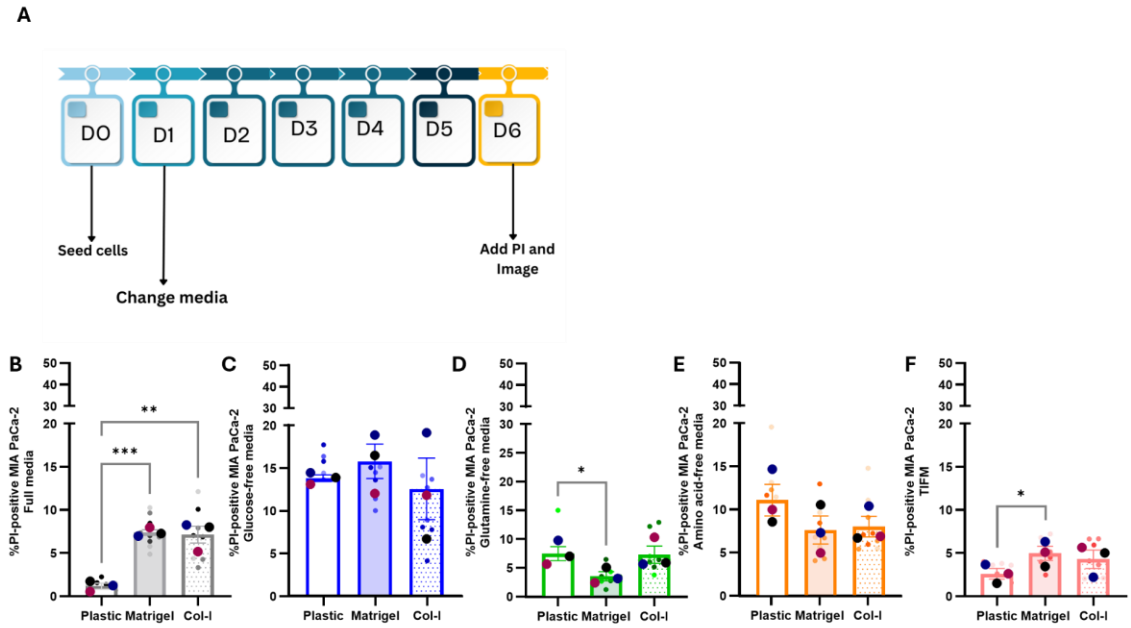

Figure 3.9 – The ECM did not reduce apoptosis in nutrient-deprived MIA PaCa-2 cells
(A) Timeline of PI incorporation experiment. MIA PaCa-2 cells were seeded on plastic, 2mg/ml collagen-I (Col-I) or a 3mg/ml Matrigel-coated 96-well plate and incubated overnight. The media were changed to (B) full media, (C) glucose-free media, (D) glutamine-free media, (E) amino acid-free media and (F) TIFM, all supplemented with dFBS and incubated for 6 days. The cells were stained with both Hoechst 33342 and PI, imaged live with an Image Xpress microscope and analysed using the MetaXpress software. Data are presented as Mean ± SEM. Significance was determined using Kruskal-Wallis and Dunn's multiple comparisons test ***p<0.001, **p<0.01, *p<0.05. N = 3 independent experiments, and the bigger dots represent the mean of each experiment.

In full media, there was a significant increase in the percentage of PI-positive cells in the presence of both Matrigel and collagen-I **(Figure 3.9B)**, also likely attributed to the slightly faster cell growth in the presence of ECM. Furthermore, unlike in SW-1990 cells, neither Matrigel nor collagen-I reduced cell death in glucose-starved MIA PaCa-2 cells **(Figure 3.9C)**. In contrast to this, Matrigel, but not collagen-I, resulted in a small but statistically significant reduction of PI-positive cells under glutamine starvation **(Figure 3.9D)**. Neither Matrigel nor collagen-I affected cell death under amino acid starvation, while Matrigel, but not collagen-I, slightly increased the % of PI-positive MIA PaCa-2 cells grown in TIFM **(Figure 3.9E, F).**

Overall, our data indicate that Matrigel, but not collagen-I, reduced cell death under glucose-free and, to a lesser extent, glutamine-free conditions in SW-1990 cells and MIA PaCa-2 cells, respectively, while neither matrix affected cell death under the other nutrient starvation conditions. This suggests that Matrigel might support cell proliferation through different mechanisms depending on the starvation conditions and in a cell type-dependent manner.

3.2.6 Matrigel increased the DNA synthesis of glucose and glutamine-deprived PDAC cells

Since Matrigel did not reduce cell death in most nutrient starvation conditions studied, we hypothesised that the Matrigel-induced increase in the proliferation of nutrient-deprived PDAC cells could be due to increased DNA synthesis. To test this, we assessed cell cycle progression in the presence of Matrigel and under different nutrient-deprived conditions using 5-Ethynyl-2'-deoxyuridine (EdU), which is incorporated in cells during DNA synthesis. SW-1990 cells were cultured in full, glucose-free, glutamine-free, amino acid-free media or TIFM, all supplemented with 10% dFBS. EdU was added to the cells on day 7 for 24 hours (**Figure 3.10A**), and the cells were imaged to determine the percentage of EdU-positive cells.

First, we assessed the effects of nutrient deprivation on EdU incorporation in cells on plastic. There were approximately 60% of EdU-positive cells in full media, followed by a reduction in the percentage of EdU-positive cells in glucose-free media (~20%) and glutamine-free media (~35%). Surprisingly, there was no difference in the percentage of EdU-positive cells in amino acid-free media (~53%) or TIFM (~56%) compared to full media (**Figure 3.10).**

Next, we investigated the impact of ECM on EdU incorporation under nutrient deprivation. We detected a modest but statistically significant increase in the proliferation of cells seeded on Matrigel compared to plastic in full media (**Figure 3.10B**). On the one hand, Matrigel increased the percentage of EdU-positive cells cultured in glucose- and, to a lesser extent, glutamine-free media **(Figure 3.10C, D)**. On the other hand, the presence of Matrigel did not affect the percentage of EdU-positive cells cultured in amino acid-free media or TIFM **(Figure 3.10E, F)**. Overall, we showed that while nutrient-deprivation reduced the ability of PDAC cells cultured in glucose-free and glutamine-free media to synthesise new DNA, the presence of Matrigel partially restored their DNA synthesis, which is likely responsible for the increase in cell proliferation despite the lack of adequate nutrients.

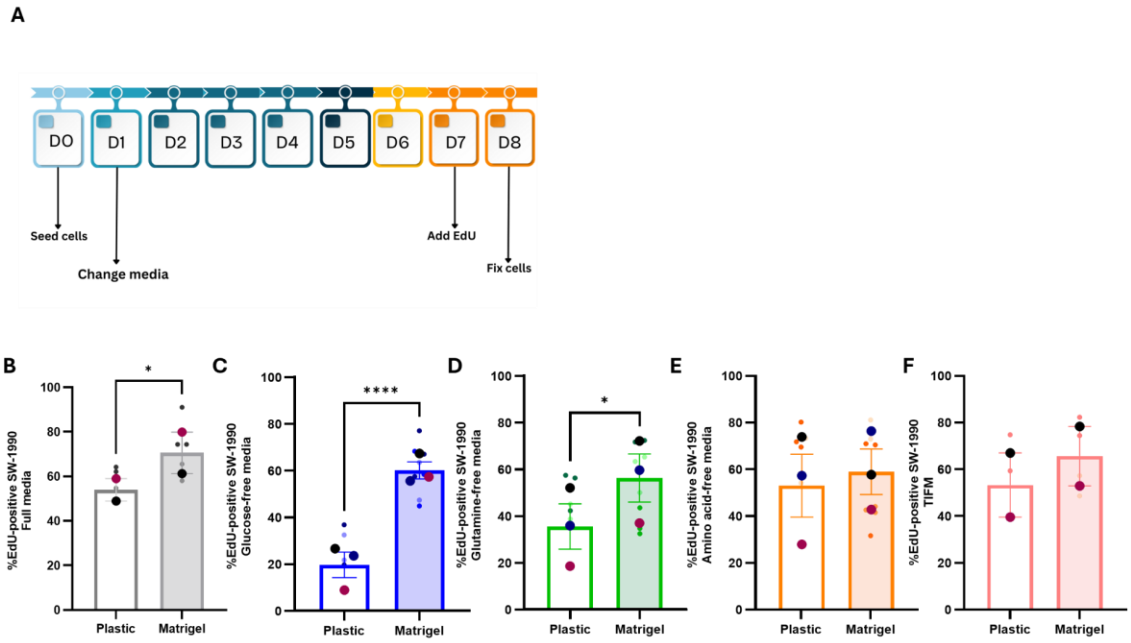

Figure 3.10 - Matrigel increased DNA synthesis in PDAC cells under nutrient deprivation
(A) Timeline of EdU incorporation experiment. SW-1990 cells were seeded on plastic or 3mg/ml Matrigel-coated 96-well plates and incubated overnight. The media were changed to (B) full media, (C) glucose-free media, (D) glutamine-free media, (E) amino acid-free media, and (F) TIFM, all supplemented with dFBS and incubated for 7 days. The cells were incubated with EdU 7 for 24 hours, fixed and stained with Hoechst33342 and EdU cell proliferation imaging kit. The samples were imaged using the InCell Analyzer 2200 and analysed using Cell Profiler. Data are presented as Mean ± SEM. Significance was determined using Kruskal-Wallis and Dunn's multiple comparisons test. ****p<0.0001, *p<0.05. N ≥2 independent experiments, and the bigger dots represent the mean of each experiment.

3.3 Discussion

In our study, we show that ECM components supported the proliferation of PDAC cells in glucose-free, glutamine-free, amino acid-free and tumour interstitial fluid media (TIFM). We also found that the ECM's role was independent of the presence or absence of KRAS mutation, as we saw similar effects on KRAS-mutated PDAC cell lines, SW-1990, PANC-1 and MIA PaCa-2, as well as on the wild-type KRAS PDAC cell line, BxPC-3. Additionally, we found that compared to collagen-I and laminin, Matrigel had a more significant effect on nutrient-starved PDAC cell proliferation **(Figure 3.11)**.

Furthermore, we found that Matrigel partially rescued the growth of PDAC cells upon pharmacological inhibition of glutaminase (which prevents glutamine metabolism), suggesting that the ECM could make PDAC cells less sensitive to pharmacological metabolism inhibitors. Mechanistically, we found that the role of Matrigel in supporting the growth of nutrient-deprived PDAC cells is likely linked to an increase in DNA synthesis and not a reduction in cell death. Taken together, our data suggest that the abundant ECM in PDAC could promote cancer cell growth in a nutrient-deprived environment and reduce the sensitivity of PDAC cells to glutamine metabolism inhibitors.

Consistently, Olivares et al reported that both collagen-I and collagen-IV supported PDAC cell survival in glucose and glutamine-starved conditions (Olivares et al., 2017). Additionally, our study showed that the role of the ECM in supporting nutrient-starved PDAC cells was independent of the presence of the KRAS mutation. This is interesting because various reports have demonstrated that KRAS-driven cells upregulate different mechanisms, such as macropinocytosis or upregulate the expression of nutrient transporters to acquire nutrients (Commisso et al., 2013; Jeong et al., 2018). While this chapter did not focus on the mechanism of nutrient acquisition, using BxPC-3 cells as a wild-type KRAS model of PDAC, we have shown that in PDAC cells, the supporting role of the ECM is independent of the oncogenic KRAS status of the cells.

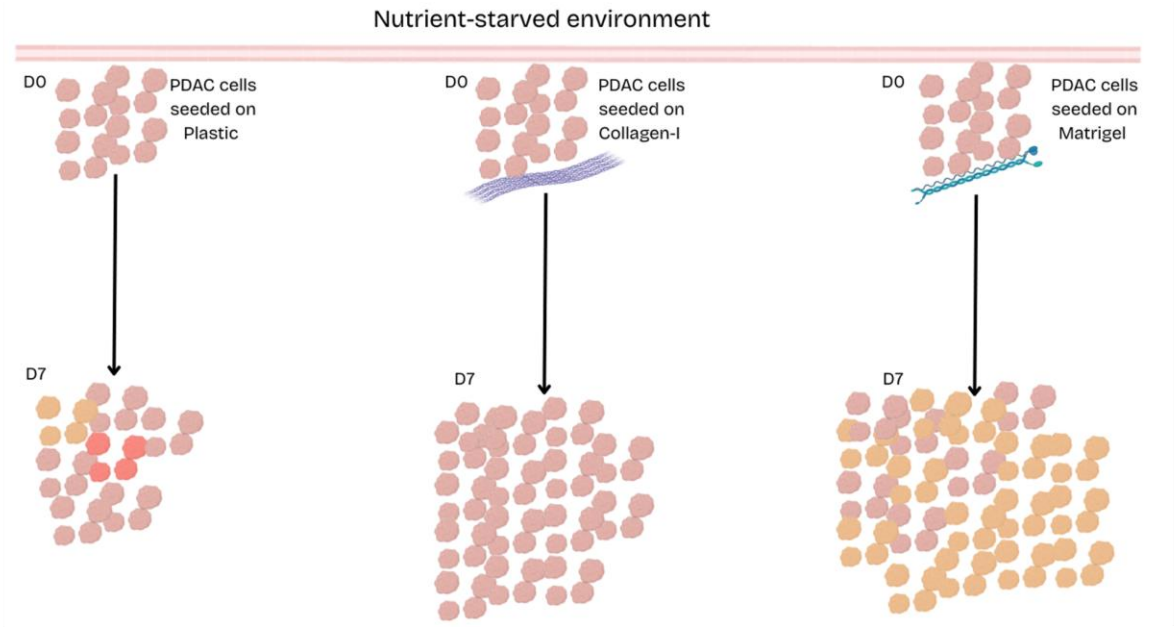

Figure 3.11 – Schematic representation of the ECM supporting PDAC cell proliferation under nutrient deprivation conditions
Nutrient-deprived PDAC cells were cultured on plastic, collagen-I, or Matrigel. Compared to the cells grown on plastic, those grown on either collagen-I or Matrigel continued to proliferate under nutrient-deprived conditions, with Matrigel having a more pronounced effect on cell proliferation than plastic or collagen-I. Furthermore, the ECM reduced the percentage of PI-positive (dead) cells (in red) in some cases, while Matrigel increased EdU incorporation (in yellow). D0 = Day 0; D7 = Day 7. Created with Canva.

Intriguingly, using TIFM, which was formulated to better depict the nutrient content of the PDAC TME (Sullivan et al., 2019), we found that, except in PANC-1 cells, where neither Matrigel nor collagen-I supported cell growth, only Matrigel supported the proliferation of all the other PDAC cell lines studied. This shows that Matrigel had a more prominent effect on nutrient-deprived PDAC cells than collagen-I. This suggests that the basement membrane components of the ECM could play a more significant role in cell survival in nutrient-starved conditions than other components of the ECM. Further work is needed to determine whether this is due to changes in matrix topology and/or stiffness or to specific basement membrane components.

Key components of Matrigel are laminins and collagen-IV. We found that seeding SW-1990 cells on a laminin/entactin-coated surface did not rescue the growth of the cells in TIFM, unlike Matrigel-coated surfaces. This suggests that the presence of laminin/entactin in Matrigel might not be the only factor responsible for its role. While we did not study the specific effects of collagen-IV, Ohlund and colleagues found that an abundant serum collagen-IV level was associated with pancreatic cancer relapse (Ohlund et al., 2009). Furthermore, while collagen-I is reported to be the most abundant ECM component in the desmoplastic reaction in PDAC TME, Ohlund et al found that, compared to normal pancreatic cells, where the expression of all basement membrane proteins is similar, collagen-IV is highly expressed in PDAC compared to other basement membrane proteins (Ohlund et al., 2013). While more studies are needed to confirm this, all this evidence points to the fact that collagen-IV could account for the significant role of Matrigel in our study. However, in addition to laminin/entactin and collagen-IV, Matrigel also contains perlecan and growth factors, which could account for its more significant effect on nutrient-deprived PDAC cells. Interestingly, perlecan was identified as a key component in the CAF-induced pro-metastatic environment in a PDAC mouse model (Vennin et al., 2019). Hence, it will be interesting to dissect the specific molecular mechanisms behind the more substantial role of basement membrane components in nutrient-deprived PDAC cells.

Given the advancement in our understanding of cancer metabolism reprogramming and the emergence of drugs that target different metabolic pathways, such GLS1 inhibitors to block glutaminolysis (Harding et al., 2021) and L-asparaginase for the treatment of paediatric acute lymphoblastic leukaemia (Garcia-Bermudez et al., 2020), it is vital to understand the possible resistance mechanisms of cancer cells to these drugs to improve efficacy and the overall survival of patients. Biancur et al found that upon treatment with 100nM CB-839, a GLS1 inhibitor, there was a significant reduction in the proliferation of PDAC cells (Biancur et al., 2017). This agrees with our findings, as we saw a concentration-dependent decrease in the proliferation of PDAC cells upon treatment with CB-839.

Furthermore, we found that the reduction in cell number seen upon treatment with CB-839 was similar to the effects of culturing PDAC cells in glutamine-free media. This shows that our model of culturing the cells in media lacking specific nutrients, while not targeting specific nutrient pathways, is adequate for depicting nutrient starvation. A more interesting discovery was that seeding the cells with Matrigel reversed the effects of CB-839, as there was a significant increase in cell number upon supplementation with Matrigel. This is of significant clinical relevance as various studies aim at disrupting different metabolic pathways to target cancer cells. Our data suggest that the abundant ECM in PDAC is not only a nutrient source or a barrier to chemotherapeutic agents but may also

contribute to resistance to therapeutic options that target metabolic pathways. More work is needed to determine whether this effect is specific to glutaminolysis inhibitors or might play a role more broadly in the response the drugs targeting energy metabolism, such as glycolysis.

Proliferating cells and indeed all cells require an optimum amount of nutrients to survive. We found that culturing the cells in glucose, glutamine, and amino acid-free media increased the percentage of non-viable cells, as evidenced by an increase in the percentage of PI-positive cells. Interestingly, the cells in TIFM had a lower percentage of PI-positive cells compared to the cells in other starvation conditions. This could suggest that TIFM contains enough nutrients to facilitate the survival of PDAC cells. In agreement with this, Apiz Saab et al used murine PDAC cell lines to study how PDAC cells survive in TIFM. They found that while their PDAC cells cultured in standard media, RPMI, grew at a faster rate, the cells cultured in TIFM also grew and survived, showing that TIFM provides enough nutrients for PDAC cell survival (Apiz Saab et al., 2023). However, they did not characterise the effect of TIFM on apoptosis or other types of cell death.

Furthermore, our data revealed that while Matrigel, but not collagen-I, reduced cell death in glucose-starved SW-1990 cells, neither Matrigel nor collagen-I affected cell death in glutamine or amino acid-starved SW-1990 cells. In agreement with this, Nazemi et al found that neither Matrigel nor collagen-I significantly reduced apoptosis in amino acid-starved breast cancer cells (Nazemi et al., 2024).

Finally, using EdU incorporation as a determinant of cell division, we found that there was a reduction in the percentage of EdU-positive cells cultured in glucose-free media and, to a lesser extent, in glutamine-free media, while there was no reduction in the percentage of EdU-positive cells cultured in amino acid-free media or TIFM. This was unexpected, as evidence has shown that nutrient starvation reduces proliferation in PDAC (Shen et al., 2025). However, our data showed that only about 60% of cells in full media were EdU positive, which could be because the cell confluency was very high in full media at the time point at which we performed the EdU incorporation experiment. This could account for the lack of difference between the cells in full media and the cells under starvation.

Interestingly, we found that seeding cells on Matrigel increased DNA synthesis of glucose and glutamine-starved PDAC cells, but not in cells cultured in amino acid-free media or TIFM (in which there was no difference in EdU incorporation between complete media and starvation on plastic). While this was contrary to the report by Nazemi et al, where they saw a Matrigel-dependent increase in EdU incorporation in breast cancer cells cultured in amino acid-free media, our data agree with their report that supplementation with Matrigel increased the EdU incorporation of glutamine-starved cells (Nazemi et al., 2024). However, it is important to note that their study was done in breast cancer cell

lines, which could account for the difference in the effects of amino acid starvation. More importantly, Matrigel's ability to support DNA synthesis was need-based. In glucose-free conditions, where there was a significant reduction in EdU incorporation, Matrigel had a more significant effect on EdU incorporation compared to glutamine-free conditions. Also, in TIFM and amino acid-free conditions, where there was no reduction in EdU incorporation, Matrigel did not affect EdU incorporation.

Conclusively, while we have shown that the ECM supported PDAC cell growth under nutrient starvation, it will be important to use a more relevant 3D model to better characterise the roles of the ECM, as this will give a more accurate depiction of the TME of PDAC. However, our 2D model has provided an interesting baseline that could be used for further studies. Additionally, the fact that Matrigel significantly reduced cell death under glucose starvation but not under glutamine starvation, especially in SW-1990 cells, suggests that Matrigel could use different mechanisms of action to support cell proliferation/survival depending on the nutrient deprivation conditions. In the following chapters, we investigated the molecular mechanisms driving Matrigel-dependent proliferation of these nutrient-deprived PDAC cells.

4 Matrigel internalisation and mTORC1 activation are required for Matrigel-dependent cell growth under nutrient deprivation

4.1 Introduction

PDAC cells, although in a nutrient-deprived environment, have been reported to adapt by upregulating metabolic pathways to acquire nutrients for their survival (Son et al., 2013), upregulating nutrient transporters (Yun et al., 2009) and making use of nutrient scavenging mechanisms such as macropinocytosis (Commisso et al., 2013; Kamphorst et al., 2015; Olivares et al., 2017; Jeong et al., 2018). Additionally, it has been shown that PDAC cells internalise ECM proteins, followed by lysosomal breakdown to supply nutrients to aid their survival in a nutrient-starved environment (Olivares et al., 2017; Nazemi et al., 2024). ECM internalisation is a process whereby cells bind to the ECM via different ECM receptors, including integrins. Uptake of ECM components then occurs via different endocytic or phagocytic mechanisms, before lysosomal degradation. Some ECM endocytic mechanisms that have been studied include macropinocytosis, clathrin-mediated endocytosis, caveolin-dependent endocytosis, and cholesterol-sensitive clathrin- and caveolae-independent endocytosis (Rainero, 2018; Ju et al., 2020) **(Figure 1.5),** with macropinocytosis being the most linked to nutrient acquisition in PDAC. Indeed, Olivares et al reported that glucose and glutamine-deprived PDAC cells internalise both collagen-I and IV, with macropinocytosis playing a role in glucose-deprived conditions but not in glutamine-deprived ones (Olivares et al., 2017).

Furthermore, while mTORC1 signalling is inactivated under nutrient deprivation (Palm et al., 2015; Lowman et al., 2019), Tsai et al reported that mTORC1 signalling is an adaptive mechanism for the survival of PDAC cells cultured in both low glucose and low glutamine media (Tsai et al., 2021). Using different human PDAC cell lines, they found that while culturing in both low glucose and low glutamine media resulted in cell death in the majority of the cells studied, a proportion of the cells, specifically in SUIT-2 and 8988-T cell lines, survived and the surviving cells upregulated mTORC1 as evidenced by increased phosphorylation of S6K and 4E-BP1, both downstream of mTORC1 (Tsai et al., 2021). Additionally, a previous study in our lab highlighted the roles of the ECM in reactivating mTORC1 under nutrient-deprived conditions. Nazemi et al reported that while culturing MDA-MB-231 cells on plastic in amino acid-free media resulted in deactivation of mTORC1 signalling, evidenced by a reduction in the phosphorylation of S6 and in mTOR lysosomal recruitment, culturing the cells on either Matrigel

or collagen-I coated surfaces resulted in an increased S6 phosphorylation compared to the cells cultured on plastic (Nazemi et al., 2024).

Understanding the molecular mechanisms behind the ability of PDAC cells to survive in their nutrient-deprived environment is vital in pancreatic cancer research, as this could lead to the discovery of novel potential therapeutic targets. Indeed, studies have found that PDAC cells can scavenge nutrients from the ECM to survive in a nutrient-starved environment and that KRAS-mutated PDAC cells upregulate macropinocytosis to facilitate this nutrient uptake (Commisso et al., 2013; Jeong et al., 2018). Also, although PDAC cells can scavenge nutrients from the extracellular space, it is unclear whether nutrient scavenging is the go-to method of nutrient acquisition under all nutrient-deprived conditions. Endocytic processes such as macropinocytosis and caveolin-mediated endocytosis are involved in PDAC cell nutrient scavenging (Commisso et al., 2013; Kamphorst et al., 2015; Wolfe et al., 2024). Here, we wanted to assess the ability of PDAC cells to internalise Matrigel in nutrient-replete conditions and characterise the mechanisms involved in Matrigel internalisation in these cells.

4.2 Results

4.2.1 PDAC cells internalised Matrigel using different endocytic routes

The previous chapter showed that Matrigel supported PDAC cell growth in different nutrient-deprived conditions. Here, we focused on the mechanisms behind Matrigel-induced proliferation of glucose and glutamine-deprived PDAC cells. To do this, 35mm dishes were coated with 1mg/ml of Matrigel and labelled with pHrodo red. pHrodo red is a pH-sensitive dye that emits red fluorescence in an acidic environment, such as the lysosome (Lindner et al., 2020), making it suitable to measure the internalisation of Matrigel into acidic endosomal compartments (Martinez et al., 2024). SW-1990 and BxPC-3 cells were seeded on pHrodo-labelled Matrigel-coated plates, in the presence or absence of EIPA, a well-known macropinocytosis inhibitor that blocks the Na^+/H^+ exchanger (NHE1) **(Figure 4.1A)** (Jeong et al., 2018).

In SW-1990 cells, Matrigel-containing vesicles are abundant in the cells treated with the vehicle control, while the addition of EIPA significantly reduced the presence of Matrigel puncta in the cells. Matrigel uptake quantification showed an 80% reduction in Matrigel internalisation upon treatment with EIPA **(Figure 4.1B)**. Similarly, in the BxPC-3 cells, the cells treated with DMSO featured abundant Matrigel-containing vesicles, while there were few or no Matrigel-containing vesicles upon treatment with EIPA. Image analysis indicated about 60% reduction in Matrigel uptake index upon treatment with EIPA **(Figure 4.1C)**. The results suggest that macropinocytosis might play a role in Matrigel internalisation in PDAC cells. Interestingly, Matrigel internalisation was more strongly induced in BxPC-

3 cells compared to SW-1990 cells. This suggests that Matrigel internalisation might be independent of the presence of oncogenic KRAS mutations.

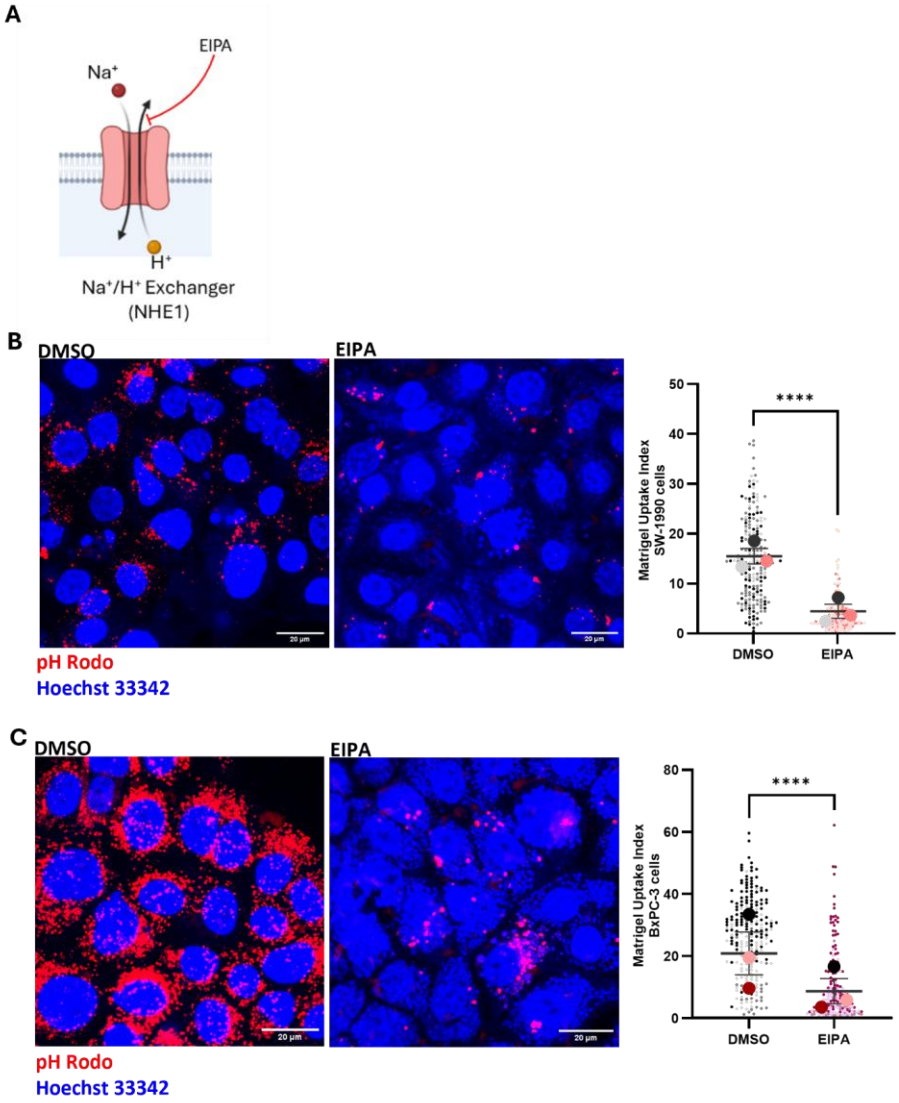

Figure 4.1 – EIPA reduced Matrigel Internalisation in PDAC cells
(A) Schematics of NHE1 inhibition by EIPA. (B) SW-1990 and (C) BxPC-3 cells were seeded on a 1mg/ml Matrigel-coated plate labelled with pH Rodo (red). DMSO or 25µM of EIPA was added to the cells and incubated overnight. The nuclei were stained with Hoechst 33342 (blue), and the cells were imaged live with a Nikon A1 confocal microscope, 60X objective and the uptake index was analysed using ImageJ. Scale bar 20µm. Data are presented as Mean ± SEM. Significance was determined using the Mann-Whitney test. ****p<0.0001. N=3 independent experiments, and the bigger dots represent the mean of each experiment.

To confirm the role of macropinocytosis in Matrigel uptake, we knocked down NHE1, the EIPA target and a regulator of ECM uptake in breast cancer cells (Martinez et al., 2024). To do this, siRNA targeting NHE1 was used in both SW-1990 and BxPC-3 cells; the knockdown efficiency was analysed via Western blotting, and we observed about a 60% reduction in NHE1 expression in both SW-1990 and BxPC-3 cells **(Figure 4.2A, B)**.

Following this, the cells were seeded on pHrodo-labelled Matrigel-coated plates to investigate the internalisation of Matrigel upon knockdown of NHE1 compared to non-targeting siRNA. In SW-1990 cells treated with a non-targeting siRNA, we detected an accumulation of Matrigel-positive vesicles, which appeared reduced upon NHE1 downregulation. Indeed, upon imaging and analysis, there was a small but statistically significant reduction (about 30%) in the presence of Matrigel-containing vesicles upon NHE1 knockdown compared to the cells containing non-targeting siRNA (**Figure 4.2C)**. In contrast, in the BxPC-3 cells, while the overall Matrigel uptake was lower compared to Figure 4.1, we could detect the presence of Matrigel-positive vesicles in the presence of either control or NHE1-targeting siRNA. Consistently, there was no reduction in Matrigel uptake index vesicles upon knockdown of NHE1 **(Figure 4.2D)**

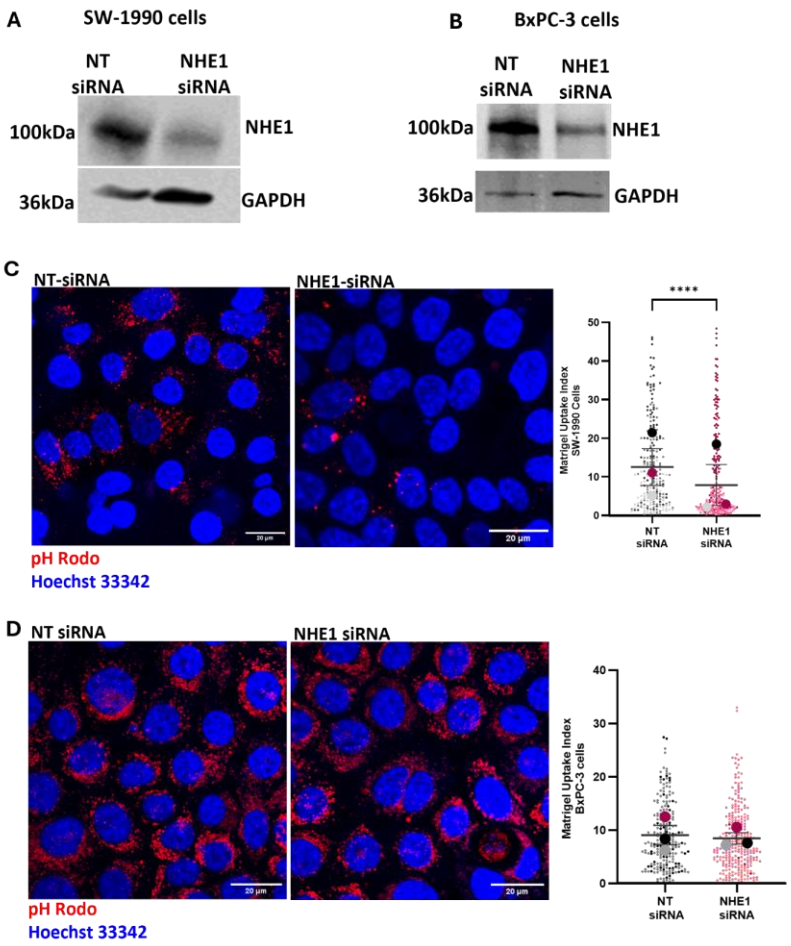

Figure 4.2 –NHE1 knockdown reduced Matrigel Internalisation in SW-1990 cells
SW-1990 and BxPC-3 cells were transfected with non-targeting siRNA (NT-siRNA) or NHE1-siRNA for 3 days. Cell lysates were collected, and NHE1 and GAPDH (control) proteins were analysed via Western blotting (A, B). (C) SW-1990 and (D) BxPC-3 cells transfected with NT-siRNA or NHE1-siRNA were seeded on a 1mg/ml Matrigel-coated plate labelled with pH Rodo (red) and incubated overnight. The nuclei were stained with Hoechst 33342 (blue), and the cells were imaged live with a Nikon A1 confocal microscope, 60X objective and the uptake index was analysed using ImageJ. Scale bar 20µm. Significance was determined using the Mann-Whitney test. ****p<0.0001. N=3 independent experiments, and the bigger dots represent the mean of each experiment.

Overall, these data suggested that macropinocytosis played an important role in Matrigel internalisation in SW-1990 cells. However, in BxPC-3 cells, other endocytic pathways are likely involved.

Class I phosphoinositide 3-kinase (PI3K) are well-established regulators of macropinocytosis that function by generating phosphatidylinositol (3,4,5)-trisphosphate (PIP_3) at the plasma membrane. The localised PIP_3 is required for actin cytoskeleton remodelling during macropinosome formation (Alonso-Curbelo et al., 2015; Salloum et al., 2019). To further validate the role of macropinocytosis in Matrigel internalisation in SW-1990 cells, the PI3K inhibitor LY294002 was used. SW-1990 cells were seeded on pHrodo-labelled Matrigel-coated plates, in the presence and absence of LY294002.

We observed a visible reduction in the number of Matrigel-containing vesicles upon treatment with LY294002 compared to DMSO. Upon quantification, there was a small but statistically significant (about 30%) reduction in Matrigel internalisation upon treatment with LY294002 **(Figure 4.3)**. Collectively, these findings indicate that macropinocytosis contributes to Matrigel internalisation in PDAC cells, especially SW-1990 cells.

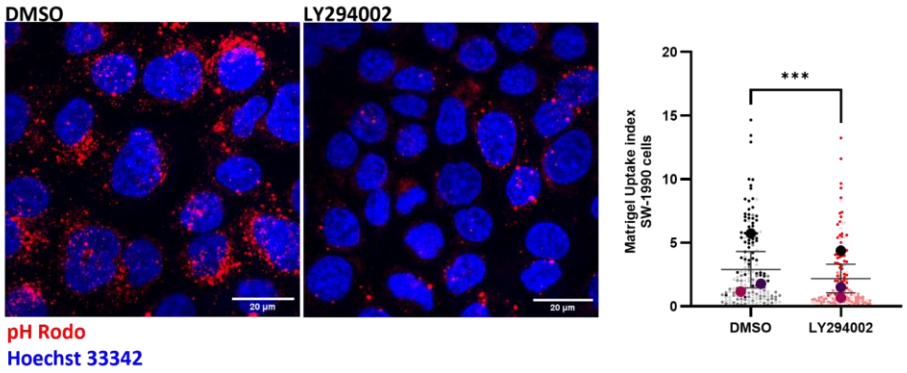

Figure 4.3 – LY294002 reduced Matrigel Internalisation in SW-1990 cells
SW-1990 cells were seeded on a 1mg/ml Matrigel-coated plate labelled with pH Rodo (red). DMSO or 5µM of LY294002 was added to the cells and incubated overnight. The nuclei were stained with Hoechst 33342 (blue), and the cells were imaged live with a Nikon A1 confocal microscope, 60X objective and the uptake index was analysed using ImageJ. Scale bar 20µm. Data are presented as Mean ± SEM. Significance was determined using the Mann-Whitney test. ****p<0.0001. N=3 independent experiments, and the bigger dots represent the mean of each experiment.

Following this, we assessed the roles of other endocytic processes in Matrigel internalisation. SW-1990 cells were seeded on pHrodo-labelled Matrigel-coated plates, and the cells were treated with DMSO (vehicle control), dynasore (a dynamin inhibitor, opposing both clathrin-mediated and caveolin-mediated endocytosis) or filipin (a lipid raft-mediated endocytosis inhibitor). Compared to the control group, there was a significant reduction in Matrigel-containing vesicles upon the addition of either dynasore or filipin**.** Statistical analysis showed approximately 40% reduction upon filipin, and

approximately 80% reduction upon Dynasore treatment **(Figure 4.4)**. These results indicate that, besides macropinocytosis, other endocytic pathways, including dynamin- and caveolin-mediated mechanisms, likely contribute to Matrigel internalisation in SW-1990 cells.

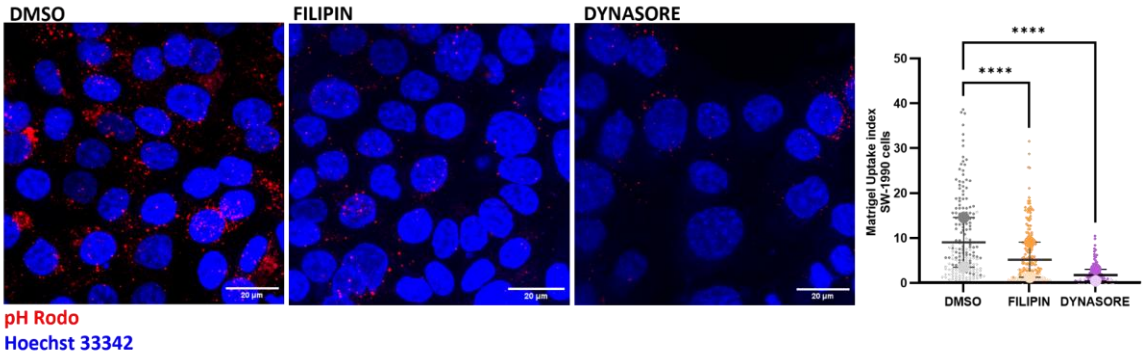

Figure 4.4 – Filipin and Dynasore reduced Matrigel Internalisation in SW-1990 cells
SW-1990 cells were seeded on a 1mg/ml Matrigel-coated plate labelled with pH Rodo (red). DMSO, 5µg/ml of filipin or 40µM of Dynasore was added to the cells and incubated overnight. The nuclei were stained with Hoechst 33342 (blue), and the cells were imaged live with a Nikon A1 confocal microscope, 60X objective and the uptake index was analysed using ImageJ. Scale bar 20µm. Data are presented as Mean ± SEM from 2 independent experiments, with 181 (DMSO), 196 (Filipin), 94 (Dynasore) cells analysed per condition. Significance was determined using Kruskal-Wallis and Dunn's multiple comparisons test. ****p<0.0001. The bigger dots represent the mean of each experiment.

4.2.2 Matrigel internalisation was induced in glutamine-deprived PDAC cells

In **4.2.1**, we showed that PDAC cells can internalise Matrigel in nutrient-replete conditions. Here, we wanted to investigate the impact of nutrient deprivation on ECM internalisation in PDAC cells. To do this, SW-1990 and BxPC-3 cells were seeded on pHrodo-labelled Matrigel and incubated for at least 3 hours for the cells to attach to the surface. Afterwards, the media was changed to full media, glucose-free or glutamine-free media, all supplemented with dFBS. The cells were incubated overnight before imaging. Expectedly, SW-1990 cells internalised Matrigel in full media; however, there was a significant reduction in Matrigel-containing vesicles in cells grown in glucose-free media compared to the cells in full media. Statistical analysis showed about a 70% reduction. Intriguingly, there was a significant increase in Matrigel-containing vesicles when the cells were grown in glutamine-free media compared to the cells in full media, statistically, about a 70% increase **(Figure 4.5A)**.

Similarly, in the BxPC-3 cells, we observed a significant reduction in Matrigel-containing vesicles in cells grown in glucose-free media compared to the cells in full media, statistically, about 50% reduction. Consistent with SW-1990 cells, there was a significant increase (statistically, about 50%) in Matrigel-containing vesicles when the cells were grown in glutamine-free media compared to the cells in full media **(Figure 4.5B)**. The data suggest that although PDAC cells internalise Matrigel under nutrient-replete conditions, glutamine deprivation induces increased internalisation of Matrigel in both SW-1990 and BxPC-3 cells, while glucose starvation impairs it.

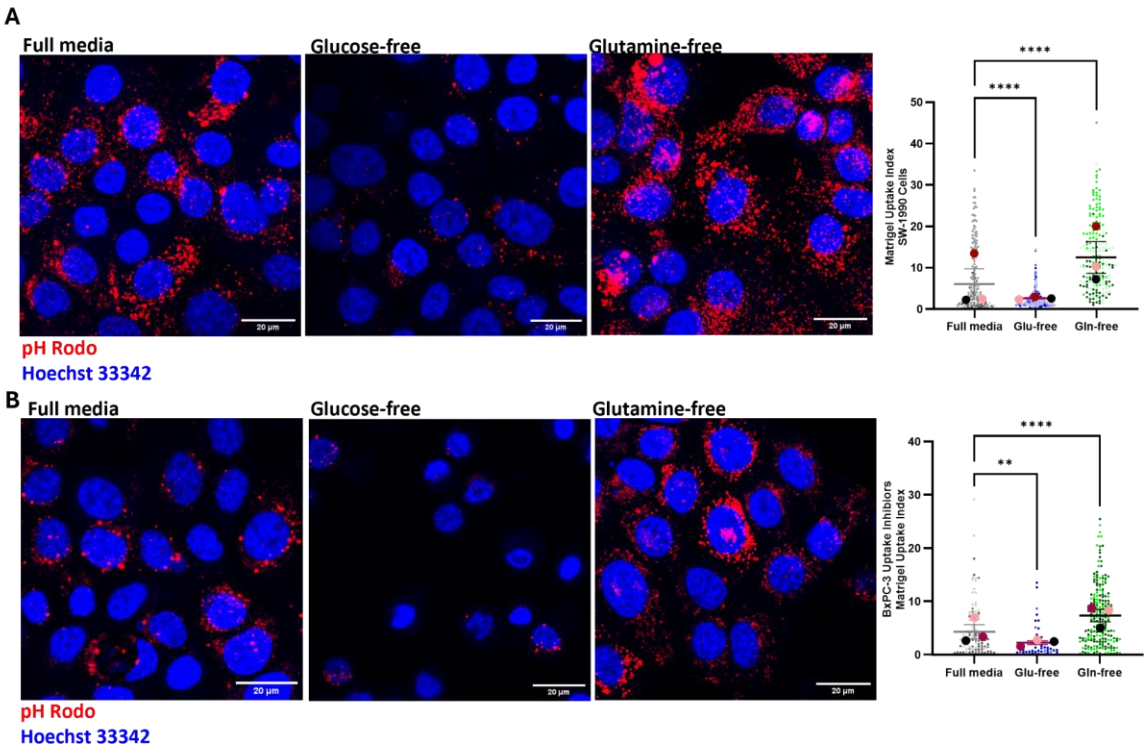

Figure 4.5 – Matrigel internalisation is upregulated under glutamine-deprived conditions in PDAC cells
(A) SW-1990 and (B) BxPC-3 cells were seeded in full media on a 1mg/ml Matrigel-coated plate labelled with pH Rodo (red) and incubated for 3 hrs. The media were changed to Full media, Glucose-free media and Glutamine-free media, all supplemented with dFBS and incubated overnight. The nuclei were stained with Hoechst 33342 (blue), and the cells were imaged live with a Nikon A1 confocal microscope, 60X objective and the uptake index was analysed using ImageJ. Scale bar 20µm. Data are presented as Mean ± SEM. Significance was determined using Kruskal-Wallis and Dunn's multiple comparisons test, ****p<0.0001, **p<0.01. N=3 independent experiments, and the bigger dots represent the mean of each experiment.

4.2.3 Matrigel internalisation was required for Matrigel-dependent proliferation of glutamine-deprived PDAC cells

As ECM uptake has been shown to represent a nutrient scavenging mechanism in PDAC (Olivares et al., 2017) and our lab recently demonstrated that ECM internalisation was required for breast cancer cell growth under amino acid starvation (Nazemi et al., 2024), we wanted to investigate whether Matrigel internalisation was needed for Matrigel-dependent proliferation of PDAC cells in glucose-free or glutamine-free conditions. We have previously shown that chemical ECM crosslinking, using glutaraldehyde (GA), strongly prevented ECM internalisation (Nazemi et al., 2024). GA is a chemical crosslinking agent that interacts with the amine group of protein (Ma et al., 2014; Kim et al., 2024), creating rigid bonds between ECM components and blocking ECM internalisation. However, while GA is an effective crosslinker, it is potentially cytotoxic (Gough et al., 2002), especially if the concentration is too high. To assess the potential toxicity of GA to PDAC cells, Matrigel was crosslinked using 1%, 2.5%, 5% or 10% GA or left untreated, and SW-1990 cells were seeded in full media on plastic, control or crosslinked Matrigel for 7 days. The cells were fixed, stained with Hoechst33342 and imaged using

an InCell Analyzer 2200. There was no significant difference in cell number between the cells on plastic, Matrigel, or 1% GA crosslinked Matrigel **(Figure 4.6A)**. Similarly, there was no significant difference in cell number between the cells on Matrigel and 2.5% GA crosslinked Matrigel **(Figure 4.6B)**. This suggests that at 2.5% GA concentration, Matrigel crosslinking did not affect the viability of PDAC cells in full media. However, at 5% or 10% GA concentration, there was a progressive reduction in cell number on crosslinked Matrigel, despite the lack of statistical significance between control and crosslinked Matrigel **(Figure 4.6B, C)**. Altogether, the data show a trend that suggests that the higher the concentration of GA, the more toxic it becomes to the PDAC cells.

Given that a GA concentration of 1% and 2.5% resulted in less toxicity, we wanted to assess the ability of GA crosslinking to reduce Matrigel internalisation at these concentrations. To do this, 35mm dishes were coated with Matrigel for at least 1 hour, Matrigel was crosslinked using 1% or 2.5% GA and the dishes were labelled with pHrodo and placed in the incubator overnight. SW-1990 cells were seeded on either the crosslinked dishes or the control dishes overnight before imaging and analysis.

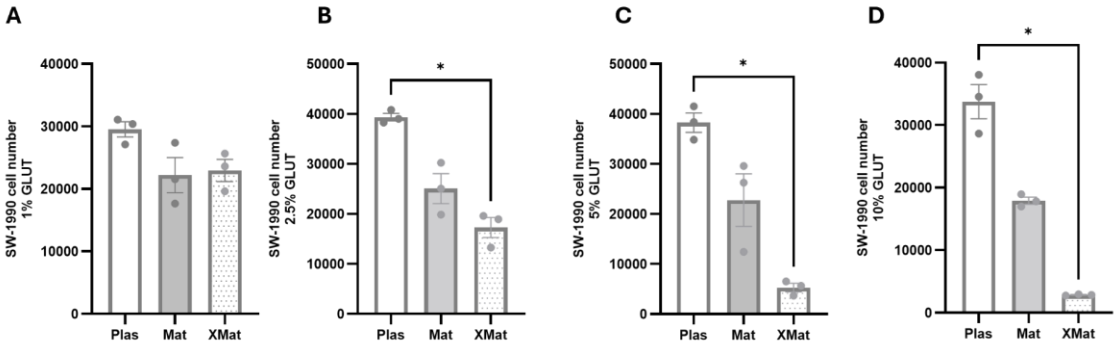

Figure 4.6 – Glutaraldehyde concentration optimisation
SW-1990 cells were seeded in full media on a plastic or 3mg/ml Matrigel-coated plate. Matrigel was crosslinked (XMat) using (A) 1% (B) 2.5% (C) 5% and (D) 10% glutaraldehyde. The cells were fixed and stained with Hoechst 33342 on day 7, imaged using In Cell Analyzer 2200 and analysed using Cell Profiler. Data are presented as Mean ± SEM, significance was determined using Kruskal-Wallis and Dunn's multiple comparisons test. *p<0.05. 3 technical replicates from 1 independent experiment..

As shown in **Figure 4.7**, while Matrigel-containing vesicles were very abundant in cells seeded on control Matrigel, only a few Matrigel puncta were present in the cells upon 1% GA crosslinking, with a further reduction observed upon 2.5% GA crosslinking. Matrigel uptake quantification showed that, compared to the cells seeded on control dishes, there was a significant reduction in Matrigel internalisation when the cells were seeded on both 1% (about 80% reduction) and 2.5% (about 90% reduction) GA crosslinked plates. This shows that both 1% and 2.5% GA concentration were enough to effectively reduce Matrigel internalisation in PDAC cells.

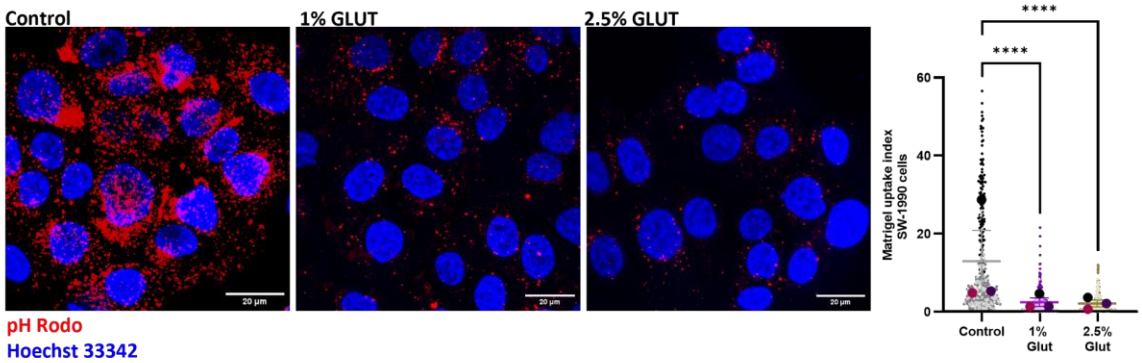

Figure 4.7 – Chemical crosslinking reduced Matrigel Internalisation in SW-1990 cells
SW-1990 cells were seeded on a 1mg/ml Matrigel-coated plate (A) control (non-crosslinked), (B) 1% or (C) 2.5% glutaraldehyde-crosslinked plate labelled with pH Rodo (red) and incubated overnight. The nuclei were stained with Hoechst 33342 (blue). The cells were imaged live with a Nikon A1 confocal microscope, 60X objective and the uptake index was analysed using ImageJ. Scale bar 20µm. Data are presented as Mean ± SEM from 3 independent experiments, with 360 (A), 353 (B), 353 (C) cells analysed per condition, Significance was determined using Kruskal-Wallis and Dunn's multiple comparisons test, ****p<0.0001. The bigger dots represent the mean of each experiment.

Afterwards, we wanted to investigate the impact of Matrigel crosslinking on Matrigel-dependent growth of glucose or glutamine-deprived PDAC cells. Given that 2.5% GA effectively reduced Matrigel internalisation without being toxic to the cells in full media, we used 2.5% of GA to crosslink the ECM for the proliferation experiments. SW-1990 or BxPC-3 cells were seeded on plastic, Matrigel, or 2.5% GA crosslinked Matrigel overnight. The media was changed to full, glucose-free or glutamine-free media, all supplemented with dFBS. The cells were fixed on day 7, stained with Hoechst33342 and imaged using an InCell Analyzer 2200.

Similar to the results in Figure 4.7B**, Figure 4.8A** showed that in SW-1990 cells, compared to cells on plastic, there was a significant reduction in cell number upon Matrigel crosslinking in full media. However, there was no significant difference between the cells on Matrigel and those on crosslinked Matrigel. This again confirmed that Matrigel crosslinking did not affect Matrigel-dependent growth of PDAC cells in full media. In glucose-free conditions, consistent with the results in Chapter 3, there was a significant increase in cell number when the cells were seeded on Matrigel-coated surfaces compared to the cells on plastic. Additionally, our data showed a small but statistically significant increase in cell number upon Matrigel crosslinking compared to the cells on plastic. Furthermore, while not statistically significant, there was a reduction in cell number between the cells on the Matrigel-coated surface and the cells on the crosslinked Matrigel-coated surface **(Figure 4.8B)**. Our data shows that Matrigel crosslinking under glucose-deprivation reduced Matrigel-induced cell proliferation but did not completely prevent it.

In glutamine-free conditions, while there was an expected significant increase in the cell number when the cells were seeded on Matrigel-coated surfaces compared to the cells on plastic, there was no

increase in cell number when the cells were seeded on crosslinked Matrigel-coated surfaces compared to the cells on plastic **(Figure 4.8C)**. This shows that Matrigel crosslinking completely abolished Matrigel-induced proliferation of glutamine-deprived PDAC cells.

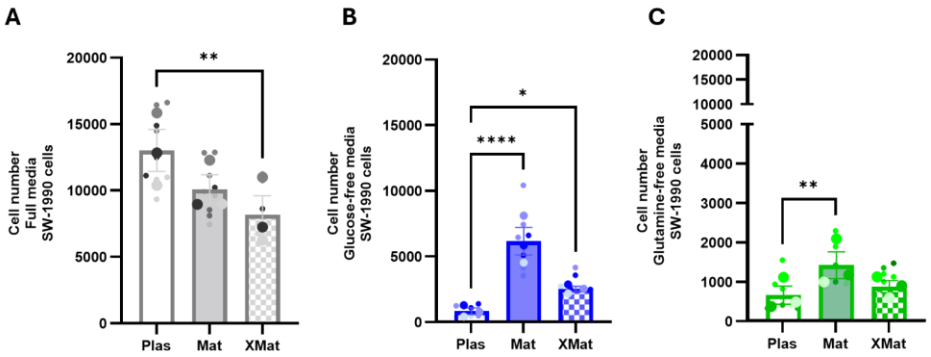

Figure 4.8 – Chemical crosslinking reduced Matrigel-dependent growth of SW-1990 cells under glutamine deprivation

SW-1990 cells were seeded on a plastic, 3mg/ml Matrigel-coated or crosslinked Matrigel-coated plate (XMat) and incubated overnight. The media was changed to (A) Full media, (B) Glucose-free media, or (C) Glutamine-free media, all supplemented with dFBS. The cells were fixed and stained with Hoechst 33342 on day 7, imaged using In Cell Analyzer 2200 and analysed using Cell Profiler. Data are presented as Mean ± SEM. Significance was determined using Kruskal-Wallis and Dunn's multiple comparisons test. ****p<0.0001, **p<0.01, *p<0.05. N=3 independent experiments, and the bigger dots represent the mean of each experiment.

In BxPC-3 cells in full media, there was a substantial reduction that did not reach statistical significance in cell number between the cells on plastic and crosslinked Matrigel and a statistically significant decrease between the cells on Matrigel and crosslinked Matrigel **(Figure 4.9A)**. In glucose-free conditions, we observed a significant increase in cell number when the cells were plated on either Matrigel or crosslinked Matrigel compared to plastic **(Figure 4.9B)**. This suggests that Matrigel crosslinking did not influence Matrigel-induced proliferation of BxPC-3 cells under glucose starvation. Also, we saw that in contrast to cells in full media, there was no difference in cell number between the cells seeded on Matrigel-coated plates and on crosslinked Matrigel-coated plates, suggesting that Matrigel uptake was not required for ECM-dependent cell growth. In glutamine-free conditions, while there was an expected increase in the number of cells on Matrigel-coated plates compared to the cells on plastic, upon crosslinking, the Matrigel-induced increase in cell proliferation was abolished as there was no difference in cell number between the cells on plastic and the cells on crosslinked Matrigel-coated surfaces **(Figure 4.9C)**.

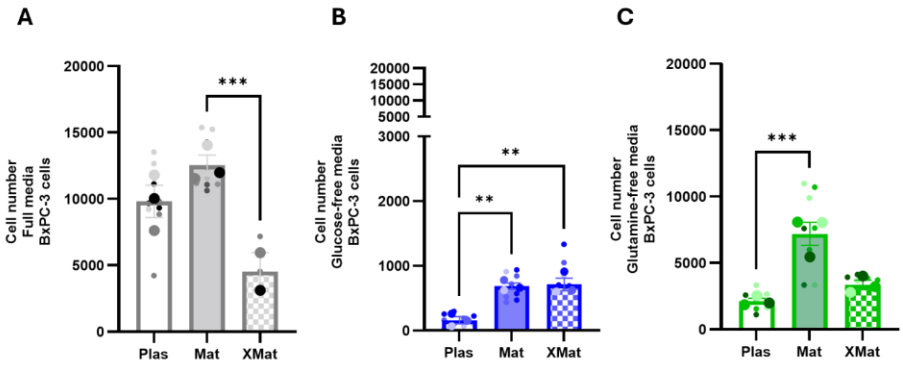

Figure 4.9 – Chemical crosslinking reduced Matrigel-dependent growth of BxPC-3 cells under glutamine deprivation
BxPC-3 cells were seeded on a plastic, 3mg/ml Matrigel-coated or crosslinked Matrigel-coated plate (XMat) and incubated overnight. The media was changed to (A) Full media, (B) Glucose-free media or (C) Glutamine-free media. The cells were fixed and stained with Hoechst 33342 on day 7, imaged using In Cell Analyzer 2200 and analysed using Cell Profiler. Data are presented as Mean ± SEM. Significance was determined using Kruskal-Wallis and Dunn's multiple comparisons test. ***p<0.001, **p<0.01. N=3 independent experiments, and the bigger dots represent the mean of each experiment.

Taken together, our data suggest that Matrigel internalisation is required for the Matrigel-dependent proliferation of glutamine-deprived PDAC cells, while a different mechanism, aside from Matrigel internalisation, might be required for the Matrigel-dependent proliferation of glucose-deprived PDAC cells.

To further validate the role of Matrigel internalisation in supporting Matrigel-dependent growth of glutamine-starved PDAC cells, we examined the effect of LY294002, previously shown to reduce Matrigel internalisation **(Figure 4.3)**. SW-1990 cells were seeded on Matrigel-coated 96-well plates and incubated overnight. The media was changed to full and glutamine-free media, both supplemented with dFBS, in the presence or absence of 5µM LY294002 or DMSO control. On day 7, the cells were fixed, stained with DRAQ5 and imaged using a LICOR Odyssey system.

In full media on plastic, LY294002 significantly reduced cell growth compared to DMSO, indicating that PI3K inhibition negatively impacts PDAC cell proliferation under nutrient-replete conditions. However, on Matrigel, LY294002 had no significant effect, suggesting that Matrigel-dependent growth is independent of macropinocytosis and/or PI3K signalling **(Figure 4.10A)**. In contrast, in glutamine-deprived conditions, LY294002 treatment did not alter the growth of cells on plastic compared to DMSO. Notably, while Matrigel significantly rescued cell proliferation in glutamine-starved cells treated with DMSO, this rescue effect was abolished by LY294002, as cell growth on Matrigel was not different from that on plastic upon treatment with LY294002 (**Figure 4.10B)**. Together, these data support our initial conclusion that ECM internalisation is required for Matrigel-dependent growth of SW-1990 cells under glutamine starvation.

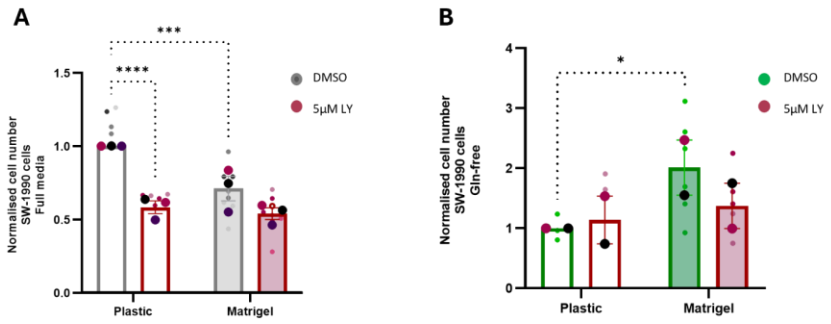

Figure 4.10 – LY294002 reduced Matrigel-dependent growth of SW-1990 cells under glutamine deprivation
SW-1990 cells were seeded on a plastic or 3mg/ml Matrigel-coated plate and incubated overnight. The media was changed to (A) full media or (B) Glutamine-free media, both supplemented with dFBS, and 5μM of LY294002 or DMSO was added to the cells. The cells were fixed, stained with DRAQ5 and imaged with a Licor Odyssey Sa system. The signal intensity was quantified using Image Studio Lite. Data are presented as Mean ± SEM. The data was normalised to the mean of each condition on plastic. Significance was determined by Two-Way Anova with Tukey's multiple comparisons. ***p<0.001, *p<0.05. N ≥2 independent experiments, and the bigger dots represent the mean of each experiment.

4.2.4 mTORC1 activation was required for Matrigel-dependent proliferation of Glucose-deprived PDAC cells

mTOR signalling is vital in regulating cellular metabolism, cell growth and survival (Xu et al., 2025). mTORC1 is activated in the presence of amino acids, glucose and growth factors, resulting in the phosphorylation of S6K and/or 4E-BP1, eventually leading to mRNA translation, protein synthesis and cell survival (Musa et al., 2016). To assess the role of mTORC1 signalling in Matrigel-dependent cell growth, we monitored the phosphorylation of S6 and 4E-BP1 under glucose or glutamine deprivation. SW-1990 cells were seeded on Matrigel-coated 6-well plates or on plastic for 24 hours. The media was changed to full media, glucose-free or glutamine-free media, all supplemented with dFBS, and cells were incubated for 7 days. The cell lysates were collected, and the phosphorylation of both S6 (pS6) and 4E-BP1 (p4E-BP1) was measured via Western blotting. Unexpectedly, as shown in **Figure 4.11A**, there was no reduction in the phosphorylation of S6 in glucose or glutamine-free conditions on plastic compared to full media, and Matrigel did not affect pS6 levels.

Contrary to pS6, we observed a significant reduction in the phosphorylation of 4E-BP1 under both glucose and glutamine-free conditions compared to full media on plastic. Interestingly, glucose-deprivation resulted in a more substantial reduction in p4E-BP1 levels than glutamine-deprivation. Furthermore, Matrigel significantly increased the levels of p4E-BP1 in glucose-free conditions, while there was a small but statistically insignificant increase in glutamine-free conditions. Importantly, Matrigel did not affect 4E-BP1 phosphorylation in full media **(Figure 4.11B)**. This suggests that Matrigel resulted in the reactivation of a specific branch of the mTORC1 signalling pathway under nutrient starvation conditions, promoting 4E-BP1, but not S6, phosphorylation.

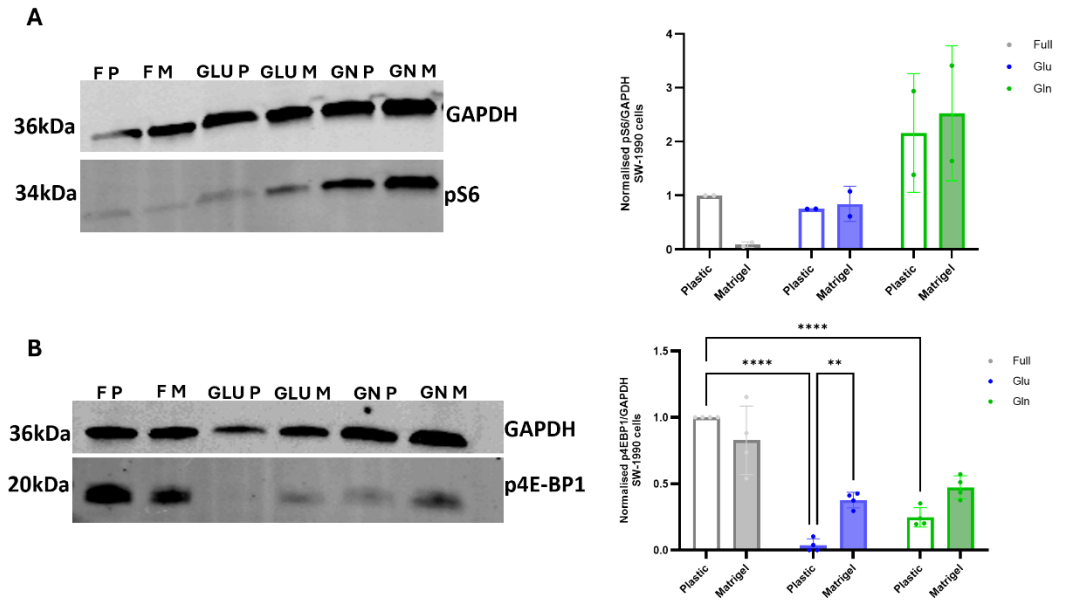

Figure 4.11 – Matrigel rescued mTORC1 activity in SW-1990 cells.
SW-1990 cells were seeded on a plastic or 3mg/ml Matrigel-coated 6-well plate and incubated overnight. The media was changed to full media (Full), glucose-free media (Glu) or glutamine-free media (Gln), all supplemented with dFBS. Cell lysates were collected, and (A) pS6 and GAPDH (control) proteins and (B) p4E-BP1 and GAPDH proteins were analysed via Western blotting. The band intensity was quantified using Image Studio Lite software. Data are presented as Mean ± SEM. Significance was determined by Two-Way Anova with Tukey's multiple comparisons test. ****p<0.0001, **p<0.01. A is N=2, B is N=4 independent experiments.

Given the Matrigel-induced activation of mTORC1 signalling, we hypothesised that mTORC1 activation might be required for Matrigel-induced proliferation in nutrient-starved PDAC cells. To test this, we used TORIN-1, a known mTORC1/2 inhibitor (Francipane and Lagasse, 2013), to deactivate mTOR. SW-1990 cells were seeded on Matrigel-coated 96-well plates and incubated overnight. The media was changed to full, glucose-free or glutamine-free media, all supplemented with dFBS, in the presence or absence of 15nM of TORIN-1 or DMSO. On day 5, the cells were fixed, stained with Hoechst33342 and imaged using an InCell Analyzer 2200. We found that TORIN-1 reduced the cell number in full media, regardless of the presence of Matrigel, indicating that mTOR signalling is required for PDAC cell proliferation **(Figure 4.12A)**. In glucose-free conditions, there was no difference in cell number upon addition of TORIN-1 on plastic, suggesting that inhibition of mTOR had no effect in glucose-deprived cells. Consistent with our previous data, there was a statistically significant increase in cell number on Matrigel compared to plastic upon addition of DMSO. Interestingly, in the presence of Matrigel, there was a small but statistically significant reduction in Matrigel-dependent proliferation of glucose-starved PDAC cells upon addition of TORIN-1 compared to DMSO (**Figure 4.12B)**. Moreover, there was no difference in cell number upon addition of TORIN-1 compared to DMSO on plastic in glutamine-free media, indicating that mTOR inhibition does not affect glutamine-deprived PDAC cells. However, there was a similar increase in cell number between cells on plastic and cells on Matrigel upon the addition of either DMSO or TORIN-1, and there was no reduction in Matrigel-dependent cell proliferation upon the addition of TORIN-1 compared to DMSO **(Figure 4.12C)**. This suggests that

mTOR activation was required for Matrigel-dependent growth of SW-1990 cells in glucose-free media. In contrast, Matrigel-dependent growth of PDAC cells in glutamine-free conditions might be independent of mTOR activation.

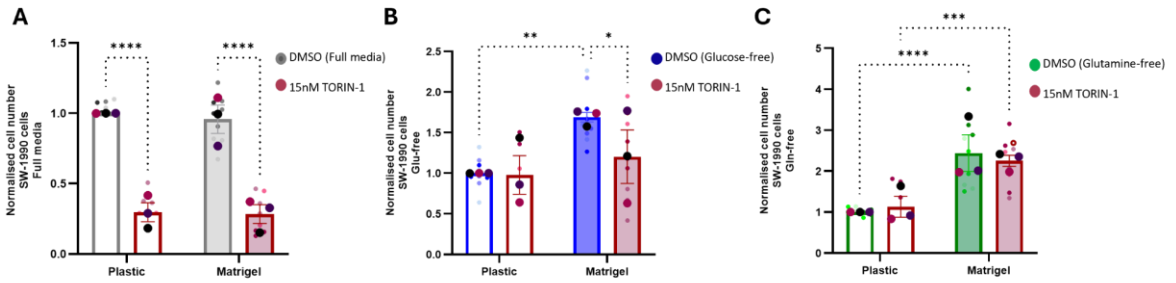

Figure 4.12 – mTOR inhibition reduced Matrigel-dependent cell growth under glucose deprivation
SW-1990 cells were seeded on plastic or a 3mg/ml Matrigel-coated 96-well plate and incubated overnight. The media were changed to (A) full media, (B) glucose-free media, and (C) glutamine-free media, all supplemented with dFBS and 15nM of TORIN-1 or DMSO was added to the cells. The cells were fixed and stained with Hoechst 33342 on day 5, imaged using InCell Analyzer 2200 and analysed using Cell Profiler. Data are presented as Mean ± SEM. The data was normalised to the mean of each condition on plastic. Significance was determined by Two-Way Anova with Tukey's multiple comparisons test. ****p<0.0001, ***p<0.001, **p<0.01, *p<0.05. N=3 independent experiments, and the bigger dots represent the mean of each experiment.

4.3 Discussion

Here, we have shown that PDAC cells use different means of proliferation/survival under glucose or glutamine-deprived conditions. While glutamine-starved PDAC cells upregulated ECM internalisation, glucose-starved PDAC cells did not do so. This suggests that Matrigel-dependent proliferation of glucose-starved PDAC cells was independent of ECM internalisation. Furthermore, while there was a Matrigel-dependent phosphorylation of the mTORC1 target 4E-BP1 under both glucose and glutamine-deprived conditions, inhibition of mTOR only disrupted Matrigel-induced proliferation of glucose-starved PDAC cells. In contrast, Matrigel-induced proliferation of glutamine-starved PDAC cells was unperturbed. This revealed that Matrigel-induced proliferation of glutamine-starved PDAC cells is independent of mTOR signalling **(Figure 4.13)**.

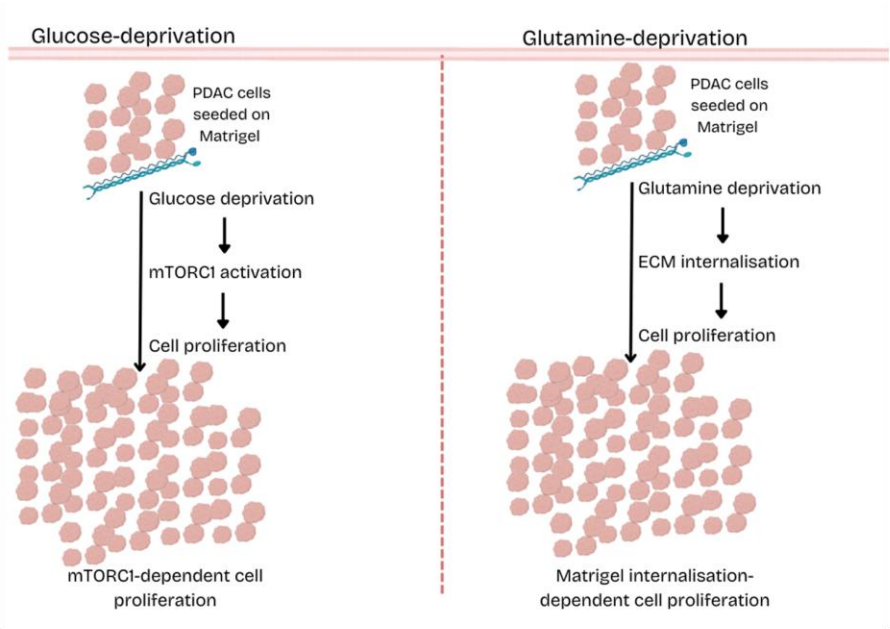

Figure 4.13 – Mechanism of ECM-dependent proliferation of glucose- and glutamine-deprived PDAC cells
Under glucose deprivation, Matrigel activates mTORC1 signalling, and this is required for Matrigel-dependent cell proliferation. Under glutamine deprivation, there is an increase in Matrigel internalisation compared to either glucose deprivation or full media and this internalisation is required for Matrigel–dependent cell proliferation. Created with Canva

Using TMR-dextran uptake as a marker of macropinocytosis, several studies have reported that KRAS-mutated PDAC cells internalise extracellular proteins via macropinocytosis, and EIPA effectively blocked the macropinocytic process (Commisso et al., 2013; Jeong et al., 2018). In agreement with this, EIPA blocked Matrigel internalisation in KRAS-mutated SW-1990 cells. Interestingly, our data revealed similar inhibition of Matrigel internalisation upon addition of EIPA to BxPC-3 cells with wild-type KRAS. However, we saw that upon knockdown of NHE1, while there was a significant reduction in Matrigel internalisation in SW-1990 cells, there was no reduction in Matrigel internalisation in BxPC-3 cells. This could be because the NHE1 knockdown efficiency was not very high in the BxPC-3 cells, and the remaining NHE1 could be sufficient to drive Matrigel internalisation. Also, EIPA has been reported to have NHE1-independent effects on the viability of breast cancer cells (Rolver et al., 2020), and it has been shown to inhibit clathrin-dependent endocytosis in breast cancer cells (Paul et al., 2023). Further work is needed to fully characterise the endocytic pathways controlling Matrigel uptake in BxPC-3 cells. For instance, knocking down PAK1, another key regulator of macropinocytosis (Nazemi et al., 2024), could clarify the role of macropinocytosis in the internalisation of Matrigel in BxPC-3 cells.

Looking at the roles of other endocytic pathways, a recent study in our lab revealed that, in addition to macropinocytosis, breast cancer cells also internalise Matrigel via dynamin-dependent endocytosis. They found that upon pharmacological inhibition of dynamin and lipid raft-mediated endocytosis by the addition of dynasore and filipin, respectively, there was a significant reduction in Matrigel internalisation in MDA-MB-231 cells (Nazemi et al., 2024). Consistent with this, our data showed a

significant decrease in Matrigel internalisation upon addition of dynasore and filipin. Furthermore, our data revealed that dynasore had a more significant effect on Matrigel internalisation. It is important to highlight that dynasore was toxic to the cells, as there was about a 50% reduction in cell number, which could account for the decrease in Matrigel internalisation. Hence, it will be necessary to knock down key regulators of these endocytic processes, like caveolin 1/2 or dynamin 2/3, to validate the results further.

Furthermore, Olivares and colleagues reported an increase in DQ fluorescein collagen-I and IV uptake under both glucose and glutamine-deprived conditions in PK4A PDAC cells compared to full media (Olivares et al., 2017). While we also saw an increase in Matrigel internalisation in glutamine-deprived conditions, we did not see an upregulation of Matrigel internalisation under glucose deprivation. It should be noted, however, that different ECM proteins were used in this study, and this could account for the differences in ECM uptake under nutrient deprivation.

Consistently, we saw that blocking Matrigel internalisation by Matrigel crosslinking had a more significant effect on Matrigel-dependent proliferation of glutamine-deprived PDAC cells than glucose-deprived PDAC cells. This agrees with a previous study in our lab that revealed that collagen-I internalisation was not required for collagen-I-dependent proliferation of breast and pancreatic cancer cells under glucose starvation (Nazemi et al., ms in preparation). Our data revealed that Matrigel internalisation was upregulated under glutamine starvation and was essential for Matrigel-dependent proliferation of glutamine-deprived PDAC cells. The next interesting step will be to identify the specific endocytic processes that facilitate Matrigel uptake, as targeting those processes may provide a strategy to inhibit Matrigel internalisation and selectively disrupt glutamine metabolism in nutrient-deprived PDAC cells. Also, while the reduced cell growth observed upon Matrigel crosslinking could be attributed to changes in its mechanical properties, such as increased stiffness, the inhibition of macropinocytosis with LY294002 produced a similar reduction in Matrigel-induced cell proliferation under glutamine-deprived conditions. This finding supports the conclusion that Matrigel internalisation is indeed required for Matrigel-induced cell growth in the absence of glutamine.

Changes in nutrient levels are well established to affect mTORC1 (Palm et al., 2015). Consistently, we found that 4E-BP1 phosphorylation downstream of mTORC1 was suppressed under nutrient deprivation. However, we saw a Matrigel-induced reactivation of mTORC1 signalling under nutrient-deprived conditions, as evidenced by phosphorylation of 4E-BP1. Surprisingly, in contrast to 4E-BP1 phosphorylation, we saw that the phosphorylation of S6 was not influenced by either nutrient starvation or the presence of Matrigel, suggesting that Matrigel-induced activation of mTORC1 might be specific for some targets. This agrees with the study by Olivares et al, where there was no collagen-

I or IV-dependent phosphorylation of S6 under glucose and glutamine starvation, which led them to conclude that collagens I or IV did not rescue mTORC1 activity under glucose or glutamine-starved conditions (Olivares et al., 2017). However, their study did not report on the activation of mTORC1 via phosphorylation of 4E-BP1. Unpublished data from our lab indicate that integrin signalling might control mTORC1 activation in glucose-deprived breast cancer and PDAC cells (Nazemi et al., ms in preparation). It would be interesting to determine whether laminin or collagen IV receptors are involved in this process and, if so, through which signalling pathway. Laminin internalisation was shown to sustain mTOR activation in serum-starved mammary epithelial cells (Muranen et al., 2017); however, our data suggest that ECM internalisation is not involved in our system. Further work is also needed to determine whether other mTORC1 targets, such as ULK1, SREBP, Lipin-1 and TFEB, are involved.

While it remains unclear why Matrigel-induced mTORC1 activation was only associated with phosphorylation of 4E-BP1 and not S6, it is likely linked to the downstream signalling pathways specific to 4E-BP1. PDAC cells have been reported to rely on the activity of e1F4A, one of the e1F4F complexes required to initiate cap-dependent mRNA translation (Chan et al., 2019). Using both in vitro murine pancreatic organoid model and in vivo orthotopic transplant model, Chan et al found that upon selective inhibition of e1F4A by CR-1-31B, there was a reduction in protein synthesis, cell viability and tumour growth (Chan et al., 2019).

Similarly, in a study by Martineau and colleagues, immunohistochemistry staining of both normal and PDAC patient samples revealed that, unlike in normal pancreas, where 4E-BP1 is expressed abundantly, there was a significantly reduced expression of 4E-BP1 protein in PDAC samples studied (Martineau et al., 2014). Their study further revealed that the loss of 4E-BP1 in PDAC cells promoted the assembly of the e1F4F complexes and allowed the phosphorylation of e1F4E, which subsequently resulted in an increased tumour growth in nude mice (Martineau et al., 2014). Altogether, these findings indicate that the e1F4F complexes play an important role in the proliferation of PDAC cells, and the Matrigel-dependent phosphorylation of 4E-BP1 upon mTORC1 activation might support the formation of the e1F4F complexes to aid cell proliferation.

We observed that inhibition of mTORC1/2 with TORIN-1 significantly reduced cell numbers under nutrient-replete conditions. However, consistent with our observation that mTORC1 activity is suppressed during glucose or glutamine starvation, TORIN-1 treatment did not further reduce cell numbers when cells were cultured on plastic under either glucose- or glutamine-deprived condition. Consistent with this, Khan et al found that glutamine-deprived hepatocellular carcinoma (HCC) cells were insensitive to TORIN-1 (Khan et al., 2018). Examining the effects of mTOR inhibition in Matrigel-

induced cell growth, our data revealed that the Matrigel-dependent activation of mTORC1 signalling under glucose starvation was accompanied by a reduction in Matrigel-dependent cell proliferation following TORIN-1 treatment. This observation is consistent with previous reports that mTOR activation promotes DNA synthesis, protein translation, and subsequent cell proliferation (Musa et al., 2016).

In contrast, TORIN-1 treatment did not reduce Matrigel-dependent cell growth under glutamine-starved conditions, indicating that mTOR activation was not required for Matrigel-driven proliferation of glutamine-deprived PDAC cells. Consistent with this, Kim et al. reported that glutamine-deprived PDAC cells supplemented with BSA were insensitive to TORIN-1, whereas those supplemented with 4mM glutamine were TORIN-1 sensitive. Under glutamine deprivation, BSA supplementation increased the viability of MIA PaCa-2 cells through macropinocytic uptake. However, TORIN-1 treatment reduced viability only in glutamine-supplemented cells and did not affect BSA-supplemented ones (Kim et al., 2022).

It is important to note that the inhibitor used in this study, TORIN-1, prevents the activation of both mTORC1 and mTORC2, so we cannot rule out an additional role of mTORC2 in controlling cell proliferation under glucose starvation. Indeed, mTORC2 has been reported to be activated by glucose starvation, resulting in increased AKT phosphorylation (Moloughney et al., 2016). It will therefore be important to determine the individual contributions of mTORC1 and mTORC2 by knocking down Raptor and Rictor, essential components of the mTORC1 and mTORC2 complexes, respectively.

Altogether, given that glucose and glutamine are two of the most important nutrients for tumour metabolism (Palm and Thompson, 2017), understanding how tumour cells adapt to survive in their absence is vital in targeting tumour metabolism. Our data have revealed that PDAC cells upregulate different pathways when grown under glucose- or glutamine-deprived conditions. Upon glutamine starvation, increased Matrigel internalisation promoted ECM-dependent cell growth; while under glucose starvation, the 4E-BP1 pathway downstream of mTORC1 was required to facilitate Matrigel-dependent proliferation.

The TME of PDAC tumours will likely present varying levels of both nutrients; therefore, a combination approach targeting both mTOR and ECM internalisation is more likely to be beneficial in vivo. This could be investigated using TIFM, which more closely recapitulates the TME nutrient levels, to determine the impact of ECM uptake and mTOR signalling on ECM-dependent cell growth.

5 Matrigel altered the metabolism of nutrient-deprived PDAC cells

5.1 Introduction

Cancer is a metabolic disease, with metabolic alteration as one of the hallmarks of cancer (Gyamfi et al., 2022; Hanahan and Weinberg, 2011; Schmidt et al., 2021). Cancer cells modify their metabolism to meet nutrient and energy requirements, allowing them to survive and thrive in an otherwise inhospitable microenvironment (Danzi et al., 2023; Suri et al., 2023). In oncology, this unique ability of cancer cells presents a therapeutic opportunity, as these altered metabolic pathways could be studied based on their unique metabolite features to develop markers for diagnostic purposes. Also, the reliance of cancer cells on specific metabolic pathways presents an opportunity for targeted treatment options (Schmidt et al., 2021). As a result, it is vital to understand the metabolic changes in cancers, such as PDAC cells that survive in a nutrient-deprived microenvironment. One of the ways of understanding these metabolic changes is metabolomics.

Metabolomics is one of the -omics technologies that has started to gain recognition in cancer research. Using different state-of-the-art techniques such as Mass spectrometry (MS) and Nuclear Magnetic Resonance (NMR), metabolomics is used to detect a pool of metabolites in cells, tissue or blood samples and identify metabolic changes that occur (Beger, 2013). With metabolomics, cancer researchers can characterise the metabolic alterations that occur in cancer cells, test hypotheses and identify common biomarkers that could aid in diagnosis, treatment and subsequent monitoring of cancer (**Figure 5.1)**.

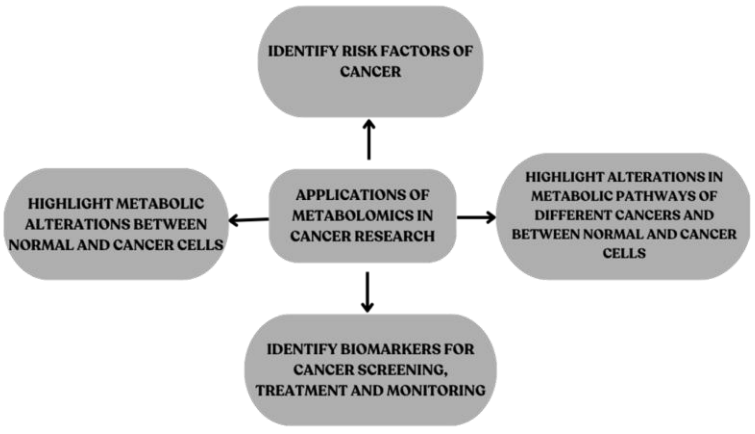

Figure 5.1 - An overview of the Applications of Metabolomics in Cancer Research
Adapted from Schmidt et al., 2021. Created with Canva

Metabolomics approaches are classified into untargeted and targeted. Untargeted metabolomics gives a comprehensive overview of all the metabolites present in each sample, while targeted metabolomics, as its name implies, gives precise quantification of specific metabolites present in a given sample based on a reference standard for each metabolite to be analysed.

In chapter 3, we showed that Matrigel and collagen-I supported the proliferation of nutrient-deprived PDAC cells, and we found that Matrigel had a more pronounced effect on PDAC cells in most nutrient-starved conditions studied. Given that Matrigel partially rescued the growth of PDAC cells under nutrient deprivation, we hypothesised that Matrigel could remodel the metabolism of PDAC cells to support their growth under nutrient deprivation.

5.2 Results

5.2.1 Untargeted metabolomics revealed Matrigel-dependent metabolic reprogramming in nutrient-deprived PDAC cells

An untargeted metabolomics approach was used to highlight the differentially expressed metabolites in PDAC cells on plastic or Matrigel. SW-1990 and MIA PaCa-2 cells were seeded on either plastic or Matrigel-coated 6-well plates and incubated for 24 hours. The media was changed to full media, glucose-free media, glutamine-free media or TIFM, incubated for 7 (SW-1990 cells) or 6 (MIA PaCa-2 cells) days, and imaged before the metabolites were extracted **(Figure 5.2)**.

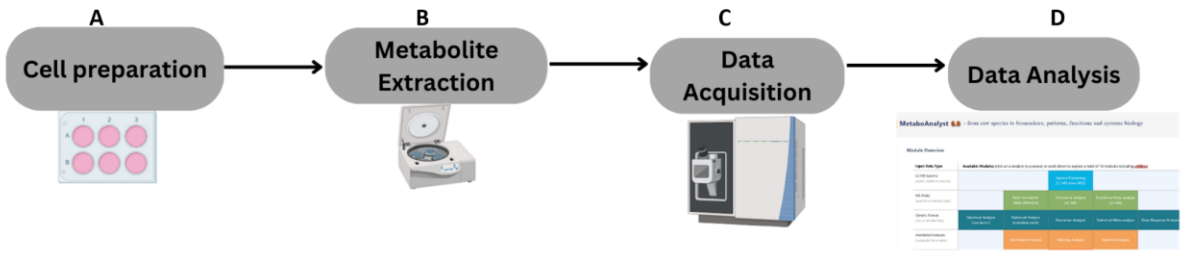

Figure 5.2 – A schematic representation of the Metabolomics Workflow
(A) PDAC cells were seeded on plastic or Matrigel-coated 6-well plates overnight. The media was changed to different starvation conditions and placed in the incubator for 6 or 7 days. (B) 800µl of metabolite extraction solution was added to each well and centrifuged at 14,000rpm, 4°C for 10 minutes to extract the metabolites. (C) The samples were run using a Waters G2 Synapt mass spectrometer in electrospray mode. (D) The data was analysed using Perseus software, and the enrichment analysis was done using the MetaboAnalyst 6.0 software. Created with Canva and Biorender.

Consistent with our results in Chapter 3, bright field imaging showed a Matrigel-dependent increase in cell proliferation under nutrient deprivation (**Figure 5.3).**

Next, the metabolites were extracted, and Ultra-Performance Liquid Chromatography-Mass spectrometry (UPLC-MS)-based untargeted metabolomics was used to identify the metabolites in the samples. The data were analysed using Perseus software to determine the metabolites that were significantly altered between the cells on Matrigel or plastic across all the conditions tested.

Table 5.1 Number of metabolites upregulated on either plastic or Matrigel. The differential metabolite abundance was generated by comparison analysis and determined in Perseus. S_o = 0.1, FDR < 0.05, N = 1.

Nutrient deprivation conditions	Number of upregulated metabolites (SW-1990 cells)	Number of upregulated metabolites (MIA PaCa-2 cells)
Full media Plastic	1202	1077
Full media Matrigel	722	1216
Glucose-free Plastic	392	1809
Glucose-free Matrigel	324	2043
Glutamine-free Plastic	1824	644
Glutamine-free Matrigel	1422	519
TIFM Plastic	1378	2060
TIFM Matrigel	1443	1882

In both SW-1990 and MIA PaCa-2 cells, there were some differentially expressed metabolites when the cells were plated on either Matrigel or plastic across all starvation conditions studied; with some metabolites slightly higher on Matrigel, while some were slightly higher on plastic **(Table 5.1).**

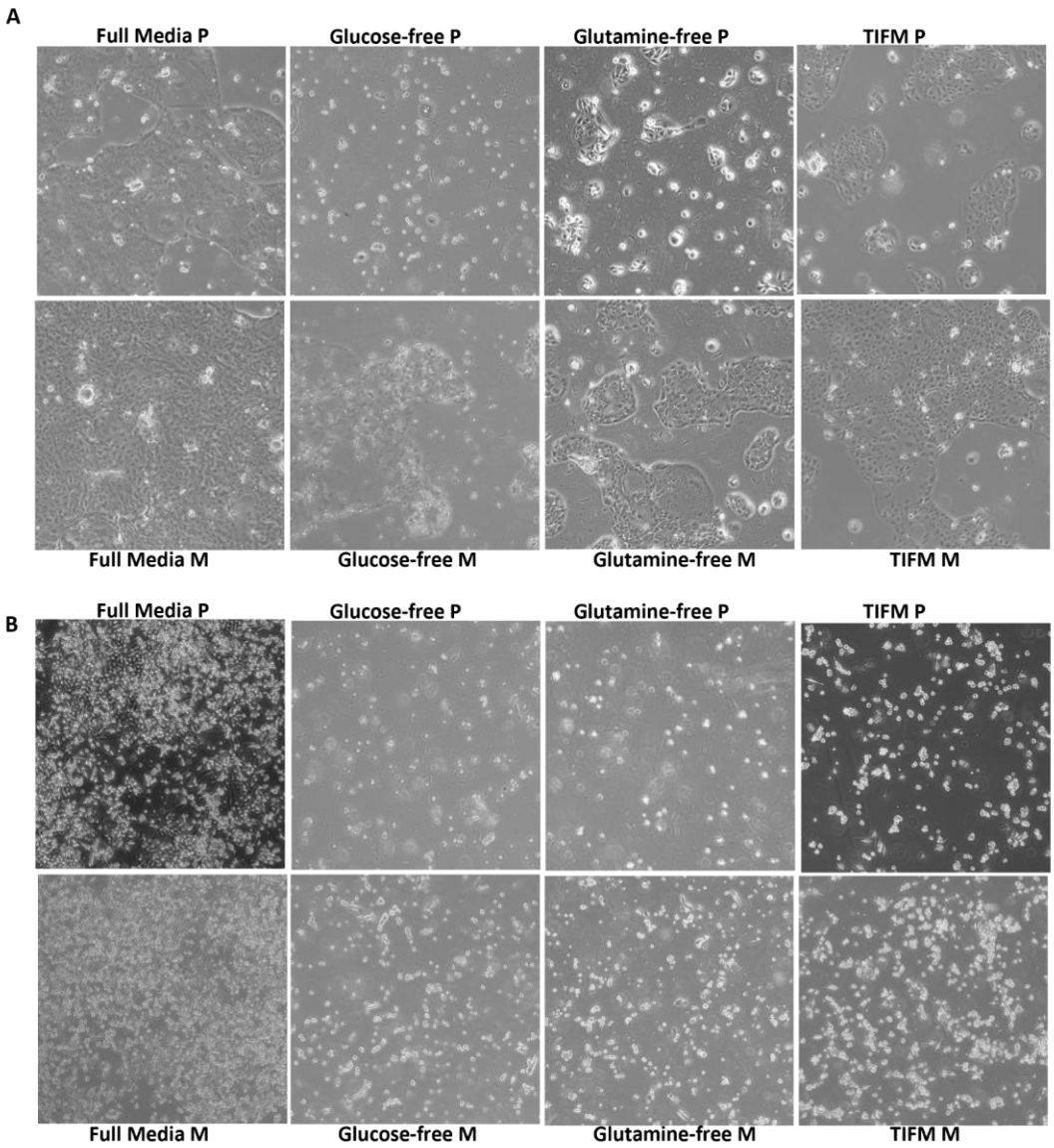

Figure 5.3 – Matrigel rescued PDAC cell growth under nutrient deprivation.
(A) SW-1990 and (B) MIA PaCa-2 cells were seeded on a plastic (P) or 3mg/ml Matrigel-coated (M) 6-well plate. The media was changed to full media, glucose-free media, glutamine-free media and TIFM, all supplemented with dFBS after 24 hours. The cells were incubated for 7 days and imaged live on Day 7 with the Olympus E450 Microscope, 10X magnification.

The red dots in the volcano plots represent metabolites that were significantly higher on either Matrigel or plastic, while the grey dots represent the metabolites that were not significantly changed **(Figure 5.4).** Overall, our results indicated that Matrigel altered the metabolite content of PDAC cells, and the changes were consistent across the two cell lines studied.

A

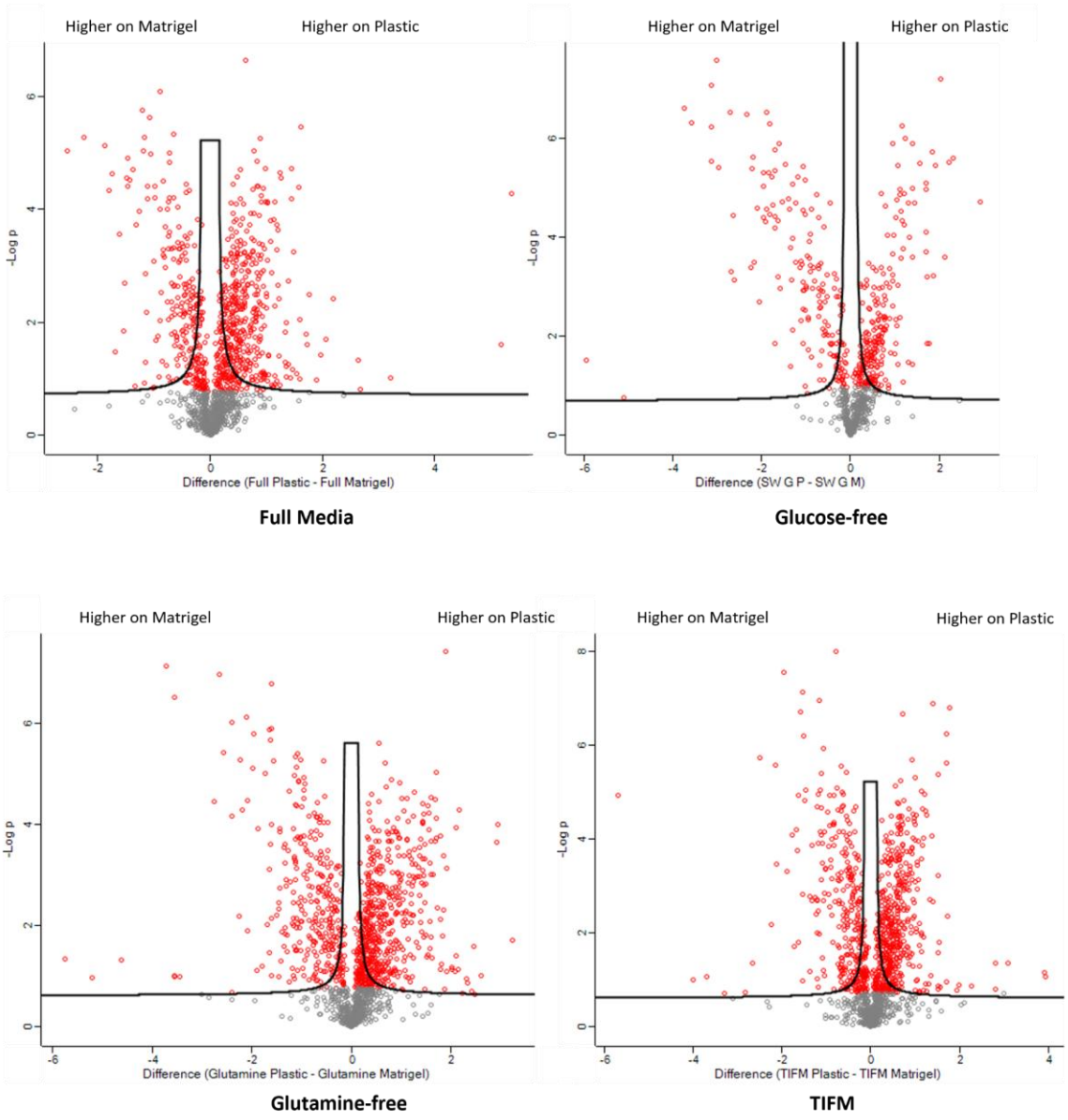
Higher on Matrigel
Higher on Plastic
-Log p
Difference (Full Plastic - Full Matrigel)
Full Media
Higher on Matrigel
Higher on Plastic
-Log p
Difference (SW G P - SW G M)
Glucose-free
Higher on Matrigel
Higher on Plastic
-Log p
Difference (Glutamine Plastic - Glutamine Matrigel)
Glutamine-free
Higher on Matrigel
Higher on Plastic
-Log p
Difference (TIFM Plastic - TIFM Matrigel)
TIFM

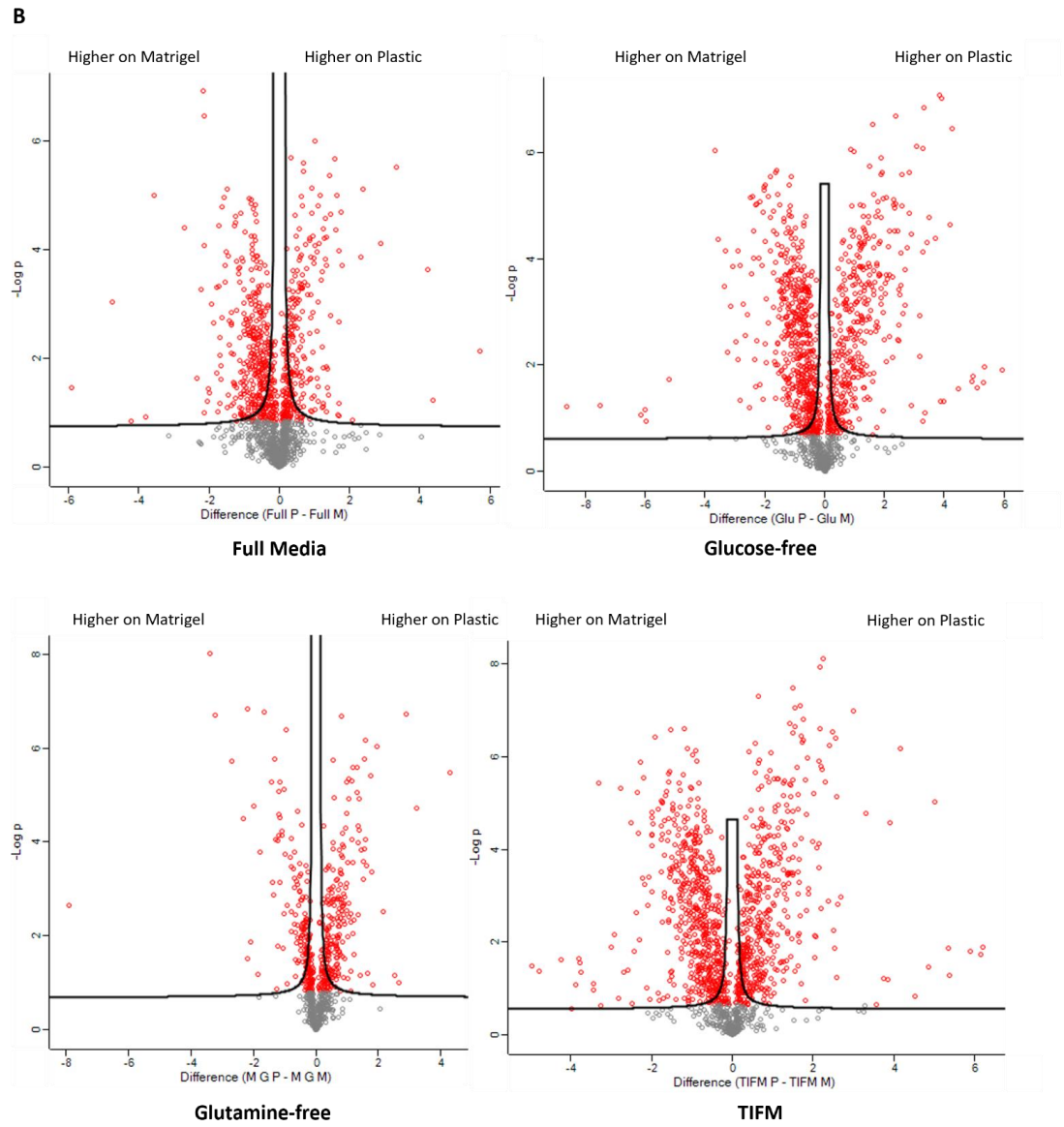

Figure 5.4 – Matrigel altered the metabolite content of PDAC cells.
(A) SW-1990 and (B) MIA PaCa-2 cells were seeded on a plastic or 3mg/ml Matrigel-coated 6-well plate. After 24 hours, the media was changed to full media, glucose-free media, glutamine-free media, and TIFM, all supplemented with dFBS and the cells were incubated for 7 days. Metabolites were extracted and analysed by untargeted LC-MS. The data was analysed using Perseus. Raw intensity values were log2-transformed before statistical analysis. Differential abundance between plastic and Matrigel conditions was assessed by a two-sample Student's T-test with an S_0 parameter of 0.1. Statistical significance was determined at FDR < 0.05. The statistically significantly higher metabolites are shown in red, while the non-significant metabolites are shown in grey.

5.2.2 Untargeted metabolomics identified Matrigel-induced upregulation of arginine and proline metabolism in nutrient-deprived PDAC cells

Given that there was a Matrigel-induced change in the metabolite content of the cells, we wanted to determine the specific metabolic pathways that were altered in the presence of Matrigel. To do this, the MetaboAnalyst database was used to perform an Enrichment Analysis. The significantly higher metabolites across each condition were uploaded to the MetaboAnalyst database and cross-

referenced to the metabolites deposited in the Human Metabolome Database. The identified metabolites were deposited on the Small Molecule Pathway Database (SMPDB) to map them to the normal human metabolic pathways on the SMPDB. **Figure 5.5** shows the top 25 enriched metabolic pathways on either plastic or Matrigel across all conditions tested in SW-1990 cells. Arginine and proline metabolism, purine metabolism and aspartate metabolism are among the top 10 upregulated metabolic pathways upregulated only in the presence of Matrigel across all the starvation conditions tested.

Glucose-free P

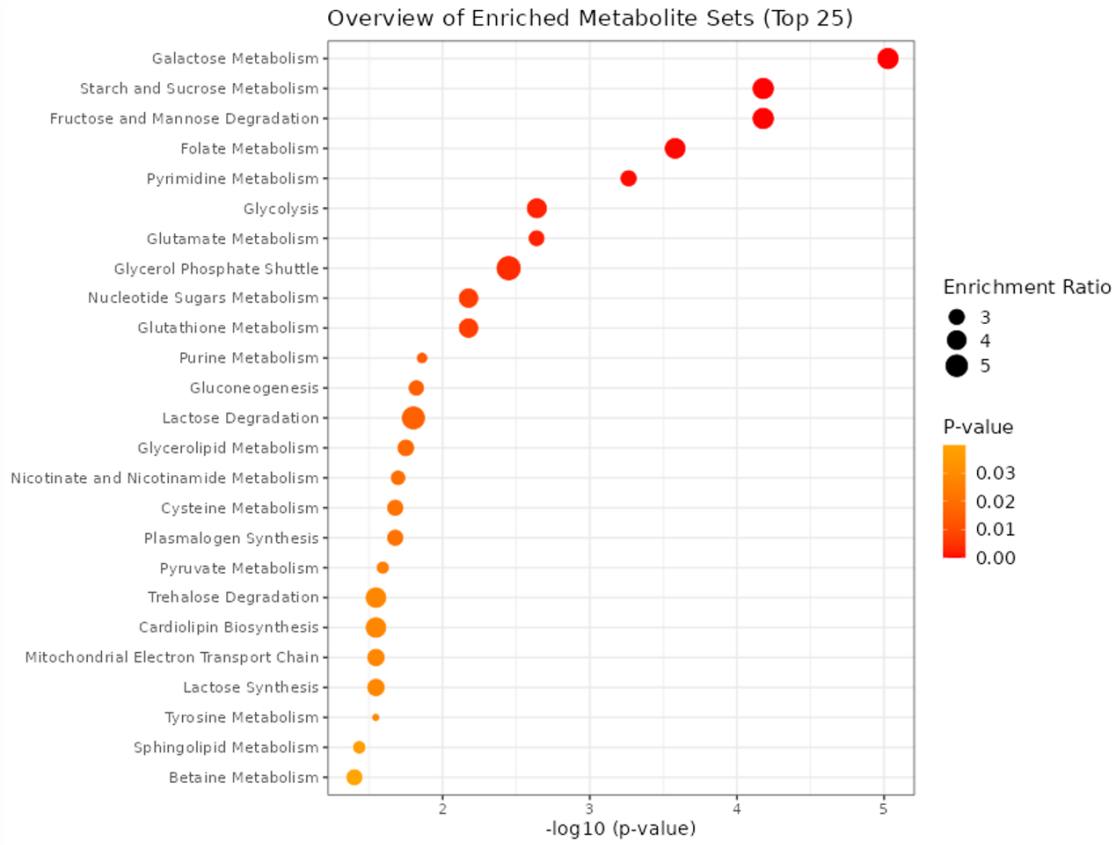

Glucose-free M

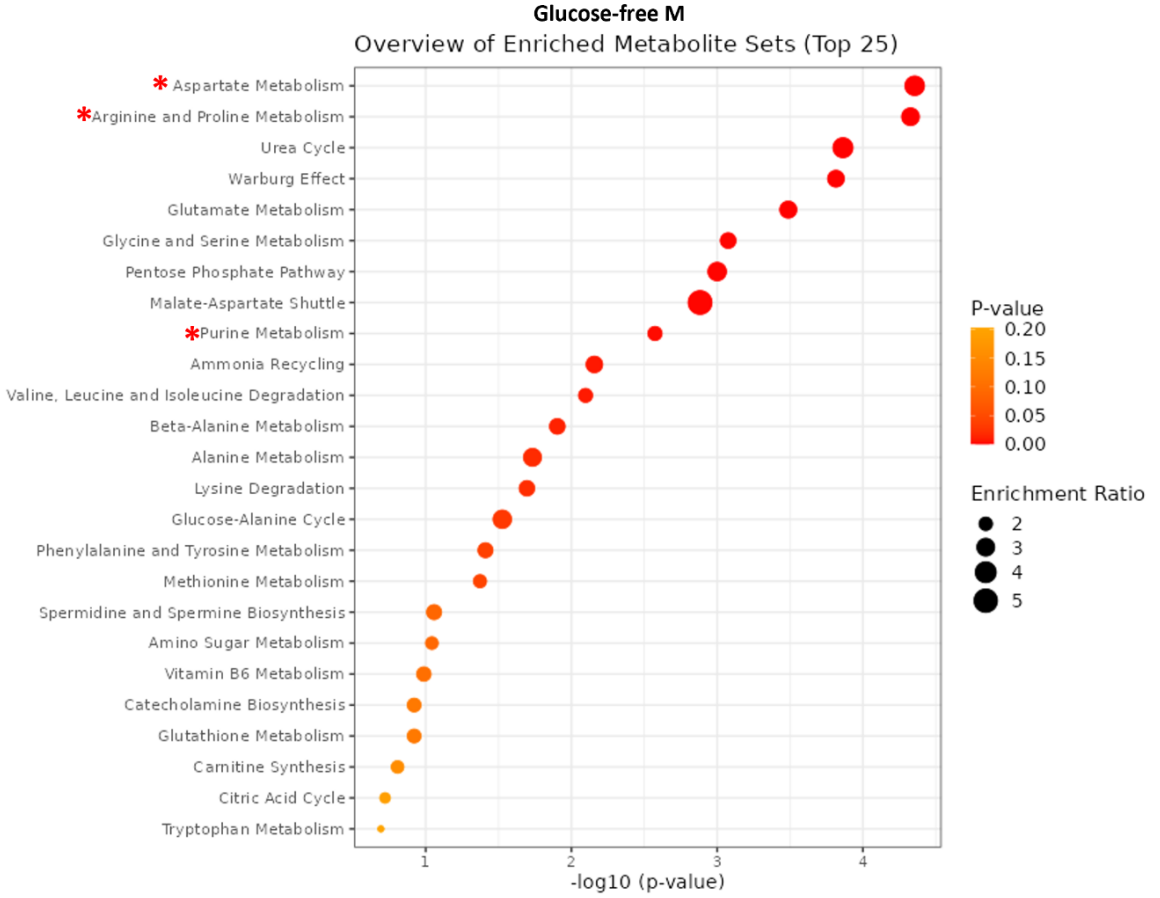

Glutamine-free P

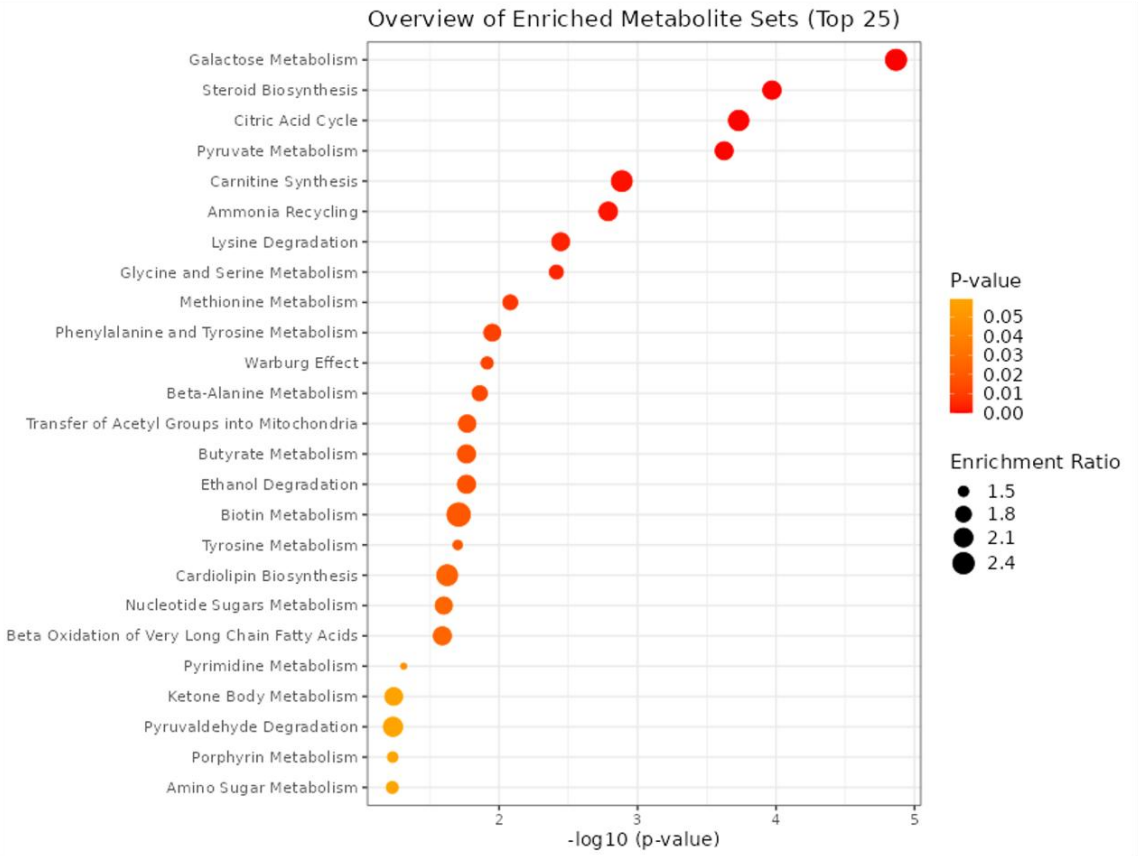

Glutamine-free M

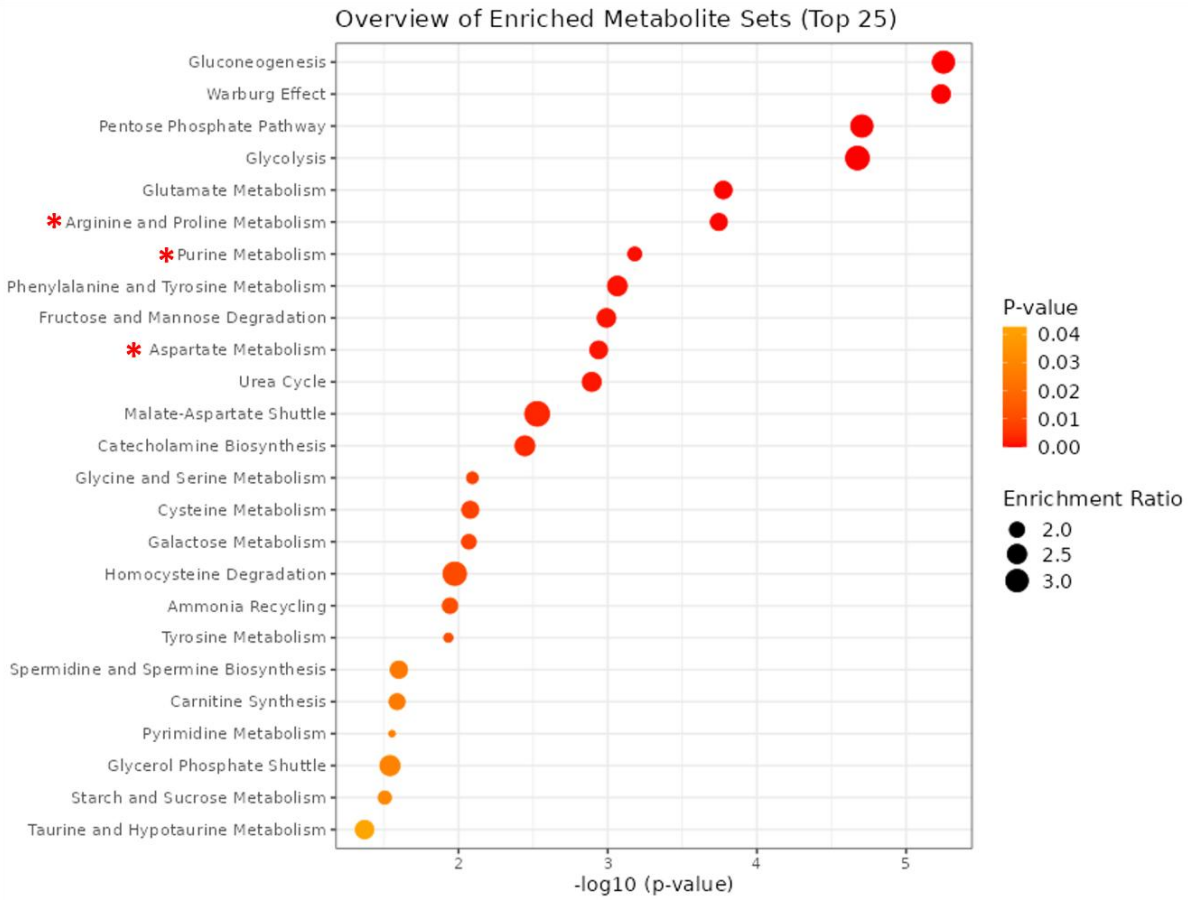

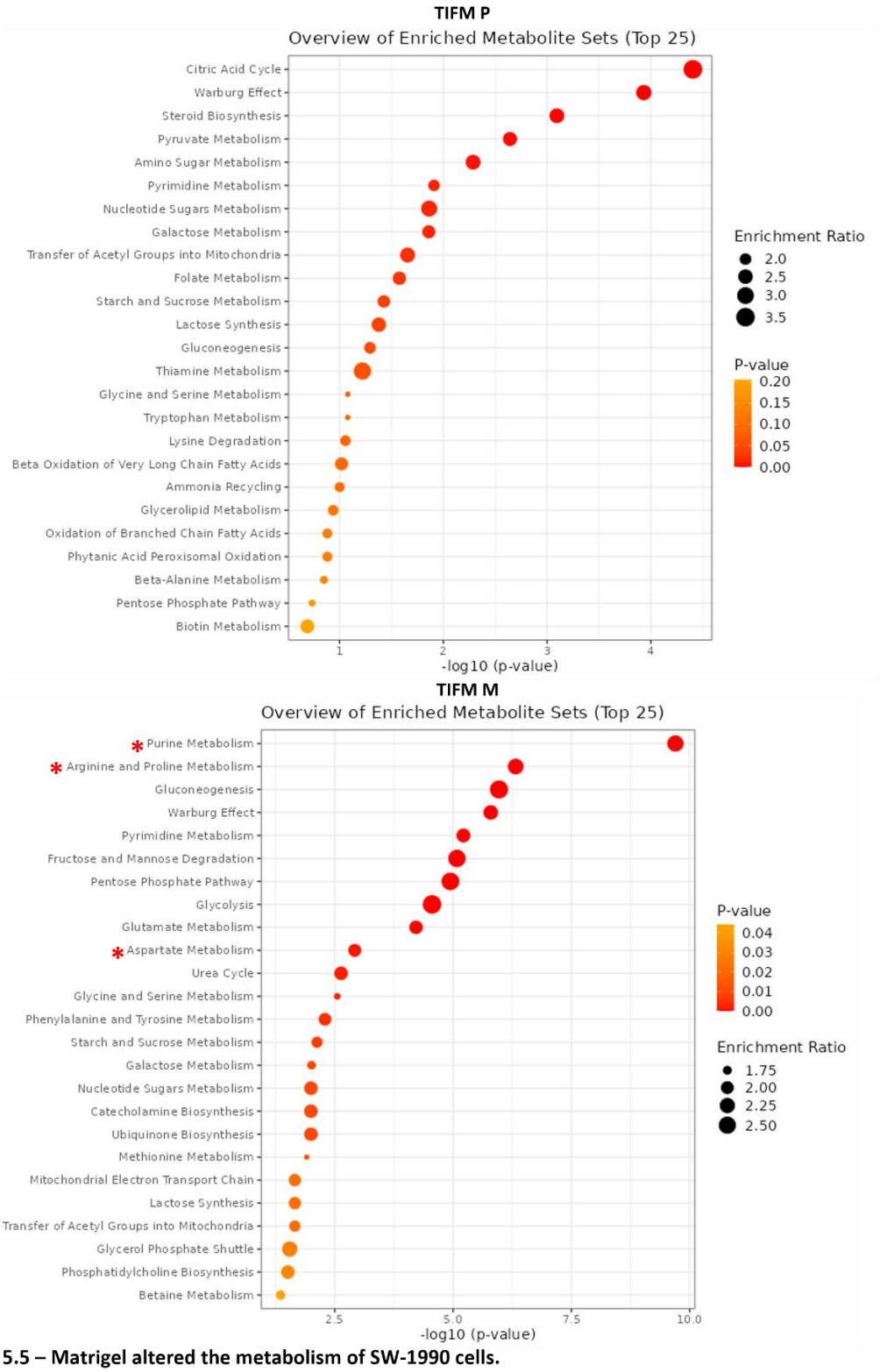

Figure 5.5 – Matrigel altered the metabolism of SW-1990 cells.
SW-1990 cells were seeded on a plastic (P) or 3mg/ml Matrigel-coated (M) 6-well plate. After 24 hours, the media was changed to full media, glucose-free media, glutamine-free media, and TIFM, all supplemented with dFBS and the cells were incubated for 7 days. Metabolites were extracted and analysed by untargeted LC-MS. The data was analysed using Perseus. Pathway enrichment analysis was performed in MetaboAnalyst 6.0. In the bubble plot, bubble size represents the number of significant metabolite hits mapped to each pathway, with larger bubbles indicating greater pathway coverage. Pathways were considered significantly enriched based on p-value.

Similarly, in MIA PaCa-2 cells, arginine and proline metabolism, glycine and serine metabolism and aspartate metabolism were among the top 10 upregulated metabolic pathways upregulated only in the presence of Matrigel across full media and all the starvation conditions tested, except in glucose-free conditions, where glycine and serine metabolism are not among the top 10 upregulated pathways **(Figure 5.6)**.

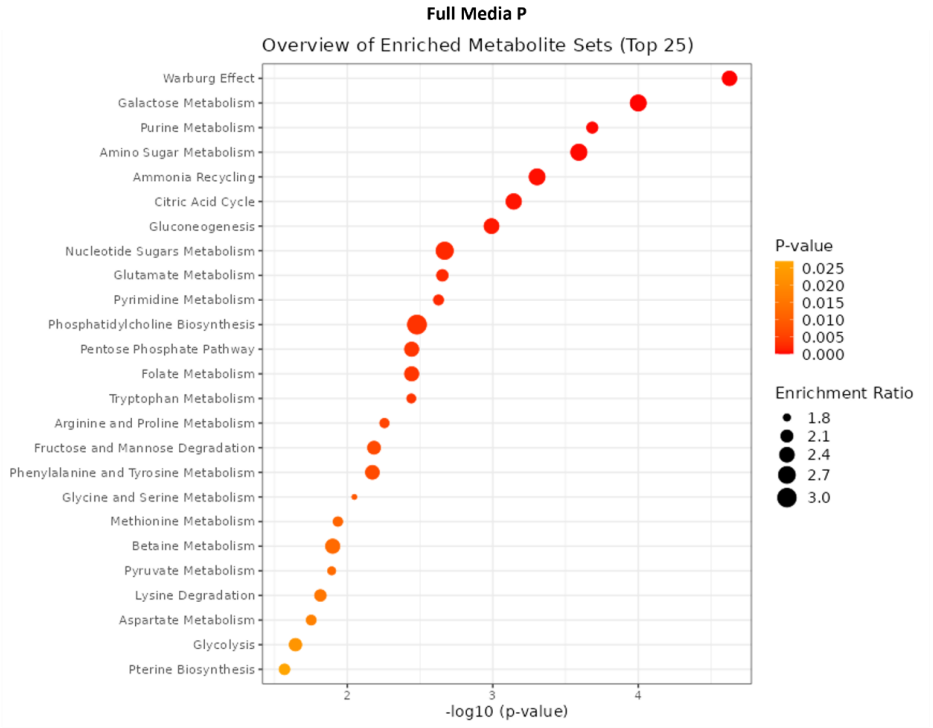

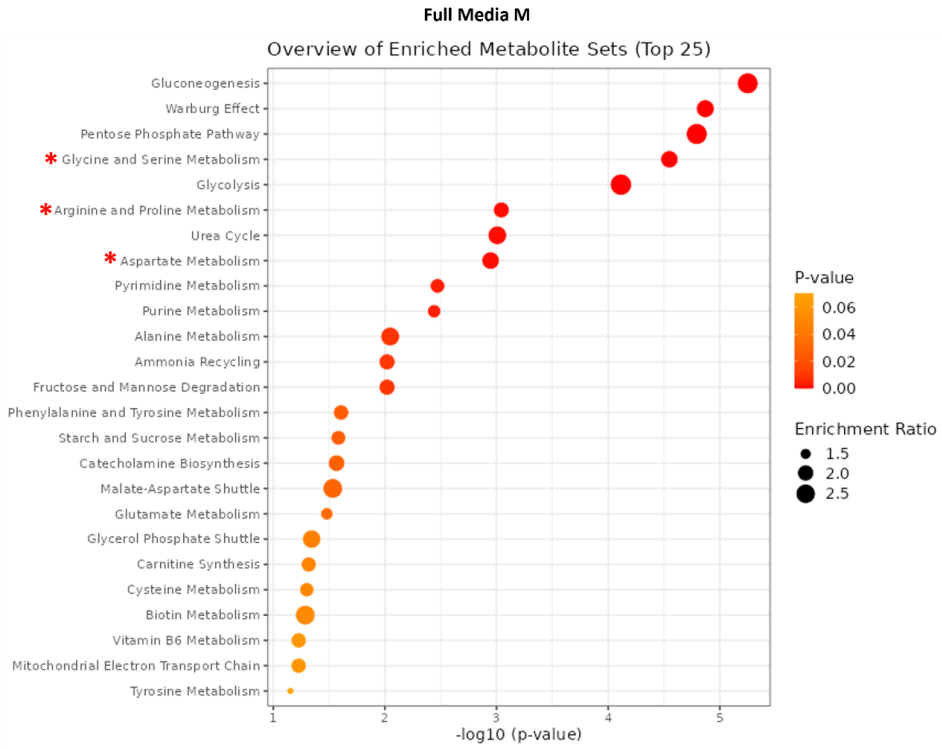

Glucose-free P

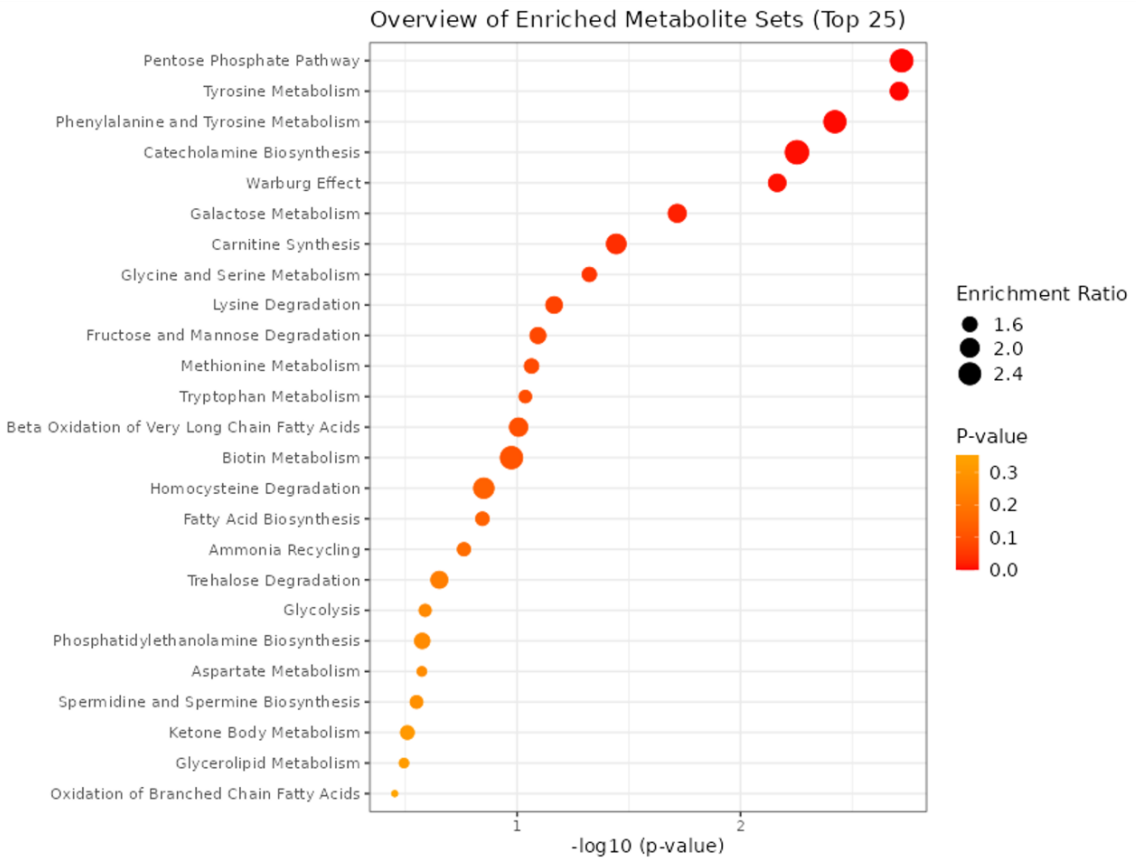

Glucose-free M

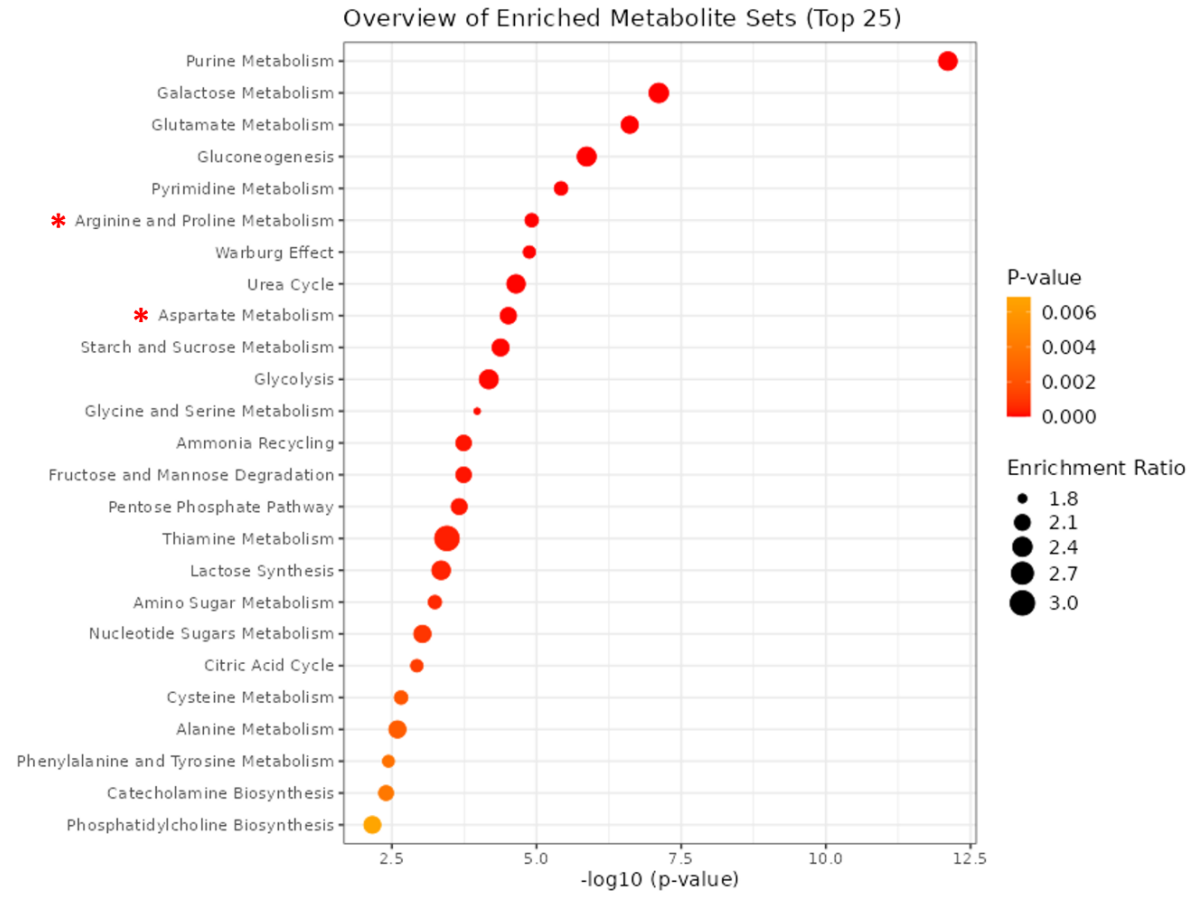

Glutamine-free P

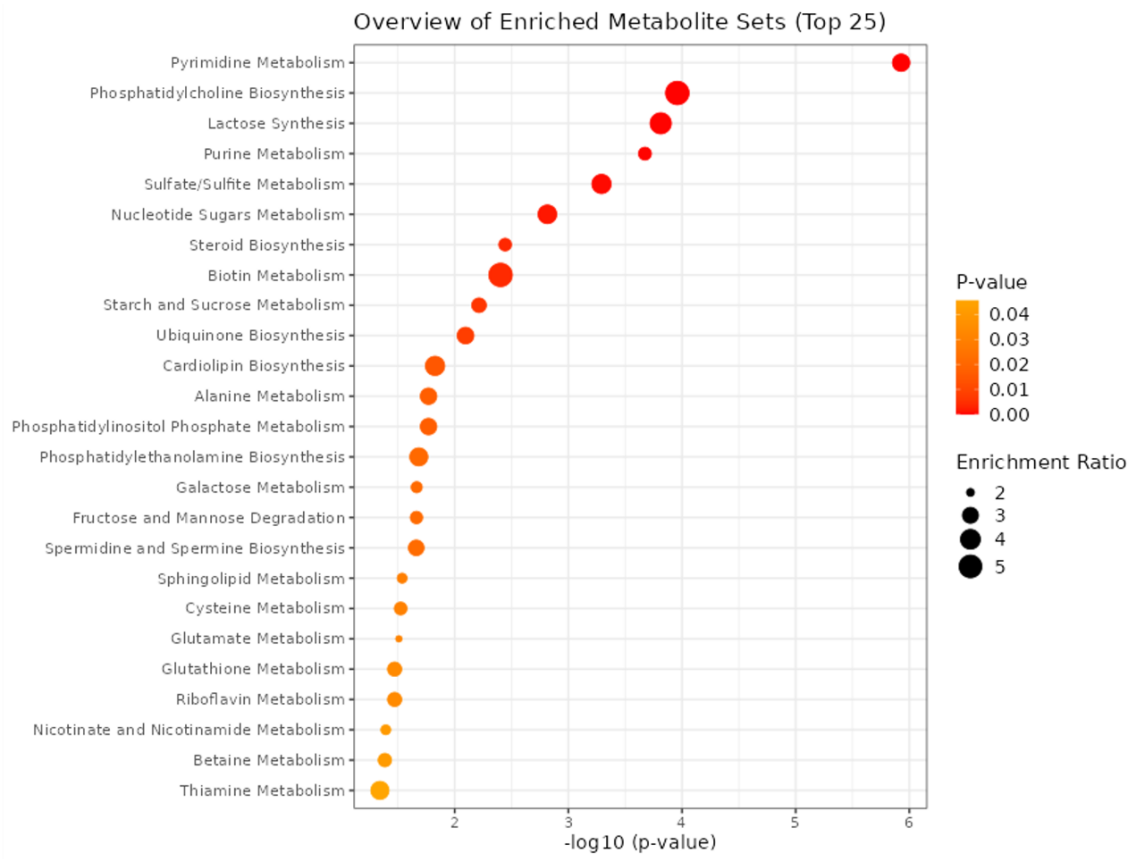

Glutamine-free M

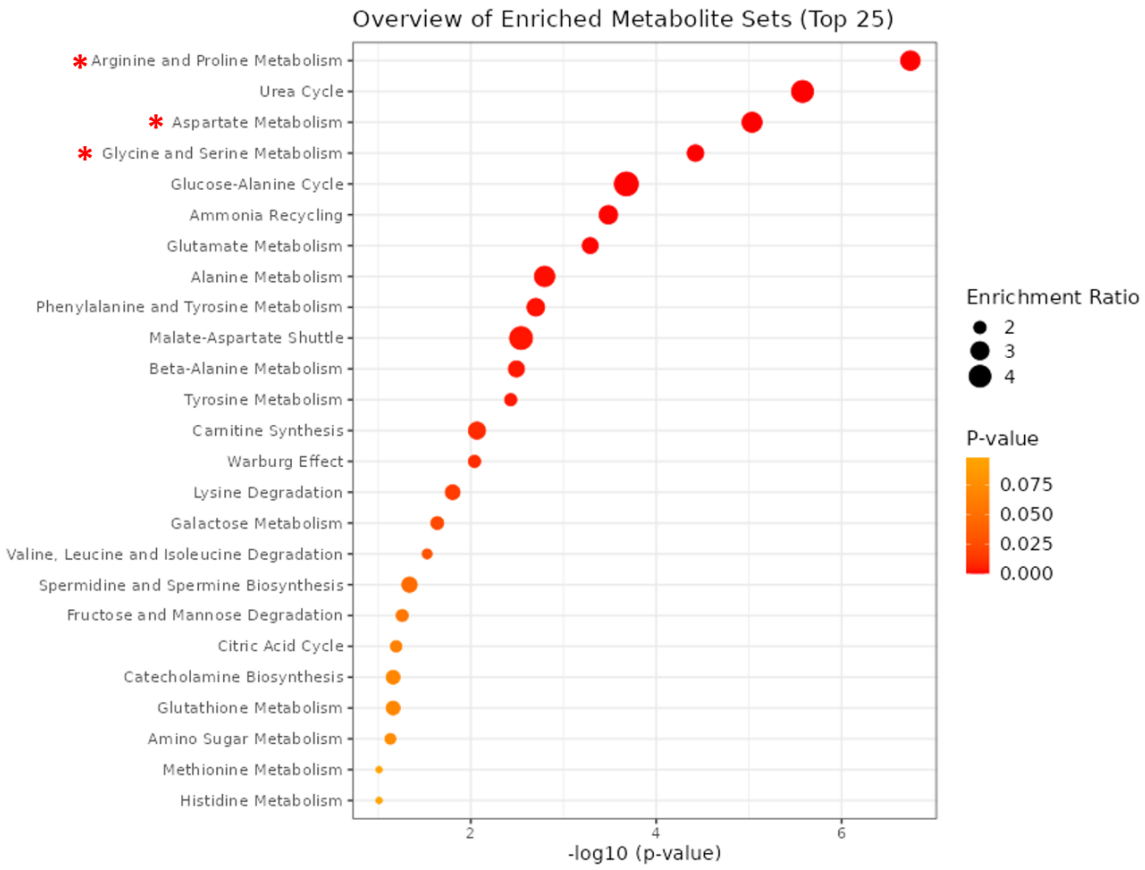

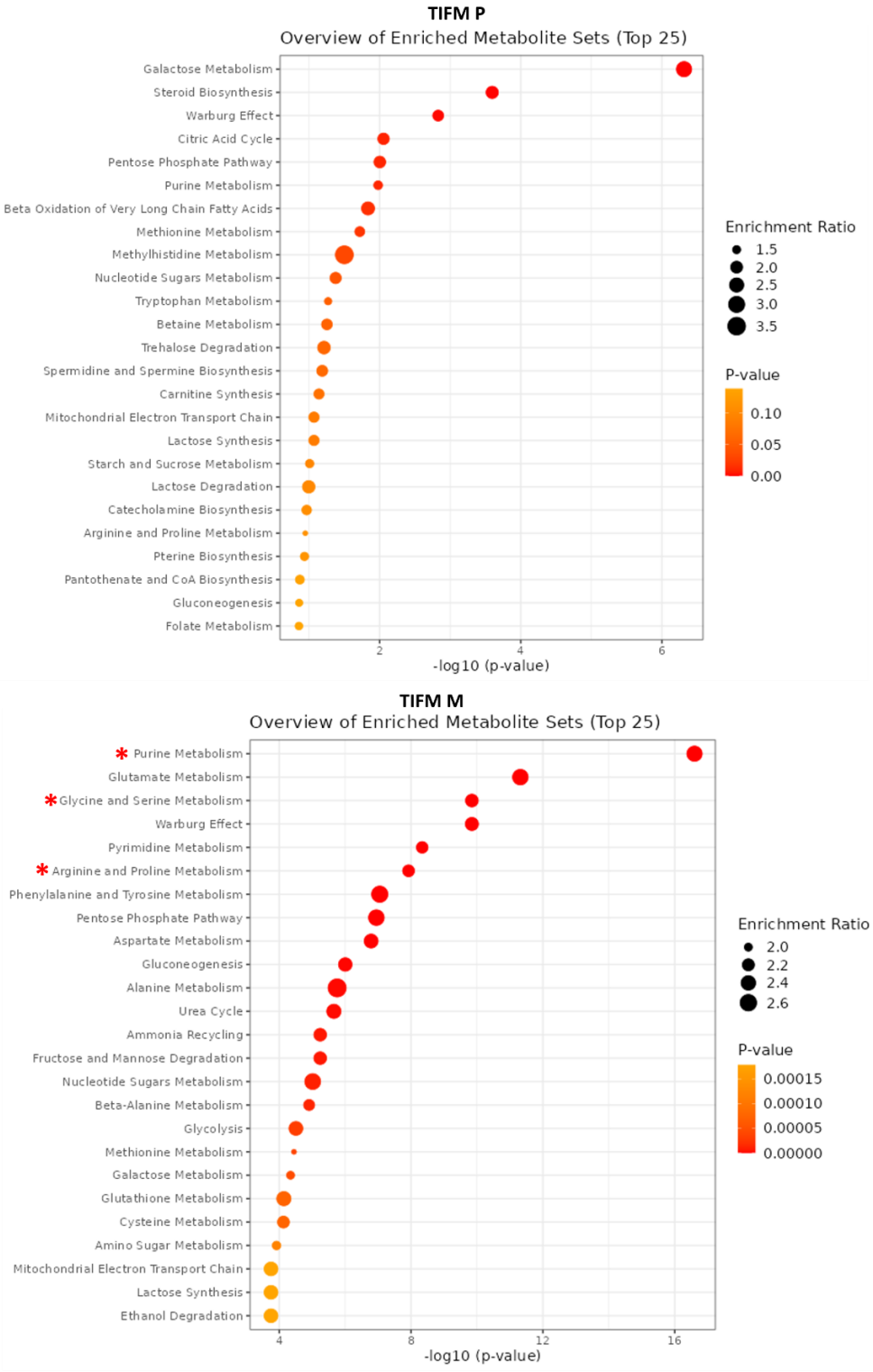

Figure 5.6 – Matrigel altered the metabolism of MIA PaCa-2 cells.
MIA PaCa-2 cells were seeded on a plastic (P) or 3mg/ml Matrigel-coated (M) 6-well plate. After 24 hours, the media was changed to full media, glucose-free media, glutamine-free media, and TIFM, all supplemented with dFBS and the cells were incubated for 7 days. Metabolites were extracted and analysed by untargeted LC-MS. The data was analysed using Perseus. Pathway enrichment analysis was performed in MetaboAnalyst 6.0. In the bubble plot, bubble size represents the number of significant metabolite hits mapped to each pathway, with larger bubbles indicating greater pathway coverage. Pathways were considered significantly enriched based on the p-value

To identify metabolic pathways consistently upregulated in cells cultured on Matrigel independently of the specific nutrient-starvation condition, a Venn diagram was constructed comparing metabolites significantly higher on Matrigel across all starvation conditions tested. This approach allowed us to identify the metabolites common to all conditions, thereby isolating matrigel-driven metabolic reprogramming from starvation-specific effects. In the SW-1990 cells, 116 metabolites were common in cells in glucose-free media, glutamine-free media and TIFM. Interestingly, TIFM and glutamine starvation shared the most metabolites in common (223), suggesting that glutamine deprivation might more closely recapitulate the TME conditions. On the other hand, this might be because the number of upregulated metabolites under glucose deprivation was lower than in other conditions in our study, as seen in Table 5.1. 188 metabolites were specifically upregulated in TIFM, 49 in glucose-starved cells and 67 in glutamine-deprived ones **(Figure 5.7A)**. The metabolites upregulated in common to all the starvation conditions were uploaded to the MetaboAnalyst database for enrichment analysis, and **Figure 5.7B** showed that arginine and proline metabolism, pentose phosphate pathway, Warburg effect, purine metabolism and glutamate metabolism were the top 5 metabolic pathways.

Similarly, 185 metabolites were common to the cells in glucose-free media, glutamine-free media, and TIFM in the MIA PaCa-2 cells. However, glucose starvation and TIFM shared the highest number of common metabolites (334). Again, this is likely because the number of upregulated metabolites under glutamine deprivation in MIA PaCa-2 cells was lower than in other conditions in our study, as seen in Table 5.1. 136 metabolites were specifically upregulated in TIFM, 69 in glucose-starved cells and 39 in glutamine-deprived ones **(Figure 5.7C)**. Upon enrichment analysis, we saw that arginine and proline metabolism, aspartate metabolism, urea cycle, phenylalanine and tyrosine metabolism, and malate-aspartate shuttle were the top five metabolic pathways upregulated across all the starvation conditions **(Figure 5.7D)**.

Given that metabolites in the arginine and proline metabolism were the most upregulated across all the starvation conditions and in the two cell lines studied, we hypothesised that this metabolic pathway could mediate Matrigel-dependent PDAC cell proliferation in nutrient-deprived conditions.

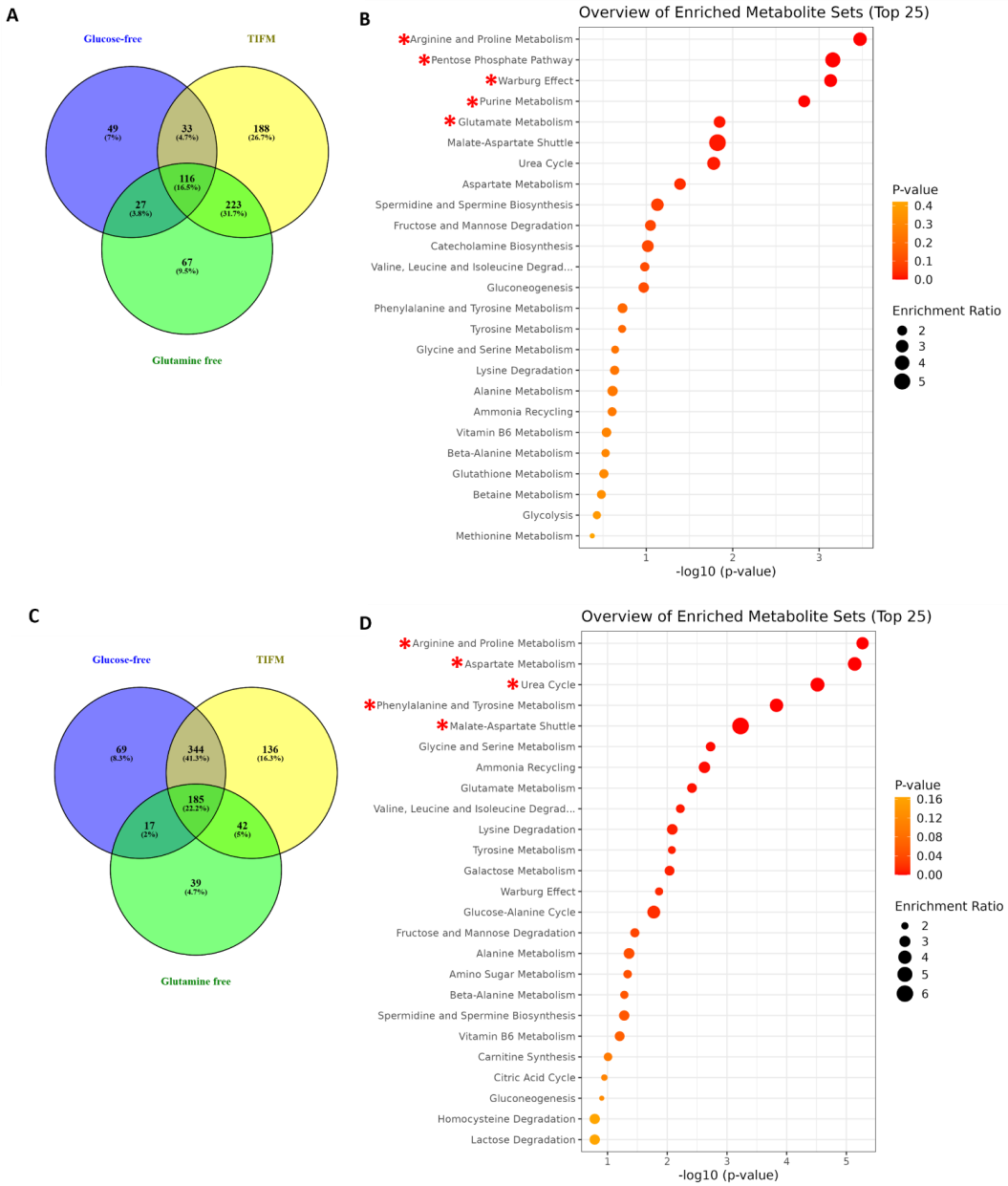

Figure 5.7 – Matrigel altered the metabolism of PDAC cells.
(A-B) SW-1990 and (C-D) MIA PaCa-2 cells were seeded on a plastic or 3mg/ml Matrigel-coated 6-well plate. The media was changed to full media, glucose-free media, glutamine-free media and TIFM, all supplemented with dFBS after 24 hours. The cells were incubated for 7 days. And the metabolites were extracted and quantified by untargeted mass spectroscopy. The Venn diagram (A, C) shows the distribution of the significantly higher metabolites under each nutrient deprivation condition. (B, D) The top 25 enriched pathways of all the metabolites common to all three starvation conditions.

5.2.3 Untargeted metabolomics identified Matrigel-induced changes in disease signature pathways in nutrient-deprived PDAC cells

Metabolomics has been used to identify common biomarkers in different diseases, including pancreatic cancer (Luo et al., 2020). One of the goals of discovering disease biomarkers is to improve diagnosis and develop a targeted and personalised treatment approach, which is expected to enhance the efficacy of treatment and reduce the side effects of regular cancer treatment techniques. To

determine the disease signatures linked to our metabolites, MetaboAnalyst was used to determine the disease pathway signatures. The identified metabolites were deposited on the Small Molecule Pathway Database (SMPDB) to map them to the previously deposited metabolites reported in human blood.

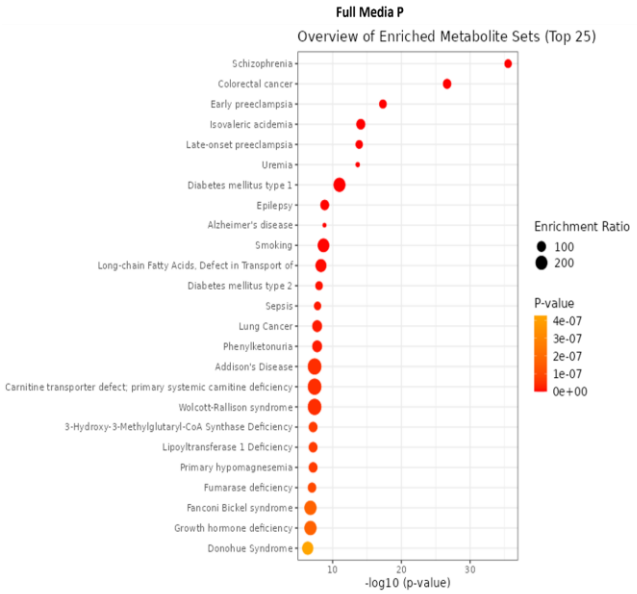

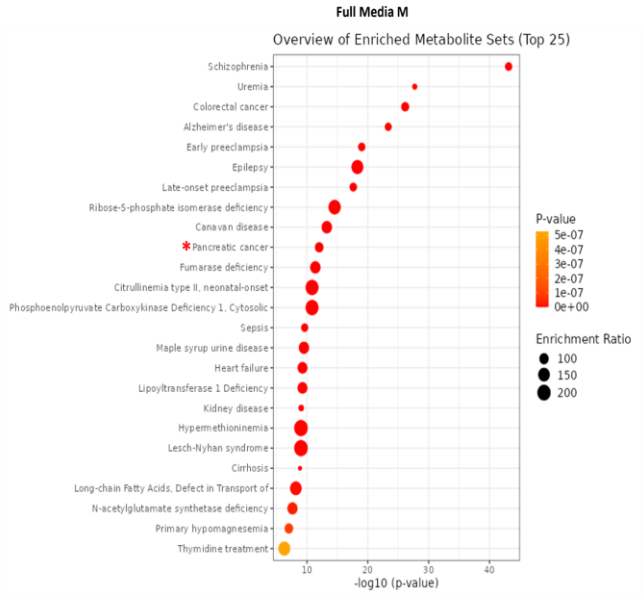

Glucose-free P

Glucose-free M

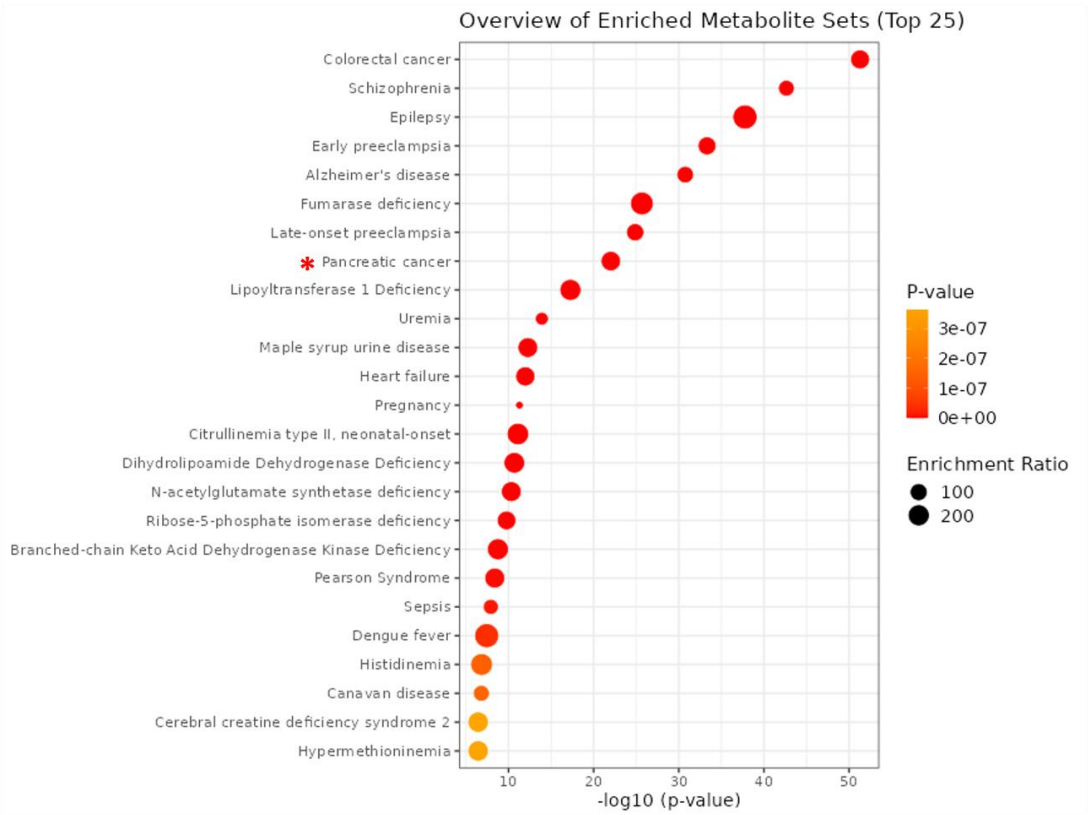

Glutamine-free P

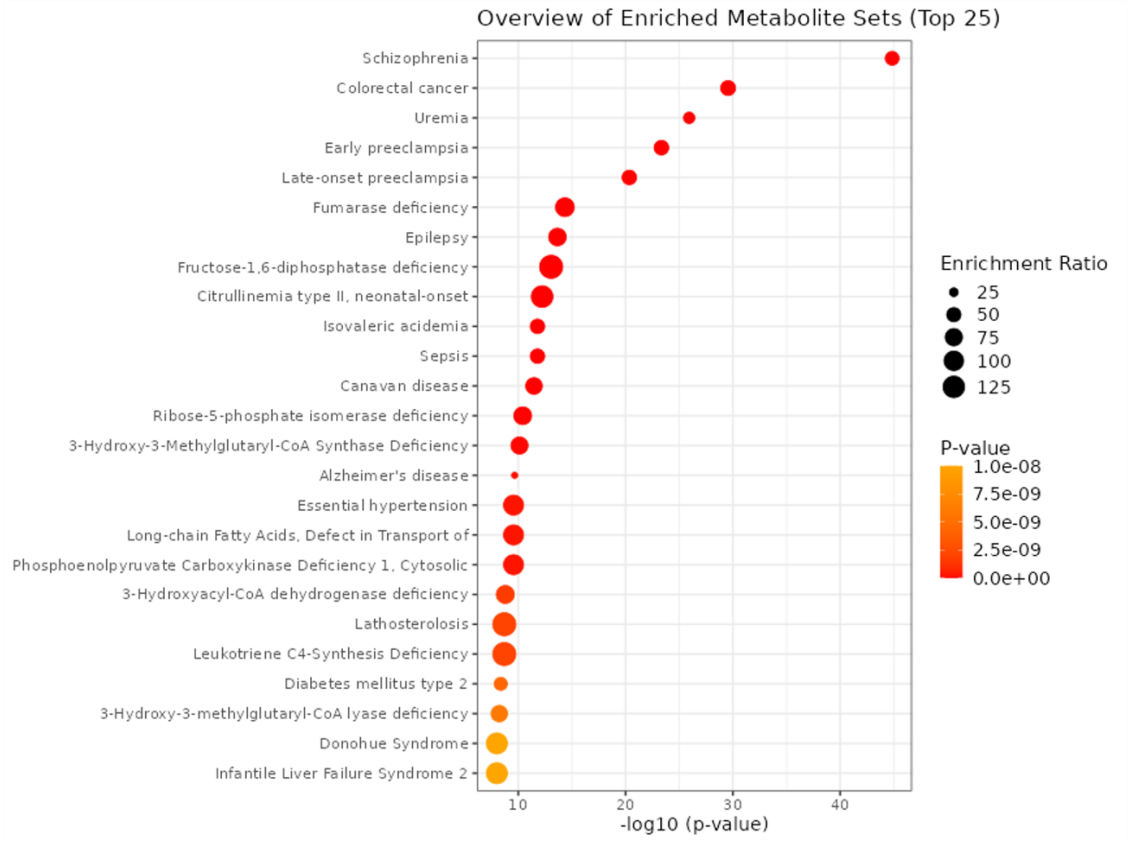

Glutamine-free M

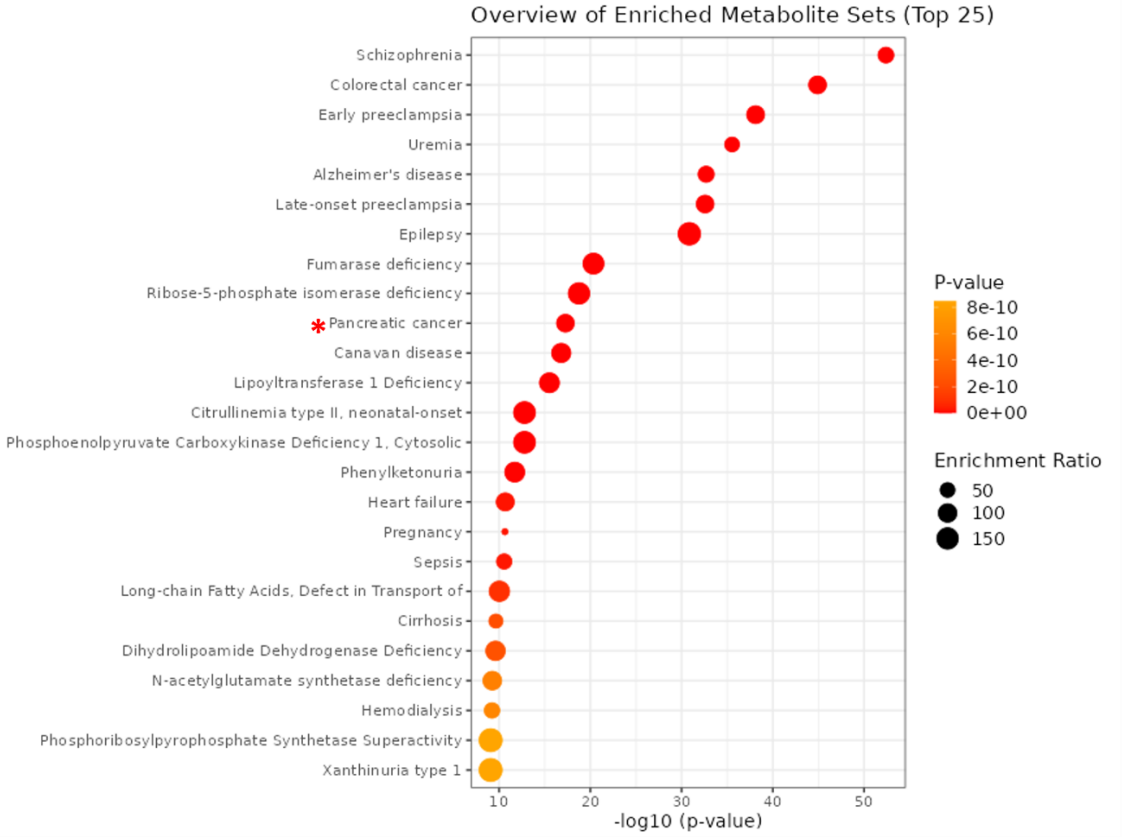

Figure 5.8 – Matrigel altered the disease signature of SW-1990 cells.
SW-1990 cells were seeded on a plastic (P) or 3mg/ml Matrigel-coated (M) 6-well plate. After 24 hours, the media was changed to full media, glucose-free media, glutamine-free media, and TIFM, all supplemented with dFBS and the cells were incubated for 7 days. Metabolites were extracted and analysed by untargeted LC-MS. The data was analysed using Perseus. Disease signature analysis was performed in MetaboAnalyst 6.0. In the bubble plot, bubble size represents the number of significant metabolite hits mapped to each pathway, with larger bubbles indicating greater pathway coverage. Disease signatures were considered significantly enriched based on the p-value

Interestingly, we found that in the presence of Matrigel, but not on plastic, pancreatic cancer emerged among the top ten disease signatures found in the metabolite sets in SW-1990 cells (**Figure 5.8**) and MIA PaCa-2 cells **(Figure 5.9)**. The only exceptions are in SW-1990 cells in TIFM and MIA PaCa-2 cells in glucose-free media, where pancreatic cancer was among the top 10 upregulated diseases in plastic and Matrigel. Some key metabolites associated with pancreatic cancer identified in our data are isoleucine, creatine, valine, lactic acid and glutamic acid. These findings indicate Matrigel specifically induced the expression of metabolites linked explicitly to pancreatic cancer, further solidifying the clinical significance of the role of the ECM in pancreatic cancer. Moreover, culturing cells on Matrigel enhances the physiological relevance of in vitro models, better recapitulating disease-associated metabolic signatures observed in patients.

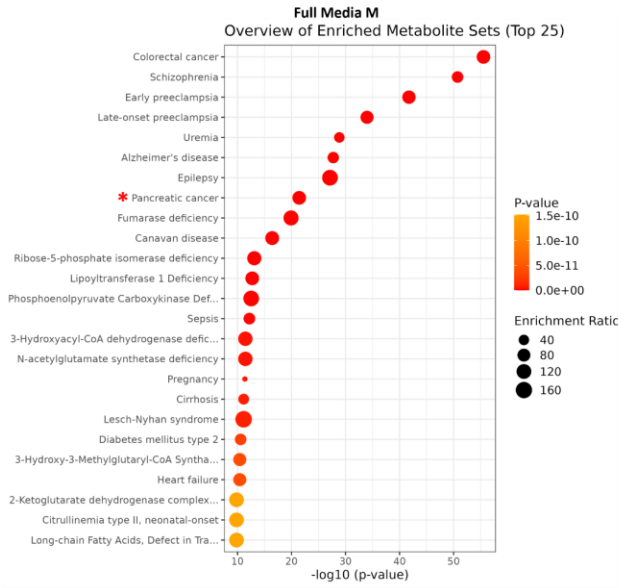

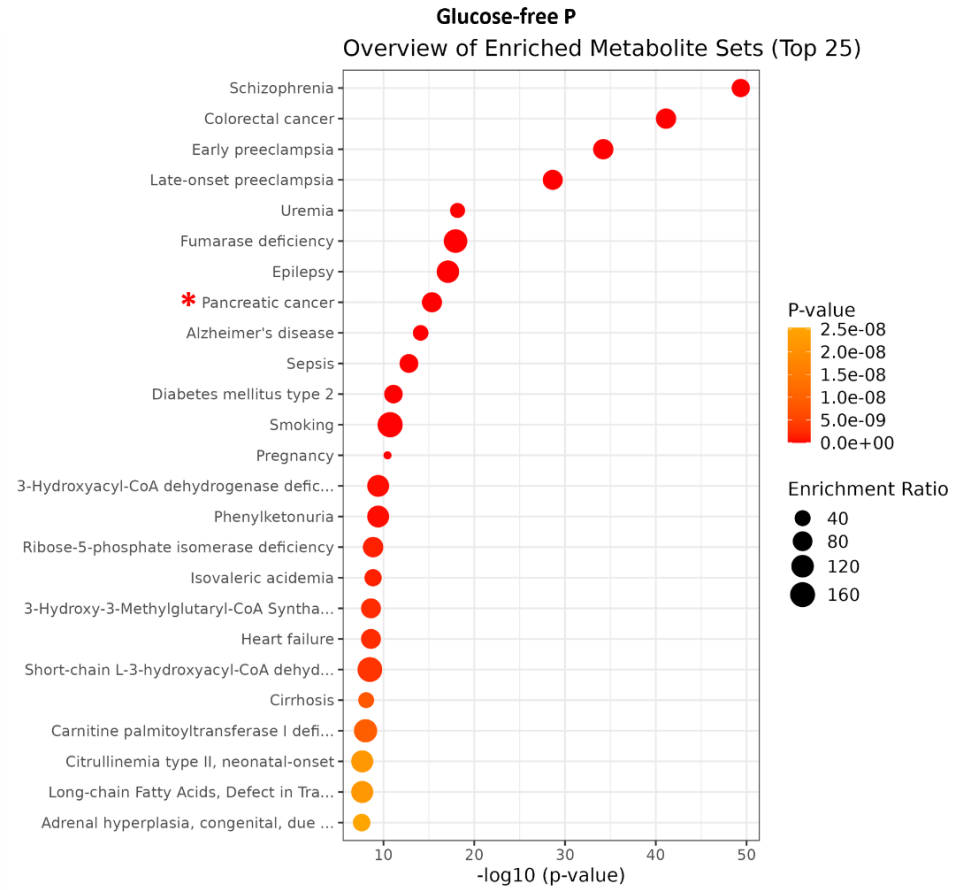
Glucose-free P
Overview of Enriched Metabolite Sets (Top 25)
Schizophrenia
Colorectal cancer
Early preeclampsia
Late-onset preeclampsia
Uremia
Fumarase deficiency
Epilepsy
* Pancreatic cancer
Alzheimer's disease
Sepsis
Diabetes mellitus type 2
Smoking
Pregnancy
3-Hydroxyacyl-CoA dehydrogenase defic...
Phenylketonuria
Ribose-5-phosphate isomerase deficiency
Isovaleric acidemia
3-Hydroxy-3-Methylglutaryl-CoA Syntha...
Heart failure
Short-chain L-3-hydroxyacyl-CoA dehyd...
Cirrhosis
Carnitine palmitoyltransferase I defi...
Citrullinemia type II, neonatal-onset
Long-chain Fatty Acids, Defect in Tra...
Adrenal hyperplasia, congenital, due ...
10
20
30
40
50
-log10 (p-value)
P-value
2.5e-08
2.0e-08
1.5e-08
1.0e-08
5.0e-09
0.0e+00
Enrichment Ratio
40
80
120
160

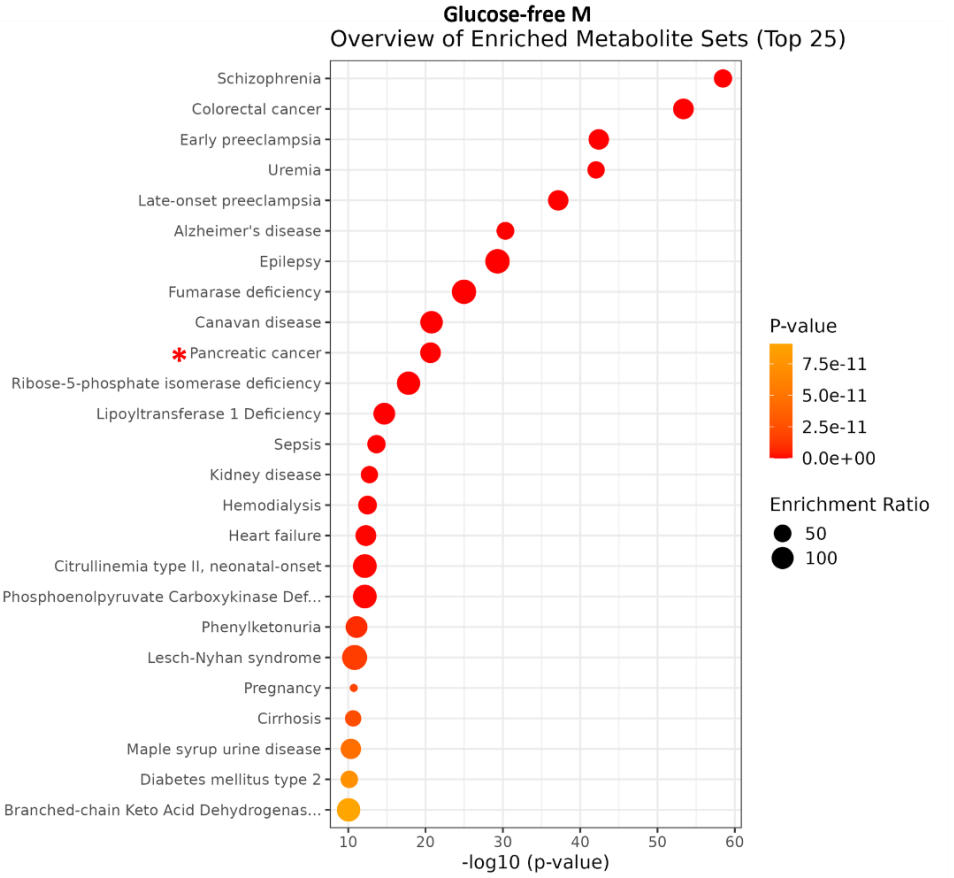
Glucose-free M
Overview of Enriched Metabolite Sets (Top 25)
Schizophrenia
Colorectal cancer
Early preeclampsia
Uremia
Late-onset preeclampsia
Alzheimer's disease
Epilepsy
Fumarase deficiency
Canavan disease
* Pancreatic cancer
Ribose-5-phosphate isomerase deficiency
Lipoyltransferase 1 Deficiency
Sepsis
Kidney disease
Hemodialysis
Heart failure
Citrullinemia type II, neonatal-onset
Phosphoenolpyruvate Carboxykinase Def...
Phenylketonuria
Lesch-Nyhan syndrome
Pregnancy
Cirrhosis
Maple syrup urine disease
Diabetes mellitus type 2
Branched-chain Keto Acid Dehydrogenas...
10
20
30
40
50
60
-log10 (p-value)
P-value
7.5e-11
5.0e-11
2.5e-11
0.0e+00
Enrichment Ratio
50
100

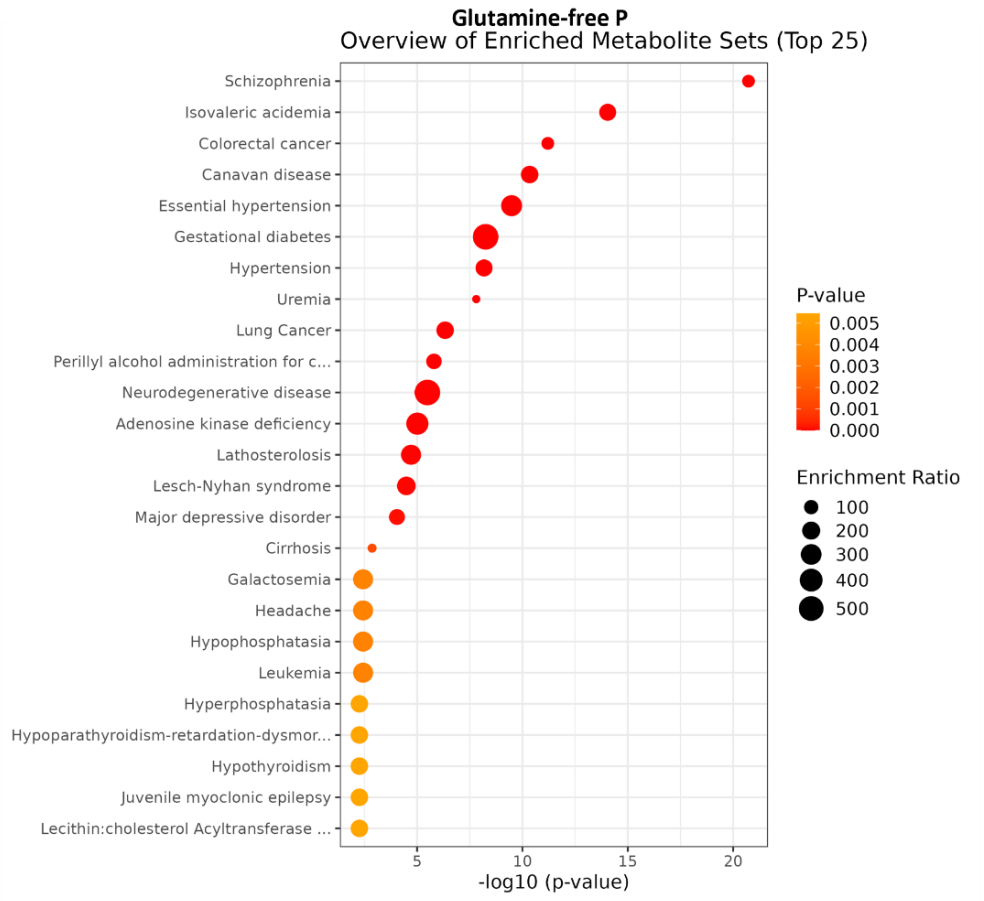
Glutamine-free P
Overview of Enriched Metabolite Sets (Top 25)
Schizophrenia
Isovaleric acidemia
Colorectal cancer
Canavan disease
Essential hypertension
Gestational diabetes
Hypertension
Uremia
Lung Cancer
Perillyl alcohol administration for c...
Neurodegenerative disease
Adenosine kinase deficiency
Lathosterolosis
Lesch-Nyhan syndrome
Major depressive disorder
Cirrhosis
Galactosemia
Headache
Hypophosphatasia
Leukemia
Hyperphosphatasia
Hypoparathyroidism-retardation-dysmor...
Hypothyroidism
Juvenile myoclonic epilepsy
Lecithin:cholesterol Acyltransferase ...
5
10
15
20
-log10 (p-value)
P-value
0.005
0.004
0.003
0.002
0.001
0.000
Enrichment Ratio
100
200
300
400
500

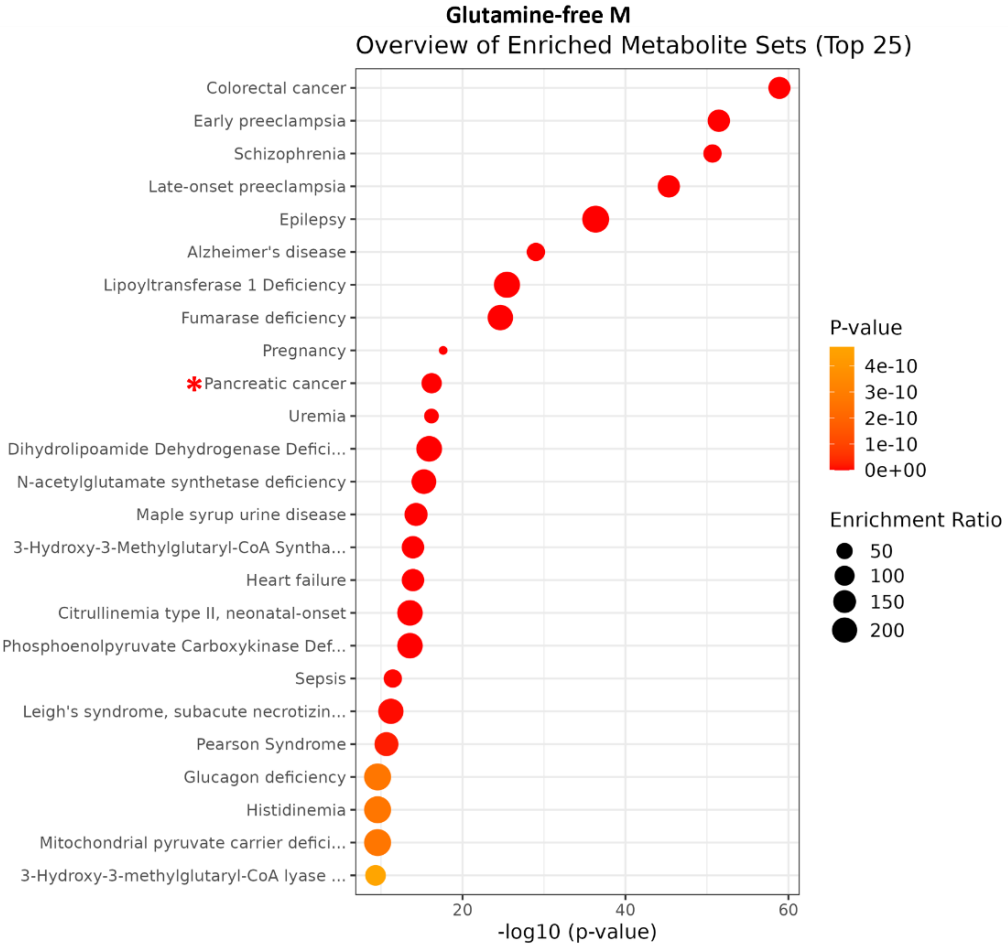
Glutamine-free M
Overview of Enriched Metabolite Sets (Top 25)
Colorectal cancer
Early preeclampsia
Schizophrenia
Late-onset preeclampsia
Epilepsy
Alzheimer's disease
Lipoyltransferase 1 Deficiency
Fumarase deficiency
Pregnancy
*Pancreatic cancer
Uremia
Dihydrolipoamide Dehydrogenase Defici...
N-acetylglutamate synthetase deficiency
Maple syrup urine disease
3-Hydroxy-3-Methylglutaryl-CoA Syntha...
Heart failure
Citrullinemia type II, neonatal-onset
Phosphoenolpyruvate Carboxykinase Def...
Sepsis
Leigh's syndrome, subacute necrotizin...
Pearson Syndrome
Glucagon deficiency
Histidinemia
Mitochondrial pyruvate carrier defici...
3-Hydroxy-3-methylglutaryl-CoA lyase ...
20
40
60
-log10 (p-value)
P-value
4e-10
3e-10
2e-10
1e-10
0e+00
Enrichment Ratio
50
100
150
200

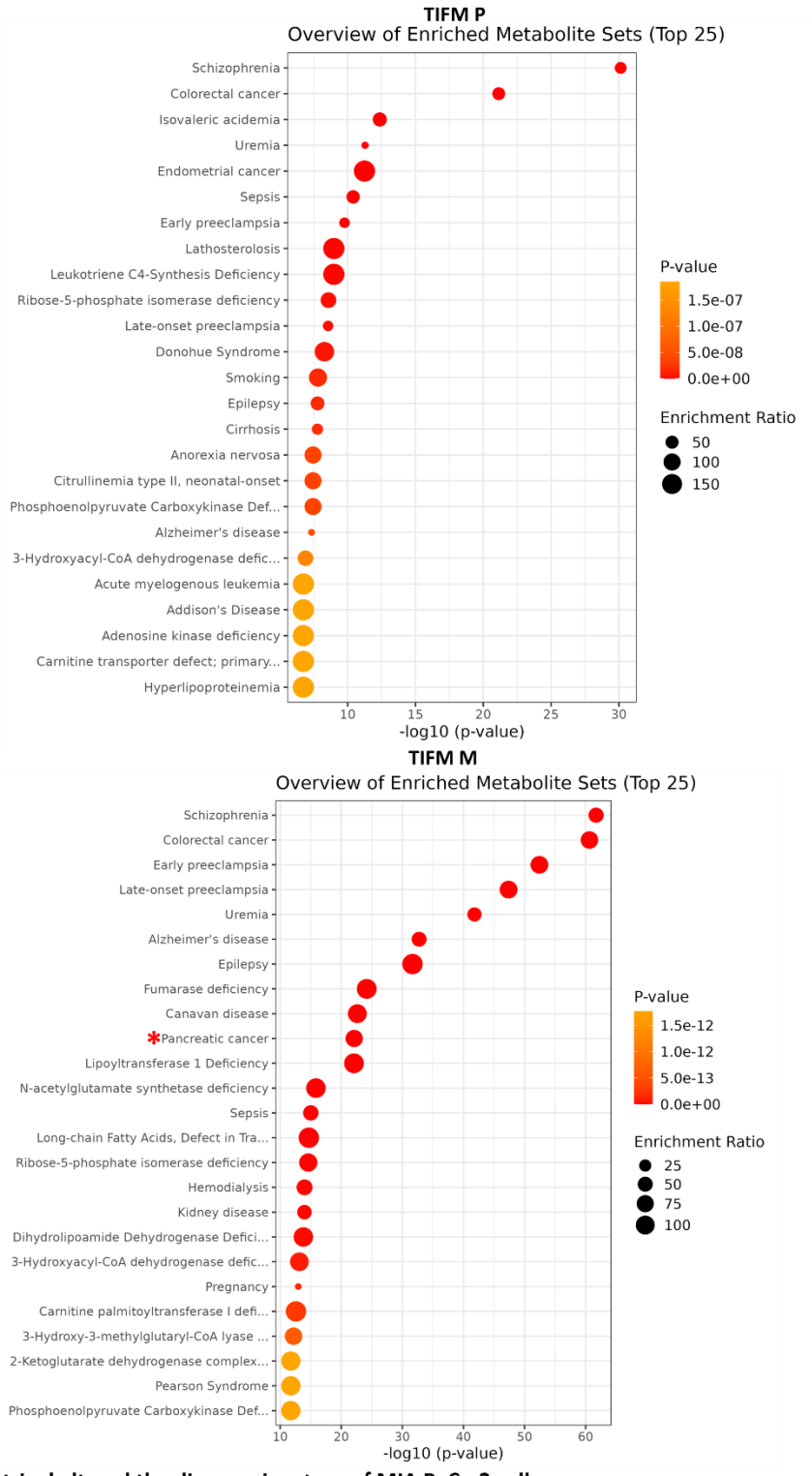

Figure 5.9 – Matrigel altered the disease signature of MIA PaCa-2 cells.
MIA PaCa-2 cells were seeded on a plastic (P) or 3mg/ml Matrigel-coated (M) 6-well plate. After 24 hours, the media was changed to full media, glucose-free media, glutamine-free media, and TIFM, all supplemented with dFBS and the cells were incubated for 7 days. Metabolites were extracted and analysed by untargeted LC-MS. The data was analysed using Perseus. Disease signature analysis was performed in MetaboAnalyst 6.0. In the bubble plot, bubble size represents the number of significant metabolite hits mapped to each pathway, with larger bubbles indicating greater pathway coverage. Disease signatures were considered significantly enriched based on the p-value.

5.2.4 Targeted metabolomics confirmed a Matrigel-induced upregulation of metabolites in the arginine and proline pathway

Targeted metabolomics can test a previously established hypothesis by quantifying a known set of metabolites in a sample based on a standard (Liu and Locasale, 2017). It accurately assesses the concentration of a specific target metabolite in each sample. To follow up on our untargeted metabolomics data, 15 metabolites were measured by targeted metabolomics to confirm their Matrigel-induced upregulation.

SW-1990 and MIA PaCa-2 cells were seeded on either plastic or Matrigel-coated 6-well plates and incubated for 24 hours. The media was changed to full media, glucose-free media, glutamine-free media, or TIFM, and the cells were incubated for 7 (SW-1990 cells) or 6 (MIA PaCa-2 cells) days. The metabolites were extracted, and a UPLC-MS-based targeted metabolomics was performed using a standard for each metabolite to determine its concentration. **Figure 5.10** shows a heatmap summary of all our targeted metabolomics data in SW-1990 cells, with the deeper shades representing a higher concentration and the lighter shades representing a lower concentration of a particular metabolite. In full media, uridine, xanthine, ornithine, arginine, isoleucine and creatine were upregulated on Matrigel versus plastic **(Figure 5.10A)**. In glucose-free media, we saw that cysteine, aspartic acid, glutamic acid, uridine, xanthine, ornithine, arginine, isoleucine and creatine were upregulated on Matrigel compared to plastic **(Figure 5.10B)**, while under glutamine-starved conditions, cysteine, ornithine, arginine, isoleucine and creatine were higher on Matrigel than on plastic **(Figure 5.10C)**. Finally, uridine, uracil, xanthine, valine, ornithine and creatine were upregulated considerably on Matrigel compared to plastic in TIFM **(Figure 5.10D)**. It should be noted that the concentration of creatine was not included in the TIFM heatmap because the concentration in TIFM was much higher than the concentration of other metabolites, which impacted our ability to accurately assess the differences between other metabolites using the heatmap. Overall, we saw that arginine was the upregulated metabolite in full media, glucose-free media (although other metabolites were upregulated to a similar extent), and glutamine-free media, but not the cells in TIFM on Matrigel compared to plastic.

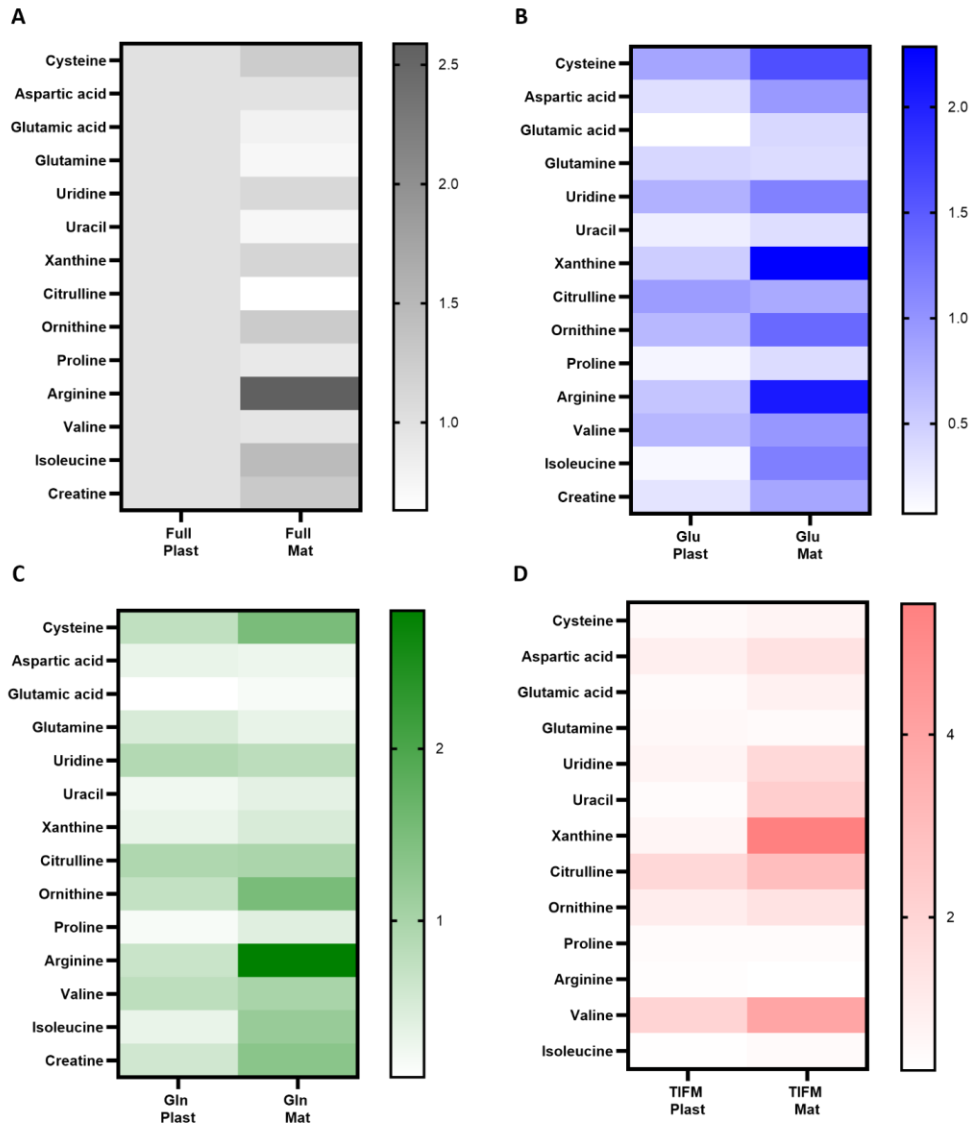

Figure 5.10 – Heatmap of Metabolites on Matrigel versus Plastic in SW-1990 cells
SW-1990 cells were seeded on a plastic (Plast) or 3mg/ml Matrigel-coated (Mat) 6-well plate. The media was changed to (A) full media, (B) glucose-free media, (C) glutamine-free media and (D) TIFM, all supplemented with dFBS after 24 hours. The cells were incubated for 7 days, and the metabolites were extracted and quantified by targeted mass spectroscopy. Each row corresponds to a detected metabolite. The data was normalised to the mean of the full media on plastic. The colour intensity indicates normalised metabolite levels, with a darker shade indicating higher and a lighter shade indicating lower relative intensity. N ≥2 independent experiments

We performed a similar analysis in MIA PaCa-2 cells (**Figure 5.11)**. In full media, xanthine, ornithine, arginine and isoleucine were upregulated on Matrigel versus plastic **(Figure 5.11A)**. In glucose-free media, uridine, xanthine, ornithine, arginine and isoleucine were upregulated on Matrigel versus plastic **(Figure 5.11B)**, while under glutamine-starved conditions, cysteine, xanthine, ornithine, arginine and isoleucine were higher on Matrigel than on plastic **(Figure 5.11C)**. Finally, in TIFM, uridine, uracil, xanthine, ornithine, valine and creatine were upregulated on Matrigel compared to plastic **(Figure 5.11D)**. Consistent with SW-1990 cells results, arginine concentration was higher on Matrigel than on plastic in full, glucose-free, and glutamine-free media, but not in TIFM.

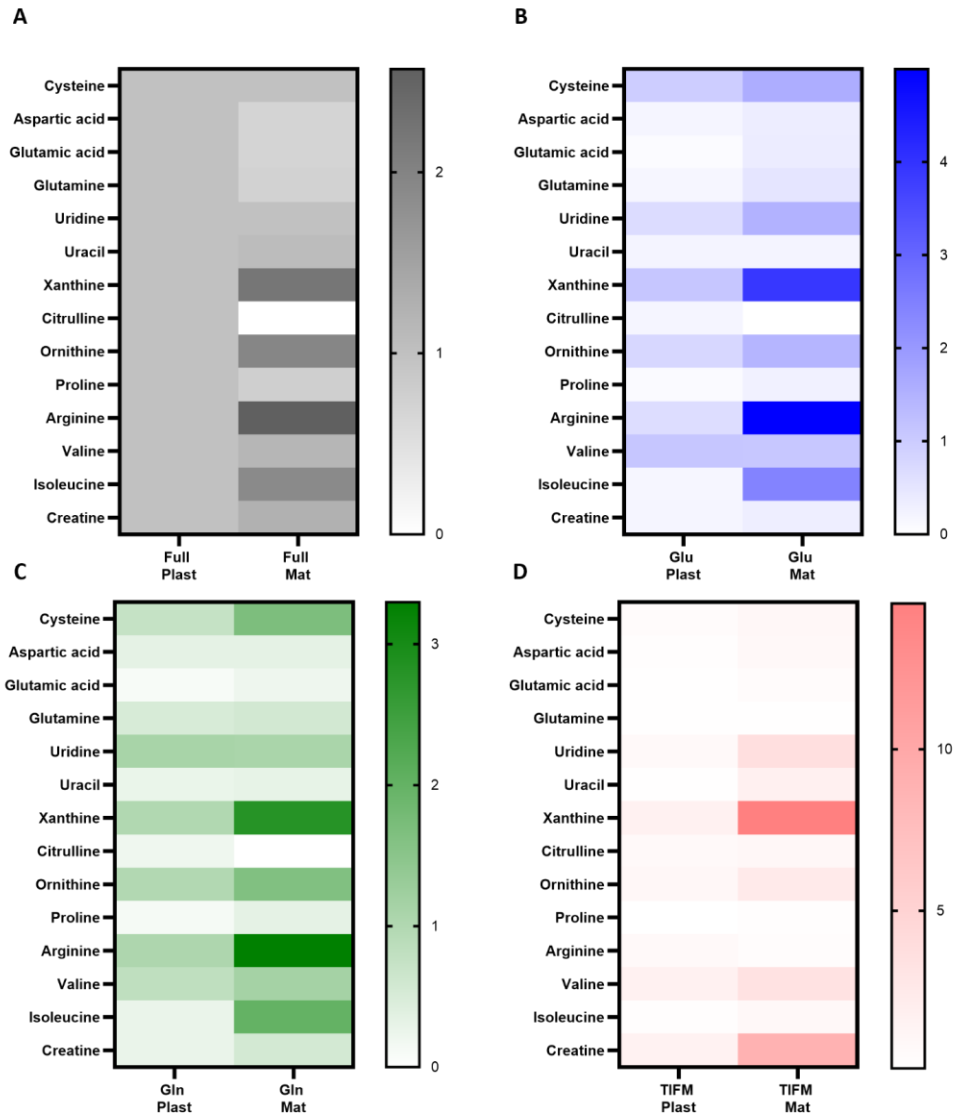

Figure 5.11 – Heatmap of Metabolites on Matrigel versus Plastic in MIA PaCa-2 cells
MIA PaCa-2 cells were seeded on a plastic (Plast) or 3mg/ml Matrigel-coated (Mat) 6-well plate. The media was changed to (A) full media, (B) glucose-free media, (C) glutamine-free media and (D) TIFM, all supplemented with dFBS after 24 hours. The cells were incubated for 6 days, and the metabolites were extracted and quantified by targeted mass spectroscopy. Each row corresponds to a detected metabolite. The data was normalised to the mean of the full media on plastic. The colour intensity indicates normalised metabolite levels, with a darker shade indicating higher and a lighter shade indicating lower relative intensity. N ≥2 independent experiments

We then focused on creatine, arginine, ornithine, and xanthine, which showed an upward trend based on our heatmaps. In SW-1990 cells, we observed a statistically significant increase in arginine concentration under both glucose and glutamine deprivation, but not in TIFM, in the presence of Matrigel compared to plastic **(Figure 5.12A)**. Under glucose and glutamine-deprived conditions, there was no statistically significant increase in the concentration of creatine and xanthine on Matrigel compared to plastic **(Figure 5.12B, C)**, while Matrigel significantly increased the intracellular levels of both creatine and xanthine in TIFM **(Figure 5.12B, C)**. Finally, there was no significant Matrigel-

dependent increase in the concentration of ornithine in all starvation conditions studied **(Figure 5.12D)**.

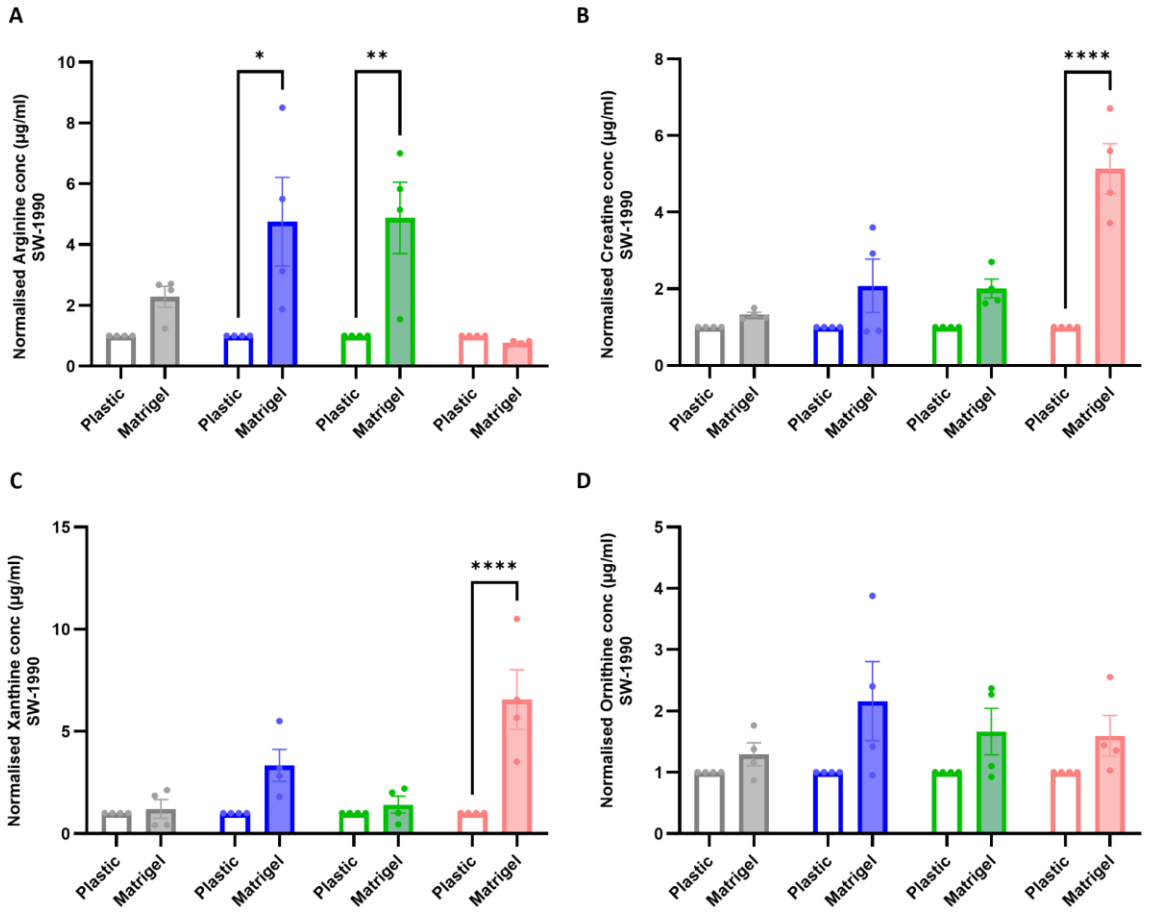

Figure 5.12 – Matrigel increased intracellular Arginine, Creatine and Xanthine levels in SW-1990 cells.
SW-1990 cells were seeded on a plastic or 3mg/ml Matrigel-coated 6-well plate. The media was changed to full media, glucose-free media, glutamine-free media and TIFM, all supplemented with dFBS after 24 hours. The cells were incubated for 7 days. The metabolites were extracted, and intracellular levels of (A) Arginine, (B) Creatine, (C) Xanthine, and (D) Ornithine were quantified by targeted mass spectroscopy. Data are presented as Mean ± SEM. The data was normalised to the mean of the plastic in each condition. Significance was determined by Two-Way Anova with Tukey's multiple comparisons test. ****p<0.0001, **p<0.01, *p<0.05. N = 4 independent experiments

Similarly, in MIA PaCa-2 cells, we observed a statistically significant Matrigel-dependent increase in arginine under glucose- and glutamine-deprivation, but not in TIFM **(Figure 5.13A)**. Moreover, under glucose or glutamine-deprived conditions, intracellular creatine and xanthine levels were not significantly increased in the presence of Matrigel, while there was a Matrigel-dependent increase in TIFM (**Figure 5.13B, C)**. Lastly, there was a trend towards an increase in intracellular levels of ornithine across all starvation conditions in the presence of Matrigel, but this was not statistically significant **(Figure 5.13D)**.

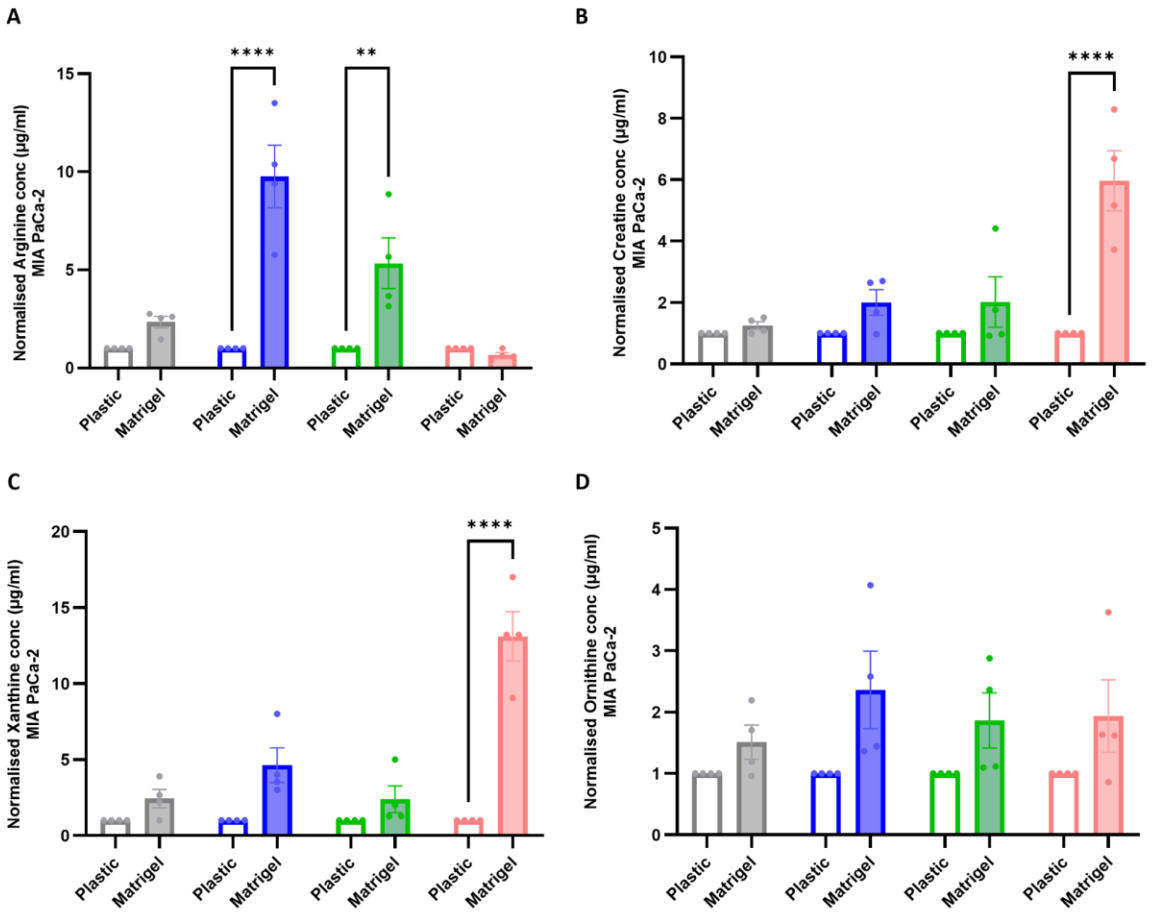

Figure 5.13 – Matrigel increased intracellular Arginine, Creatine and Xanthine levels in MIA PaCa-2 cells.
MIA PaCa-2 cells were seeded on a plastic or 3mg/ml Matrigel-coated 6-well plate. The media was changed to full media, glucose-free media, glutamine-free media and TIFM, all supplemented with dFBS after 24 hours. The cells were incubated for 6 days. The metabolites were extracted, and intracellular levels of (A) Arginine, (B) Creatine, (C) Xanthine, and (D) Ornithine were quantified by targeted mass spectroscopy. Data are presented as Mean ± SEM. The data was normalised to the mean of the plastic in each condition. Significance was determined by Two-Way Anova with Tukey's multiple comparisons test. ****p<0.0001, **p<0.01, *p<0.05. N = 4 independent experiments

The observed upregulation of arginine and creatine, both components of the arginine and proline metabolic pathway, corroborated our untargeted metabolomics data and confirmed that Matrigel induced arginine and proline metabolism in PDAC cells.

5.2.5 Matrigel-dependent growth of nutrient-deprived PDAC cells is independent of ASS1 expression

Our targeted metabolomics data have shown that arginine increased in a Matrigel-dependent fashion, especially under glucose and glutamine deprivation. **Figure 5.14** schematically represents the arginine and proline metabolic pathway, highlighting the enzymes and metabolites that could be involved in Matrigel-dependent cell proliferation in our study.

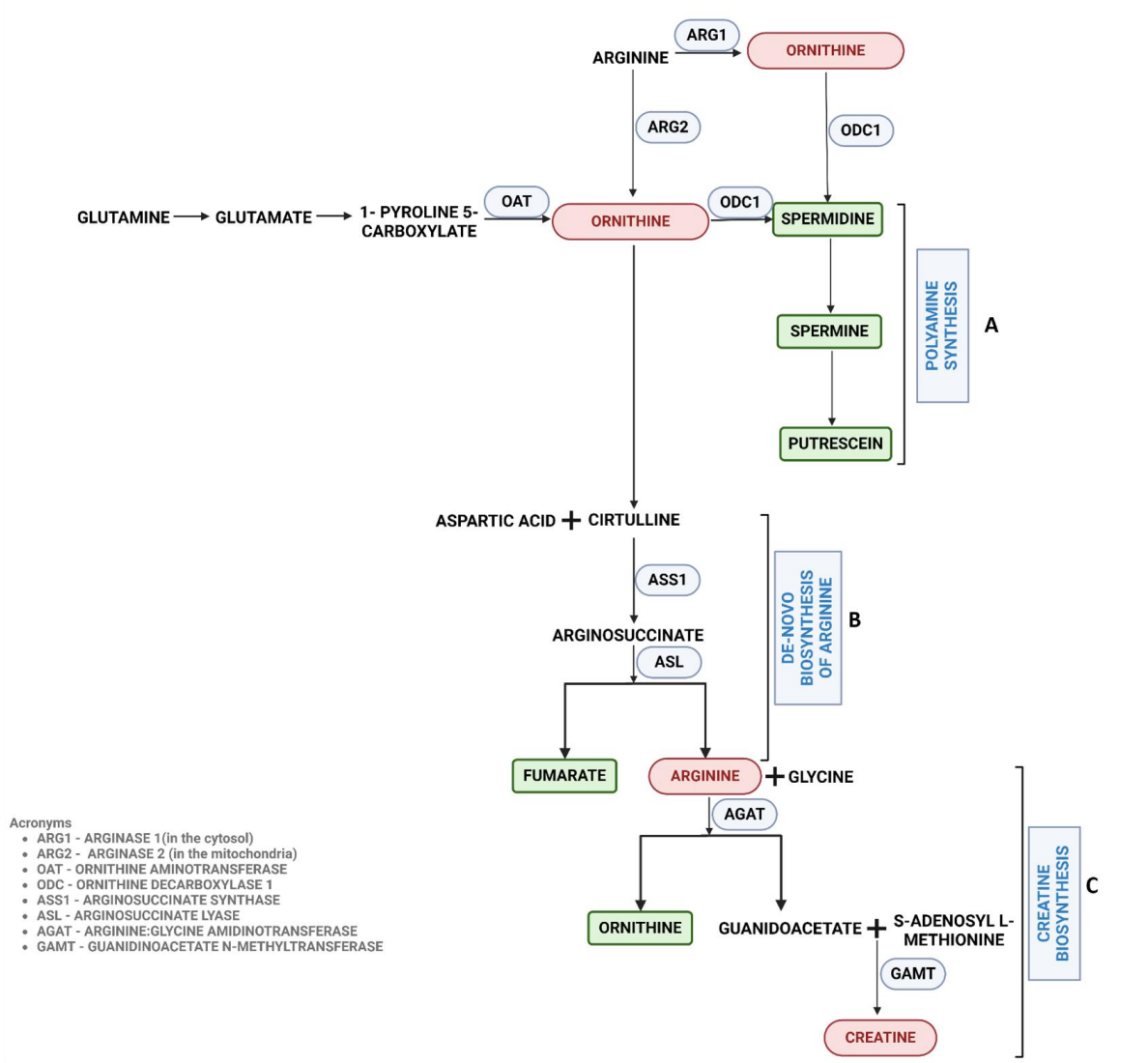

Figure 5.14 – Schematic representation of metabolites and enzymes in the Arginine and proline metabolic pathway
Arginine is converted to ornithine via ARG1 (Arginase 1) in the cytosol or ARG2 (Arginase 2) in the mitochondria. ODC1 (Ornithine Decarboxylase 1) catalyses the synthesis of Polyamines (spermidine, spermine and putrescein) from ornithine (A). For the De novo synthesis of Arginine, ornithine produces citrulline, which, in combination with aspartic acid, produces arginosuccinate, catalysed by ASS1 (Arginosuccinate synthase 1). Arginosuccinate is converted to arginine and fumarate in a reaction catalysed by Arginosuccinate lyase (ASL) (B). For Creatine synthesis, arginine and glycine are converted to ornithine and guanidinoacetate, catalysed by Arginine: Glycine Amidinotransferase (AGAT). Creatine is synthesised from guanidinoacetate and S-adenosyl L-methionine in a reaction catalysed by Guanidinoacetate N-methyltransferase (GAMT) (C). The metabolites highlighted in red are the metabolites upregulated in our samples. Created with Biorender.com

Arginosuccinate synthase 1 (ASS1) plays a role in the de novo synthesis of arginine **(Figure 5.14)**. We hypothesised that the presence of Matrigel promotes de novo arginine synthesis; hence, we assessed the effects of Matrigel on the mRNA expression of ASS1. To do this, SW-1990 cells were seeded on either Matrigel or plastic-coated 6-well plates and incubated for 24 hours. The media was changed to full, glucose-free, glutamine-free media or TIFM and incubated for 7 days. The mRNA was extracted, and qPCR was used to determine ASS1 expression levels. There was no significant difference in ASS1 mRNA expression between cells cultured on Matrigel and those on plastic in full media or TIFM **(Figure**

5.15A, D). However, under glucose- and, to a lesser extent, glutamine-deprived conditions, a small but statistically significant increase in ASS1 mRNA expression was observed in cells grown on Matrigel compared to plastic **(Figure 5.15B, C)**. These findings suggest that elevated arginine concentrations on Matrigel under nutrient-deprived conditions, but not in full media or TIFM, could be mediated by increased ASS1 expression.

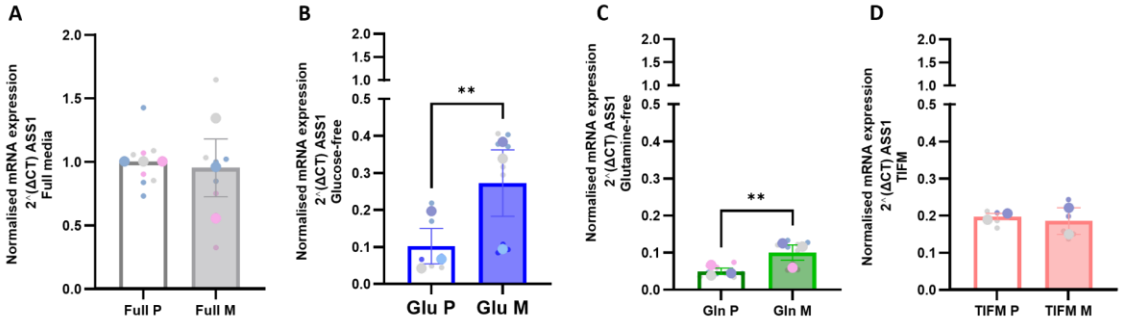

Figure 5.15 – Matrigel increased the mRNA expression of ASS1 under glucose and glutamine deprivation.
SW-1990 cells were seeded on a plastic or 3mg/ml Matrigel-coated 6-well plate and incubated overnight. After 24 hours, the media was changed to (A) full media, (B) glucose-free media, (C) glutamine-free media, and (D) TIFM, all supplemented with dFBS, and the cells were incubated for 7 days. The mRNA was extracted, and SYBR-green-based qPCR was used to determine the mRNA expression of ASS1. GAPDH was used as the control housekeeping gene, and the data were normalised to the mean of full media on plastic. Data are presented as Mean ± SEM. Significance was determined using the Mann-Whitney test. **p<0.01. independent experiments, and the bigger dots represent the mean of each experiment. N ≥2 independent experiments

To determine whether ASS1-dependent arginine synthesis was required for the Matrigel-dependent growth of PDAC cells, an siRNA targeting ASS1 was used to knock down ASS1 in SW-1990 cells, where we achieved an ~80% reduction in ASS1 levels, measured by qPCR. **(Figure 5.16A)**. Next, the proliferation of SW-1990 cells in the presence of Matrigel or plastic in full or glucose-free media upon ASS1 knockdown was assessed, as we detected a more profound induction of ASS1 expression in glucose-starved cells compared to glutamine-starved ones. SW-1990 cells were seeded on Matrigel-coated 96-well plates, and the cells were transfected with siRNA targeting ASS1 or a non-targeting control and incubated overnight. The media was changed to full or glucose-free media, both supplemented with dFBS. On day 5, the cells were fixed, stained with Hoechst33342 and imaged using an InCell Analyzer 2200. We observed no significant difference in cell number upon knockdown of ASS1 on plastic or Matrigel compared to the control in full media **(Figure 5.16B)**. Surprisingly, under glucose-free conditions, ASS1 knockdown on plastic led to a significant increase in cell number compared to the control; however, there was no difference in cell number on Matrigel upon knockdown of ASS1 compared to the control **(Figure 5.16C)**.

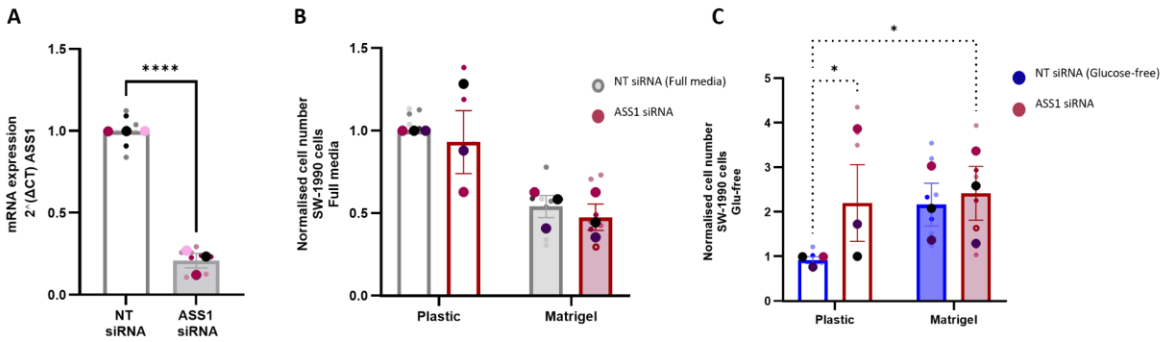

Figure 5.16 – ASS1 did not reduce Matrigel-induced cell proliferation under glucose deprivation
(A) SW-1990 cells were transfected with non-targeting siRNA (NT-siRNA) or ASS1-siRNA for 5 days, mRNA was extracted, and SYBR-green-based qPCR was used to determine the mRNA expression of ASS1. GAPDH was used as the control housekeeping gene, and the data were normalised to the mean of NT siRNA. SW-1990 cells were seeded on plastic or a 3mg/ml Matrigel-coated 96-well plate and incubated for 3 hours. The cells were transfected with NT siRNA or ASS1 siRNA and incubated overnight. The media were changed to (B) full media and (C) glucose-free media, supplemented with dFBS. The cells were fixed and stained with Hoechst 33342 on day 5, imaged using InCell Analyzer 2200 and analysed using Cell Profiler. The data was normalised to the mean of each condition on plastic. Data are presented as Mean ± SEM. Significance was determined using the Mann-Whitney test (A), Two-Way Anova with Tukey's multiple comparisons test (B-D). ****p<0.0001 *p<0.05. N=3 independent experiments, and the bigger dots represent the mean of each experiment.

5.3 Discussion

Metabolic remodelling is one of the main hallmarks of cancer, and various studies have highlighted how cancer cells remodel their metabolism to upregulate specific metabolic pathways required for sustained cell proliferation and metastasis (Shiratori et al., 2019; Yang et al., 2023; Nazemi et al., 2024; Yang et al., 2024). Here, we showed a Matrigel-dependent remodelling of PDAC metabolism under nutrient deprivation. We found a significant difference in the metabolite content in the presence of Matrigel compared to plastic, which alters the samples' disease signature. Notably, pancreatic cancer was among the top upregulated disease signatures in the presence of Matrigel, further solidifying the clinical relevance of our model. In addition, colorectal cancer signatures were consistently enriched across both plastic- and Matrigel-grown cells under all starvation conditions and in full media, suggesting that the metabolic adaptations observed here may extend beyond pancreatic cancer. Pathway analysis further identified upregulation of several metabolic pathways, including arginine and proline metabolism, purine metabolism, and aspartate metabolism. Moreover, we observed a Matrigel-dependent increase in ASS1 expression during glucose starvation; however, this enzyme was not required for Matrigel-dependent proliferation. This suggests that the primary source of arginine is likely the extracellular environment, rather than de novo synthesis.

A recently published work in our lab demonstrated that the ECM influences cancer metabolism under nutrient starvation. Nazemi and colleagues found that collagen-I and Matrigel upregulated phenylalanine and tyrosine catabolism, thereby supporting invasive breast cancer cell proliferation

under amino acid starvation (Nazemi et al., 2024). Our untargeted metabolomics also revealed that under glutamine and amino acid deprivation (amino acid data not shown), there was a Matrigel-dependent upregulation of phenylalanine and tyrosine metabolism in PDAC cells. These findings suggest that ECM-mediated metabolic remodelling may represent a conserved mechanism across tumour types, enabling cancer cells to remodel their metabolism and maintain proliferation under amino acid deprivation.

To identify biomarkers that could aid with the diagnosis of pancreatic cancer, Luo and colleagues used plasma and tissue samples from pancreatic cancer patients and healthy controls to analyse the specific metabolites that could be linked to pancreatic cancer. Their targeted metabolomics data showed that creatine, inosine, beta-sitosterol, sphinganine and glycocholic acid were upregulated in pancreatic cancer patients compared to healthy controls and could be used as biomarkers for the precise diagnosis of pancreatic cancer (Luo et al., 2020). Consistently, our study revealed a Matrigel-induced increase in the concentration of creatine in the cells exposed to TIFM (which reflects the physiological nutrient composition of PDAC microenvironment). Additionally, their enrichment analysis revealed that the upregulated metabolites were linked to purine metabolism, glycine and serine metabolism, arginine and proline metabolism, steroid biosynthesis, sphingolipid metabolism and bile metabolism. Similarly, in our study, arginine and proline metabolism, purine metabolism, glycine and serine metabolism, and aspartate metabolism were among the top upregulated metabolic pathways in the presence of Matrigel and under nutrient-deprived conditions. Together, these findings suggest that ECM-mediated metabolic remodelling in PDAC cells closely mirrors clinically observed metabolic alterations, underscoring the clinical relevance of our model for studying the role of the ECM in PDAC metabolism.

Furthermore, using gene expression profiling, a study by Agarwal et al found that phosphoribosylaminoimidazole succinocarboxamide synthetase (PAICS), a key enzyme in purine metabolism, is overexpressed in PDAC cells compared to normal controls. They found that knockdown of PAICS induced apoptosis in PDAC cells, highlighting the importance of purine metabolism in PDAC survival (Agarwal et al., 2020). In agreement with these findings, our untargeted metabolomics showed that purine metabolism is upregulated in the presence of Matrigel across all nutrient-deprivation conditions studied. It is important to note, however, that while our untargeted data indicated an overall increase in purine metabolism, our targeted metabolomics specifically measured xanthine, a metabolite within the purine salvage pathway, rather than intermediates of de novo purine biosynthesis where PAICS functions. This distinction highlights that both salvage and synthetic arms of purine metabolism may contribute to ECM-dependent metabolic adaptation in PDAC cells.

In an effort to adequately mimic the nutrient contents of the TME of PDAC, Sullivan and colleagues used metabolomics to quantify the nutrient content of the interstitial fluid of a murine model of PDAC and subsequently formulated the TIFM used in our study. They found that arginine was the most depleted nutrient in their model (Sullivan et al., 2019; Apiz Saab et al., 2023). Consistent with this observation, while our untargeted metabolomics showed an upregulation of the arginine and proline metabolism in the presence of Matrigel, our targeted metabolomics data revealed that Matrigel did not increase the intracellular arginine levels in the cells cultured in TIFM. Also, while there was a Matrigel-induced upregulation of the ASS1 gene under both glucose and glutamine deprivation, there was no difference in the expression of ASS1 in the presence of Matrigel in TIFM.

Furthermore, a recent review by Lee and colleagues emphasised the need for a more stringent approach while interpreting pathway enrichment analysis results from untargeted metabolomics data. They shed light on some factors that may be responsible for the upregulation of some metabolic pathways in untargeted metabolomics without an increase in the concentration of metabolites in such pathways in targeted metabolomics. They stated that there might be an increase in the end-product metabolite of some pathways but not in the intermediate metabolites in such pathways, some metabolites may be rapidly produced and consumed by cells and finally, that a single metabolite may be made from multiple metabolic pathways and may be used to perform different functions within a cell (Lee et al., 2025). These considerations highlight the complexity of interpreting metabolomic data and provide a plausible explanation for why some metabolic pathways appear upregulated in our untargeted dataset, even in the absence of measurable changes in specific metabolites in our targeted analysis.

Interestingly, our targeted metabolomics revealed that in TIFM, creatine, a key end-product metabolite in the arginine and proline metabolic pathway, was significantly upregulated in the presence of Matrigel compared to plastic. This agrees with Lee and colleagues' thoughts on interpreting untargeted metabolomics data. Moreover, the intracellular creatine levels in cells in TIFM were markedly higher compared to cells in full media or other nutrient-deprivation conditions used in our study. This indicates that creatine might be vital to the role of Matrigel in supporting PDAC cells cultured in TIFM. To have a better understanding of the specific role of creatine in TIFM, it will be interesting to knock down genes that are involved in creatine biosynthesis, such as the guanidinoacetate N-methyltransferase (GAMT) and assess their effects on Matrigel-induced cell proliferation in TIFM.

In conclusion, our untargeted and targeted metabolomics data demonstrate that Matrigel alters the metabolism of PDAC cells, leading to increased intracellular metabolites such as arginine and creatine.

However, ASS1 knockdown did not alter Matrigel-dependent proliferation of PDAC cells under nutrient deprivation. Importantly, a key limitation that must be considered when interpreting this finding is that although ASS1 knockdown was confirmed at the mRNA level, the absence of protein-level verification means that residual ASS1 protein may have remained functionally sufficient during the proliferation assay, given that the half-life of ASS1 protein is not well established. Hence, the lack of phenotypic effect may reflect insufficient protein depletion rather than the role of ASS1 in this context. Nonetheless, these findings raise the possibility that metabolic compensatory mechanisms exist to mitigate the blockade of de novo arginine synthesis, or that alternative ECM-mediated processes, such as macropinocytosis-driven nutrient scavenging, contribute to PDAC cell growth under nutrient-limited conditions. Future studies should confirm ASS1 depletion at the protein level by western blot and further dissect the precise mechanisms by which the ECM supports metabolic adaptation and proliferation in nutrient-deprived environments

6 KRAS Inhibition results in the formation of quiescent, slow-cycling cells

6.1 Introduction

Tumour cells have been known to exist in a reversible quiescent state characterised by a lack of cell proliferation, the ability to evade assaults from chemotherapeutic agents and the ability to re-enter the cell cycle to resume proliferation (Ortmayr and Zampieri, 2022). Clinically, reactivation of quiescent/dormant tumour cells is one of the causes of cancer relapse (Yabuuchi et al., 2020). For example, a study by Yabuuchi and colleagues reported a recurrence of ER-positive breast cancer in the lungs about 23 years after initial successful treatment. Their morphological and immunohistochemical staining revealed that the lung metastasis was related to the initial breast cancer, leading them to conclude that the newly reported lung cancer was a result of reawakened dormant breast cancer cells (Yabuuchi et al., 2020).

Unlike breast cancers, a few studies have highlighted the presence of quiescent tumour cells in pancreatic cancer. For example, in their study on the role of copper in pancreatic cancer progression, Yu and colleagues found that both pharmacological deprivation of copper and siRNA knockdown of the copper transporter SLC31A1 resulted in a reduction in proliferation of PDAC cells without increasing cell death, with the majority of the cells in the G0 /G1 phase of the cell cycle, indicating quiescence (Yu et al., 2019).

More than 90% of pancreatic cancers are driven by activating mutations in the KRAS oncogene, with a codon 12-point mutation that changes glycine to aspartic acid being the most common (Hezel et al., 2006). Unlike wild-type KRAS, which switches between the inactive GDP-bound state and active GTP-bound state, mutated KRAS has impaired GTPase activity, thereby preventing the hydrolysis of GTP to GDP, leaving KRAS in the active GTP-bound state (Tu et al., 2024). Subsequently, the downstream signalling pathways, such as ERK and PI3K/AKT/mTOR, remain activated, eventually driving cell proliferation, migration, and survival.

After years of research into developing RAS-specific inhibitors, Wang et al reported the discovery of a potent G12D-specific inhibitor, MRTX1133, which was in the phase I/II clinical trial for solid tumours such as PDAC, colorectal cancer and non-small cell lung carcinoma (Wang et al., 2022). However, the study was recently terminated before entering phase II clinical trials. Structurally, KRAS is composed of a Guanine nucleotide-binding domain (G-domain) that mediates the GTPase activity of KRAS via its active site, a phosphate-binding loop (P-loop), a switch I and a switch II (Wittinghofer and Vetter, 2011;

Zeissig et al., 2023). The switch I and II regions change their conformation depending on whether KRAS is in a GDP-bound or GTP-bound state, allowing the binding of RAS downstream effectors such as RAF and PI3K (Zeissig et al., 2023). MRTX1133 selectively binds to the switch II pocket of the G-domain of G12D mutated KRAS in the GDP-bound state, resulting in a change in conformation that disrupts its ability to bind to its effectors, thereby blocking the cellular processes facilitated by the downstream effectors of KRAS (**Figure 6.1)** (Hallin et al., 2022; Wang et al., 2022).

In vivo and in vitro studies on KRAS G12D-mutated PDAC models have reported the efficacy of MRTX1133 in reducing the proliferation of PDAC cells and blocking phosphorylation of ERK, downstream of KRAS (Gulay et al., 2023; Kemp et al., 2023; Mahadevan et al., 2023). However, some studies have also reported that PDAC cells could acquire resistance to MRTX1133 (Feng et al., 2023; Singhal et al., 2024; Jiang et al., 2025). To our knowledge, no study has linked treatment with MRTX1133 with the development of quiescent PDAC cells.

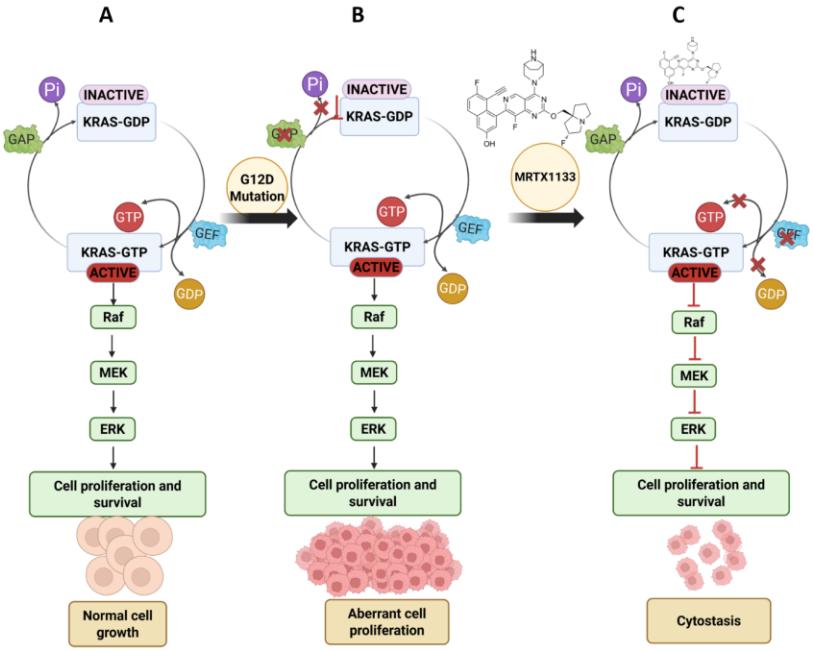

Figure 6.1 - Mechanism of Action of MRTX1133
(A) Wild-type KRAS switches between the inactive GDP-bound state and active GTP-bound state, facilitated by GAPs and GEFs, respectively. (B) Mutated KRAS has an impaired GAP-induced GTPase activity, thereby preventing the hydrolysis of GTP to GDP, leaving KRAS in the active GTP-bound state, resulting in sustained activation of its downstream effectors, and eventually leading to uncontrolled cell proliferation. (C) MRTX1133 selectively binds to G12D-mutated KRAS in the GDP-bound state, resulting in a change in conformation that disrupts its GEF activity, thereby blocking binding of KRAS to GTP and blocking its downstream effectors, and eventually blocking cell proliferation. Created with Biorender.com

Studies have reported that knockdown of the KRAS oncogene results in the formation of slow-cycling quiescent cells in PDAC (Viale et al., 2014; Rajbhandari et al., 2017). Therefore, we hypothesised that

treatment with MRTX1133 could yield a population of cells with a quiescent phenotype with the ability to re-enter the cell cycle and resume proliferation in the presence of appropriate signals.

6.2 Results

6.2.1 KRAS inhibition prevented ERK phosphorylation

The activation of MAPK was evaluated to assess the efficacy of the KRAS inhibitors in blocking downstream signalling. SW-1990 and MIA PaCa-2 cells were treated with MRTX1133 (a KRAS G12D inhibitor) or MRTX849 (a KRAS G12C inhibitor), respectively, for 4 days. The cell lysates were collected, and the expression of ERK and phosphorylated ERK (pERK) was measured via Western blotting. **Figure 6.2A** showed a significant reduction in the phosphorylation of ERK in SW-1990 cells upon treatment with MRTX1133 compared to the vehicle control, coupled with an overall reduction in ERK levels. Similarly, upon treatment with MRTX849, there was a reduction in phosphorylation of ERK and total ERK levels in MIA PaCa-2 cells (**Figure 6.2B)**. Thus, our data confirm the efficacy of both KRAS inhibitors in impairing signalling downstream of KRAS.

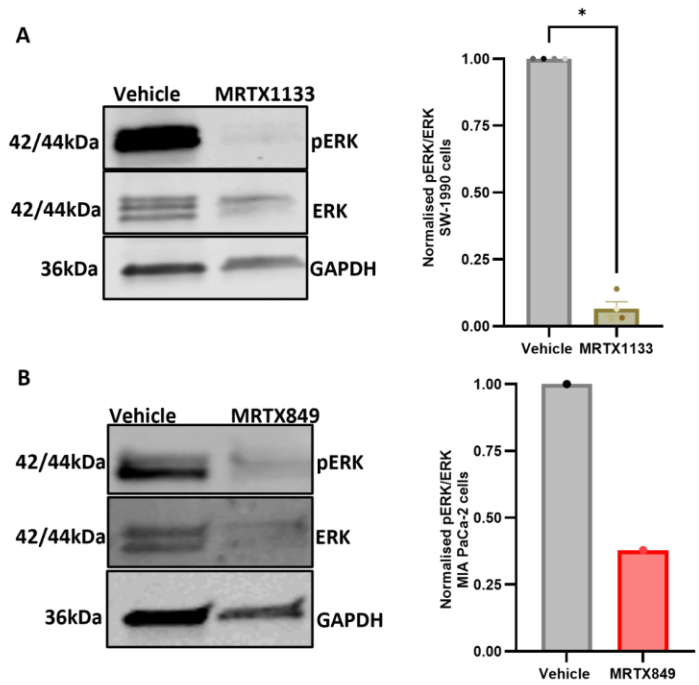

Figure 6.2 – KRAS Inhibition blocked ERK phosphorylation in PDAC cells
(A) SW-1990 and (B) MIA PaCa-2 cells were seeded on a 6-well plate and incubated overnight. The media was changed to (A) media containing DMSO (vehicle) or 200nM MRTX1133. (B) media containing DMSO (Vehicle) or 100nM MRTX849. The cell lysates were collected on Day 4, and the expression of ERK and pERK proteins was measured via Western blotting. The band intensity was quantified using Image Studio Lite software. Data are presented as Mean ± SEM. Significance was determined using the Mann-Whitney test. *p<0.05. N=4 (A), N =1 (B).

6.2.2 KRAS inhibition significantly reduced the proliferation of SW-1990 cells without an increase in cell death

To investigate the effects of KRAS inhibition, nutrient deprivation and serum deprivation on PDAC cell proliferation, human PDAC cell lines, SW-1990 and PANC-1, were treated with MRTX1133 (200nM) or exposed to glutamine-free media, serum-free media or vehicle control. After 4 days, the cells were fixed, stained with DRAQ5 and imaged using a LICOR Odyssey system. There was a significant reduction in the signal intensity of SW-1990 cells treated with MRTX1133 compared to the vehicle control. Similarly, there was a significant reduction in signal intensity upon glutamine deprivation. In contrast, there was no reduction in the signal intensity of SW-1990 cells when grown in serum-free media **(Figure 6.3A)**, suggesting that while SW-1990 cells were sensitive to treatment with MRTX1133 and a lack of glutamine, they were less sensitive to culture in serum-free media for the duration of the study.

On the other hand, signal intensity was not reduced upon treatment of PANC-1 cells with MRTX1133, suggesting that the cells were more resistant to MRTX1133 than SW-1990 cells. Furthermore, unlike SW-1990 cells, PANC-1 cells were sensitive to the lack of serum, as there was a significant reduction in signal intensity of PANC-1 cells exposed to serum-free media compared to the vehicle control. Similar to SW-1990 cells, there was a significant reduction in signal intensity upon glutamine deprivation compared to the control group **(Figure 6.3B)**.

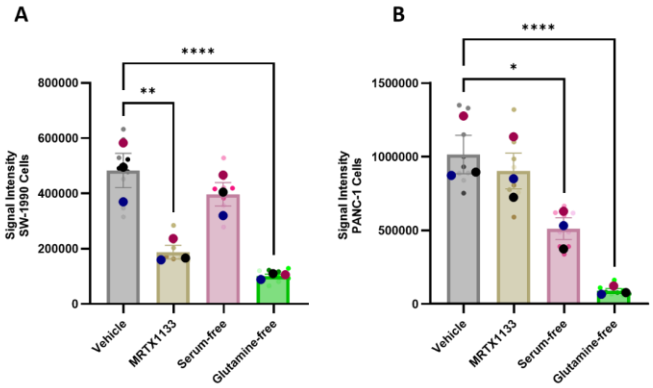

Figure 6.3 - KRAS inhibition reduced the growth of SW-1990 cells
(A) SW-1990 and (B) PANC-1 cells were seeded on 96-well plates and incubated overnight. The media was changed to media containing DMSO (Vehicle), media with 200nM MRTX1133, serum-free media and glutamine-free media supplemented with dFBS, and the cells were incubated for 4 days. The cells were fixed, stained with DRAQ5 and imaged with a Licor Odyssey Sa system. The signal intensity was quantified using Image Studio Lite software. Data are presented as Mean ± SEM. Significance was determined using Kruskal-Wallis and Dunn's multiple comparisons test.. ****p<0.0001, **p<0.01, *p<0.05. N=3 independent experiments, and the bigger dots represent the mean of each experiment.

Overall, these data showed that, while exposure to glutamine-free media significantly affected the cell proliferation of both SW-1990 and PANC-1 cells, SW-1990 cells were more resistant to serum-free

media compared to PANC-1 cells, while PANC-1 cells were more resistant to KRAS inhibition by MRTX1133 compared to SW-1990 cells.

To assess apoptosis, SW-1990 cells were treated with MRTX1133, glutamine-free media, serum-free media or vehicle control. The cells were co-stained with propidium iodide (PI) **(Figure 6.4A)** and Hoechst33342 and imaged live 4 days post-treatment. Live cell imaging showed that there was no significant difference in the percentage of PI-positive cells upon treatment with MRTX1133 compared to the vehicle control, while there was a small, but statistically significant, increase in the percentage of PI-positive cells upon exposure to glutamine-free and serum-free media **(Figure 6.4B)**. This suggests that although there was a substantial reduction in cell numbers upon treatment with MRTX1133, this was not accompanied by an increase in cell death.

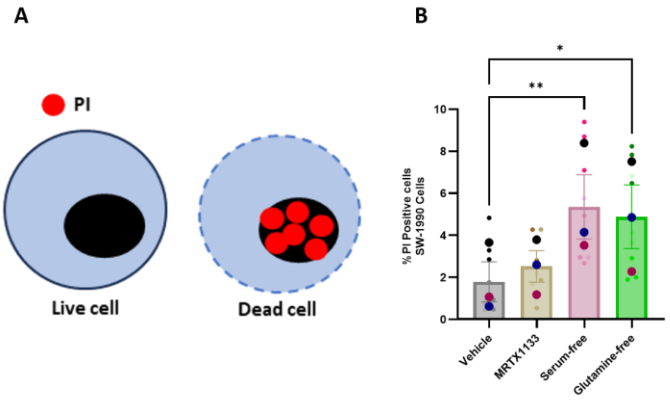

Figure 6.4 - KRAS inhibition did not increase apoptosis in SW-1990 cells
(A) Schematic representation of propidium iodide (PI) staining. (B) SW-1990 cells were seeded on 96-well plates and incubated overnight. The media was changed to media containing DMSO (Vehicle), media with 200nM MRTX1133, serum-free media and glutamine-free media supplemented with dFBS, and the cells were incubated for 4 days. The cells were stained with both Hoechst 33342 and PI, imaged live with an Image Xpress microscope and analysed using the MetaXpress software. Data are presented as Mean ± SEM. Significance was determined using Kruskal-Wallis and Dunn's multiple comparisons test. **p<0.01, *p<0.05. N=3 independent experiments, and the bigger dots represent the mean of each experiment.

To further characterise the effects of KRAS inhibition on cell viability, SW-1990 cells were treated with different concentrations of MRTX1133 (20nM and 200nM) for 4 days and 7 days, to determine the effect of a lower concentration and a longer-term exposure to the inhibitor on the cells. In addition, the cells were treated with gemcitabine, a known chemotherapeutic agent used to treat pancreatic cancer. The cells were co-stained with both Hoechst33342 and PI to determine the effects of the treatment on cell proliferation and cell death. As shown in **Figure 6.5A**, a lower concentration (20nM) of MRTX1133 resulted in a small and statistically insignificant reduction in cell number at day 4, while there was a significant reduction in cell number upon treatment with 200nM of MRTX1133. Expectedly, there was a significant reduction in cell number upon treatment with gemcitabine.

Similarly, at day 7, 20nM of MRTX1133 did not significantly reduce the cell number, while there was a significant reduction upon treatment with 200 nM MRTX1133 and gemcitabine **(Figure 6.5C)**.

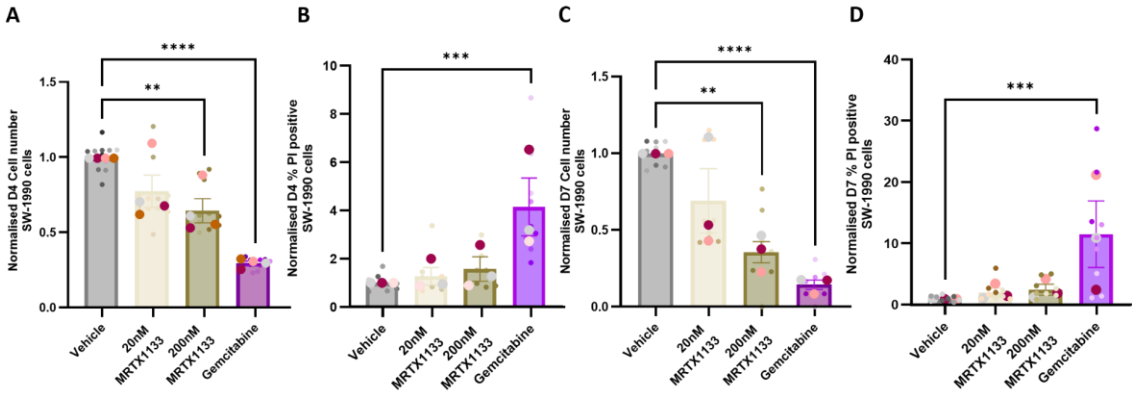

Figure 6.5 – KRAS G12D inhibition reduced proliferation but not apoptosis of SW-1990 cells
SW-1990 cells were seeded on 96-well plates and incubated overnight. The media was changed to media containing DMSO (Vehicle), 20nM MRTX1133, 200nM MRTX1133 and 10nM Gemcitabine and the cells were incubated for 4 days (A, B) and 7 days (C, D). The cells were stained with Hoechst 33342 and PI, imaged live with an Image Xpress microscope and analysed using the MetaXpress software. (A, C) The cell number was measured via Hoechst33342 nuclear staining. (B, D) The % PI was measured as a percentage of PI-positive cells. Data are presented as Mean ± SEM. Significance was determined using Kruskal-Wallis and Dunn's multiple comparisons test. ****p<0.0001, ***p<0.001, **p<0.01, *p<0.05. N ≥ 3 independent experiments, and the bigger dots represent the mean of each experiment.

In terms of cell death, at day 4, there was no increase in the percentage of PI-positive cells upon treatment with 20nM or 200nM of MRTX1133, while there was a small, but statistically significant, increase in the percentage of PI-positive cells upon treatment with gemcitabine **(Figure 6.5B)**. Similarly, at day 7, while there was a significant increase in the percentage of PI-positive cells upon treatment with gemcitabine, the percentage of PI-positive cells was not affected by treatment with 20nM or 200nM of MRTX1133 **(Figure 6.5D)**. This further indicates that MRTX1133 had a negligible effect on cell death.

To test whether the effects of KRAS inhibition on SW-1990 cell number and cell death could be replicated in KRAS G12C-mutated PDAC cells, MIA PaCa-2 cells were treated with 100nM of MRTX849, a known KRAS G12C inhibitor (Hallin et al., 2020). Like SW-1990 cells, while there was a significant reduction in cell number upon treatment with MRTX849, there was no increase in cell death, while treatment with gemcitabine resulted in a significant decrease in cell numbers coupled with a small, but statistically significant, increase in cell death (**Figure 6.6).**

Overall, the data showed that while treatment with both KRAS inhibitors, MRTX1133 and MRTX849, reduced cell number, there was no increase in cell death as seen in gemcitabine-treated cells. This suggests that treatment with KRAS inhibitors is cytostatic but not cytotoxic.

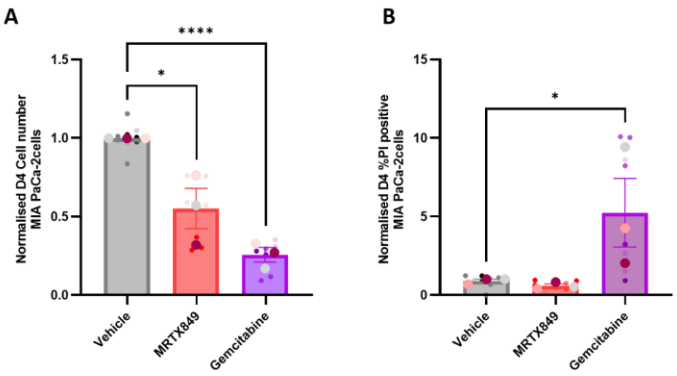

Figure 6.6 – KRAS G12C inhibition reduced proliferation but not apoptosis of MIA PaCa-2 cells
MIA PaCa-2 cells were seeded on 96-well plates and incubated overnight. The media was changed to media containing DMSO (Vehicle), 100nM MRTX849 or 10nM Gemcitabine and the cells were incubated for 4 days. The cells were stained with Hoechst33342 and PI, imaged live with an Image Xpress microscope and analysed using the MetaXpress software. (A) The cell number was measured via Hoechst33342 nuclear staining. (B) The % PI was measured as a percentage of PI-positive cells. Data are presented as Mean ± SEM. Significance was determined using Kruskal-Wallis and Dunn's multiple comparisons test. ****p<0.0001, *p<0.05. N=3 independent experiments, and the bigger dots represent the mean of each experiment.

6.2.3 MRTX1133 reduced EdU incorporation in PDAC cells

5-Ethynyl-2'-deoxyuridine (EdU) is a thymidine analogue that is incorporated in cells during DNA synthesis, i.e. in the S-phase of the cell cycle. As shown earlier, MRTX1133 treatment reduced cell number without affecting cell death. Therefore, EdU incorporation was used further to characterise the effects of MRTX1133 on cell division. SW-1990 cells were treated with MRTX1133 for 4 days, EdU was added to the cells on day 4 for 24 hours, and the cells were imaged to determine the percentage of EdU-positive cells. The result shows that only about 30% of MRTX1133-treated cells were EdU positive, compared to >60% of vehicle control cells (**Figure 6.7)**. This suggests that the progression through the cell cycle was impaired after treatment.

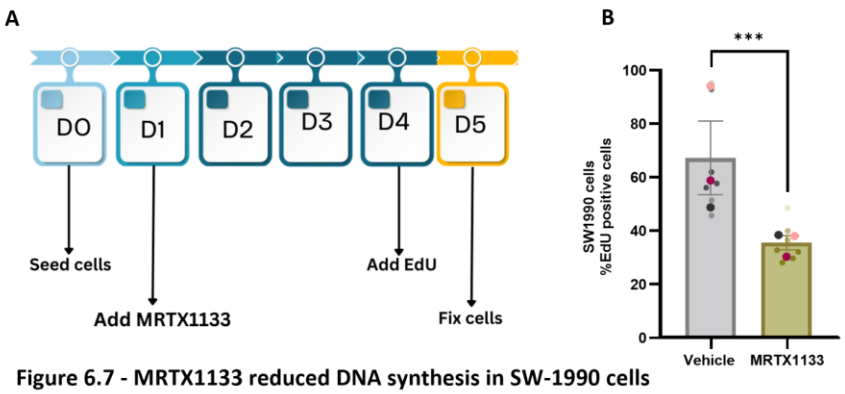

Figure 6.7 - MRTX1133 reduced DNA synthesis in SW-1990 cells
(A) Timeline of EdU incorporation experiment. (B) SW-1990 cells were seeded on a 96-well plate and incubated overnight. The media was changed to media containing DMSO (vehicle) or 200nM MRTX1133. The cells were incubated with EdU 4 days post-treatment, fixed and stained with Hoechst33342 and EdU cell proliferation imaging kit on Day 5. The samples were imaged using InCell Analyzer 2200 and analysed using Cell Profiler. Data are presented as Mean ± SEM. Significance was determined using the Mann-Whitney test. ***p<0.001. N=3 independent experiments, and the bigger dots represent the mean of each experiment.

6.2.4 MRTX1133-treated PDAC cells accumulated in the G0 phase of the cell cycle

So far, our data show that MRTX1133 effectively reduced cell proliferation without increasing cell death, suggesting that the cells may be quiescent. Here, we wanted to more directly quantify quiescent PDAC cells. A known method of distinguishing quiescent cells from cells in other phases of the cell cycle is by co-staining with Hoechst33342 and pyronin Y, followed by flow cytometry analysis as described by Eddaoudi and colleagues (Eddaoudi et al., 2018). Hoechst33342 stains the DNA, while pyronin Y stains both the DNA and RNA; when cells are stained with both Hoechst33342 and pyronin Y, Hoechst33342 binds to the DNA with more affinity while pyronin Y only binds to the RNA (Eddaoudi et al., 2018). While cells in G0 have the same DNA content as cells in the G1 phase of the cell cycle, they have a lower RNA content; therefore, low pyronin Y staining identifies quiescent cells.

Here, SW-1990 cells were grown in glutamine-free, serum-free media or treated with MRTX1133 for 4 days. Afterwards, they were stained with Hoechst33342 and pyronin Y and analysed via flow cytometry. As shown in **Figure 6.8,** about 60% of MRTX1133-treated cells were in the G0 phase, while culturing in vehicle control, glutamine-free media and FBS-free media resulted in approximately 35%, 40% and 38% of the cells, respectively, in the G0 phase of the cell cycle. Overall, the results indicate that compared to other treatment groups, treatment with MRTX1133 drove more cells into the G0 phase of the cell cycle.

6.2.5 MRTX1133 treatment resulted in the formation of a label-retaining population of SW-1990 cells

To further characterise the quiescent state of MRTX1133-treated cells, we performed a label retention assay. This is based on the principle that when cells are labelled with a dye, rapidly growing cells dilute the dye as they divide, while slow-dividing quiescent cells retain the dye (Moore et al., 2011). Since we have previously shown that MRTX1133 drove SW-1990 cells into a quiescent state, we hypothesise that the treated cells should retain the dye over time, as most are not proliferating. SW-1990 cells were treated with MRTX1133 for 4 days, labelled with Cell Tracker Red **(Figure 6.9A)**, plated in a 96-well plate and imaged live every day over 4 days post labelling. To image the cells, the nucleus was stained with Hoechst33342 to determine the percentage of cells positive for Cell Tracker Red in the entire cell population.

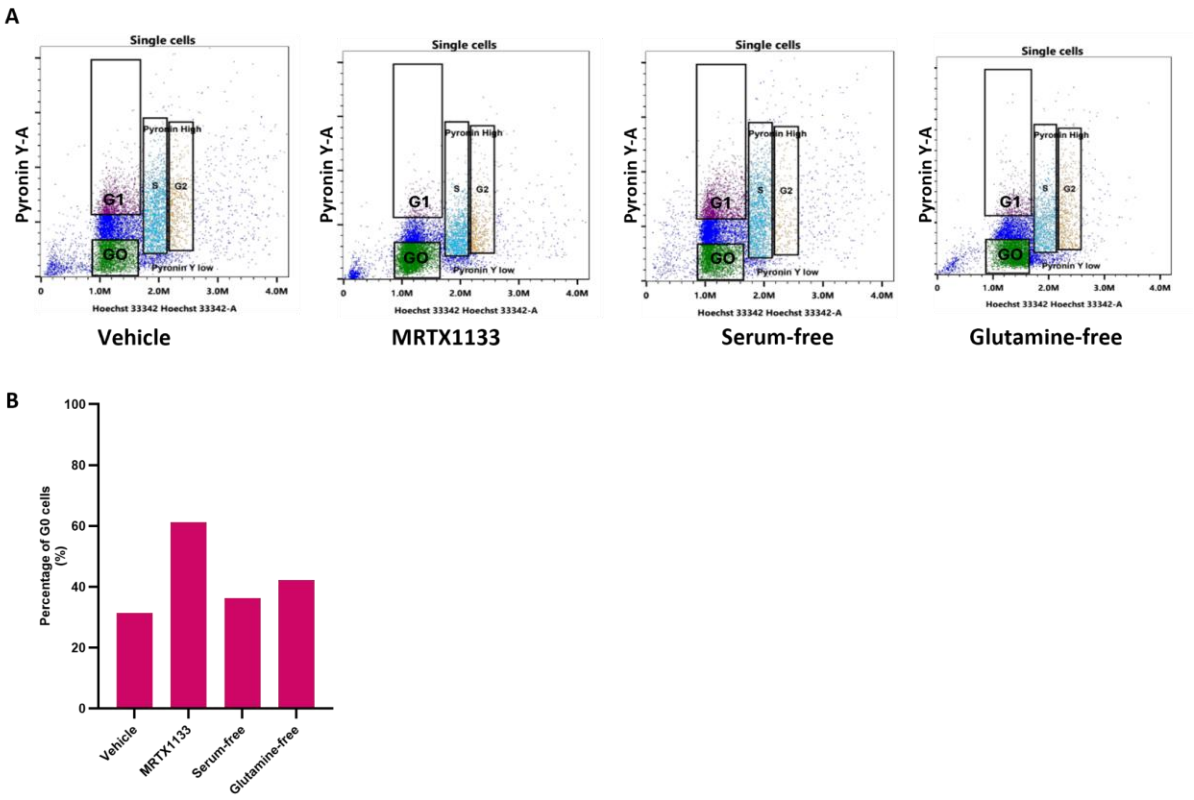

Figure 6.8 - SW-1990 cells are enriched in G0 phase upon treatment with MRTX1133
SW-1990 cells were seeded on a 6-well plate and incubated overnight. The media was changed to media containing DMSO (vehicle) or 200nM MRTX1133, serum-free and glutamine-free media supplemented with dFBS and incubated for 4 days. The cells were stained with both Hoechst33342 (10µg/ml) and Pyronin Y (5µg/ml) before flow cytometry analysis. (A) The bivariate plot showing DNA content (x axis - Hoechst33342) and RNA content (y axis = Pyronin Y fluorescence) (B). Data are presented as Mean, N=3 independent experiments.

As shown in **Figure 6.9B**, most of the cells in the vehicle control and the MRTX1133-treated group were positive for the cell tracker red on day 0. However, by day 4, while only a few of the cells in the control group were cell tracker red-positive, many of the cells in the MRTX1133-treated group were positive for the cell tracker red. Statistical analysis revealed that in the vehicle control cells, there was a progressive reduction in the percentage of Cell Tracker Red-positive cells from day 0 (≃90%), day 1 (≃50%), day 2 (≃20%), day 3 (≃5%) and day 4 (≃5%) **(Figure 6.9C)**. In contrast, in the MRTX1133-treated cells, there was limited reduction in the percentage of Cell Tracker Red-positive cells from day 0 (≃90%), day 1 (≃90%), day 2 (≃80%), day 3 (≃75%) and day 4 (≃70%) **(Figure 6.9C)**. More specifically, this indicated that treating SW-1990 cells with MRTX1133 drives the cells into a non-proliferative quiescent state.

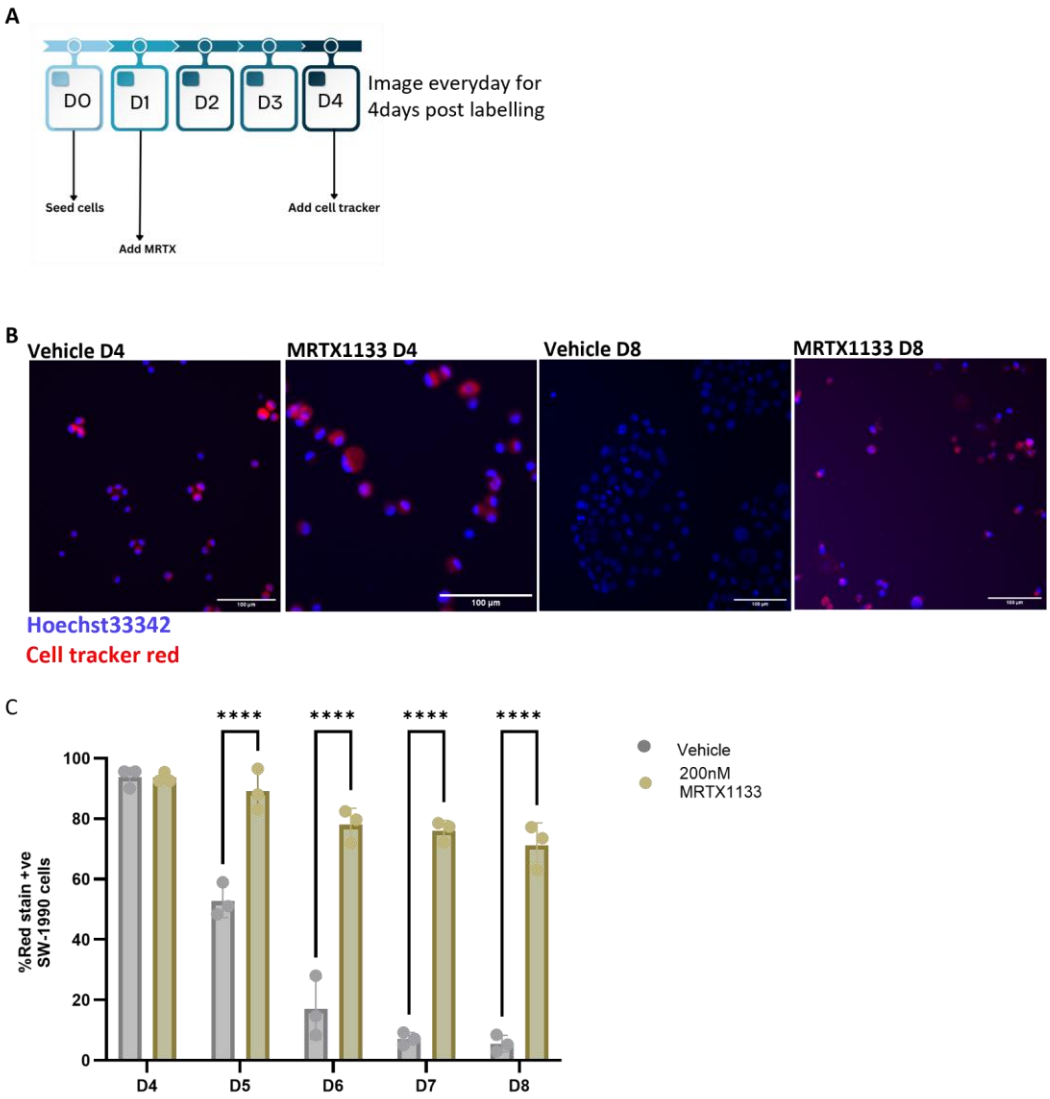

Figure 6.9 – MRTX1133 treatment resulted in the formation of a label-retaining population of SW-1990 cells
(A) Timeline of the experiment. (B) SW-1990 cells were seeded on a 6-well plate and incubated overnight. The media was changed to media containing DMSO (vehicle) or 200nM MRTX1133. The cells were labelled with cell tracker red (1:3000 dilution in serum-free media) on D4 and imaged for 4 days post labelling. Representative images (B) were taken on Day 4 and Day 8 using InCell Analyzer 2200 and analysed using Cell Profiler. Scale bar 100µm (C) Data are presented as Mean ± SEM. Significance was determined by a 2-Way Anova test with a Tukey's Multiple comparisons test. ****p<0.0001. N=3 independent experiments. D4 = Day 4, D5 = Day 5, D6 = Day 6, D7 = Day 7, D8 = Day 8.

6.2.6 MRTX1133 reduced the activation of mTORC1 in PDAC cells

mTOR can be activated downstream of KRAS signalling and has been implicated in tumour quiescence. Specifically, downregulation of mTOR signalling, evidenced by reduced phosphorylation of pS6 downstream of mTORC1, is reported to be a characteristic of quiescent tumour cells (Khalil et al., 2021). To determine the effects of MRTX1133 on mTORC1 signalling, the phosphorylation of S6 (pS6), a downstream mTORC1 target, was determined via Western blotting. 96 hours of treatment with MRTX1133 resulted in a significant reduction in S6 phosphorylation, compared to the vehicle control

(Figure 6.10). This indicates that KRAS inhibition impaired mTORC1 activation, a feature of quiescent PDAC cells.

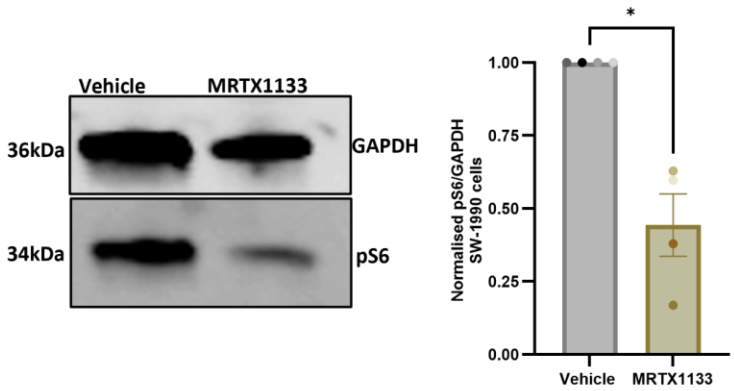

Figure 6.10 - MRTX1133 reduced mTORC1 signalling in SW-1990 cells
SW-1990 cells were seeded on a 6-well plate and incubated overnight. The media was changed to media containing DMSO (vehicle) or 200nM MRTX1133. The cell lysates were collected on Day 4, and S6 phosphorylation was measured via Western blotting. The band intensity was quantified using Image Studio Lite software. Data are presented as Mean ± SEM. Significance was determined using the Mann-Whitney test. *p<0.05. N=4 independent experiments.

6.2.7 PDAC cells restarted proliferation upon removal of MRTX1133

To confirm the reversibility of the growth arrest upon treatment with MRTX1133, SW-1990 cells were treated with MRTX1133 for 4 days, and the media were changed to fresh media in the presence or absence of MRTX1133 for 8 days (**Figure 6.11A)**. The cells were then stained with Hoechst33342 and imaged. **Figure 6.11B** shows a significant increase in the number of cells upon removal of MRTX1133 compared to the controls treated with MRTX1133 throughout the whole experiment. This suggests that the cells could regain their proliferative properties upon removal of MRTX1133.

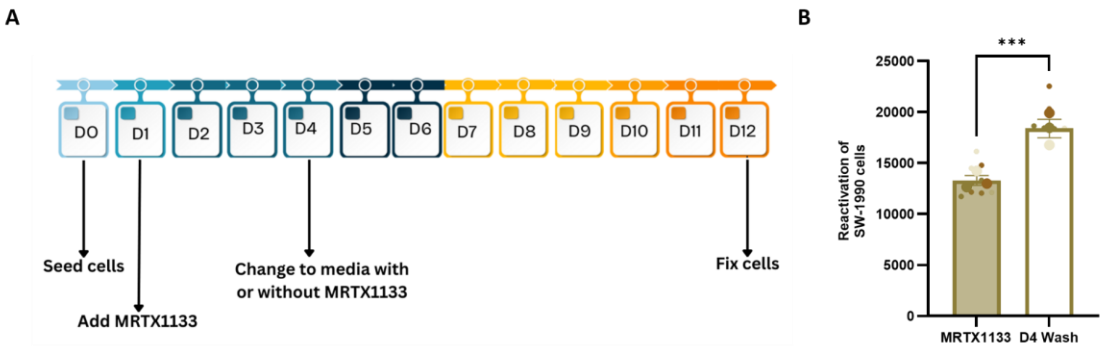

Figure 6.11 - Removal of MRTX1133 reversed its growth inhibition effects on SW-1990 cells
(A) Timeline of MRTX1133 removal experiment. (B) SW-1990 cells were seeded on a 96-well plate and incubated overnight. The media was changed to media containing DMSO (vehicle) or 200nM MRTX1133. The cells were washed and media replaced with fresh media without MRTX1133 4 days post-treatment, and the cells were fixed and stained with Hoechst33342 8days post-wash. The samples were imaged using InCell Analyzer 2200 and analysed using Cell Profiler. Data are presented as Mean ± SEM. Significance was determined using the Mann-Whitney test. ***p<0.001. N=3 independent experiments, and the bigger dots represent the mean of each experiment.

6.2.8 MRTX1133 treatment altered the metabolic profile of PDAC cells

6.2.8.1 Untargeted metabolomics showed intracellular metabolite alterations in MRTX1133-treated cells

Metabolic adaptations are a hallmark of cancer (Hanahan and Weinberg, 2011); however metabolic requirements of quiescent cancer cells have been largely understudied. Here, we wanted to identify the metabolic pathways that might play a role in the survival of MRTX1133-induced quiescent PDAC cells. To do this, metabolites were extracted from MRTX1133-treated cells, vehicle control and a 3rd group treated with palbociclib (Pb), a known cyclin-dependent kinase 4/6 inhibitor which arrests the cells in the late G1 phase of the cell cycle, as an additional control to exclude metabolic changes associated with the lack of proliferation. UPLC-MS-based untargeted metabolomics was used to identify all the metabolites in the samples. Perseus was used to analyse the untargeted metabolomics data by comparing the metabolites present in the vehicle (V) control versus MRTX1133-treated cells (MRTX) (Group A) and vehicle (V) control versus Pb-treated cells (Pb) (Group B). The volcano plots **(Figure 6.12 A, B)** show that there were differentially expressed metabolites in Group A (V vs MRTX) and Group B (V vs Pb). The red dots represent the metabolites that were upregulated in each group, while the grey dots indicate the metabolites that were not significantly changed in each group. In Group A, about 2000 metabolites were significantly upregulated in the vehicle control group; similarly, about 2000 metabolites were significantly upregulated in the MRTX1133-treated cells. Additionally, in Group B, about 1500 metabolites were significantly upregulated in the vehicle control group, and about 1500 metabolites were significantly upregulated in the Pb-treated cells.

Next, a Venn diagram was used to determine the metabolites that were specifically upregulated in each treatment group. To do this, all the metabolites significantly higher in the MRTX1133-treated group in Group A, the metabolites that were significantly higher in the palbociclib-treated group in Group B, and the metabolites that were significantly higher in the vehicle control were put in a Venn diagram. While there were some metabolites common to each treatment group, 361 of the metabolites were specific to the vehicle control group, while 65 and 48 were specific to the samples in the MRTX1133-treatment group and the palbociclib-treatment group, respectively **(Figure 6.12C)**.

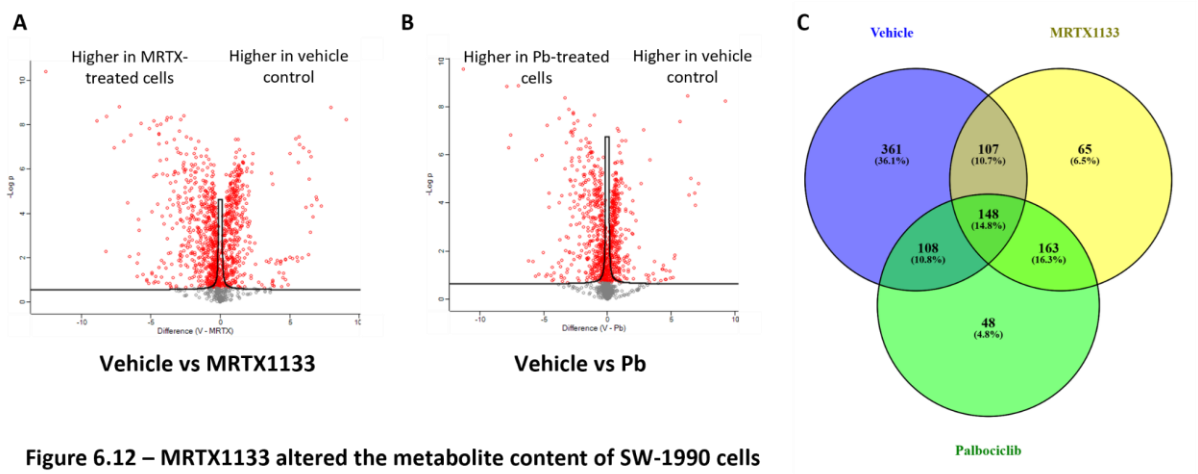

Figure 6.12 – MRTX1133 altered the metabolite content of SW-1990 cells
SW-1990 cells were seeded on a 6-well plate and incubated overnight. The media was changed to media containing DMSO (vehicle), 200nM MRTX1133 or 1µM Palbociclib (Pb). The metabolites were extracted on day 4 and analysed by untargeted LC-MS. The volcano plots (A, B) were plotted using Perseus by comparing the fold change and adjusted q-value between Vehicle and MRTX1133 (A) and Vehicle and Palbociclib (B). Raw intensity values were log2-transformed before statistical analysis. Differential abundance between the treatment conditions was assessed by a two-sample Student's T-test with an S_0 parameter of 0.1. Statistical significance was determined at FDR < 0.05. The statistically significantly higher metabolites are shown in red, while the non-significant metabolites are shown in grey. (C) The Venn diagram shows the distribution of the significantly higher metabolites in each treatment condition.

To determine the specific metabolic pathways upregulated in each group, Metaboanalyst 6.0 was used to perform an Enrichment Analysis. The metabolites unique to each condition were uploaded to the Metaboanalyst database, and they were cross-referenced to the metabolites deposited in the Human Metabolome Database. The identified metabolites were deposited on the Small Molecule Pathway Database (SMPDB) to map them to the normal human metabolic pathways on the SMPDB. Our results showed that the top 5 enriched pathways in the vehicle control group were purine metabolism, glutamate metabolism, glycine and serine metabolism, aspartate metabolism, and the urea cycle (**Figure 6.13A)**. In contrast, the top 5 enriched pathways in MRTX1133-treated cells were lysine degradation, carnitine synthesis, methionine metabolism, β-oxidation of very long chain fatty acid and fatty acid biosynthesis (**Figure 6.13B)**. Finally, the top 5 enriched pathways in Pb-treated cells were alpha linolenic acid metabolism, inositol phosphate metabolism, plasmalogen synthesis, pterine biosynthesis and β-oxidation of long chain fatty acid (**Figure 6.13C)**.

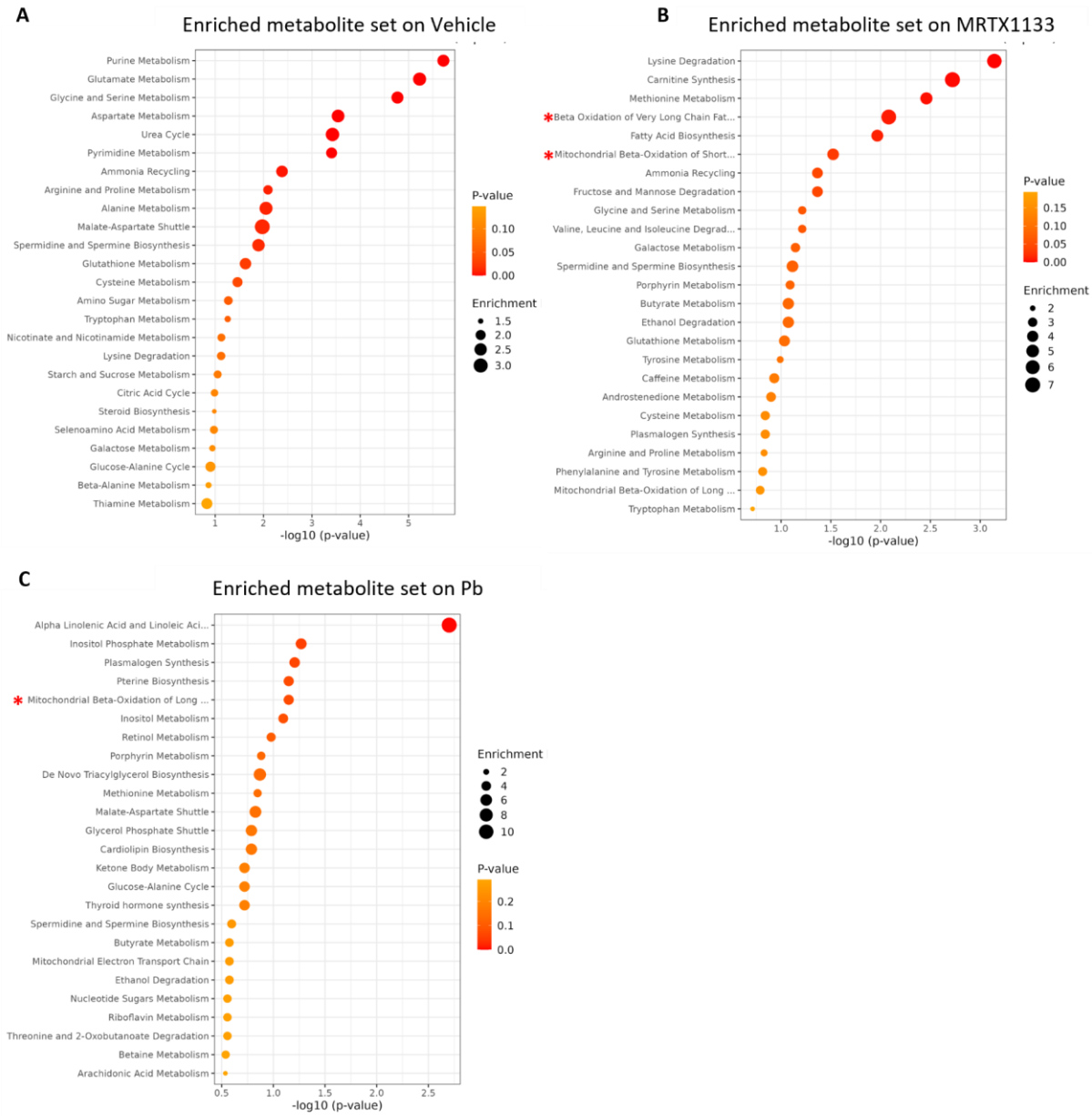

Figure 6.13 – MRTX1133 altered the metabolism of SW-1990 cells
SW-1990 cells were seeded on a 6-well plate and incubated overnight. The media was changed to media containing DMSO (vehicle), 200nM MRTX1133 or 1µM Palbociclib (Pb). The metabolites were extracted on Day 4 and quantified by untargeted mass spectroscopy. Metaboanalyst was used to determine the top 25 enriched pathways on (A) vehicle alone, (B) MRTX1133 alone and (C) Palbociclib (Pb) alone.

Altogether, our enrichment analysis showed that while most of the enriched metabolic pathways in the vehicle control group were linked to amino acid metabolism, the majority of the enriched metabolic pathways in the MRTX1133- and Pb-treated groups were related to fatty acids.

6.2.8.2 Targeted metabolomics showed upregulation of metabolites in the β-oxidation of fatty acids pathway in MRTX1133-treated cells

As stated in Chapter 5, targeted metabolomics can be used to test a previously established hypothesis based on the data from untargeted metabolomics by quantifying a known set of metabolites in each sample. Given that the untargeted metabolomics data showed that β-oxidation of fatty acid **(Figure**

6.14A) was one of the most enriched pathways in MRTX1133-treated cells, we performed targeted metabolomics on 16 selected metabolites (the majority of them in the β-oxidation of fatty acid pathway) to confirm their upregulation upon treatment with MRTX1133.

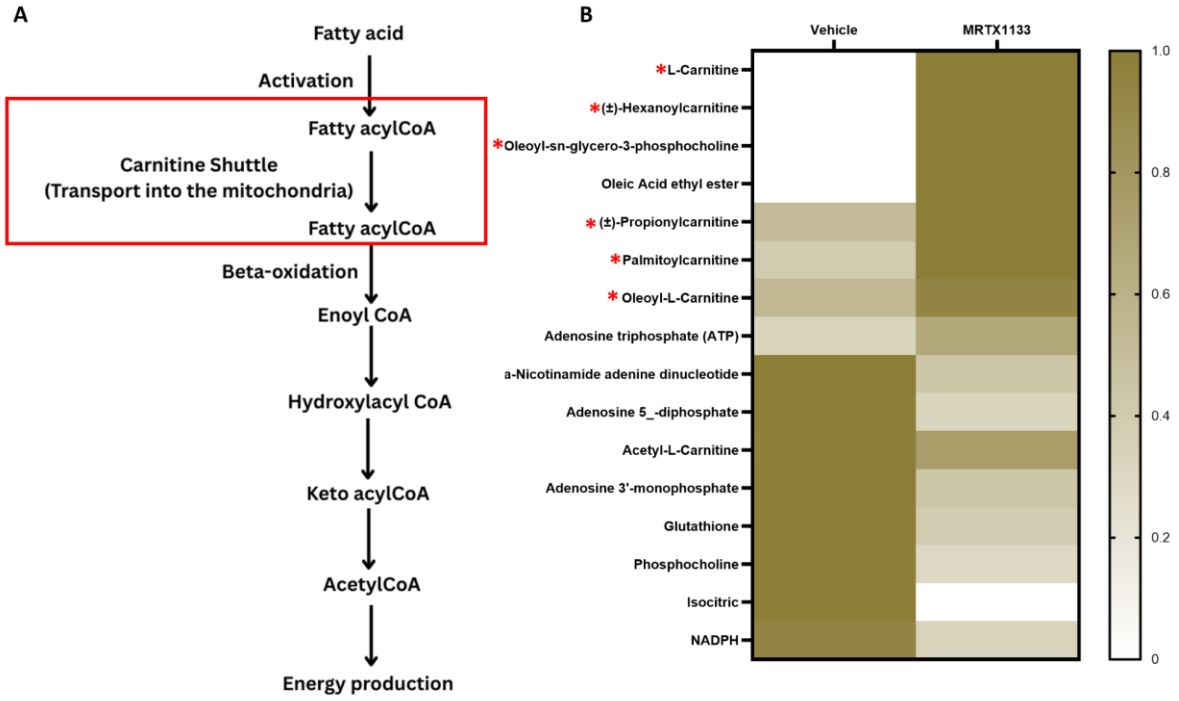

Figure 6.14 – Heatmap of Metabolite Intensities in Vehicle and MRTX1133-treated groups
(A) The β-oxidation of fatty acids begins with the activation of fatty acids to fatty acyl-CoA in the cytoplasm. The activated fatty acyl-CoA is then transported into the mitochondrial matrix via the carnitine shuttle system. Within the mitochondria, β-oxidation sequentially shortens the fatty acyl-CoA chain, generating acetyl-CoA, which subsequently enters the tricarboxylic acid (TCA) cycle for energy production in the form of ATP. (B) SW-1990 cells were seeded on a 6-well plate. The media was changed to media containing DMSO (vehicle) or 200nM MRTX1133 after 24 hours. The metabolites were extracted on Day 4 and quantified by targeted mass spectroscopy. Each column represents an individual sample, and each row corresponds to a detected metabolite. The data was normalised to the highest value within each group. The colour intensity indicates normalised metabolite levels, with gold indicating higher and white indicating lower relative intensity. N = 3

All our targeted metabolomics data are summarised as a heatmap, with the deeper shades representing a higher intensity of a specific metabolite and the lighter shades representing a lower intensity of a specific metabolite **(Figure 6.14B)**. In vehicle control cells, we saw elevated levels of phosphocholine, beta-nicotinamide adenine dinucleotide (NAD), ADP, AMP, Glutathione, Isocitric acid and NADPH compared to the MRTX1133-treated cells. Interestingly, none of these metabolites is directly involved in the β-oxidation of fatty acids. Contrarily, in MRTX1133-treated cells, we saw an upregulation of propionyl carnitine, hexanoyl carnitine and oleyl-L carnitine, all of which are intermediates in the carnitine shuttle system that promotes the transport of fatty acids into the mitochondria, where β-oxidation takes place.

In summary, using metabolomics, we showed that treatment with MRTX1133 upregulated metabolic pathways linked to β-oxidation of fatty acids. This suggests that MRTX1133-treated cells rely on β-

oxidation for energy generation to facilitate their survival, and disrupting this pathway could improve the efficacy of MRTX1133.

6.3 Discussion

KRAS mutation is found in about 90% of PDAC cases, and among all the KRAS mutations, the G12D mutation is found in about half of KRAS-mutated PDAC (Hezel et al., 2006). Hence, the discovery of MRTX1133, a G12D-specific inhibitor, represents a breakthrough in PDAC. However, given the propensity of cancer cells to evolve and develop new mechanisms of survival when targeted, it is vital to extensively characterise the effects of treatment with MRTX1133 on PDAC cells. In this chapter, we showed that treatment of PDAC cells, specifically, SW-1990 cells, with MRTX1133 resulted in reduced cell proliferation, no significant increase in cell death and accumulation of cells in a quiescent G0 phase of the cell cycle. Notably, using metabolomics approaches, we found that upon treatment with MRTX1133, PDAC cells might rely on energy generation via β-oxidation of fatty acids to survive in their quiescent state.

Several studies have reported the cytostatic effects of MRTX1133 in both in vitro and in vivo models of PDAC (Gulay et al., 2023; Mahadevan et al., 2023). Similarly, we found that treatment with MRTX1133 resulted in a significant reduction in the proliferation of SW-1990 cells; however, we did not see a similar decrease in PANC-1 cells at the same concentration. This agrees with the study of Jiang and colleagues, who highlighted that PANC-1 cells were less sensitive to MRTX1133 than other G12D-mutated PDAC cell lines (Jiang et al., 2025). In agreement with the study by Kemp et al, we found that MRTX1133 is specific to G12D-mutated PDAC cells, as treatment of BxPC-3 cells (with wild-type KRAS) with MRTX1133 did not affect cell proliferation (data not shown) (Kemp et al., 2023).

One of the downstream effectors of KRAS is ERK, and activation of ERK via phosphorylation triggers a series of processes that result in cell proliferation and survival. Expectedly, MRTX1133 impaired the phosphorylation of ERK in SW-1990 cells as previously reported (Gulay et al., 2023; Kemp et al., 2023). In addition to ERK, mTORC1 signalling is another signalling pathway activated downstream of KRAS. Like our findings, Hallin et al reported that treatment with MRTX1133 reduced S6 phosphorylation in G12D-mutated pancreatic and colorectal cell lines (Hallin et al., 2022). However, it is noteworthy that in our study, downregulation of mTORC1 signalling could be a quiescence marker. Consistent with this, studies have reported that inactivation of mTORC1 signalling has driven cells into a quiescent state (Terzi et al., 2016; Aleksandrova et al., 2024). For example, a study by Khalil et al revealed that nuclear receptor NR2F1 induced dormancy in HNSCC mouse models, and they found that, in addition to other markers of dormancy, low phosphorylation of S6 was seen upon induction of dormancy (Khalil et al.,

2021). In contrast to this, using a breast cancer model of tumour quiescence/dormancy, and pS6 as a readout of mTORC1 signalling, Hampsch and colleagues found that there was no reduction in mTORC1 signalling when they compared their quiescent models to the proliferative model (Hampsch et al., 2020). While the inconsistency in S6 phosphorylation as a quiescence marker is unclear, it might be due to different genetic markers in the cell lines or in the drivers of quiescence used in the other studies.

Furthermore, via flow cytometry and dye retention assay, we showed that treatment with MRTX1133 drove the cells into a non-proliferative G0 phase. While we do not know of any studies that have looked at the specific role of MRTX1133 in driving PDAC cells to a quiescent state, using a KRAS G12D-mutated model of pancreatic cancer, Rajbhandari et al found that genetic knockdown of KRAS in these cells resulted in a population of cells with a quiescent phenotype (Rajbhandari et al., 2017). This agrees with our findings that disrupting KRAS mutations, specifically the G12D mutation, could result in a population of quiescent tumour cells.

Additionally, given that one of the main properties of quiescent cells is their ability to re-enter the cell cycle (Endo and Inoue, 2019; Ortmayr and Zampieri, 2022), we saw that the removal of MRTX1133 allowed the cells to resume proliferation, as evidenced by the significant increase in cell proliferation in our data. In agreement with this, Feng et al reported that cytostatic effects of MRTX1133 were reversible in colorectal cancer cells, as they found that removal of MRTX1133 resulted in increased cell proliferation of G12D-mutated colorectal cell lines (Feng et al., 2023)

Proliferative cells, with the need to produce building blocks to continue cell proliferation, have different metabolic demands when compared to quiescent cells (Diehl et al., 2024). Quiescent cells, given that they are not actively proliferating, largely depend on catabolic metabolism such as β-oxidation of fatty acids and oxidative phosphorylation to produce ATP to sustain them in their quiescent state (Ortmayr and Zampieri, 2022; Suomalainen and Nunnari, 2024). In agreement with this, our untargeted metabolomics data revealed that compared to cells in the vehicle control that showed upregulation of amino acid and nucleotide metabolic pathways, MRTX1133-treated cells upregulated pathways linked to mitochondrial β-oxidation of fatty acids. Furthermore, our targeted metabolomics data confirmed the increased levels of metabolites in the β-oxidation of fatty acid metabolism pathway, such as propionyl carnitine, hexanoyl carnitine and oleyl-L carnitine. Interestingly, several studies have highlighted the role of β-oxidation of fatty acids in quiescent tumour cells (Hampsch et al., 2020; Ortmayr and Zampieri, 2022). More specifically, Hampsch and colleagues showed that in a breast cancer model of dormancy/quiescence, there was an upregulation of β-oxidation of fatty acid pathway, and the cells were sensitive to pharmacological inhibition of carnitine

palmitoyl transferase 1 (CPT1) (the rate-limiting enzyme in β-oxidation pathway) (Hampsch et al., 2020). Ortmayr and Zampieri also found that while actively proliferating cells were insensitive to pharmacological inhibition of 3-ketoacyl-CoA thiolase, one of the enzymes involved in fatty acid oxidation, it increased cell death in the quiescent lung and colon cancer models used in their study (Ortmayr and Zampieri, 2022).

It is important to highlight that the fact that most of our experiments were performed in a single cell line and using only MRTX1133 is a limitation of this study. Subsequent work could assess the roles of different mutant KRAS-specific inhibitors, as well as PAN-RAS inhibitors like RMC-7977, with various concentrations and in other KRAS-mutated PDAC cell lines like SU86.86 to better understand the quiescent-inducing role of KRAS inhibitors. Also, our EdU incorporation data showed that about 35% of the cells were positive for EdU, and it could be argued that the increase in cell number upon removal of MRTX1133 could be from the 35% of cells already positive for EdU.

Reactivation of quiescent cells has been reported to be responsible for cancer relapse after initial successful treatment (Yabuuchi et al., 2020). A breakthrough in cancer research would be to eradicate quiescent tumour cells before they could become reactivated to cause cancer relapse. Understanding and disrupting the survival mechanism of quiescent tumour cells is vital to do this. Here, we have not only shown that treatment with MRTX1133 could result in the formation of quiescent cells, but our data also suggest that these cells upregulated β-oxidation of fatty acids, which could be a vulnerability that could be exploited for cancer therapy. This suggests that disrupting the β-oxidation of fatty acid pathways might have the potential to improve the efficacy of MRTX1133 and eradicate these quiescent cells, further highlighting the potential benefits of combination treatment in cancer research.

7 Discussion

7.1 Matrigel supports the proliferation of nutrient-deprived PDAC cells by promoting ECM internalisation or mTORC1 activation, in a starvation-dependent manner

The understanding that even in nutrient-deprived conditions, PDAC cells survive by scavenging nutrients from the extracellular environment via macropinocytosis and other endocytic pathways (Olivares et al., 2017), upregulate nutrient transporters (Parker et al., 2020), and upregulate different metabolic pathways (Cheng et al., 2025) has garnered increased interest in understanding the metabolic flexibility of PDAC. PDAC cells have a dense fibrotic microenvironment (Hidalgo, 2010) characterised by an extensive deposition of ECMs. They scavenge nutrients from extracellular proteins and the ECM to support their survival, and macropinocytosis plays a role in the internalisation of ECM proteins (Olivares et al., 2017).

In our study, using different nutrient-starvation conditions, we have shown that ECM proteins, specifically Matrigel, support the growth of nutrient-starved PDAC cells. Consistently, collagen I and IV have been shown to promote pancreatic and breast cancer cell growth under glucose, glutamine or amino acid-deprived conditions (Olivares et al., 2017; Nazemi et al., 2024). Previous work by Olivares et al using KPC PDAC cells reported that PDAC cells internalise collagen I and IV under both glucose and glutamine-deprived conditions (Olivares et al., 2017). However, our study did not observe a similar increase in ECM internalisation under glucose-free conditions.

Our data revealed that Matrigel internalisation is upregulated under glutamine-deprived conditions compared to glucose-deprived conditions or in nutrient-replete conditions in both KRAS-mutated and wild-type KRAS PDAC cells. A possible explanation for the difference in Matrigel internalisation is that our ECM internalisation assay did not account for lysosomal degradation of internalised ECM, which may have occurred under glucose starvation. Thus, ECM internalisation might still occur under glucose deprivation, but the ECM could be degraded faster than under glutamine deprivation. Further experiments could test this hypothesis by blocking lysosomal degradation after ECM internalisation using inhibitors such as E-64D, an irreversible inhibitor of cysteine proteases (Fujishima et al., 1997), to determine whether preventing ECM degradation alters the apparent rate of ECM internalisation.

Furthermore, while it is well known that PDAC cells, especially KRAS-mutated cells, internalise extracellular proteins to scavenge nutrients via macropinocytosis (Commisso et al., 2013; Kamphorst et al., 2015; Jeong et al., 2018), and that macropinocytosis facilitates the internalisation of collagens I and IV under glucose deprivation (Olivares et al., 2017), the endocytic pathways that facilitate Matrigel internalisation under glutamine deprivation remain unclear. Although our study did not highlight the specific nutrient scavenging pathways that play a role in Matrigel internalisation under glutamine deprivation, possible pathways are macropinocytosis (widely studied in PDAC), clathrin-mediated endocytosis or caveolae-mediated endocytosis.

Additionally, we found that Matrigel internalisation was required for Matrigel-dependent cell proliferation under glutamine-deprived conditions but not in glucose-deprived conditions. Supporting the relevance of ECM-internalisation under nutrient stress, Hsu et al used colorectal (SW620), lung (PC9), and pancreatic (HPAC) cancer cells to demonstrate that tumour-cell survival under nutrient stress is not directly dependent on collagen internalisation by tumour cells. Instead, they showed that tumour-associated stromal cells, rather than cancer cells, internalise and degrade collagen I via Tumour Endothelial Marker 8 (TEM8) to generate glutamine, which sustains cancer cell survival under nutrient stress. Notably, pharmacological inhibition or genetic knockout of TEM8 disrupted this metabolic support and suppressed tumour growth (Hsu et al., 2022). While our study focused on Matrigel internalisation by PDAC cells, Hsu's findings complement our observation by highlighting that ECM internalisation, whether by cancer or stromal cells, serves as a critical mechanism of metabolic adaptation under nutrient stress. Together, these studies highlight the importance of ECM-derived nutrient scavenging as a survival strategy in nutrient-deprived tumour microenvironments.

Taken together, our results indicate that nutrient scavenging is the preferred means of nutrient acquisition under glutamine deprivation, leading us to hypothesise that glutamine-deprived PDAC cells upregulate nutrient scavenging mechanisms to facilitate Matrigel internalisation followed by lysosomal degradation, resulting in increased intracellular arginine levels, which can feed into the TCA cycle to support cell survival and proliferation **(Figure 7.1A)**.

Furthermore, our study revealed that Matrigel activates mTORC1 signalling in both glucose and glutamine-deprived conditions, with a more profound effect seen under glucose-starved conditions. Following up on this, we found that upon mTORC1 inhibition, there was a significant reduction in Matrigel-dependent cell proliferation in glucose-starved conditions. In contrast, in glutamine-deprived conditions, where cells depend on Matrigel internalisation for proliferation, mTORC1 signalling was not required for Matrigel-induced growth. These results align with a study by Palm et al, where they found that when cells depend on extracellular proteins like albumin to supply amino acids under

essential amino acid-deprived conditions, mTORC inhibition by TORIN-1 further enhanced cell proliferation by promoting lysosomal degradation of internalised proteins (Palm et al., 2015). Their findings provide a rationale for why mTORC1 signalling is dispensable in Matrigel-dependent growth under glutamine deprivation, as seen in our study.

Previous work has shown that SLC38A9 senses intracellular arginine to trigger the recruitment and activation of mTORC1 to support cell growth under leucine deprivation in PDAC cells (Wyant et al., 2017). However, analysis of Human Protein Atlas data indicates that although SLC38A9 is expressed at the mRNA level in the majority of PDAC cell lines, it is not expressed at the protein level. In contrast, SLC7A1, a well-characterised amino acid transporter that transports arginine, lysine, and ornithine from the extracellular space to the cytosol (You et al., 2022), is expressed at the protein level in SW-1990 cells used in our study (Pontén et al., 2008).

Based on these findings, we propose that under glucose deprivation, SLC7A1 might facilitate the import of Arginine into the cytosol, leading to a Matrigel-dependent increase in intracellular Arginine. This, in turn, activates mTORC1 signalling to promote protein translation and cell proliferation **(Figure 7.1B)**.

Furthermore, as PDAC cells have been found to upregulate different metabolic pathways for survival (Cheng et al., 2025), we also saw that Matrigel altered PDAC cells' metabolism in nutrient-replete and nutrient-starved conditions. Our untargeted metabolomics data revealed a Matrigel-induced upregulation of arginine and proline metabolism, purine metabolism and aspartate metabolism. Similar to our findings, the Arginine and proline metabolic pathway was the most enriched pathway in KPC PDAC cells cultured on fibronectin-coated hydrogels (Papalazarou et al., 2020).

Additionally, we observed that intracellular arginine levels are higher when cells are cultured on Matrigel compared to plastic. Interestingly, while we saw an increase in the intracellular arginine levels under both glucose and glutamine deprivation, we did not see a corresponding increase in TIFM. Instead, there was a significant increase in the intracellular levels of creatine in cells cultured in TIFM, while there was only a modest increase in the intracellular creatine levels of cells cultured under glucose and glutamine deprivation. Given that arginine is a semi-essential amino acid that serves as a precursor in the production of proline, nitric oxide, polyamines, and, importantly, in this context, creatine (Zou et al., 2019; Papalazarou et al., 2020; Xu et al., 2020), it is plausible that the arginine produced in TIFM is rapidly used up to synthesise creatine, accounting for the Matrigel-induced high intracellular creatine levels seen in TIFM while intracellular arginine remains comparatively unchanged.

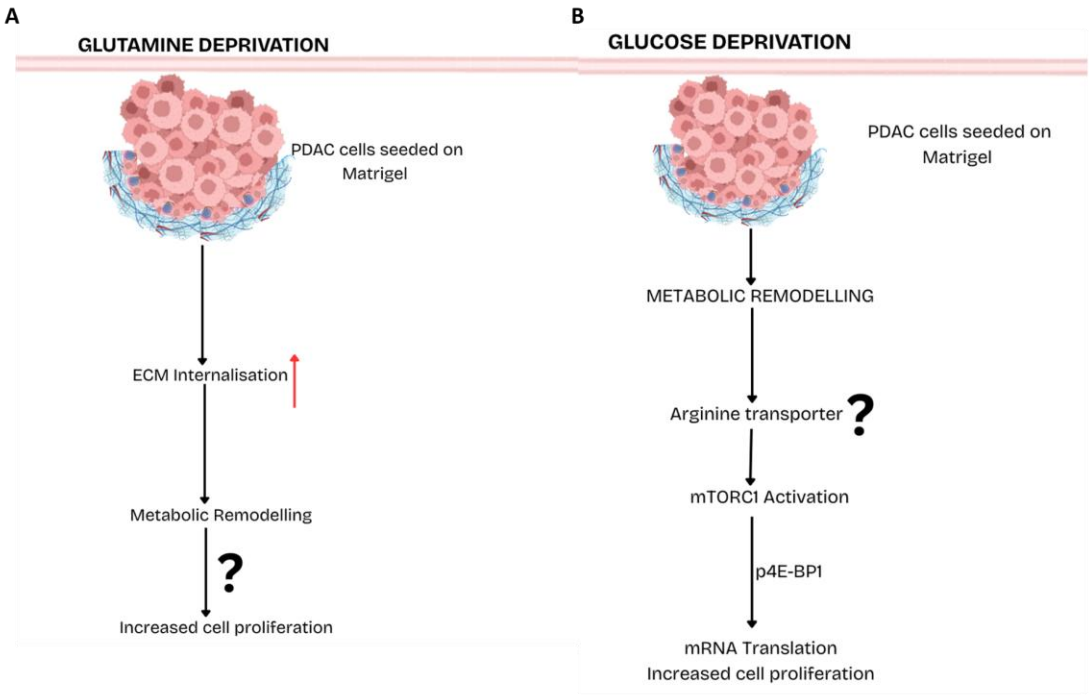

Figure 7.1 – Proposed Mechanism of Action
(A) Under glutamine deprivation, PDAC cells upregulate Matrigel internalisation, followed by a Matrigel-dependent metabolic remodelling that aids in producing nutrients required for cell proliferation. (B) Under glucose deprivation, Arginine transporters facilitate the import of Arginine into the cytosol, resulting in a Matrigel-dependent increase in intracellular Arginine that activates mTORC1, which in turn results in the phosphorylation of 4E-BP1 to promote cap-dependent mRNA translation and cell proliferation. Created with Canva

Next, our data revealed a Matrigel-dependent upregulation of the ASS1 gene, the rate-limiting enzyme in arginine biosynthesis, under both glucose and glutamine-starved conditions but not in nutrient-replete conditions. However, ASS1 was not required for Matrigel-dependent cell growth under starvation, suggesting that de novo synthesis of Arginine is not required for Matrigel-induced cell proliferation.

In addition to the role of the ECM in supporting nutrient-deprived breast cancer cells, which was previously reported in our lab (Nazemi et al., 2024), Hsu's study, highlighted above, extends the role of the ECM to colorectal cancer (CRC) (Hsu et al., 2022). Interestingly, our untargeted metabolomics data revealed that colorectal cancer was among the upregulated disease signatures on plastic and Matrigel, indicating the possibility of an expansion of the roles of Matrigel beyond PDAC. Indeed, similar to PDAC, a dense TME associated with accumulated deposition of collagens I, VI, VII, and VII is reported to be a hallmark of CRC cells (Le et al., 2020). Furthermore, using atomic force microscopy, Wang and colleagues reported that CRC cells have higher stiffness than normal colorectal cells, and the increased stiffness is associated with high collagen-I and fibronectin deposition, which is associated with increased proliferation, invasion and metastasis in both CRC in vivo and in vitro models (Wang et al., 2025).

Additionally, α1β1 integrin is upregulated in CRC tissues and cell lines, and it was reported to facilitate tumour progression (Boudjadi et al., 2017). Altogether, these studies highlight the roles of the ECM in supporting CRC progression; however, their roles in supporting nutrient-starved CRC cells have not been explored. Indeed, nutrient-deprived CRC cells have been found to upregulate autophagy to survive under amino acid deprivation (Sato et al., 2007). Similarly, KRAS-driven CRC cells reprogram their metabolism by upregulating asparagine synthetase (ASNS) enzyme to produce asparagine to facilitate their survival under glutamine deprivation (Toda et al., 2016). Overall, our findings suggest that the ECM might play a role in supporting nutrient-deprived CRC cells, extending the applicability of our findings beyond PDAC.

Overall, our work highlights several key questions at the core of PDAC metabolism, particularly regarding how nutrient-deprived PDAC cells utilise nutrients from the ECM to sustain proliferation under nutrient deprivation. Our findings suggest that different nutrient limitations engage distinct ECM-derived nutrient acquisition pathways, highlighting the metabolic adaptability of PDAC cells within their matrix-rich microenvironment.

7.2 Inhibition of KRAS results in the formation of quiescent, slow-cycling cells

Recent advances in cancer research have led to the development of inhibitors against KRAS, which was thought to be undruggable. The development of MRTX1133, a KRAS G12D-specific inhibitor (Wang et al., 2022), MRTX849, a KRAS G12C-specific inhibitor (Hallin et al., 2020) and other pan-RAS inhibitors, including RMC-7977 and RMC-6389 (Cregg et al., 2025), has provided hope for better targeted treatment options for PDAC. However, it is important to understand the modes of action of these inhibitors to reduce the possibility of treatment resistance and improve the overall survival of patients.

Our study revealed that upon treatment with MRTX1133, while there was a reduction in cell number, there was no increase in cell death. Furthermore, our data revealed similar results in MIA PaCa-2 cells treated with the KRAS G12C inhibitor, MRTX849. It is intriguing to consider that while MRTX1133 is a non-covalent inhibitor and MRTX849 is a covalent inhibitor, they are both KRAS OFF inhibitors, which means they bind to and lock KRAS in its GDP state (Hallin et al., 2020; Wang et al., 2022), and this could account for the similarity in their cytostatic effects; however, more work needs to be done on other KRAS ON inhibitors (that bind to KRAS in its active, GTP-bound state) to confirm this.

Previous studies have shown that genetic knockdown of the KRAS oncogene resulted in the formation of cells with quiescent features, such as lack of proliferation, apoptosis, and ability to resume proliferation upon re-expression of KRAS (Rajbhandari et al., 2017). Consistently, we found that KRAS inhibition, following treatment with MRTX1133, resulted in the formation of cells with quiescent features, such as inactivation of mTORC1 (Khalil et al., 2021), reduction of EdU incorporation, the ability to retain labelling in a dye retention assay and accumulation of cells in the G0 phase of the cell cycle (Rajbhandari et al., 2017). While there is a possibility that cells in the G0 phase could be senescent and not quiescent cells, our β-galactosidase assay (data not shown) revealed that there was no significant increase in the percentage of β-galactosidase-positive cells in the MRTX1133-treated cells versus the control group. Moreover, the cells resumed proliferation upon removal of MRTX1133, indicating their ability to re-enter the cell cycle.

Additionally, while there are no specific quiescent markers for PDAC, other commonly known markers of quiescent cells are p21 upregulation or lack of Ki67 (Li et al., 2019). Our attempts to assess the expression of these proteins gave inconclusive results. This could be because MRTX1133-treated cells contain both quiescent and proliferative populations, making it difficult to assess the expression of proteins only seen in quiescent cells. One way to overcome this would be to use the Flow cytometry-based fluorescence-activated cell Sorting (FACS) technique to isolate quiescent cells in the population for a more accurate characterisation.

More importantly, we found that MRTX1133-treated cells upregulated fatty acid β-oxidation. Consistently, metabolic reprogramming towards the β-oxidation pathway has been reported in quiescent breast and PDAC cells as well as in pancreatic cancer stem cells (Viale et al., 2014; Hampsch et al., 2020; Mascaraque et al., 2024). Given that quiescent cells, though metabolically active, are not rapidly proliferating, their focus would be to maintain energy balance and avoid the accumulation of ROS that could increase the possibility of oxidative stress. The shift to a catabolic and low-energy-requiring metabolism, like the β-oxidation of fatty acids to drive ATP production through oxidative phosphorylation (OXPHOS), might be favourable to generate energy. While our data showed an abundance of metabolic intermediates specific to β-oxidation like L-carnitine, propionylcarnitine, hexanoylcarnitine, palmitoylcarnitine and oleyl-L-carnitine, as well as a trend that suggests higher ATP production in the MRTX1133-treatment group compared to the vehicle control, more experiments are needed to confirm ATP generation via OXPHOS. An interesting future direction would be to measure the oxygen consumption rate (OCR) to assess mitochondrial respiratory capacity, as higher OCR indicates more ATP generation via OXPHOS, or pharmacological inhibition of OXPHOS using oligomycin to confirm dependency on OXPHOS for ATP generation (Viale et al., 2014).

Finally, it is important to note that the majority of our experiments were conducted in a single cell line, so it will be important to replicate our work in more cell lines, with different types of KRAS inhibitors. Overall, we propose that the quiescent PDAC cells induced by KRAS inhibition survive by upregulating fatty acid β-oxidation to produce acetyl CoA for ATP generation via OXPHOS (**Figure 7.2)**

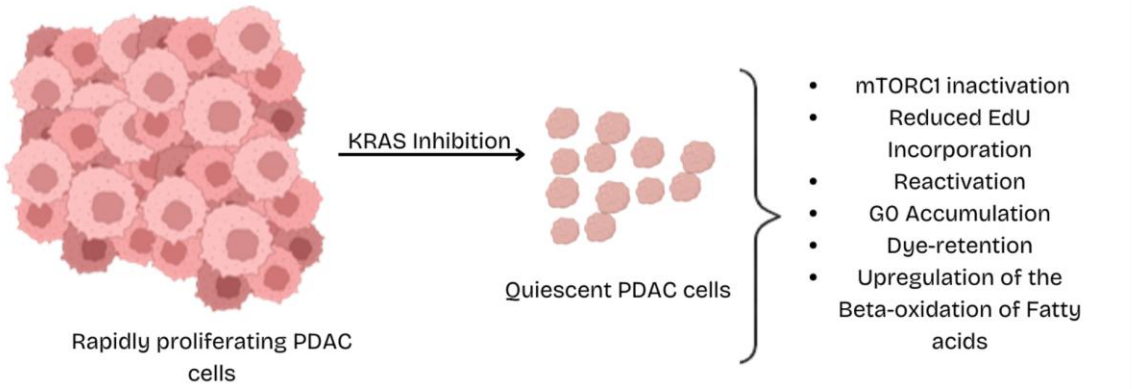

Figure 7.2 – KRAS Inhibition resulted in the formation of slow cycling cells with quiescent features
The addition of KRAS inhibitor, MRTX1133, results in a cytostatic growth arrest where the cells enter into a reversible quiescence state that is characterised by reduced cell proliferation without increased cell death, reduced EdU incorporation, mTORC1 inactivation, accumulation in the G0 phase of the cell cycle, retention of dye, via dye retention assay and reactivation upon removal of MRTX1133. Furthermore, metabolomics analysis revealed an upregulation of the beta-oxidation of fatty acid pathway. Created with Canva

7.3 Clinical relevance

We have shown that distinct nutrient starvation conditions elicited different adaptive responses in PDAC cells, leading to ECM-dependent cell proliferation. One such adaptation involves the acquisition of arginine from the ECM and/or the extracellular space to sustain growth under nutrient stress. Furthermore, using a known GLS1 inhibitor, CB-839, we found that the ECM can confer treatment resistance in PDAC cells as evidenced by the increase in cell proliferation following GLS1 inhibition using C8-839, which is currently in phase I/II clinical trials for the treatment of metastatic melanoma, renal cell carcinoma and NSCLC (Gouda et al., 2025). These findings indicate that the ECM-dependent metabolic adaptation may support the persistence and growth of PDAC tumours despite metabolic stress and may contribute to resistance against therapies targeting nutrient metabolism.

Our findings are of clinical importance because understanding how PDAC cells exploit the ECM to survive under nutrient-starved conditions will provide valuable insights into developing therapeutic strategies aimed at disrupting ECM scavenging or arginine metabolism to disrupt tumour survival. However, it is important to note that using nutrient deprivation as a therapeutic approach in PDAC is not a one-size-fits-all approach; instead, a more targeted or combinatorial approach should be considered. For instance, our data suggest that targeting arginine metabolism could be selectively

toxic to tumour cells that depend on ECM-derived arginine, while sparing normal cells. This is supported by the study of Singh et al, who demonstrated that ADI-PEG20, a pegylated arginine deiminase, sensitised ASS1-deficient PDAC cells to radiation both in vitro and in vivo (Singh et al., 2019). While targeting metabolic pathways has been explored in preclinical and clinical settings, adequately targeting specific metabolic pathways in tumour cells without harming normal cells remains challenging.

Another emerging strategy involves targeting ECM internalisation, a vulnerability that has not yet been clinically exploited. Future work could explore agents that inhibit macropinocytosis or other endocytic pathways, potentially in combination with other conventional chemotherapeutic agents, to adequately disrupt ECM-dependent support of PDAC cell proliferation.

One of the major challenges in PDAC is late diagnosis, which limits effective therapeutic intervention. The recent development of KRAS inhibitors has offered hope to pancreatic cancer patients, as the KRAS mutation is one of the main drivers of pancreatic cancer. With different KRAS inhibitors in clinical trials for the possible treatment of pancreatic cancer and other solid tumours **(Table 7.1)**, it is crucial to pre-empt the possible ways cancer cells can evade these therapeutic options and survive, thereby improving the efficacy of these drugs. While sotorasib has been approved for use in combination with panitumumab for KRAS G12C-mutated colorectal cancer and MRTX849 was recently approved for KRAS G12C-mutated NSCLC, no KRAS inhibitor has been approved for PDAC to date.

Our findings that PDAC cells could become quiescent upon treatment with KRAS inhibitors, with the capacity to become reactivated following drug withdrawal, together with the evidence that the β-oxidation of fatty acid pathway is upregulated, suggest potential strategies to overcome resistance to KRAS inhibitors. Hence, combining KRAS inhibitors with drugs that target β-oxidation of fatty acids could prevent metabolic reprogramming and survival of quiescent PDAC cells. For example, etomoxir, an inhibitor of CPT1, has been widely used in experimental studies to block fatty acid oxidation in PDAC, breast and bladder cancer models (Cheng et al., 2019; Hampsch et al., 2020; Mascaraque et al., 2024). Another known fatty acid β-oxidation inhibitor, perhexiline, a CPT1 and CPT2 inhibitor, has been used to block fatty acid β-oxidation in experimental models of gastrointestinal cancers (Wang et al., 2020). However, to date, none of these have been approved for clinical use in cancer treatment.

Conclusively, by elucidating how PDAC cells exploit fatty acid β-oxidation to persist in a quiescent state following KRAS inhibition, our study supports the development of combination therapies that target both oncogenic KRAS signalling and metabolic dependencies to improve treatment efficacy and patient outcomes.

Table 7.1 - KRAS inhibitors in clinical trials
The table shows some KRAS inhibitors in or out of clinical trials. Listed are compounds selective for specific KRAS mutations (e.g., G12C or G12D), their cancer targets, and current clinical trial status. *ClinicalTrials.gov*. U.S. National Library of Medicine. Retrieved October 23, 2025, from https://clinicaltrials.gov. The table was generated using draw.io

Drug	Target KRAS Mutation	Cancer type	Clinical trial status
MRTX849	G12C	NSCLC	Phase III
Sotorasib	G12C	NSCLC	Phase II
MRTX1133	G12D	Advanced solid tumours	Terminated
RMC-9805	G12D	NSCLS, PDAC, CRC	Phase I
HRS-4642	G12D	Advanced solid tumours	Phase I
RMC-6236	G12	NSCLC, PDAC, CRC	Phase III

7.4 Future Direction

7.4.1 Role of the ECM in supporting PDAC cell growth under nutrient deprivation

While we have been able to successfully highlight the role of the ECM in supporting nutrient-deprived PDAC cells, as well as some of the molecular mechanisms controlling ECM-dependent growth of nutrient-deprived PDAC cells, this thesis has generated more questions that can be further explored to have a more robust understanding of the roles of the ECM and possibly translate into clinical use. Some of the options to be explored are highlighted below:

- While we found that arginine and proline metabolism, as well as the ASS1 gene, were upregulated in the presence of Matrigel, the knockdown of the ASS1 gene did not affect Matrigel-induced proliferation of nutrient-deprived cells. It is possible that upon knockdown of ASS1, a different nutrient scavenging pathway is upregulated to compensate for the loss of ASS1 to sustain Matrigel-dependent cell proliferation. Hence, we could knock down some of the transporters like SLC38A9 and SLC7A1 that we have hypothesised to play a role in arginine transport and mTORC1 activation.

- We showed that Matrigel supported the growth of PDAC cells in TIFM (Chapter 3); however, unlike other nutrient starvation conditions studied, neither arginine nor ASS1 was upregulated in the presence of Matrigel. Given the potentially clinically relevant role of TIFM as a nutrient-deprivation model in PDAC, it would be interesting to characterise other metabolic pathways that could be responsible for the ECM-dependent growth of PDAC cells in TIFM. Intracellular levels of xanthine (a metabolite in the purine salvage pathway) and creatine have been identified to be significantly upregulated in the cells in TIFM. The purine salvage pathway involves recycling of free purine bases to synthesise new nucleotides (Tran et al., 2024). To characterise their roles in Matrigel-induced cell proliferation in TIFM, we could assess the mRNA expression of genes involved in the purine salvage pathway, such as the Hypoxanthine-Guanine Phosphoribosyltransferase 1 (HGPRT1), which produces hypoxanthine from inosine 5'-monophosphate (IMP) (Tran et al., 2024) and knock down the gene to assess its role in the production of xanthine or Matrigel-induced cell proliferation in TIFM. Interestingly, human protein atlas data revealed that HGPRT1 is highly expressed in the majority of PDAC cells, including SW-1990 cells used in the majority of our study (Pontén et al., 2008). It is important to note, however, that we focused on the purine salvage pathway and not the de novo purine synthesis pathway because we did not assess the intracellular content of metabolites in the de novo purine synthesis pathway.
- Using a more physiologically relevant model, such as 3D cell culture or organoids, to confirm the data from our 2D studies and improve the relevance of our discoveries.
- While our metabolomics data gave significant insight into the metabolic pathways linked to ECM-dependent proliferation of nutrient-deprived PDAC cells, other omics techniques, such as phospho-proteomics, would give a more elaborate understanding of the signalling pathways that are upregulated upon Matrigel-dependent proliferation. Phospho-proteomics can be used to identify kinases or phosphorylation sites in the presence of Matrigel compared to plastic, and the data would be validated via Western blotting. This would complement our metabolomics data by highlighting the specific signalling pathways that drive the metabolic pathways identified in our study.
- Our data showed that Matrigel-dependent activation of mTORC1 promoted the phosphorylation of 4E-BP1 and not S6. Characterisation of the roles of other e1F4F complexes would aid in confirming the specific role of 4E-BP1 in Matrigel-dependent activation of mTORC1, for example, by treating the cells with CR-13-1B, an e1F4A-specific inhibitor.

7.4.2 Tumour Quiescence in response to KRAS pharmacological inhibition

Here, we have shown that upon treatment with MRTX1133, a KRAS G12D inhibitor, a population of PDAC cells becomes quiescent and upregulates different metabolic pathways, such as fatty acid β-oxidation. Further studies to explore include:

- Characterising the possible role of other KRAS inhibitors, such as G12D inhibitors, like RMC-9805, or pan RAS inhibitors, such as RMC 7977, in inducing quiescence in a panel of PDAC cells.
- Characterising how the PDAC microenvironment contributes to the formation of quiescent cells upon KRAS inhibition. Given that all our studies were done in 2D, which does not adequately depict the microenvironment of PDAC, it will be interesting to use a more clinically relevant model, such as organoids, to better understand the effects of KRAS inhibitors on PDAC cells.
- Given the desmoplastic and nutrient-deprived nature of the PDAC TME, assessing the roles of the ECM or nutrient deprivation in inducing quiescence upon KRAS inhibition will be beneficial.
- We have highlighted β-oxidation of fatty acids among other pathways upregulated in MRTX1133-treated PDAC cells. The next steps would be to investigate the effects of disrupting metabolic pathways that could be responsible for the survival of quiescent PDAC cells. Inhibitors of β-oxidation of fatty acid pathways, such as etomoxir, could be used in combination with KRAS inhibitors to improve the efficacy of KRAS inhibition in PDAC cells.

Collectively, the findings from this thesis highlight the remarkable metabolic plasticity of PDAC cells, which enables survival under nutrient deprivation and targeted therapy, highlighting the need for combination strategies that block compensatory metabolic pathways to achieve better treatment response.

8 References

2025. *American Cancer Society. Cancer Facts & Figures 2025. Atlanta: American Cancer Society; 2025* [Online].Available:https://www.cancer.org/content/dam/cancer-org/research/cancer-facts-and-statistics/annual-cancer-facts-and-figures/2025/2025-cancer-facts-and-figures-acs.pdf [Accessed].

AGARWAL, S., CHAKRAVARTHI, B., KIM, H. G., GUPTA, N., HALE, K., BALASUBRAMANYA, S. A. H., OLIVER, P. G., THOMAS, D. G., ELTOUM, I. A., BUCHSBAUM, D. J., MANNE, U. & VARAMBALLY, S. 2020. PAICS, a De Novo Purine Biosynthetic Enzyme, Is Overexpressed in Pancreatic Cancer and Is Involved in Its Progression. *Transl Oncol,* 13**,** 100776.

AGUIRRE-GHISO, J. A., ESTRADA, Y., LIU, D. & OSSOWSKI, L. 2003. ERKMAPK Activity as a Determinant of Tumour Growth and Dormancy; Regulation by p38SAPK1. *Cancer Research,* 63**,** 1684-1695.

AGUIRRE-GHISO, J. A. 2007. Models, mechanisms and clinical evidence for cancer dormancy. *Nature Reviews Cancer,* 7**,** 834-846.

AISENBREY, E. A. & MURPHY, W. L. 2020. Synthetic alternatives to Matrigel. *Nat Rev Mater,* 5**,** 539-551.

ALEKSANDROVA, K. V., VOROBEV, M. L. & SUVOROVA, I. I. 2024. mTOR pathway occupies a central role in the emergence of latent cancer cells. *Cell Death & Disease,* 15**,** 176.

ALIPOUR, H., RAZ, A., ZAKERI, S. & DINPARAST DJADID, N. 2016. Therapeutic applications of collagenase (metalloproteases): A review. *Asian Pacific Journal of Tropical Biomedicine,* 6**,** 975-981.

ALONSO-CURBELO, D., OSTERLOH, L., CAÑÓN, E., CALVO, T. G., MARTÍNEZ-HERRANZ, R., KARRAS, P., MARTÍNEZ, S., RIVEIRO-FALKENBACH, E., ROMERO, P.-O., RODRÍGUEZ-PERALTO, J. L., PASTOR, J. & SOENGAS, M. S. 2015. RAB7 counteracts PI3K-driven macropinocytosis activated at early stages of melanoma development. *Oncotarget; Vol 6, No 14*.

ALTMAN, B. J., STINE, Z. E. & DANG, C. V. 2016. From Krebs to clinic: glutamine metabolism to cancer therapy. *Nature Reviews Cancer,* 16**,** 619-634.

APIZ SAAB, J. J., DZIEROZYNSKI, L. N., JONKER, P. B., AMINITABRIZI, R., SHAH, H., MENJIVAR, R. E., SCOTT, A. J., NWOSU, Z. C., ZHU, Z., CHEN, R. N., OH, M., SHEEHAN, C., WAHL, D. R., PASCA DI MAGLIANO, M., LYSSIOTIS, C. A., MACLEOD, K. F., WEBER, C. R. & MUIR, A. 2023. Pancreatic Tumours Exhibit Myeloid-Driven Amino Acid Stress and Upregulate Arginine Biosynthesis. *Elife,* 12.

ARDALAN, B., CINER, A., BACA, Y., HINTON, A., DARABI, S., KASI, A., LOU, E., AZQUETA, J. I., XIU, J., DATTA, J., SHIELDS, A. F., AGUIRRE, A., SINGH, H., SHROFF, R. T., PISHVAIAN, M. J. & GOEL, S.

2025. Distinct Molecular and Clinical Features of Specific Variants of KRAS Codon 12 in Pancreatic Adenocarcinoma. *Clinical Cancer Research,* 31**,** 1082-1090.

AUDIT, N. P. C. 2024. *National Pancreatic Cancer Audit State of the Nation Report 2024* [Online]. Available: https://www.hqip.org.uk/wp-content/uploads/2024/09/1_REF463_NATCAN-NPaCA-SoN-v20240912_FINAL.pdf [Accessed].

BARKAN, D., EL TOUNY, L. H., MICHALOWSKI, A. M., SMITH, J. A., CHU, I., DAVIS, A. S., WEBSTER, J. D., HOOVER, S., SIMPSON, R. M., GAULDIE, J. & GREEN, J. E. 2010. Metastatic Growth from Dormant Cells Induced by a Col-I–Enriched Fibrotic Environment. *Cancer Research,* 70**,** 5706-5716.

BARKAN, D., GREEN, J. E. & CHAMBERS, A. F. 2010. Extracellular matrix: A gatekeeper in the transition from dormancy to metastatic growth. *European Journal of Cancer,* 46**,** 1181-1188.

BEGER, R. D. 2013. A Review of Applications Of Metabolomics In Cancer. *Metabolites,* 3**,** 552-74.

BEN-SAHRA, I. & MANNING, B. D. 2017. mTORC1 signalling and the metabolic control of cell growth. *Current Opinion in Cell Biology,* 45**,** 72-82.

BENTON, G., KLEINMAN, H. K., GEORGE, J. & ARNAOUTOVA, I. 2011. Multiple uses of basement membrane-like matrix (BME/Matrigel) in vitro and in vivo with cancer cells. *International Journal of Cancer,* 128**,** 1751-1757.

BIANCUR, D. E., PAULO, J. A., MAŁACHOWSKA, B., QUILES DEL REY, M., SOUSA, C. M., WANG, X., SOHN, A. S. W., CHU, G. C., GYGI, S. P., HARPER, J. W., FENDLER, W., MANCIAS, J. D. & KIMMELMAN, A. C. 2017. Compensatory metabolic networks in pancreatic cancers upon perturbation of glutamine metabolism. *Nature Communications,* 8**,** 15965.

BOUDJADI, S., BERNATCHEZ, G., SÉNICOURT, B., BEAUSÉJOUR, M., VACHON, P. H., CARRIER, J. C. & BEAULIEU, J.-F. 2017. Involvement of the Integrin α1β1 in the Progression of Colorectal Cancer. *Cancers* [Online], 9.

BOYERINAS, B., ZAFRIR, M., YESILKANAL, A. E., PRICE, T. T., HYJEK, E. M. & SIPKINS, D. A. 2013. Adhesion to osteopontin in the bone marrow niche regulates lymphoblastic leukaemia cell dormancy. *Blood,* 121**,** 4821-4831.

Cancer Research UK, https://www.cancerresearchuk.org/health-professional/cancer-statistics/statistics-by-cancer-type/pancreatic-cancer#pancreatic_stats0, Accessed: July 2025. [Online]. [Accessed].

CECILIA BONOLO DE, C., YUAN XIAO, Z., NIKOLAI, S., SERGEI, R., LAURA ANN, B., CHANG-XIN, S., CALEB, K. S., JOACHIM, L. P., ALYSIA, N. P., MEAGHEN, E. S., ERIN, W. M., GREGORY, J. A., ILSEL, D. L. A., JONAS, K., BERGSAGEL, P. L., MARTA, C., NATHALIE, M., ESTEBAN, B. &

STEWART, A. K. 2020. Identification of PIKfyve kinase as a target in multiple myeloma. *Haematologica,* 105**,** 1641-1649.

CHAN, K., ROBERT, F., OERTLIN, C., KAPELLER-LIBERMANN, D., AVIZONIS, D., GUTIERREZ, J., HANDLY-SANTANA, A., DOUBROVIN, M., PARK, J., SCHOEPFER, C., DA SILVA, B., YAO, M., GORTON, F., SHI, J., THOMAS, C. J., BROWN, L. E., PORCO, J. A., POLLAK, M., LARSSON, O., PELLETIER, J. & CHIO, I. I. C. 2019. eIF4A supports an oncogenic translation program in pancreatic ductal adenocarcinoma. *Nature Communications,* 10**,** 5151.

CHEN, M. & HUANG, J. 2019. The expanded role of fatty acid metabolism in cancer: new aspects and targets. *Precision Clinical Medicine,* 2**,** 183-191.

CHEN, L., KONG, X., FANG, Y., PAUNIKAR, S., WANG, X., BROWN, J. A. L., BOURKE, E., LI, X. & WANG, J. 2021. Recent Advances in the Role of Discoidin Domain Receptor Tyrosine Kinase 1 and Discoidin Domain Receptor Tyrosine Kinase 2 in Breast and Ovarian Cancer. *Frontiers in Cell and Developmental Biology,* Volume 9 - 2021.

CHENG, S., WANG, G., WANG, Y., CAI, L., QIAN, K., JU, L., LIU, X., XIAO, Y. & WANG, X. 2019. Fatty acid oxidation inhibitor etomoxir suppresses tumor progression and induces cell cycle arrest via PPARγ-mediated pathway in bladder cancer. *Clinical Science,* 133**,** 1745-1758.

COLLINS, M. A., BEDNAR, F., ZHANG, Y., BRISSET, J.-C., GALBÁN, S., GALBÁN, C. J., RAKSHIT, S., FLANNAGAN, K. S., ADSAY, N. V. & PASCA DI MAGLIANO, M. 2012. Oncogenic Kras is required for both the initiation and maintenance of pancreatic cancer in mice. *The Journal of Clinical Investigation,* 122**,** 639-653.

COMMISSO, C., DAVIDSON, S. M., SOYDANER-AZELOGLU, R. G., PARKER, S. J., KAMPHORST, J. J., HACKETT, S., GRABOCKA, E., NOFAL, M., DREBIN, J. A., THOMPSON, C. B., RABINOWITZ, J. D., METALLO, C. M., VANDER HEIDEN, M. G. & BAR-SAGI, D. 2013. Macropinocytosis of protein is an amino acid supply route in Ras-transformed cells. *Nature,* 497**,** 633-7.

CREGG, J., EDWARDS, A. V., CHANG, S., LEE, B. J., KNOX, J. E., TOMLINSON, A. C. A., MARQUEZ, A., LIU, Y., FREILICH, R., AAY, N., WANG, Y., JIANG, L., JIANG, J., WANG, Z., FLAGELLA, M., WILDES, D., SMITH, J. A. M., SINGH, M., WANG, Z., GILL, A. L. & KOLTUN, E. S. 2025. Discovery of Daraxonrasib (RMC-6236), a Potent and Orally Bioavailable RAS(ON) Multi-selective, Noncovalent Tri-complex Inhibitor for the Treatment of Patients with Multiple RAS-Addicted Cancers. *Journal of Medicinal Chemistry,* 68**,** 6064-6083.

CROWLEY, L. C., SCOTT, A. P., MARFELL, B. J., BOUGHABA, J. A., CHOJNOWSKI, G. & WATERHOUSE, N. J. 2016. Measuring Cell Death by Propidium Iodide Uptake and Flow Cytometry. *Cold Spring Harbor Protocols,* 2016**,** pdb.prot087163.

DANZI, F., PACCHIANA, R., MAFFICINI, A., SCUPOLI, M. T., SCARPA, A., DONADELLI, M. & FIORE, A. 2023. To Metabolomics and Beyond: A Technological Portfolio to Investigate Cancer Metabolism. *Signal Transduct Target Ther,* 8**,** 137.

DEBERARDINIS, R. J., LUM, J. J., HATZIVASSILIOU, G. & THOMPSON, C. B. 2008. The Biology of Cancer: Metabolic Reprogramming Fuels Cell Growth and Proliferation. *Cell Metabolism,* 7**,** 11-20.

DI MARTINO, J. S., NOBRE, A. R., MONDAL, C., TAHA, I., FARIAS, E. F., FERTIG, E. J., NABA, A., AGUIRRE-GHISO, J. A. & BRAVO-CORDERO, J. J. 2022. A tumour-derived type III collagen-rich ECM niche regulates tumour cell dormancy. *Nat Cancer,* 3**,** 90-107.

DIEHL, F. F., SAPP, K. M. & VANDER HEIDEN, M. G. 2024. The bidirectional relationship between metabolism and cell cycle control. *Trends in Cell Biology,* 34**,** 136-149.

DU, Y., GUPTA, P., QIN, S. & SIEBER, M. 2023. The role of metabolism in cellular quiescence. *Journal of Cell Science,* 136**,** jcs260787.

DWYER, S., RUTH, J., SEIDEL, H. E., RAZ, A. A. & CHODOSH, L. A. 2024. Autophagy is required for mammary tumour recurrence by promoting dormant tumour cell survival following therapy. *Breast Cancer Research,* 26**,** 143.

EDDAOUDI, A., CANNING, S. L. & KATO, I. 2018. Flow Cytometric Detection of G0 in Live Cells by Hoechst 33342 and Pyronin Y Staining. *In:* LACORAZZA, H. D. (ed.) *Cellular Quiescence: Methods and Protocols.* New York, NY: Springer New York.

ELLENRIEDER, V., ALBER, B., LACHER, U., HENDLER, S. F., MENKE, A., BOECK, W., WAGNER, M., WILDA, M., FRIESS, H., BÜCHLER, M., ADLER, G. & GRESS, T. M. 2000. Role of MT-MMPs and MMP-2 in pancreatic cancer progression. *International Journal of Cancer,* 85**,** 14-20.

ENCARNACIÓN-ROSADO, J., SOHN, A. S. W., BIANCUR, D. E., LIN, E. Y., OSORIO-VASQUEZ, V., RODRICK, T., GONZÁLEZ-BAERGA, D., ZHAO, E., YOKOYAMA, Y., SIMEONE, D. M., JONES, D. R., PARKER, S. J., WILD, R. & KIMMELMAN, A. C. 2024. Targeting pancreatic cancer metabolic dependencies through glutamine antagonism. *Nature Cancer,* 5**,** 85-99.

ENDO, H. & INOUE, M. 2019. Dormancy in cancer. *Cancer Science,* 110**,** 474-480.

ENG, C., HU, J., MANNAN, R., HE, T., BHATTACHARYYA, R., MAGNUSON, B., WISNIEWSKI, J. P., PETERS, S., KARIM, S. A., MACLEAN, D. J., KARABÜRK, H., ZHANG, L., ROSSITER, N. J., ZHENG, Y., XIAO, L., LI, C., AWAD, D., MAHAPATRA, S., BAO, Y., ZHANG, Y., CAO, X., WANG, Z., MEHRA, R., MORLACCHI, P., SAHAI, V., PASCA DI MAGLIANO, M., SHAH, Y. M., WEISMAN, L. S., MORTON, J. P., DING, K., QIAO, Y., LYSSIOTIS, C. A. & CHINNAIYAN, A. M. 2025. Targeting PIKfyve-driven lipid metabolism in pancreatic cancer. *Nature,* 642**,** 776-784.

FENG, J., HU, Z., XIA, X., LIU, X., LIAN, Z., WANG, H., WANG, L., WANG, C., ZHANG, X. & PANG, X. 2023. Feedback activation of EGFR/wild-type RAS signalling axis limits KRASG12D inhibitor efficacy in KRASG12D-mutated colorectal cancer. *Oncogene,* 42**,** 1620-1633.

FERRARA, B., PIGNATELLI, C., COSSUTTA, M., CITRO, A., COURTY, J. & PIEMONTI, L. 2021. The Extracellular Matrix in Pancreatic Cancer: Description of a Complex Network and Promising Therapeutic Options. *Cancers (Basel),* 13.

FINICLE, B. T., JAYASHANKAR, V. & EDINGER, A. L. 2018. Nutrient scavenging in cancer. *Nature Reviews Cancer,* 18**,** 619-633.

FRANCIPANE, M. G. & LAGASSE, E. 2013. Selective targeting of human colon cancer stem-like cells by the mTOR inhibitor Torin-1. *Oncotarget; Vol 4, No 11: November 2013*.

FUJISHIMA, A., IMAI, Y., NOMURA, T., FUJISAWA, Y., YAMAMOTO, Y. & SUGAWARA, T. 1997. The crystal structure of human cathepsin L complexed with E-64. *FEBS Letters,* 407**,** 47-50.

GARCIA-BERMUDEZ, J., WILLIAMS, R. T., GUARECUCO, R. & BIRSOY, K. 2020. Targeting extracellular nutrient dependencies of cancer cells. *Mol Metab,* 33**,** 67-82.

GAUTAM, B., SHARMA, A., JATAVATH, M., POTHURAJU, R., CHAUDHARY, S., GAUTAM, S. K. & BHATIA, R. 2026. Acinar cell plasticity and subtype specification during acinar-to-ductal metaplasia and pancreatic cancer progression. *Biochimica et Biophysica Acta (BBA) - Reviews on Cancer,* 1881**,** 189549.

GAYLE, S., LANDRETTE, S., BEEHARRY, N., CONRAD, C., HERNANDEZ, M., BECKETT, P., FERGUSON, S. M., MANDELKERN, T., ZHENG, M., XU, T., ROTHBERG, J. & LICHENSTEIN, H. 2017. Identifying apilimod as a first-in-class PIKfyve kinase inhibitor for treating B-cell non-Hodgkin lymphoma. *Blood,* 129**,** 1768-1778.

GOUDA, M. A., VOSS, M. H., TAWBI, H., GORDON, M., TYKODI, S. S., LAM, E. T., VAISHAMPAYAN, U., TANNIR, N. M., CHAVES, J., NIKOLINAKOS, P., FAN, A., LEE, R., MCDERMOTT, D., SHAPIRO, G. I., GANDHI, L., BHATIA, S., KATRAGADDA, V. & MERIC-BERNSTAM, F. 2025. A phase I/II study of the safety and efficacy of telaglenastat (CB-839) in combination with nivolumab in patients with metastatic melanoma, renal cell carcinoma, and non-small-cell lung cancer. *ESMO Open,* 10.

GOUGH, J. E., SCOTCHFORD, C. A. & DOWNES, S. 2002. Cytotoxicity of glutaraldehyde crosslinked collagen/poly(vinyl alcohol) films is by the mechanism of apoptosis. *Journal of Biomedical Materials Research,* 61**,** 121-130.

GUERTIN, D. A. & SABATINI, D. M. 2007. Defining the Role of mTOR in Cancer. *Cancer Cell,* 12**,** 9-22.

GULAY, K. C. M., ZHANG, X., PANTAZOPOULOU, V., PATEL, J., ESPARZA, E., PRAN BABU, D. S., OGAWA, S., WEITZ, J., NG, I., MOSE, E. S., PU, M., ENGLE, D. D., LOWY, A. M. & TIRIAC, H. 2023. Dual

Inhibition of KRASG12D and Pan-ERBB Is Synergistic in Pancreatic Ductal Adenocarcinoma. *Cancer Research,* 83**,** 3001-3012.

GUO, J. Y., CHEN, H. Y., MATHEW, R., FAN, J., STROHECKER, A. M., KARSLI-UZUNBAS, G., KAMPHORST, J. J., CHEN, G., LEMONS, J. M., KARANTZA, V., COLLER, H. A., DIPAOLA, R. S., GELINAS, C., RABINOWITZ, J. D. & WHITE, E. 2011. Activated Ras requires autophagy to maintain oxidative metabolism and tumourigenesis. *Genes Dev,* 25**,** 460-70.

GYAMFI, J., KIM, J. & CHOI, J. 2022. Cancer As a Metabolic Disorder. *Int J Mol Sci,* 23.

HALBROOK, C. J., LYSSIOTIS, C. A., PASCA DI MAGLIANO, M. & MAITRA, A. 2023. Pancreatic cancer: Advances and challenges. *Cell,* 186**,** 1729-1754.

HALLIN, J., BOWCUT, V., CALINISAN, A., BRIERE, D. M., HARGIS, L., ENGSTROM, L. D., LAGUER, J., MEDWID, J., VANDERPOOL, D., LIFSET, E., TRINH, D., HOFFMAN, N., WANG, X., DAVID LAWSON, J., GUNN, R. J., SMITH, C. R., THOMAS, N. C., MARTINSON, M., BERGSTROM, A., SULLIVAN, F., BOUHANA, K., WINSKI, S., HE, L., FERNANDEZ-BANET, J., PAVLICEK, A., HALING, J. R., RAHBAEK, L., MARX, M. A., OLSON, P. & CHRISTENSEN, J. G. 2022. Anti-tumour efficacy of a potent and selective non-covalent KRASG12D inhibitor. *Nature Medicine,* 28**,** 2171-2182.

HALLIN, J., ENGSTROM, L. D., HARGIS, L., CALINISAN, A., ARANDA, R., BRIERE, D. M., SUDHAKAR, N., BOWCUT, V., BAER, B. R., BALLARD, J. A., BURKARD, M. R., FELL, J. B., FISCHER, J. P., VIGERS, G. P., XUE, Y., GATTO, S., FERNANDEZ-BANET, J., PAVLICEK, A., VELASTAGUI, K., CHAO, R. C., BARTON, J., PIEROBON, M., BALDELLI, E., PATRICOIN, E. F., III, CASSIDY, D. P., MARX, M. A., RYBKIN, I. I., JOHNSON, M. L., OU, S.-H. I., LITO, P., PAPADOPOULOS, K. P., JÄNNE, P. A., OLSON, P. & CHRISTENSEN, J. G. 2020. The KRASG12C Inhibitor MRTX849 Provides Insight toward Therapeutic Susceptibility of KRAS-Mutant Cancers in Mouse Models and Patients. *Cancer Discovery,* 10**,** 54-71.

HAMPSCH, R. A., WELLS, J. D., TRAPHAGEN, N. A., MCCLEERY, C. F., FIELDS, J. L., SHEE, K., DILLON, L. M., POOLER, D. B., LEWIS, L. D., DEMIDENKO, E., HUANG, Y. H., MAROTTI, J. D., GOEN, A. E., KINLAW, W. B. & MILLER, T. W. 2020. AMPK Activation by Metformin Promotes Survival of Dormant ER+ Breast Cancer Cells. *Clinical Cancer Research,* 26**,** 3707-3719.

HANAHAN, D. & WEINBERG, R. A. 2000. The Hallmarks of Cancer. *Cell,* 100**,** 57-70.

HANAHAN, D. & WEINBERG, R. A. 2011. Hallmarks of cancer: the next generation. *Cell,* 144**,** 646-74.

HANAHAN, D. 2022. Hallmarks of Cancer: New Dimensions. *Cancer Discovery,* 12**,** 31-46.

HARDING, J. J., TELLI, M., MUNSTER, P., VOSS, M. H., INFANTE, J. R., DEMICHELE, A., DUNPHY, M., LE, M. H., MOLINEAUX, C., ORFORD, K., PARLATI, F., WHITING, S. H., BENNETT, M. K., TANNIR, N. M. & MERIC-BERNSTAM, F. 2021. A Phase I Dose-Escalation and Expansion Study of

Telaglenastat in Patients with Advanced or Metastatic Solid tumours. *Clinical Cancer Research,* 27**,** 4994-5003.

HAY, N. 2016. Reprogramming glucose metabolism in cancer: can it be exploited for cancer therapy? *Nature Reviews Cancer,* 16**,** 635-649.

HE, S., HUANG, Q., HU, J., LI, L., XIAO, Y., YU, H., HAN, Z., WANG, T., ZHOU, W., WEI, H. & XIAO, J. 2019. EWS-FLI1-mediated tenascin-C expression promotes tumour progression by targeting MALAT1 through integrin α5β1-mediated YAP activation in Ewing sarcoma. *British Journal of Cancer,* 121**,** 922-933.

HEZEL, A. F., KIMMELMAN, A. C., STANGER, B. Z., BARDEESY, N. & DEPINHO, R. A. 2006. Genetics and biology of pancreatic ductal adenocarcinoma. *Genes Dev,* 20**,** 1218-49.

HIDALGO, M. 2010. <Pancreatic cancer.pdf>. *N Engl J Med,* 362**,** 1605-1617.

HINGORANI, S. R., WANG, L., MULTANI, A. S., COMBS, C., DERAMAUDT, T. B., HRUBAN, R. H., RUSTGI, A. K., CHANG, S. & TUVESON, D. A. 2005. Trp53R172H and KrasG12D cooperate to promote chromosomal instability and widely metastatic pancreatic ductal adenocarcinoma in mice. *Cancer Cell,* 7**,** 469-483.

HO, W. J., JAFFEE, E. M. & ZHENG, L. 2020. The tumour microenvironment in pancreatic cancer — clinical challenges and opportunities. *Nature Reviews Clinical Oncology,* 17**,** 527-540.

HOBBS, G. A., BAKER, N. M., MIERMONT, A. M., THURMAN, R. D., PIEROBON, M., TRAN, T. H., ANDERSON, A. O., WATERS, A. M., DIEHL, J. N., PAPKE, B., HODGE, R. G., KLOMP, J. E., GOODWIN, C. M., DELIBERTY, J. M., WANG, J., NG, R. W. S., GAUTAM, P., BRYANT, K. L., ESPOSITO, D., CAMPBELL, S. L., PETRICOIN, E. F., III, SIMANSHU, D. K., AGUIRRE, A. J., WOLPIN, B. M., WENNERBERG, K., RUDLOFF, U., COX, A. D. & DER, C. J. 2020. Atypical KRASG12R Mutant Is Impaired in PI3K Signaling and Macropinocytosis in Pancreatic Cancer. *Cancer Discovery,* 10**,** 104-123.

HOUTEN, S. M. & WANDERS, R. J. A. 2010. A general introduction to the biochemistry of mitochondrial fatty acid β-oxidation. *Journal of Inherited Metabolic Disease,* 33**,** 469-477.

HOWELLS, C. C., BAUMANN, W. T., SAMUELS, D. C. & FINKIELSTEIN, C. V. 2011. The Bcl-2-associated death promoter (BAD) lowers the threshold at which the Bcl-2-interacting domain death agonist (BID) triggers mitochondria disintegration. *Journal of Theoretical Biology,* 271**,** 114-123.

HSU, K.-S., DUNLEAVEY, J. M., SZOT, C., YANG, L., HILTON, M. B., MORRIS, K., SEAMAN, S., FENG, Y., LUTZ, E. M., KOOGLE, R., TOMASSONI-ARDORI, F., SAHA, S., ZHANG, X. M., ZUDAIRE, E., BAJGAIN, P., ROSE, J., ZHU, Z., DIMITROV, D. S., CUTTITTA, F., EMENAKER, N. J., TESSAROLLO,

L. & ST. CROIX, B. 2022. Cancer cell survival depends on collagen uptake into tumor-associated stroma. *Nature Communications,* 13**,** 7078.

HU, C., CHEN, Y., YIN, X., XU, R., YIN, C., WANG, C. & ZHAO, Y. 2025. Pancreatic endocrine and exocrine signaling and crosstalk in physiological and pathological status. *Signal Transduction and Targeted Therapy,* 10**,** 39.

HUANG, C. & CHEN, J. 2021. Laminin-332 mediates proliferation, apoptosis, invasion, migration and epithelial-to-mesenchymal transition in pancreatic ductal adenocarcinoma. *Mol Med Rep,* 23**,** 11.

HUANG, J., ZHANG, L., WAN, D., ZHOU, L., ZHENG, S., LIN, S. & QIAO, Y. 2021. Extracellular matrix and its therapeutic potential for cancer treatment. *Signal Transduction and Targeted Therapy,* 6**,** 153.

HUO, Y., YANG, M., LIU, W., YANG, J., FU, X., LIU, D., LI, J., ZHANG, J., HUA, R. & SUN, Y. 2015. High expression of DDR1 is associated with the poor prognosis in Chinese patients with pancreatic ductal adenocarcinoma. *Journal of Experimental & Clinical Cancer Research,* 34**,** 88.

IZUISHI, K., KATO, K., OGURA, T., KINOSHITA, T. & ESUMI, H. 2000. Remarkable tolerance of tumour cells to nutrient deprivation: Possible new biochemical target for cancer therapy. *Cancer research (Chicago, Ill.),* 60**,** 6201-6207.

JEONG, S., BYUN, J.-K., CHO, S. J., CHIN, J., LEE, I.-K., CHOI, Y.-K. & PARK, K.-G. 2018. Transcription Factor Eb Is Required for Macropinocytosis-Mediated Growth Recovery of Nutrient-Deprived Kras-Mutant Cells. *Nutrients* [Online], 10.

JIANG, S., REN, B., DING, C., DU, C., CAO, Z., YANG, G., HUANG, H. & ZHANG, T. 2025. Polyamines in pancreatic cancer: reshaping the immunosuppressive tumour microenvironment. *Cancer Letters,* 633**,** 218016.

JIANG, X., WANG, T., ZHAO, B., SUN, H., DONG, Y., MA, Y., LI, Z., WU, Y., WANG, K., GUAN, X., LONG, B., QIN, L., SHI, W., SHI, L., HE, Q., LIU, W., LI, M., XIAO, L., ZHOU, C., SUN, H., YANG, J., GUAN, J., ZHOU, H., YU, Z. & JIAO, Z. 2025. KRASG12D-driven pentose phosphate pathway remodelling imparts a targetable vulnerability synergising with MRTX1133 for durable remissions in PDAC. *Cell Reports Medicine,* 6**,** 101966.

JIN, J., BYUN, J.-K., CHOI, Y.-K. & PARK, K.-G. 2023. Targeting glutamine metabolism as a therapeutic strategy for cancer. *Experimental & Molecular Medicine,* 55**,** 706-715.

JU, Y., GUO, H., EDMAN, M. & HAMM-ALVAREZ, S. F. 2020. Application of advances in endocytosis and membrane trafficking to drug delivery. *Adv Drug Deliv Rev,* 157**,** 118-141.

KAIRA, K., SUNOSE, Y., ARAKAWA, K., OGAWA, T., SUNAGA, N., SHIMIZU, K., TOMINAGA, H., ORIUCHI, N., ITOH, H., NAGAMORI, S., KANAI, Y., SEGAWA, A., FURUYA, M., MORI, M., OYAMA, T. &

TAKEYOSHI, I. 2012. Prognostic significance of L-type amino-acid transporter 1 expression in surgically resected pancreatic cancer. *British Journal of Cancer,* 107**,** 632-638.

KAMPHORST, J. J., CROSS, J. R., FAN, J., DE STANCHINA, E., MATHEW, R., WHITE, E. P., THOMPSON, C. B. & RABINOWITZ, J. D. 2013. Hypoxic and Ras-transformed cells support growth by scavenging unsaturated fatty acids from lysophospholipids. *Proceedings of the National Academy of Sciences,* 110**,** 8882-8887.

KAMPHORST, J. J., NOFAL, M., COMMISSO, C., HACKETT, S. R., LU, W., GRABOCKA, E., VANDER HEIDEN, M. G., MILLER, G., DREBIN, J. A., BAR-SAGI, D., THOMPSON, C. B. & RABINOWITZ, J. D. 2015. Human pancreatic cancer tumours are nutrient poor and tumour cells actively scavenge extracellular protein. *Cancer Res,* 75**,** 544-53.

KEERATICHAMROEN, S., LIRDPRAPAMONGKOL, K. & SVASTI, J. 2018. Mechanism of ECM-induced dormancy and chemoresistance in A549 human lung carcinoma cells. *Oncol Rep,* 39**,** 1765-1774.

KEMP, S. B., CHENG, N., MARKOSYAN, N., SOR, R., KIM, I.-K., HALLIN, J., SHOUSH, J., QUINONES, L., BROWN, N. V., BASSETT, J. B., JOSHI, N., YUAN, S., SMITH, M., VOSTREJS, W. P., PEREZ-VALE, K. Z., KAHN, B., MO, F., DONAHUE, T. R., RADU, C. G., CLENDENIN, C., CHRISTENSEN, J. G., VONDERHEIDE, R. H. & STANGER, B. Z. 2023. Efficacy of a Small-Molecule Inhibitor of KrasG12D in Immunocompetent Models of Pancreatic Cancer. *Cancer Discovery,* 13**,** 298-311.

KHALIL, B. D., SANCHEZ, R., RAHMAN, T., RODRIGUEZ-TIRADO, C., MORITSCH, S., MARTINEZ, A. R., MILES, B., FARIAS, E., MEZEI, M., NOBRE, A. R., SINGH, D., KALE, N., SPROLL, K. C., SOSA, M. S. & AGUIRRE-GHISO, J. A. 2021. An NR2F1-specific agonist suppresses metastasis by inducing cancer cell dormancy. *Journal of Experimental Medicine,* 219**,** e20210836.

KHAN, M. W., LAYDEN, B. T. & CHAKRABARTI, P. 2018. Inhibition of mTOR complexes protects cancer cells from glutamine starvation-induced cell death by restoring Akt stability. *Biochimica et Biophysica Acta (BBA) - Molecular Basis of Disease,* 1864**,** 2040-2052.

KIM, J. K., JUNG, Y., WANG, J., JOSEPH, J., MISHRA, A., HILL, E. E., KREBSBACH, P. H., PIENTA, K. J., SHIOZAWA, Y. & TAICHMAN, R. S. 2013. TBK1 Regulates Prostate Cancer Dormancy through mTOR Inhibition. *Neoplasia,* 15**,** 1064-1074.

KIM, K. S., LEE, Y., LEE, J. H., LEE, S. S., CHUNG, J. M. & JUNG, H. S. 2024. Optimising protein crosslinking control: Synergistic quenching effects of glycine, histidine, and lysine on glutaraldehyde reactions. *Biochemical and Biophysical Research Communications,* 702**,** 149567.

KIM, S. H., SONG, J. H., KIM, M. J., SONG, M. G., KU, A. A., BANDYOPADHYAY, S., MCCORMICK, F. & KIM, S. E. 2022. Novel Regulators of Macropinocytosis-Dependent Growth Revealed by Informer Set Library Screening in Pancreatic Cancer Cells. *Metabolites* [Online], 12.

KISHIKAWA, T., OTSUKA, M., SENG, T. P., OHNO, M., SUN, X., YOSHIKAWA, T., SHIBATA, C., TAKATA, A., KOJIMA, K., TAKEHANA, K., OHISHI, M., OTA, S., NOYAMA, T., KONDO, Y., SATO, M., SOGA, T., HOSHIDA, Y. & KOIKE, K. 2015. Decreased miR122 in hepatocellular carcinoma leads to chemoresistance with increased arginine. *Oncotarget; Vol 6, No 10*.

KLEINMAN, H. K. & MARTIN, G. R. 2005. Matrigel: Basement membrane matrix with biological activity. *Seminars in Cancer Biology,* 15**,** 378-386.

LAWRENCE, R. E. & ZONCU, R. 2019. The lysosome as a cellular centre for signalling, metabolism and quality control. *Nature Cell Biology,* 21**,** 133-142.

LE, C. C., BENNASROUNE, A., LANGLOIS, B., SALESSE, S., BOULAGNON-ROMBI, C., MORJANI, H., DEDIEU, S. & APPERT-COLLIN, A. 2020. Functional Interplay Between Collagen Network and Cell Behavior Within Tumor Microenvironment in Colorectal Cancer. *Frontiers in Oncology,* Volume 10 - 2020.

LEE, K. S., SU, X. & HUAN, T. 2025. Metabolites are not genes - avoiding the misuse of pathway analysis in metabolomics. *Nat Metab*.

LEVINE, B. & KROEMER, G. 2008. Autophagy in the Pathogenesis of Disease. *Cell,* 132**,** 27-42.

LI, B., SUN, C., SUN, J., YANG, M.-H., ZUO, R., LIU, C., LAN, W.-R., LIU, M.-H., HUANG, B. & ZHOU, Y. 2019. Autophagy mediates serum starvation-induced quiescence in nucleus pulposus stem cells by the regulation of P27. *Stem Cell Research & Therapy,* 10**,** 118.

LI, X., PENG, X., LI, Y., WEI, S., HE, G., LIU, J., LI, X., YANG, S., LI, D., LIN, W., FANG, J., YANG, L. & LI, H. 2024. Glutamine addiction in tumour cell: oncogene regulation and clinical treatment. *Cell Communication and Signaling,* 22**,** 12.

LI, Z., LIN, P., GAO, C., PENG, C., LIU, S., GAO, H., WANG, B., WANG, J., NIU, J. & NIU, W. 2016. Integrin β6 acts as an unfavourable prognostic indicator and promotes cellular malignant behaviours via ERK-ETS1 pathway in pancreatic ductal adenocarcinoma (PDAC). *Tumour Biology,* 37**,** 5117-5131.

LIM, R. M., LU, A., CHUANG, B. M., ANARAKI, C., CHU, B., HALBROOK, C. J. & EDINGER, A. L. 2024. CARMIL1-AA selectively inhibits macropinocytosis while sparing autophagy. *Molecular Biology of the Cell,* 36**,** ar4.

LINDNER, B., BURKARD, T. & SCHULER, M. 2020. Phagocytosis Assays with Different pH-Sensitive Fluorescent Particles and Various Readouts. *BioTechniques,* 68**,** 245-250.

LIOT, S., BALAS, J., AUBERT, A., PRIGENT, L., MERCIER-GOUY, P., VERRIER, B., BERTOLINO, P., HENNINO, A., VALCOURT, U. & LAMBERT, E. 2021. Stroma Involvement in Pancreatic Ductal Adenocarcinoma: An Overview Focusing on Extracellular Matrix Proteins. *Frontiers in Immunology,* Volume 12 - 2021.

LIU, X. & LOCASALE, J. W. 2017. Metabolomics: A Primer. *Trends Biochem Sci,* 42**,** 274-284.

LÓPEZ DE LA OLIVA, A. R., CAMPOS-SANDOVAL, J. A., GÓMEZ-GARCÍA, M. C., CARDONA, C., MARTÍN-RUFIÁN, M., SIALANA, F. J., CASTILLA, L., BAE, N., LOBO, C., PEÑALVER, A., GARCÍA-FRUTOS, M., CARRO, D., ENRIQUE, V., PAZ, J. C., MIRMIRA, R. G., GUTIÉRREZ, A., ALONSO, F. J., SEGURA, J. A., MATÉS, J. M., LUBEC, G. & MÁRQUEZ, J. 2020. Nuclear Translocation of Glutaminase GLS2 in Human Cancer Cells Associates with Proliferation Arrest and Differentiation. *Scientific Reports,* 10**,** 2259.

LORD, S. J., VELLE, K. B., MULLINS, R. D. & FRITZ-LAYLIN, L. K. 2020. SuperPlots: Communicating reproducibility and variability in cell biology. *Journal of Cell Biology,* 219**,** e202001064.

LOWMAN, X. H., HANSE, E. A., YANG, Y., ISHAK GABRA, M. B., TRAN, T. Q., LI, H. & KONG, M. 2019. p53 Promotes Cancer Cell Adaptation to Glutamine Deprivation by Upregulating Slc7a3 to Increase Arginine Uptake. *Cell Rep,* 26**,** 3051-3060 e4.

LU, S. & ARCHER, M. C. 2005. Fatty acid synthase is a potential molecular target for the chemoprevention of breast cancer. *Carcinogenesis,* 26**,** 153-157.

LUO, X., LIU, J., WANG, H. & LU, H. 2020. Metabolomics Identified New Biomarkers for The Precise Diagnosis of Pancreatic Cancer and Associated Tissue Metastasis. *Pharmacol Res,* 156**,** 104805.

MA, B., WANG, X., WU, C. & CHANG, J. 2014. Crosslinking strategies for preparation of extracellular matrix-derived cardiovascular scaffolds. *Regenerative Biomaterials,* 1**,** 81-89.

MAHADEVAN, D. & VON HOFF, D. D. 2007. tumour-stroma interactions in pancreatic ductal adenocarcinoma. *Mol Cancer Ther,* 6**,** 1186-97.

MAHADEVAN, K. K., MCANDREWS, K. M., LEBLEU, V. S., YANG, S., LYU, H., LI, B., SOCKWELL, A. M., KIRTLEY, M. L., MORSE, S. J., MORENO DIAZ, B. A., KIM, M. P., FENG, N., LOPEZ, A. M., GUERRERO, P. A., PARADISO, F., SUGIMOTO, H., ARIAN, K. A., YING, H., BAREKATAIN, Y., STHANAM, L. K., KELLY, P. J., MAITRA, A., HEFFERNAN, T. P. & KALLURI, R. 2023. KRAS G12D inhibition reprograms the microenvironment of early and advanced pancreatic cancer to promote FAS-mediated killing by CD8+ T cells. *Cancer Cell,* 41**,** 1606-1620.e8.

MARSTRAND-DAUCÉ, L., LORENZO, D., CHASSAC, A., NICOLE, P., COUVELARD, A. & HAUMAITRE, C. 2023. Acinar-to-Ductal Metaplasia (ADM): On the Road to Pancreatic Intraepithelial

Neoplasia (PanIN) and Pancreatic Cancer. International Journal of Molecular Sciences [Online], 24.

MARTINEAU, Y., AZAR, R., MÜLLER, D., LASFARGUES, C., EL KHAWAND, S., ANESIA, R., PELLETIER, J., BOUSQUET, C. & PYRONNET, S. 2014. Pancreatic tumours escape from translational control through 4E-BP1 loss. *Oncogene,* 33**,** 1367-1374.

MARTINEZ, M. L., NAN, K., BAO, Z., BACCHETTI, R., YUAN, S., TYLER, J., GUEZENNEC, X. L., BARD, F. A. & RAINERO, E. 2024. Novel kinase regulators of extracellular matrix internalisation identified by high-content screening modulate invasive carcinoma cell migration. *PLOS Biology,* 22**,** e3002930.

MASCARAQUE, M., COURTOIS, S., ROYO-GARCÍA, A., BARNEDA, D., STOIAN, A. M., VILLAOSLADA, I., ESPIAU-ROMERA, P., BOKIL, A., CANO-GALIANO, A., JAGUST, P., HEESCHEN, C. & SANCHO, P. 2024. Fatty acid oxidation is critical for the tumorigenic potential and chemoresistance of pancreatic cancer stem cells. *Journal of Translational Medicine,* 22**,** 797.

MASSARO, C., THOMAS, J. & PHANSTIEL, O. 2017. Investigation of Polyamine Metabolism and Homeostasis in Pancreatic Cancers. *Medical Sciences* [Online], 5.

MEHTA, D., RAJPUT, K., JAIN, D., BAJAJ, A. & DASGUPTA, U. 2024. Unveiling the Role of Mechanistic Target of Rapamycin Kinase (MTOR) Signalling in Cancer Progression and the Emergence of MTOR Inhibitors as Therapeutic Strategies. *ACS Pharmacology & Translational Science,* 7**,** 3758-3779.

MIAO, R., LI, M., ZHANG, Q., YANG, C. & WANG, X. 2020. An ECM-to-Nucleus Signaling Pathway Activates Lysosomes for C. elegans Larval Development. *Developmental Cell,* 52**,** 21-37.e5.

MICHALOPOULOU, E., AUCIELLO, F. R., BULUSU, V., STRACHAN, D., CAMPBELL, A. D., TAIT-MULDER, J., KARIM, S. A., MORTON, J. P., SANSOM, O. J. & KAMPHORST, J. J. 2020. Macropinocytosis Renders a Subset of Pancreatic tumour Cells Resistant to mTOR Inhibition. *Cell Reports,* 30**,** 2729-2742.e4.

MIYAMOTO, H., MURAKAMI, T., TSUCHIDA, K., SUGINO, H., MIYAKE, H. & TASHIRO, S. 2004. Tumour-Stroma Interaction of Human Pancreatic Cancer: Acquired Resistance to Anticancer Drugs and Proliferation Regulation Is Dependent on Extracellular Matrix Proteins. *Pancreas,* 28**,** 38-44.

MOLOUGHNEY, J. G., KIM, P. K., VEGA-COTTO, N. M., WU, C.-C., ZHANG, S., ADLAM, M., LYNCH, T., CHOU, P.-C., RABINOWITZ, J. D., WERLEN, G. & JACINTO, E. 2016. mTORC2 Responds to Glutamine Catabolite Levels to Modulate the Hexosamine Biosynthesis Enzyme GFAT1. *Molecular Cell,* 63**,** 811-826.

MOORE, N., HOUGHTON, J. & LYLE, S. 2011. Slow-Cycling Therapy-Resistant Cancer Cells. *Stem Cells and Development,* 21**,** 1822-1830.

MOSSMANN, D., PARK, S. & HALL, M. N. 2018. mTOR signalling and cellular metabolism are mutual determinants in cancer. *Nature Reviews Cancer,* 18**,** 744-757.

MURANEN, T., IWANICKI, M. P., CURRY, N. L., HWANG, J., DUBOIS, C. D., COLOFF, J. L., HITCHCOCK, D. S., CLISH, C. B., BRUGGE, J. S. & KALAANY, N. Y. 2017. Starved epithelial cells uptake extracellular matrix for survival. *Nature Communications,* 8**,** 13989.

MURPHY, G. & NAGASE, H. 2008. Progress in matrix metalloproteinase research. *Molecular Aspects of Medicine,* 29**,** 290-308.

MURPHY, K. J., ZHU, J., TRPCESKI, M., PEREIRA, B. A., TIMPSON, P. & HERRMANN, D. 2022. Focal adhesion kinase priming in pancreatic cancer, altering biomechanics to improve chemotherapy. *Biochemical Society Transactions,* 50**,** 1129-1141.

MUSA, J., ORTH, M. F., DALLMAYER, M., BALDAUF, M., PARDO, C., ROTBLAT, B., KIRCHNER, T., LEPRIVIER, G. & GRÜNEWALD, T. G. P. 2016. Eukaryotic initiation factor 4E-binding protein 1 (4E-BP1): a master regulator of mRNA translation involved in tumourigenesis. *Oncogene,* 35**,** 4675-4688.

National Cancer Institute Surveillance, Epidemiology, and End Results (SEER) Program. Cancer Stat Facts: Pancreatic Cancer https://seer.cancer.gov/statfacts/html/pancreas.html. Accessed: July 2025.

NAZEMI, M., YANES, B., MARTINEZ, M. L., WALKER, H. J., PHAM, K., COLLINS, M. O., BARD, F. & RAINERO, E. 2024. The Extracellular Matrix Supports Breast Cancer Cell Growth Under Amino Acid Starvation by Promoting Tyrosine Catabolism. *Plos Biol,* 22**,** E3002406.

NIK NABIL, W. N., XI, Z., SONG, Z., JIN, L., ZHANG, X. D., ZHOU, H., DE SOUZA, P., DONG, Q. & XU, H. 2021. Towards a Framework for Better Understanding of Quiescent Cancer Cells. *Cells* [Online], 10.

NONG, S., QIAN, Y., ZHANG, T., ZHOU, X., WEI, Y., YIN, X. & MA, X. 2022. Mechanism and application of nonessential amino acid deprivation associated with tumour therapy. *MedComm – Future Medicine,* 1**,** e12.

OHLUND, D., LUNDIN, C., ARDNOR, B., OMAN, M., NAREDI, P. & SUND, M. 2009. Type IV collagen is a tumour stroma-derived biomarker for pancreas cancer. *Br J Cancer,* 101**,** 91-7.

ÖHLUND, D., FRANKLIN, O., LUNDBERG, E., LUNDIN, C. & SUND, M. 2013. Type IV collagen stimulates pancreatic cancer cell proliferation, migration, and inhibits apoptosis through an autocrine loop. *BMC Cancer,* 13**,** 154.

OLIVARES, O., MAYERS, J. R., GOUIRAND, V., TORRENCE, M. E., GICQUEL, T., BORGE, L., LAC, S., ROQUES, J., LAVAUT, M.-N., BERTHEZÈNE, P., RUBIS, M., SECQ, V., GARCIA, S., MOUTARDIER, V., LOMBARDO, D., IOVANNA, J. L., TOMASINI, R., GUILLAUMOND, F., VANDER HEIDEN, M. G. & VASSEUR, S. 2017. Collagen-derived proline promotes pancreatic ductal adenocarcinoma cell survival under nutrient-limited conditions. *Nature Communications,* 8**,** 16031.

ORTMAYR, K. & ZAMPIERI, M. 2022. Sorting-free metabolic profiling uncovers the vulnerability of fatty acid β-oxidation in vitro in quiescence models. *Molecular Systems Biology,* 18**,** e10716.

PALM, W. & THOMPSON, C. B. 2017. Nutrient acquisition strategies of mammalian cells. *Nature,* 546**,** 234-242.

PALM, W., PARK, Y., WRIGHT, K., PAVLOVA, N. N., TUVESON, D. A. & THOMPSON, C. B. 2015. The Utilization of Extracellular Proteins as Nutrients Is Suppressed by mTORC1. *Cell,* 162**,** 259-270.

PANTSAR, T. 2020. The current understanding of KRAS protein structure and dynamics. *Computational and Structural Biotechnology Journal,* 18**,** 189-198.

PAPALAZAROU, V., ZHANG, T., PAUL, N. R., JUIN, A., CANTINI, M., MADDOCKS, O. D. K., SALMERON-SANCHEZ, M. & MACHESKY, L. M. 2020. The creatine-phosphagen system is mechanoresponsive in pancreatic adenocarcinoma and fuels invasion and metastasis. *Nat Metab,* 2**,** 62-80.

PARKER, S. J., AMENDOLA, C. R., HOLLINSHEAD, K. E. R., YU, Q., YAMAMOTO, K., ENCARNACIÓN-ROSADO, J., ROSE, R. E., LARUE, M. M., SOHN, A. S. W., BIANCUR, D. E., PAULO, J. A., GYGI, S. P., JONES, D. R., WANG, H., PHILIPS, M. R., BAR-SAGI, D., MANCIAS, J. D. & KIMMELMAN, A. C. 2020. Selective Alanine Transporter Utilisation Creates a Targetable Metabolic Niche in Pancreatic Cancer. *Cancer Discovery,* 10**,** 1018-1037.

PARZYCH, K. R. & KLIONSKY, D. J. 2013. An Overview of Autophagy: Morphology, Mechanism, and Regulation. *Antioxidants & Redox Signaling,* 20**,** 460-473.

PAUL, D., STERN, O., VALLIS, Y., DHILLON, J., BUCHANAN, A. & MCMAHON, H. 2023. Cell surface protein aggregation triggers endocytosis to maintain plasma membrane proteostasis. *Nature Communications,* 14**,** 947.

PEREZ, V. M., KEARNEY, J. F. & YEH, J. J. 2021. The PDAC Extracellular Matrix: A Review of the ECM Protein Composition, tumour Cell Interaction, and Therapeutic Strategies. *Front Oncol,* 11**,** 751311.

PONTÉN, F., JIRSTRÖM, K. & UHLEN, M. 2008. The Human Protein Atlas—a tool for pathology. *The Journal of Pathology,* 216**,** 387-393.

PRAKASH, J. & SHAKED, Y. 2024. The Interplay between Extracellular Matrix Remodelling and Cancer Therapeutics. *Cancer Discovery,* 14**,** 1375-1388.

PROVENZANO, PAOLO P., CUEVAS, C., CHANG, AMY E., GOEL, VIKAS K., VON HOFF, DANIEL D. & HINGORANI, SUNIL R. 2012. Enzymatic Targeting of the Stroma Ablates Physical Barriers to Treatment of Pancreatic Ductal Adenocarcinoma. *Cancer Cell,* 21**,** 418-429.

QUINTANILLA-DIECK, M. J., CODRIANSKY, K., KEADY, M., BHAWAN, J. & RÜNGER, T. M. 2008. Cathepsin K in Melanoma Invasion. *Journal of Investigative Dermatology,* 128**,** 2281-2288.

RABANAL-RUIZ, Y., OTTEN, ELSJE G. & KOROLCHUK, VIKTOR I. 2017. mTORC1 as the main gateway to autophagy. *Essays in Biochemistry,* 61**,** 565-584.

RAINERO, E. 2016. Extracellular matrix endocytosis in controlling matrix turnover and beyond: emerging roles in cancer. *Biochem Soc Trans,* 44**,** 1347-1354.

RAINERO, E. 2018. Extracellular matrix internalisation links nutrient signalling to invasive migration. *International Journal of Experimental Pathology,* 99**,** 4-9.

RAJBHANDARI, N., LIN, W.-C., WEHDE, B. L., TRIPLETT, A. A. & WAGNER, K.-U. 2017. Autocrine IGF1 Signaling Mediates Pancreatic tumour Cell Dormancy in the Absence of Oncogenic Drivers. *Cell Reports,* 18**,** 2243-2255.

REN, L. L., MAO, T., MENG, P., ZHANG, L., WEI, H. Y. & TIAN, Z. B. 2023. Glutamine addiction and therapeutic strategies in pancreatic cancer. *World J Gastrointest Oncol,* 15**,** 1852-1863.

RICCIARDI, M. R., MIRABILII, S., ALLEGRETTI, M., LICCHETTA, R., CALARCO, A., TORRISI, M. R., FOÀ, R., NICOLAI, R., PELUSO, G. & TAFURI, A. 2015. Targeting the leukaemia cell metabolism by the CPT1a inhibition: functional preclinical effects in leukemias. *Blood,* 126**,** 1925-1929.

ROLVER, M. G., ELINGAARD-LARSEN, L. O., ANDERSEN, A. P., COUNILLON, L. & PEDERSEN, S. F. 2020. Pyrazine ring-based Na+/H+ exchanger (NHE) inhibitors potently inhibit cancer cell growth in 3D culture, independent of NHE1. *Scientific Reports,* 10**,** 5800.

ROY, R., MORAD, G., JEDINAK, A. & MOSES, M. A. 2020. Metalloproteinases and their roles in human cancer. *The Anatomical Record,* 303**,** 1557-1572.

SALLOUM, G., JAKUBIK, C. T., ERAMI, Z., HEITZ, S. D., BRESNICK, A. R. & BACKER, J. M. 2019. PI3Kβ is selectively required for growth factor-stimulated macropinocytosis. *Journal of Cell Science,* 132**,** jcs231639.

SATO, K., TSUCHIHARA, K., FUJII, S., SUGIYAMA, M., GOYA, T., ATOMI, Y., UENO, T., OCHIAI, A. & ESUMI, H. 2007. Autophagy Is Activated in Colorectal Cancer Cells and Contributes to the Tolerance to Nutrient Deprivation. *Cancer Research,* 67**,** 9677-9684.

SAWAI, H., OKADA, Y., FUNAHASHI, H., TAKAHASHI, H., MATSUO, Y., YASUDA, A., OCHI, N., TAKEYAMA, H. & MANABE, T. 2008. Basement Membrane Proteins Play an Important Role in

the Invasive Processes of Human Pancreatic Cancer Cells. *Journal of Surgical Research,* 144**,** 117-123.

SCHLAEPFER, I. R., RIDER, L., RODRIGUES, L. U., GIJÓN, M. A., PAC, C. T., ROMERO, L., CIMIC, A., SIRINTRAPUN, S. J., GLODÉ, L. M., ECKEL, R. H. & CRAMER, S. D. 2014. Lipid Catabolism via CPT1 as a Therapeutic Target for Prostate Cancer. *Molecular Cancer Therapeutics,* 13**,** 2361-2371.

SCHMIDT, D. R., PATEL, R., KIRSCH, D. G., LEWIS, C. A., VANDER HEIDEN, M. G. & LOCASALE, J. W. 2021. Metabolomics In Cancer Research and Emerging Applications In Clinical Oncology. *Ca Cancer J Clin,* 71**,** 333-358.

SEO, J. W., CHOI, J., LEE, S. Y., SUNG, S., YOO, H. J., KANG, M. J., CHEONG, H. & SON, J. 2016. Autophagy is required for PDAC glutamine metabolism. *Sci Rep,* 6**,** 37594.

SHEN, X., CHEN, Y., TANG, Y., LU, P., LIU, M., MAO, T., WENG, Y., YU, F., LIU, Y., TANG, Y., WANG, L., NIU, N. & XUE, J. 2025. Targeting pancreatic cancer glutamine dependency confers vulnerability to GPX4-dependent ferroptosis. *Cell Reports Medicine,* 6.

SHI, Y., ZHENG, H., WANG, T., ZHOU, S., ZHAO, S., LI, M. & CAO, B. 2025. Targeting KRAS: from metabolic regulation to cancer treatment. *Mol Cancer,* 24**,** 9.

SHIN, S., SOLORZANO, J., LIAUZUN, M., PYRONNET, S., BOUSQUET, C. & MARTINEAU, Y. 2022. Translational alterations in pancreatic cancer: a central role for the integrated stress response. *NAR Cancer,* 4**,** zcac031.

SHIRATORI, R., FURUICHI, K., YAMAGUCHI, M., MIYAZAKI, N., AOKI, H., CHIBANA, H., ITO, K. & AOKI, S. 2019. Glycolytic suppression dramatically changes the intracellular metabolic profile of multiple cancer cell lines in a mitochondrial metabolism-dependent manner. *Sci Rep,* 9**,** 18699.

SINGH, P. K., DEORUKHKAR, A. A., VENKATESULU, B. P., LI, X., TAILOR, R., BOMALASKI, J. S. & KRISHNAN, S. 2019. Exploiting Arginine Auxotrophy with Pegylated Arginine Deiminase (ADI-PEG20) to Sensitize Pancreatic Cancer to Radiotherapy via Metabolic Dysregulation. *Molecular Cancer Therapeutics,* 18**,** 2381-2393.

SINGHAL, A., STYERS, H. C., RUB, J., LI, Z., TORBORG, S. R., KIM, J. Y., GRBOVIC-HUEZO, O., FENG, H., TARCAN, Z. C., SAHIN OZKAN, H., HALLIN, J., BASTURK, O., YAEGER, R., CHRISTENSEN, J. G., BETEL, D., YAN, Y., CHIO, I. I. C., DE STANCHINA, E. & TAMMELA, T. 2024. A Classical Epithelial State Drives Acute Resistance to KRAS Inhibition in Pancreatic Cancer. *Cancer Discovery,* 14**,** 2122-2134.

SIPOS, B., HAHN, D., CARCELLER, A., PIULATS, J., HEDDERICH, J., KALTHOFF, H., GOODMAN, S. L., KOSMAHL, M. & KLÖPPEL, G. 2004. Immunohistochemical screening for β6-integrin subunit

expression in adenocarcinomas using a novel monoclonal antibody reveals strong up-regulation in pancreatic ductal adenocarcinomas in vivo and in vitro. *Histopathology,* 45**,** 226-236.

SNEEGGEN, M., GUADAGNO, N. A. & PROGIDA, C. 2020. Intracellular Transport in Cancer Metabolic Reprogramming. *Front Cell Dev Biol,* 8**,** 597608.

SON, J., LYSSIOTIS, C. A., YING, H., WANG, X., HUA, S., LIGORIO, M., PERERA, R. M., FERRONE, C. R., MULLARKY, E., SHYH-CHANG, N., KANG, Y., FLEMING, J. B., BARDEESY, N., ASARA, J. M., HAIGIS, M. C., DEPINHO, R. A., CANTLEY, L. C. & KIMMELMAN, A. C. 2013. Glutamine supports pancreatic cancer growth through a KRAS-regulated metabolic pathway. *Nature,* 496**,** 101-5.

SPRANGERS, S. & EVERTS, V. 2019. Molecular pathways of cell-mediated degradation of fibrillar collagen. *Matrix Biology,* 75-76**,** 190-200.

STORZ, P. 2017. Acinar cell plasticity and development of pancreatic ductal adenocarcinoma. *Nature Reviews Gastroenterology & Hepatology,* 14**,** 296-304.

SULLIVAN, M. R., DANAI, L. V., LEWIS, C. A., CHAN, S. H., GUI, D. Y., KUNCHOK, T., DENNSTEDT, E. A., VANDER HEIDEN, M. G. & MUIR, A. 2019. Quantification of microenvironmental metabolites in murine cancers reveals determinants of tumour nutrient availability. *Elife,* 8.

SUN, Z., SCHWENZER, A., RUPP, T., MURDAMOOTHOO, D., VEGLIANTE, R., LEFEBVRE, O., KLEIN, A., HUSSENET, T. & OREND, G. 2018. Tenascin-C Promotes Tumour Cell Migration and Metastasis through Integrin α9β1–Mediated YAP Inhibition. *Cancer Research,* 78**,** 950-961.

SUOMALAINEN, A. & NUNNARI, J. 2024. Mitochondria at the crossroads of health and disease. *Cell,* 187**,** 2601-2627.

SURI, G. S., KAUR, G., CARBONE, G. M. & SHINDE, D. 2023. Metabolomics In Oncology. *Cancer Rep (Hoboken),* 6**,** E1795.

TABANG, D. N., CUI, Y., TREMMEL, D. M., FORD, M., LI, Z., SACKETT, S. D., ODORICO, J. S. & LI, L. 2021. Analysis of pancreatic extracellular matrix protein post-translational modifications via electrostatic repulsion-hydrophilic interaction chromatography coupled with mass spectrometry. *Molecular Omics,* 17**,** 652-664.

TERZI, M. Y., IZMIRLI, M. & GOGEBAKAN, B. 2016. The cell fate: senescence or quiescence. *Molecular Biology Reports,* 43**,** 1213-1220.

TIAN, T., LI, X. & ZHANG, J. 2019. mTOR Signalling in Cancer and mTOR Inhibitors in Solid tumour Targeting Therapy. *International Journal of Molecular Sciences* [Online], 20.

TODA, K., KAWADA, K., IWAMOTO, M., INAMOTO, S., SASAZUKI, T., SHIRASAWA, S., HASEGAWA, S. & SAKAI, Y. 2016. Metabolic Alterations Caused by KRAS Mutations in Colorectal Cancer

Contribute to Cell Adaptation to Glutamine Depletion by Upregulation of Asparagine Synthetase. *Neoplasia,* 18**,** 654-665.

TRAN, D. H., KIM, D., KESAVAN, R., BROWN, H., DEY, T., SOFLAEE, M. H., VU, H. S., TASDOGAN, A., GUO, J., BEZWADA, D., AL SAAD, H., CAI, F., SOLMONSON, A., RION, H., CHABATYA, R., MERCHANT, S., MANALES, N. J., TCHEUYAP, V. T., MULKEY, M., MATHEWS, T. P., BRUGAROLAS, J., MORRISON, S. J., ZHU, H., DEBERARDINIS, R. J. & HOXHAJ, G. 2024. De novo and salvage purine synthesis pathways across tissues and tumors. *Cell,* 187**,** 3602-3618 e20.

TSAI, P.-Y., LEE, M.-S., JADHAV, U., NAQVI, I., MADHA, S., ADLER, A., MISTRY, M., NAUMENKO, S., LEWIS, C. A., HITCHCOCK, D. S., ROBERTS, F. R., DELNERO, P., HANK, T., HONSELMANN, K. C., MORALES OYARVIDE, V., MINO-KENUDSON, M., CLISH, C. B., SHIVDASANI, R. A. & KALAANY, N. Y. 2021. Adaptation of pancreatic cancer cells to nutrient deprivation is reversible and requires glutamine synthetase stabilisation by mTORC1. *Proceedings of the National Academy of Sciences,* 118**,** e2003014118.

TSAI, W.-B., AIBA, I., LEE, S.-Y., FEUN, L., SAVARAJ, N. & KUO, M. T. 2009. Resistance to arginine deiminase treatment in melanoma cells is associated with induced argininosuccinate synthetase expression involving c-Myc/HIF-1α/Sp4. *Molecular Cancer Therapeutics,* 8**,** 3223-3233.

TU, G., GONG, Y., YAO, X., LIU, Q., XUE, W. & ZHANG, R. 2024. Pathways and mechanism of MRTX1133 binding to KRAS G12D elucidated by molecular dynamics simulations and Markov state models. *International Journal of Biological Macromolecules,* 274**,** 133374.

VALCOURT, J. R., LEMONS, J. M. S., HALEY, E. M., KOJIMA, M., DEMUREN, O. O. & COLLER, H. A. 2012. Staying alive. *Cell Cycle,* 11**,** 1680-1696.

VALENTE, R., COPPOLA, A., SCANDAVINI, C. M., HALIMI, A., MAGNUSSON, A., LAURO, A., SOTIROVA, I., ARNELO, U. & FRANKLIN, O. 2024. Interactions between the Exocrine and the Endocrine Pancreas. *Journal of Clinical Medicine* [Online], 13.

VANDER HEIDEN, M. G., CANTLEY, L. C. & THOMPSON, C. B. 2009. Understanding the Warburg Effect: The Metabolic Requirements of Cell Proliferation. *Science,* 324**,** 1029-1033.

VENNIN, C., MÉLÉNEC, P., ROUET, R., NOBIS, M., CAZET, A. S., MURPHY, K. J., HERRMANN, D., REED, D. A., LUCAS, M. C., WARREN, S. C., ELGUNDI, Z., PINESE, M., KALNA, G., RODEN, D., SAMUEL, M., ZARATZIAN, A., GREY, S. T., DA SILVA, A., LEUNG, W., JOHNS, A. L., CHANTRILL, L. A., CHOU, A., STEINMANN, A., ARSHI, M., DWARTE, T., FROIO, D., PEREIRA, B., RITCHIE, S., CHAMBERS, C. R., METCALF, X., WADDELL, N., PEARSON, J. V., PATCH, A.-M., NONES, K., NEWELL, F., MUKHOPADHYAY, P., ADDALA, V., KAZAKOFF, S., HOLMES, O., LEONARD, C.,

WOOD, S., GRIMMOND, S. M., HOFMANN, O., CHRIST, A., BRUXNER, T., SAMRA, J. S., PAVLAKIS, N., HIGH, H. A., ASGHARI, R., MERRETT, N. D., PAVEY, D., DAS, A., COSMAN, P. H., ISMAIL, K., O'CONNNOR, C., STOITA, A., WILLIAMS, D., SPIGELLMAN, A., LAM, V. W., MCLEOD, D., KIRK, J., KENCH, J. G., GRIMISON, P., COOPER, C. L., SANDROUSSI, C., GOODWIN, A., MEAD, R. S., TUCKER, K., ANDREWS, L., TEXLER, M., FOREST, C., EPARI, K. P., BALLAL, M., FLETCHER, D. R., MUKHEDKAR, S., ZEPS, N., BEILIN, M., FEENEY, K., NGUYEN, N. Q., RUSZKIEWICZ, A. R., WORTHLEY, C., CHEN, J., BROOKE-SMITH, M. E., PAPANGELIS, V., CLOUSTON, A. D., BARBOUR, A. P., O'ROURKE, T. J., FAWCETT, J. W., SLATER, K., HATZIFOTIS, M., HODGKINSON, P., NIKFARJAM, M., ESHLEMAN, J. R., HRUBAN, R. H., WOLFGANG, C. L., LAWLOR, R. T., BEGHELLI, S., CORBO, V., SCARDONI, M., BASSI, C., et al. 2019. CAF hierarchy driven by pancreatic cancer cell p53-status creates a pro-metastatic and chemoresistant environment via perlecan. *Nature Communications,* 10**,** 3637.

VIALE, A., PETTAZZONI, P., LYSSIOTIS, C. A., YING, H., SÁNCHEZ, N., MARCHESINI, M., CARUGO, A., GREEN, T., SETH, S., GIULIANI, V., KOST-ALIMOVA, M., MULLER, F., COLLA, S., NEZI, L., GENOVESE, G., DEEM, A. K., KAPOOR, A., YAO, W., BRUNETTO, E., KANG, Y. A., YUAN, M., ASARA, J. M., WANG, Y. A., HEFFERNAN, T. P., KIMMELMAN, A. C., WANG, H., FLEMING, J. B., CANTLEY, L. C., DEPINHO, R. A. & DRAETTA, G. F. 2014. Oncogene ablation-resistant pancreatic cancer cells depend on mitochondrial function. *Nature,* 514**,** 628-632.

WAGNER, M. & WIIG, H. 2015. Tumour Interstitial Fluid Formation, Characterisation, and Clinical Implications. *Frontiers in Oncology,* Volume 5 - 2015.

WANG, K., NING, S., ZHANG, S., JIANG, M., HUANG, Y., PEI, H., LI, M. & TAN, F. 2025a. Extracellular matrix stiffness regulates colorectal cancer progression via HSF4. *Journal of Experimental & Clinical Cancer Research,* 44**,** 30.

WANG, X., ALLEN, S., BLAKE, J. F., BOWCUT, V., BRIERE, D. M., CALINISAN, A., DAHLKE, J. R., FELL, J. B., FISCHER, J. P., GUNN, R. J., HALLIN, J., LAGUER, J., LAWSON, J. D., MEDWID, J., NEWHOUSE, B., NGUYEN, P., O'LEARY, J. M., OLSON, P., PAJK, S., RAHBAEK, L., RODRIGUEZ, M., SMITH, C. R., TANG, T. P., THOMAS, N. C., VANDERPOOL, D., VIGERS, G. P., CHRISTENSEN, J. G. & MARX, M. A. 2022. Identification of MRTX1133, a Noncovalent, Potent, and Selective KRASG12D Inhibitor. *Journal of Medicinal Chemistry,* 65**,** 3123-3133.

WANG, Y., LIU, L., ZHANG, X., LIANG, T. & BAI, X. 2025b. Cancer dormancy and metabolism: From molecular insights to translational opportunities. *Cancer Letters,* 635**,** 218097.

WANG, Y., LU, J.-H., WANG, F., WANG, Y.-N., HE, M.-M., WU, Q.-N., LU, Y.-X., YU, H.-E., CHEN, Z.-H., ZHAO, Q., LIU, J., CHEN, Y.-X., WANG, D.-S., SHENG, H., LIU, Z.-X., ZENG, Z.-L., XU, R.-H. & JU,

H.-Q. 2020. Inhibition of fatty acid catabolism augments the efficacy of oxaliplatin-based chemotherapy in gastrointestinal cancers. *Cancer Letters,* 473**,** 74-89.

WEI, D., WANG, L., ZUO, X., MAITRA, A. & BRESALIER, R. S. 2024. A Small Molecule with Big Impact: MRTX1133 Targets the KRASG12D Mutation in Pancreatic Cancer. *Clinical Cancer Research,* 30**,** 655-662.

WENIGER, M., HONSELMANN, K. C. & LISS, A. S. 2018. The Extracellular Matrix and Pancreatic Cancer: A Complex Relationship. *Cancers (Basel),* 10.

WHITE, E. Z., PENNANT, N. M., CARTER, J. R., HAWSAWI, O., ODERO-MARAH, V. & HINTON, C. V. 2020. Serum deprivation initiates adaptation and survival to oxidative stress in prostate cancer cells. *Scientific Reports,* 10**,** 12505.

WILLUMSEN, N., BAGER, C. L., LEEMING, D. J., SMITH, V., KARSDAL, M. A., DORNAN, D. & BAY-JENSEN, A.-C. 2013. Extracellular matrix-specific protein fingerprints measured in serum can separate pancreatic cancer patients from healthy controls. *BMC Cancer,* 13**,** 554.

WINKLER, J., ABISOYE-OGUNNIYAN, A., METCALF, K. J. & WERB, Z. 2020. Concepts of extracellular matrix remodelling in tumour progression and metastasis. *Nature Communications,* 11**,** 5120.

WITTINGHOFER, A. & VETTER, I. R. 2011. Structure-Function Relationships of the G Domain, a Canonical Switch Motif. *Annual Review of Biochemistry,* 80**,** 943-971.

WOLFE, A. R., CUI, T., BAIE, S., CORRALES-GUERRERO, S., WEBB, A., CASTRO-ACEITUNO, V., SHYU, D.-L., KARASINSKA, J. M., TOPHAM, J. T., RENOUF, D. J., SCHAEFFER, D. F., HALLORAN, M., PACKARD, R., ROBB, R., CHEN, W., DENKO, N., LISANTI, M., THOMPSON, T. C., FRANK, P. & WILLIAMS, T. M. 2024. Nutrient scavenging-fueled growth in pancreatic cancer depends on caveolae-mediated endocytosis under nutrient-deprived conditions. *Science Advances,* 10**,** eadj3551.

World Cancer Research Fund https://www.wcrf.org/preventing-cancer/cancer-statistics/pancreatic-cancer-statistics/ Accessed: July 2025.

WU, H., FU, M., WU, M., CAO, Z., ZHANG, Q. & LIU, Z. 2024. Emerging mechanisms and promising approaches in pancreatic cancer metabolism. *Cell Death Dis,* 15**,** 553.

WU, H., OU, S., ZHANG, H., HUANG, R., YU, S., ZHAO, M. & TAI, S. 2022. Advances in biomarkers and techniques for pancreatic cancer diagnosis. *Cancer Cell Int,* 22**,** 220.

WYANT, G. A., ABU-REMAILEH, M., WOLFSON, R. L., CHEN, W. W., FREINKMAN, E., DANAI, L. V., VANDER HEIDEN, M. G. & SABATINI, D. M. 2017. mTORC1 Activator SLC38A9 Is Required to Efflux Essential Amino Acids from Lysosomes and Use Protein as a Nutrient. *Cell,* 171**,** 642-654.e12.

XU, G., ZHANG, Q., CHENG, R., QU, J. & LI, W. 2025. Survival strategies of cancer cells: the role of macropinocytosis in nutrient acquisition, metabolic reprogramming, and therapeutic targeting. *Autophagy,* 21**,** 693-718.

XU, R., YANG, J., REN, B., WANG, H., YANG, G., CHEN, Y., YOU, L. & ZHAO, Y. 2020. Reprogramming of Amino Acid Metabolism in Pancreatic Cancer: Recent Advances and Therapeutic Strategies. *Frontiers in Oncology,* Volume 10 - 2020.

YABUUCHI, Y., NAKAGAWA, T., SHIMANOUCHI, M., USUI, S., HAYASHIHARA, K., OH-ISHI, S., SAITO, T., KANAZAWA, J., MIURA, Y., KUBOTA, S., KAWASHIMA, K., SHIMADA, T., OSHIMA, H., HIRANO, H., NONAKA, M., KITAOKA, Y., ARAI, N., HYODO, K., NAKAZAWA, A. & MINAMI, Y. 2020. A Case of Pulmonary Metastasis of Breast Cancer 23 Years after Surgery Accompanied with Non-Tuberculous Mycobacterium Infection. *Case Reports in Oncology,* 13**,** 1357-1363.

YAN, L., RAJ, P., YAO, W. & YING, H. 2019. Glucose Metabolism in Pancreatic Cancer. *Cancers* [Online], 11.

YANG, D., LIU, J., QIAN, H. & ZHUANG, Q. 2023a. Cancer-associated fibroblasts: from basic science to anticancer therapy. *Exp Mol Med,* 55**,** 1322-1332.

YANG, J., REN, B., REN, J., YANG, G., FANG, Y., WANG, X., ZHOU, F., YOU, L. & ZHAO, Y. 2023b. Epigenetic reprogramming-induced guanidinoacetic acid synthesis promotes pancreatic cancer metastasis and transcription-activating histone modifications. *J Exp Clin Cancer Res,* 42**,** 155.

YANG, S., WANG, X., CONTINO, G., LIESA, M., SAHIN, E., YING, H., BAUSE, A., LI, Y., STOMMEL, J. M., DELL'ANTONIO, G., MAUTNER, J., TONON, G., HAIGIS, M., SHIRIHAI, O. S., DOGLIONI, C., BARDEESY, N. & KIMMELMAN, A. C. 2011. Pancreatic cancers require autophagy for tumour growth. *Genes Dev,* 25**,** 717-29.

YING, H., KIMMELMAN, ALEC C., LYSSIOTIS, COSTAS A., HUA, S., CHU, GERALD C., FLETCHER-SANANIKONE, E., LOCASALE, JASON W., SON, J., ZHANG, H., COLOFF, JONATHAN L., YAN, H., WANG, W., CHEN, S., VIALE, A., ZHENG, H., PAIK, J.-H., LIM, C., GUIMARAES, ALEXANDER R., MARTIN, ERIC S., CHANG, J., HEZEL, ARAM F., PERRY, SAMUEL R., HU, J., GAN, B., XIAO, Y., ASARA, JOHN M., WEISSLEDER, R., WANG, Y. A., CHIN, L., CANTLEY, LEWIS C. & DEPINHO, RONALD A. 2012. Oncogenic Kras Maintains Pancreatic tumours through Regulation of Anabolic Glucose Metabolism. *Cell,* 149**,** 656-670.

YOU, S., ZHU, X., YANG, Y., DU, X., SONG, K., ZHENG, Q., ZENG, P. & YAO, Q. 2022. SLC7A1 Overexpression Is Involved in Energy Metabolism Reprogramming to Induce Tumor Progression in Epithelial Ovarian Cancer and Is Associated with Immune-Infiltrating Cells. *Journal of Oncology,* 2022**,** 5864826.

YU, B., SHAO, S. & MA, W. 2025. Frontiers in pancreatic cancer on biomarkers, microenvironment, and immunotherapy. *Cancer Lett,* 610**,** 217350.

YU, W., YANG, X., ZHANG, Q., SUN, L., YUAN, S. & XIN, Y. 2021. Targeting GLS1 to cancer therapy through glutamine metabolism. *Clinical and Translational Oncology,* 23**,** 2253-2268.

YU, Z., ZHOU, R., ZHAO, Y., PAN, Y., LIANG, H., ZHANG, J. S., TAI, S., JIN, L. & TENG, C. B. 2019. Blockage of SLC31A1-dependent copper absorption increases pancreatic cancer cell autophagy to resist cell death. *Cell Prolif,* 52**,** e12568.

YUN, J., MULLARKY, E., LU, C., BOSCH, K. N., KAVALIER, A., RIVERA, K., ROPER, J., CHIO, I. I. C., GIANNOPOULOU, E. G., RAGO, C., MULEY, A., ASARA, J. M., PAIK, J., ELEMENTO, O., CHEN, Z., PAPPIN, D. J., DOW, L. E., PAPADOPOULOS, N., GROSS, S. S. & CANTLEY, L. C. 2015. Vitamin C selectively kills KRAS and BRAF mutant colorectal cancer cells by targeting GAPDH. *Science,* 350**,** 1391-1396.

YUN, J., RAGO, C., CHEONG, I., PAGLIARINI, R., ANGENENDT, P., RAJAGOPALAN, H., SCHMIDT, K., WILLSON, J. K. V., MARKOWITZ, S., ZHOU, S., DIAZ, L. A., VELCULESCU, V. E., LENGAUER, C., KINZLER, K. W., VOGELSTEIN, B. & PAPADOPOULOS, N. 2009. Glucose Deprivation Contributes to the Development of KRAS Pathway Mutations in tumour Cells. *Science,* 325**,** 1555-1559.

ZEISSIG, M. N., ASHWOOD, L. M., KONDRASHOVA, O. & SUTHERLAND, K. D. 2023. Next batter up! Targeting cancers with KRAS-G12D mutations. *Trends in Cancer,* 9**,** 955-967.

Zhao, Y., Sepehr, E., Vaught, C., Yourick, J. & Sprando, R. L. 2024. Cellular Metabolomics: From Sample Preparation to High-Throughput Data Analysis. *Journal Of Agriculture and Food Research,* 15.

ZHOU, S., CHEN, S., PEI, Y. A. & PEI, M. 2022. Nidogen: A matrix protein with potential roles in musculoskeletal tissue regeneration. *Genes & Diseases,* 9**,** 598-609.

ZOU, S., WANG, X., LIU, P., KE, C. & XU, S. 2019. Arginine metabolism and deprivation in cancer therapy. *Biomedicine & Pharmacotherapy,* 118**,** 109210.